Design and Operation of Intensified Multiphase Processes

by

Fouad Azizi

Submitted in partial fulfillment of the requirements
for the degree of Doctor of Philosophy

at

Dalhousie University
Halifax, Nova Scotia
April, 2009

Your file Votre référence
ISBN: 978-0-494-50287-7
Our file Notre référence
ISBN: 978-0-494-50287-7

DALHOUSIE UNIVERSITY

To comply with the Canadian Privacy Act the National Library of Canada has requested that the following pages be removed from this copy of the thesis:

Preliminary Pages
- Examiners Signature Page
- Dalhousie Library Copyright Agreement

Appendices
- Copyright Releases (if applicable)

TABLE OF CONTENTS

LIST OF TABLES

LIST OF FIGURES

ABSTRACT

Systems containing bubbles and/or drops are encountered in a wide range of industrial operations. Nevertheless, designing multiphase reactors that offer high selectivity and yield remains a major challenge because of the complex hydrodynamic conditions prevalent in conventional reactor configurations, and the use of CFD to simulate such conditions is clouded by uncertainties related to the accurate representation of bubble and drop breakage and coalescence. Most of these hydrodynamic difficulties are however overcome when multi-stage screen-type static mixers are used as reactors.

The current thesis work aims towards developing a better understanding of the factors that influence the use of the population balance equation (PBE) in simulating multi-fluid dispersed systems as well as the application of screen-type static mixers in intensifying multiphase operations.

For that purpose, an approach for predicting the spatial variation of the energy dissipation rate downstream of a screen was developed and validated with experimental results. Furthermore, a new methodology for solving the discretized PBE employing a novel algorithm that prevents error propagation was also developed and successfully tested for stability, accuracy, reliability and robustness at low to very high shear rate conditions.

In addition, successful attempts to model turbulently flowing gas-liquid and liquid-liquid dispersions through multi-stage screen-type static mixers were undertaken. Good agreement between model predictions and experimentally determined dispersion characteristics was obtained under various operating and design conditions as well as interfacial characteristics.

Moreover, a model for estimating the dispersed phase mass transfer coefficient was developed then incorporated in the aforementioned PBE algorithm to calculate the local volumetric mass transfer coefficients in regions of varying turbulent energy dissipation rates. This model was found to be capable of predicting the experimental data well over a wide range of design and operating conditions. It also provided a hydrodynamic justification for the commonly used effective diffusivity correction factor which is reported to vary between 1 and 50.

Finally, an attempt to intensify gas-liquid contacting using screen-type static mixers was also undertaken. While investigating the effect of varying the hydrodynamic conditions and interfacial characteristics, $k_L a$ values as high as 4.08 s^{-1} were achieved even in the presence of contaminants.

NOMENCLATURE

a	Interfacial area of contact between the phases	$[m^2.m^{-3}]$
$A(d,t)$	Probability density of a drop/bubble of diameter d at time t	$[m^{-3}.s^{-1}]$
b	Wire diameter	[m]
B_b	Rate of particle generation by breakage per unit volume	$[m^{-3}.s^{-1}]$
B_c	Rate of particle generation by coalescence per unit volume	$[m^{-3}.s^{-1}]$
C	Bulk surfactant concentration	[ppm]
C_{1-3}	Empirical constants	[–]
C_4	Coalescence efficiency constant	$[m^2]$
$C^*_{O_2}$	Oxygen concentration in liquid phase at equilibrium	[ppm]
C_{O_2}	Oxygen concentration in liquid phase	[ppm]
C_{SDS}	Concentration of SDS in the continuous phase	[ppm]
C_{vm}	Coefficient of virtual mass	[–]
d	Bubble or drop diameter	[m]
d_{32}	Sauter mean diameter	[m]
D	Diffusivity	$[m^2.s^{-1}]$
D	Pipe diameter or tank diameter	[m]
D_b	Rate of particle destruction by breakage per unit volume	$[m^{-3}.s^{-1}]$
D_c	Rate of particle destruction by coalescence per unit volume	$[m^{-3}.s^{-1}]$
D_{oe}	Overall effective diffusivity	$[m^2.s^{-1}]$
E	Energy dissipation rate	[kW]
E_m	Energy dissipation per unit mass of the liquid	[W/kg]
E_v	Energy dissipation per unit of the reactor volume	$[kW/m^3]$
E_{spm}	Specific energy consumption rate	[kW/kg]

E_t	Amount of oxygen transported to/or from liquid phase per unit of energy dissipated	[kgO_2/kWh]
f_c	Contamination factor	[–]
$g(d')$	Breakage frequency of drops of diameter d'	[s^{-1}]
$h(d,d')$	Collision frequency of bubbles of diameter d and d'	[s^{-1}]
k	Individual mass transfer coefficient	[$m.s^{-1}$]
k	Kinetic energy	[$m^2.s^{-2}$]
k_L	Mass transfer coefficient	[$m\ s^{-1}$]
k_La	Volumetric mass transfer coefficient	[s^{-1}]
K	overall mass transfer coefficient	[$m.s^{-1}$]
L	Distance between two consecutive screens	[mm]
L_{screen}	Inter-screen spacing in the mixing section	[m]
L_M	Length of the mixing section	[m]
m	Distribution coefficient	[–]
M	Screen mesh size	[m]
M_{O2}	Amount of oxygen transported from liquid phase to the gas	[kg/h]
n	number density probability	[m^{-4}]
n	Turbulence decay equation exponent	[–]
$N(d,t)$	Number density function	[m^{-3}]
$N(t)$	Total number of drops/bubbles in volume V	[–]
n_i	Probability density	[–]
Q	Volumetric flow rate	[m^3/s]
R	Enhancement factor (D_{oe}/D_d)	[–]
r	Radial coordinate	[m]

Re	Pipe Reynolds number	[s]
Re_b	Wire Reynolds number	[–]
t	residence time	[s]
t_e	exposure time	[s]
U	Superficial velocity	[m.s^{-1}]
u'	Root mean square velocity fluctuation	[m.s^{-1}]
u_p	Particle velocity	[m.s^{-1}]
V	Contactor volume	[m^3]
v	Droplet volume	[m^3]
v_s	slip velocity	[m.s^{-1}]
x	Distance downstream of the screen	[m]
x_o	Virtual origin of turbulence decay	[m]

Greek Letters

α	Fraction open area of the screen	[–]
$\beta(d,d')$	Probability that a drop of size d' is formed when a drop d breaks	[–]
ΔP	Pressure drop	[N.m^{-2}]
ε	Energy dissipation rate	[m^2.s^{-3}]
$\lambda(d,d')$	Coalescence efficiency	[–]
μ	Dynamic viscosity	[kg.m^{-1}.s^{-1}]
$\nu(d)$	Number of daughter bubbles formed by breakage of bubble d	[–]
ρ	Density	[kg.m^{-3}]
σ	Static interfacial tension	[N.m^{-1}]
ϕ	Dispersed phase volume fraction	[–]
Π	Surface pressure	[mN/m]

Ψ	Drag coefficient of the screen	[–]

Subscripts

c	continuous phase
d	dispersed phase
exp	experimental data
sim	simulated data
mix	mixture
L	liquid phase
G	gas phase

ACKNOWLEDGEMENTS

I would like to express my deep appreciation to my research supervisor, Dr A. M. Al Taweel for his criticism, guidance, encouragement, and support throughout the course of this work. I am also grateful to the members of my thesis guiding committee: Dr. Y. Gupta, Dr. M. Fels, and Dr. I. Ugursal for their interest and helpful comments.

The financial support of NSERC through the PGS-D scholarships and that of Dalhousie University are greatly appreciated.

I would also like to thank all the faculty and staff at the Chemical Engineering Programme at Dalhousie University for all their help throughout the past years.

Special thanks are expressed to K. Podila, for his support, help, and companionship throughout the time we spent sharing the same office.

I am indebted to my parents, Toni and Colette Azizi, for their constant support, encouragement and dedication to my education.

Deepest gratitude is also expressed to my friends and family for their support, and understanding during the years of study.

Chapter 1.
Introduction

Systems containing bubbles, drops are encountered in a wide range of industrial and environmental operations such as the production, storage and transport of oil and gas resources, oil sand extraction and processing, power generation, biotechnology, mineral and metal processing, water and waste water treatment, soil remediation, as well as various operations encountered in the chemical process industry. Unfortunately, design information concerning processing units handling multi-fluid systems is traditionally obtained using experimental, semi-theoretical, and simplified mathematical methods; a practice that conceals many of the hydrodynamic details and non-idealities. In addition, the use of empirical correlations is limited due to the over simplifications associated with their development, thus, rendering them inapplicable to many practical situations without the incorporation of excessive safety margins. Consequently, the majority of the multiphase contactors/reactors presently used are inefficiently designed with subsequent adverse effects on the reaction yield and selectivity and/or the mass transfer performance.

Furthermore, in order to improve sustainability, the chemical process industry is rapidly moving towards cleaner synthesis, reduced environmental impact, improved energy efficiency, and the use of smaller and safer multifunctional process plants. Process intensification [PI] is one of the most effective approaches by which these objectives can be accomplished and relies on the use of innovative approaches to achieve dramatic reductions in the size of the plant needed to attain a certain production capacity.

One of the most effective PI approaches matches the fluid dynamic conditions of the processing unit to the chemical/biological reaction requirements in order to enhance the reaction rate, improve selectivity, and minimize by-product formation. This approach is particularly effective in multiphase systems where the need to transfer material and/or energy across the interface between phases can often be the main factor affecting the overall performance of many industrial operations such as multiphase reactions, absorption, distillation, liquid-liquid extraction, direct contact heat exchangers, stripping

of VOC, aerobic wastewater treatment, Ozone disinfection, and high-temperature catalytic oxidation. Unfortunately, our ability to design effective multiphase contactors, or even predict the performance of such units, is limited by inadequate understanding of the factors affecting bubble/drop breakage and coalescence and the absence of tools by which the performance of multiphase systems can be accurately predicted (Azizi and Al Taweel, 2007). It is estimated that less than 2% of the energy input to most present day contactors is utilized to form liquid-liquid and gas-liquid dispersions and maintain inter-phase contact.

Traditionally, mechanically agitated tanks (MAT) have been used for mixing multiphase systems as they offered the ability to easily change the stirring power and residence time. However, these types of reactors suffer from many drawbacks as they lack uniformity, where mixing intensity, drop/bubble size distributions, and hold-up have large local variations. Consequently, temperature control in the reaction regions becomes very difficult (Andersson et al., 2004). On the contrary, plug flow reactors/contactors serve as a better choice in order to understand the complex phenomena taking place as well as providing better performance and control over the mixing, breaking of drops and bubbles, as well as temperature. This choice can be reinforced by the fact that the turbulence characteristics of single phase pipe flows are relatively simple and have been well investigated and are clearly understood. A large database of experimental investigations in which information pertinent to the validation of models (e.g. volume fraction distributions, turbulence intensity, drop/bubble size distribution, etc...) is also available. Further, the symmetrical nature of pipe flow reduces drastically the computational requirements for their simulation.

Lately, there has been a growing interest in the use of tubular reactors equipped with static mixers as they present an attractive alternative to conventional agitation due to their inherent advantages whereby similar or better performance can be achieved at lower capital and operating costs (Thakur et al., 2003). A common feature for these reactors is that turbulence is continuously produced and dissipated along the reactor length. The turbulence is more homogeneous and nearly isotropic compared to a stirred tank reactor where most turbulence is produced and dissipated in the impeller region. They also provide large interfacial area of contact, effective radial mixing and narrow residence

time distribution (Turunen and Haario 1994; Al Taweel et al., 2003; Andersson et al., 2004). In addition, the mass transfer efficiency can be easily adjusted according to the requirements of the reaction by modifying the flow velocity, the type of mixer used, or inter-mixer spacing. For example, using mixers that provide high energy dissipation allow the formation of small drop/bubble diameters which favours the processes with high reaction rates since they require large interfacial area of contact between the phases. Similar results can also be achieved by operating under high flow velocities or short inter-mixer distances.

While a variety of inline static mixers (e.g. Kenics, Sulzer, Lightnin) differing in their geometries and ranges of applicability exist on the market, a new static mixing element was recently introduced in which screens or grids are used to repetitively superimpose an adjustable uniformly-distributed turbulence field on the nearly plug flow conditions encountered in high velocity pipe flows. This characteristic made them particularly effective in processing multiphase systems and their ability to promote contact between immiscible liquids were found to be about 5-fold more energy efficient than mechanically agitated tanks equipped with Rushton-type impellers (Al Taweel and Chen, 1996). Interfacial areas as high as 2200 m^2/m^3 could also be efficiently generated in the case of gas-liquid systems (Chen, 1996). The very high turbulence intensities generated in the regions adjacent to the screens result not only in the formation of fine dispersed phase entities (bubbles and/or drops) but also considerably enhance the value of the inter-phase mass transfer coefficient. The combined effect of these two factors resulted in inter-phase mass transfer coefficients as high as 13 s^{-1} being achieved in the case of liquid-liquid dispersions (Al Taweel et al., 2007) and allow for 99% of equilibrium conditions to be achieved in less than 1 s. The use of multi-stage screen-type contactors to promote gas-liquid mass transfer in an energy efficient fashion also resulted in oxygen transfer efficiencies as high as 4.2 kg/kWh being achieved even in the presence of surfactants (Al Taweel et al., 2005).

However, the design of these contactors/reactors requires not only a knowledge of the dynamic properties of the dispersion, such as drop/bubble size distributions and residence time, but also the dynamic rate characteristics of drop/bubble breakup and coalescence. Hence, better understanding of the factors governing the evolution of drop/bubble size,

the interfacial area of contact, and mass transfer coefficient in turbulent systems is an area of major interest since it forms the basis for generating rational and acceptable design and scale-up methodologies for multiphase contactors/reactors and can thus help in optimizing the performance, economy, and safety of these industrial systems. To achieve such a goal, mathematical models capable of accurately predicting drop size and motion within the contactor/reactor in question (including drop breakage and coalescence), as well as the mass transfer coefficient within the contactor, are needed. This requires the use of population balance equations (PBE) to handle bubble breakage and coalescence within various regions of the contactor, and the identification of the breakage/coalescence kernels that can accurately describe these processes.

A detailed description of the dispersed phase characteristics can be obtained by using the population balance models introduced in the mid-60s to simulate chemical engineering operations. PBE have since become a well established tool that is widely used for simulating dispersed phase operations because it has the advantage of being able to describe drop/bubble breakage and coalescence processes in terms of identifiable physical parameters and operational conditions. However, the biggest uncertainty associated with the use of PBE to simulate multi-fluid processing (i.e. immiscible liquid-liquid and gas-liquid system) remains the identification of the breakage and coalescence kernels that can accurately describe what happens in turbulent flows. Most of the models developed over the past several decades were verified using experimental data obtained in mechanically-agitated tanks (MAT) in which the dispersed phase holdup, drop size distribution, and energy dissipation rate are assumed to be uniformly distributed throughout the volume of the mixing vessel. The fact that such units exhibit a broad residence time distribution and that drops periodically circulate between the regions of high and low energy dissipation rates present in the mixing tank (where the local energy dissipation rates can vary by a factor of more than 10,000) are usually overlooked.

Another factor which limited the widespread use of PBE is the ability to obtain accurate numerical solutions as the analytical solutions are rare and include major simplifying assumptions that may not be met in practice. Unfortunately, while simulating multiphase systems using PBE, little attention was given to the sources of errors arising from improper modeling of the hydrodynamic situation (e.g. the assumption that the energy

dissipation rate is uniform throughout the vessel). In recent years, computational fluid dynamics (CFD) has emerged as a powerful tool for the understanding of the fluid mechanics existing in the reactors/contactors rendering its use in conjunction with PBE to become more popular particularly because of its ability to provide good estimates of the hydrodynamic conditions prevailing at different parts of the processing vessel (Alopaeus et al., 1999; Agetrof et al., 2003). Lately, stirred reactors have become a showcase for the development of CFD simulation technology (Harris et al., 1996; Sahu et al., 1999; Sommerfeld and Decker 2004), where the availability of large computational facilities allowed higher accuracy of results from finer and finer griddings of the domain and especially from the application and tuning of more advanced turbulence models (Brucato et al., 2000). However, the ultimate success of this approach in the case of multi-fluid systems relies on the ability of PBE to yield realistic and accurate description of the overall drop breakage/coalescence processes.

Since the hydrodynamic conditions prevailing in screen-type static mixers closely approach those of isotropic homogeneous turbulence with alternating breakage-dominated and coalescence-dominated regions, they offer an ideal situation to test the various breakage/coalescence models proposed in the literature and validate the simulation results. The models identified using such geometries (e.g. drop/bubble breakage and coalescence kernels as well as the mass transfer models) are expected to apply to other more complex hydrodynamic conditions such as those encountered in MAT provided that the contactor/reactor volume is subdivided into a large number of segments where isotropic homogeneous turbulence can be correctly assumed to prevail.

This investigation aims towards developing a better understanding of the factors that influence the use of the population balance equation in simulating multi-fluid dispersed systems (*i.e.* gas-liquid, liquid-liquid) as well as the application of screen-type static mixers in intensifying multiphase operations. Therefore, the objective of this work is to further explore the possibility of using PBE to accurately simulate multiphase operations, particularly drop/bubble breakage and coalescence as well as inter-phase mass transfer processes, and to employ such knowledge to determine the optimum conditions under which multiphase contacting can be intensified. Furthermore, an attempt to intensify gas-liquid contacting using screen-type static mixers was also undertaken.

This thesis consists of eight chapters and is a compilation of six manuscripts, of which one is published (Azizi and Al Taweel, 2007), four are currently in review (Azizi and Al Taweel, 2008a; Azizi and Al Taweel, 2008b; Azizi and Al Taweel, 2009a; Azizi and Al Taweel, 2009b) and one technical report to be submitted for publication. The importance, relevance, and objective of the current work are presented in Chapter 1. In Chapter 2, PBE were used to simulate the temporal/spatial variation of bubble size distribution for gas-liquid dispersions turbulently flowing through multi-stage screen-type static mixers. This methodology was found to be capable of accurately simulating the gas-liquid contacting performance achieved in screen-type static mixers over a wide range of operating conditions. However, the monotonic decay function used to simulate the turbulence intensity in screen-type static mixers was found to be incapable of fully accounting for the total pressure drop across screens. An approach for predicting the spatial variation of the energy dissipation rate downstream of a screen was therefore developed in Chapter 3 and tested and validated by comparing the experimentally-determined volume average energy dissipation rate in the system, with the spatial average rate obtained using the developed simulation approach. The very high local energy dissipation rates encountered in screen-type static mixers pose particular problems while solving PBE because of the very large breakage and coalescence frequencies that are expected to dominate in the reactor/contactor. Therefore, a new methodology for solving the discretized population balance equation was developed in Chapter 4. It uses a novel algorithm (which relies on monitoring the onset of errors and allows for corrective action to be undertaken before the errors propagate in an uncontrollable fashion) to enhance the numerical stability, accuracy and reliability of the solution. This method was also successfully employed by Al Taweel et al. (2008a) to model the more demanding case of flocculating particles. Furthermore, the knowledge and capabilities accrued from the methodologies developed in Chapters 3 and 4 were tested in Chapter 5, where an attempt to model liquid-liquid dispersions flowing through screen-type static mixers was undertaken. Model predictions were then validated through the good agreement with the large set of experimental results obtained under a wide range of design and operating conditions. In Chapter 6, a new model for estimating the dispersed phase mass transfer coefficient in liquid-liquid dispersions was developed and then incorporated in the PBE

algorithm. The combined equations were then used to calculate the local volumetric mass transfer coefficients, *ka*, in regions of varying turbulent energy dissipation rates and the model was found capable of predicting the experimental data, obtained using screen-type static mixers, reasonably well over a wide range of design and operating conditions. In addition, the developed model not only provided a hydrodynamic justification for the commonly used effective diffusivity correction factor, but also a better accuracy of the predictions. Finally, the possibility to intensify the volumetric mass transfer coefficient in gas-liquid systems by using screen-type static mixers was presented in Chapter 7, where the effect of varying the hydrodynamic conditions and interfacial characteristics of the system were taken into consideration. Chapter 8 summarizes the conclusions and recommendations resulting from this work.

Chapter 2.
Population Balance Simulation of Gas-Liquid Contacting

F. Azizi and A.M. Al Taweel*

Multiphase Mixing and Separations Research Lab, Department of Process Engineering and Applied Sciences, Dalhousie University, Halifax NS, Canada B3J 2X4 (Al.Taweel@Dal.Ca)

Published in *Chemical Engineering Science*, vol. 62, pp. 7436–7445 (2007)

Abstract

A successful attempt to simulate turbulently flowing gas-liquid dispersions was undertaken in this work where the turbulent dispersion/coalescence of bubbles was accurately predicted over a wide range of operating conditions by incorporating the effect of virtual mass into the phenomenological model developed by Coulaloglou and Tavlarides (1977) for liquid-liquid dispersions. The population balance equation was numerically solved and the results obtained were compared with the experimental data obtained from an intensified gas-liquid reactor/contactor in which screen-type static mixers were used to superimpose an adjustable uniformly-distributed turbulence field on the nearly plug flow conditions encountered in high velocity pipe flows.

The model was also found to be capable of predicting gas-liquid contacting for the case of industrial streams where the presence of amphiphilic constituents was found to retard coalescence and result in average interfacial areas as high as 2,100 being achieved.

The fact that the model was capable to match experimental results obtained under very demanding/extreme conditions (where the flowing dispersion is successively exposed to breakage-dominated and coalescence dominated regions with local energy dissipation ratios as high as 400) suggests that it may be used for simulating other more complex gas-liquid contacting conditions such as those encountered in MAT.

Keywords: Process Intensification, Gas-liquid reactors, Static Mixers, Population Balance, Bubble breakage and coalescence.

2.1 Introduction

Gas–liquid mixing has one key objective namely the dispersion of gases into fine bubbles that possess large interfacial area of contact and relatively high inter-phase mass transfer coefficient. The high volumetric mass transfer coefficients, k_La, thus achieved allow for the use of smaller and safer reactors and can significantly increase the selectivity and yield of mass-transfer-controlled chemical reactions. Several contactor types such as bubble columns and mixing tanks are used for this purpose, but due to the very complex hydrodynamic conditions prevalent in these contactors/reactors, designing such units is very difficult without the employment of empirical knowledge and experience and an extensive amount of pilot-scale testing. Lately, there has been a growing interest in the use of tubular reactors equipped with static mixers as they present an attractive alternative to conventional agitation due to their inherent advantages whereby similar or better performance can be achieved at lower capital and operating costs (Thakur *et al.*, 2003).

Recently, a new type of static mixing element was introduced in which screens or grids are used to repetitively superimpose an adjustable uniformly-distributed turbulence field on the nearly plug flow conditions encountered in high velocity pipe flows. This characteristic made them particularly effective in processing multiphase systems and their ability to promote contact between immiscible liquids were found to be about 5-fold more energy efficient than mechanically agitated tanks equipped with Rushton-type impellers (Al Taweel and Chen, 1996). Interfacial areas as high as 2700 m^2/m^3 could also be efficiently generated in the case of gas-liquid systems (Chen and Al Taweel, 2007). The very high turbulence intensities generated in the regions adjacent to the screens result not only in the formation of fine dispersed phase entities (bubbles and/or drops) but also considerably enhance the value of the interphase mass transfer coefficient. The combined effect of these two factors resulted in inter-phase mass transfer coefficients as high as 13 s^{-1} being achieved in the case of liquid-liquid dispersions (Al Taweel et al., 2007) and allow for 99% of equilibrium conditions to be achieved in less than 1 s. The use of multi-stage screen-type contactors to promote gas-liquid mass transfer in an energy efficient

fashion also resulted in oxygen transfer efficiencies as high as 4.2 kg/kWh being achieved even in the presence of surfactants (Al Taweel *et al.*, 2005).

These performance improvements were achieved using phenomenological interpretation of the role turbulence has on multiphase contacting. However, mathematical models capable of accurately predicting bubble size and motion are needed in order to optimize the performance of multiphase contactors/reactors. This requires the use of population balance equations, PBE, to handle bubble breakage and coalescence within various regions of the contactor, and the identification of the breakage/coalescence kernels that can accurately describe these processes.

Population balance models, introduced in the mid-60s to simulate chemical engineering operations, can be used to obtain a detailed description of the dispersed phase characteristics. They have become a well established tool that is widely used for simulating dispersed phase operations because they have the advantage of being able to describe bubble breakage and coalescence processes in terms of identifiable physical parameters and operational conditions. However, the biggest uncertainty associated with their use remains to be the identification of the most appropriate breakage and coalescence kernels that can accurately describe what happens in turbulent flows.

The objective of this work is to explore the possibility of using PBE to accurately simulate bubble breakage and coalescence processes taking place in multi-stage screen-type static mixers (with alternating breakage-dominated and coalescence dominated regions), and to use such knowledge to determine the optimum conditions under which gas-liquid contacting in tubular reactors can be intensified.

Furthermore, since the hydrodynamic conditions prevailing in screen-type static mixers closely approach those of isotropic homogeneous turbulence, the bubble breakage/coalescence kernels identified in this investigation are expected to apply to other more complex hydrodynamic conditions (such as those encountered in MAT) provided that the contactor/reactor volume is subdivided into a large number of segments where isotropic homogeneous turbulence can be correctly assumed to prevail.

2.2 Modelling Bubble Breakage and Coalescence in Turbulently Flowing Gas-Liquid Dispersions

Population balance equations describe the temporal variation in dispersed phase characteristics (*e.g.* size, mass, temperature, age, and species concentration) where the dispersed phase is considered as an assembly of bubbles whose individual identities are being continually destroyed and recreated by the dynamic processes occurring within the system. Under such conditions, the hydrodynamics and the interfacial forces are the major factors affecting the changes in the interfacial area of contact between the phases. In a two-phase turbulent flow, breakage and coalescence processes take place simultaneously until a quasi-equilibrium state is reached, where the dispersion and coalescence rates become comparable and no net changes in bubble size and bubble size distribution are observed.

Even though most of the breakage/coalescence models were developed using sound thermo-, and hydro-dynamical theories, most of their validation was conducted using data obtained in mechanically agitated tanks where the complex hydrodynamics encountered in such units were often over-simplified by assuming perfectly mixed conditions with uniform energy dissipation rates. This deficiency was recently mitigated by sub-dividing the contactor volume into 2–24 compartments (Alexopoulos *et al.*, 2002; Laakkonen *et al.*, 2006) where different, but uniform value of the turbulent energy dissipation rate is assumed to exist in each compartment. The errors introduced from such a discretization approach are practically eliminated when CFD is used where the contactor volume is divided into a very large number of sub-regions. Unfortunately, most CFD tests used to test pertinent PB kernels suffer from the uncertainties associated with the use of incomplete inter-phase momentum closures, and turbulence modulation relations, needed to accurately describe the interaction between the phases in the Eulerian-Eulerian approach (Al Taweel *et al.*, 2006).

Conversely, most of the aforementioned hydrodynamic modeling difficulties are eliminated under the flow conditions encountered in multi-stage screen-type static mixers developed by Al Taweel and Chen (1996). The residence time distributions are very narrow (essentially plug flow) and the characteristics of the turbulence generated in the

region downstream from each consecutive screen are well known. These mixers therefore offer a good alternative to conventional MAT mixers for developing and testing the various hydrodynamic models as they overcome the difficulties associated with the high spatial variations of the energy dissipation rates as well as flow/recirculation non-uniformities. In addition, the nearly plug flow conditions present in the multi-stage screen-type contactor allow for the direct integration of the non-linear integro-differential equations obtained by applying the PBE, thereby eliminating any computational uncertainties and errors introduced through the use of CFD.

In the following sections, the hydrodynamic conditions prevalent in screen type static mixers are discussed with an emphasis on the model used for simulating bubble breakage and coalescence in turbulent flows.

2.2.1 Modeling the Rate of Energy Dissipation in Screen-type Static Mixers

The rate of energy dissipation within screen-type mixers plays a crucial role in determining the bubble size distribution of the flowing dispersion as well as the rate at which mass is transferred between the phases. Information concerning the axial variation of this parameter is therefore essential for the accurate modeling of the mixer dispersive performance.

A relatively large body of knowledge is available concerning the nature of grid-generated turbulence and how it is affected by the nature of flow as well as by the characteristics of the wire mesh used (Groth and Johansson, 1988; Briassulis et al., 2001; Kang et al., 2003). Its most distinctive characteristic is the generation of nearly isotropic turbulence where the local turbulent energy dissipation rate undergoes dramatic variation along the axis of flow with the maximum value being encountered in the immediate vicinity of the screen. This behaviour can be described using the following power law expression (Bourne and Lips, 1991),

$$\varepsilon = \frac{3 \cdot U^3}{2 \cdot M \cdot C} \cdot \left[\frac{x}{M} - \left(\frac{x}{M} \right)_o \right]^{-2} \tag{2.1}$$

where C is the decay coefficient, the value of which varies widely with screen geometry.

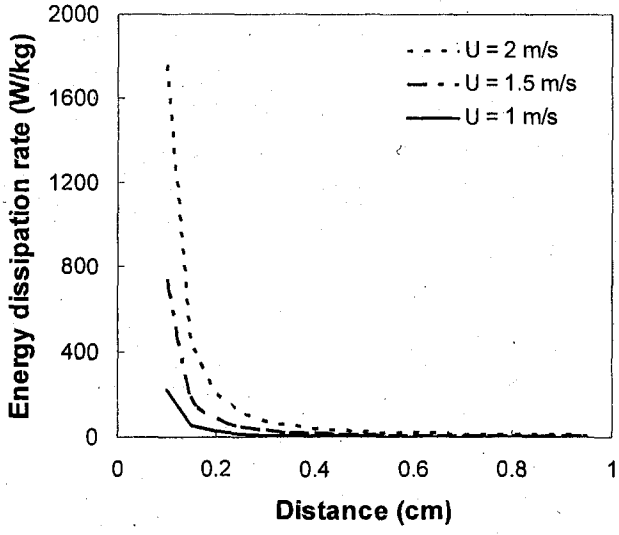

Figure 2.1: Effect of velocity on the axial variation of turbulent energy dissipation rate.

This equation clearly shows that the turbulence structure generated downstream of the screen is controlled by the upstream superficial velocity as well as by the mesh size (M). For the screen used in this investigation (a = 0.27; b = 0.508 mm; M = 0.55 mm) C was taken as equal to 15 and the results obtained are shown in Figure 2.1.

2.2.2 Modeling of Bubble Breakup and Coalescence in Screen-type Static Mixers

The extent of bubble breakup and coalescence in turbulently flowing gas-liquid mixtures govern the evolution of the bubble size distribution (BSD) in the dispersion, and consequently the interfacial area of contact between the phases. The use of PBE to model these processes often leads to an integro-partial-differential equation for which there exists very limited analytical solutions, usually obtained at the expense of assuming unrealistic major simplifications. A discretization scheme is therefore generally used to transform the partial differential equation into an ordinary differential equation which is easier to solve numerically.

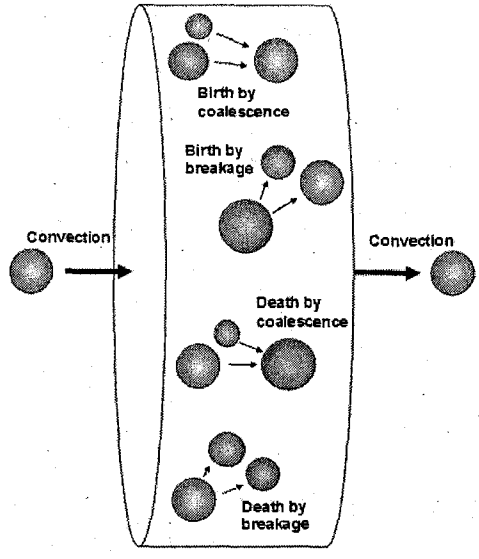

Figure 2.2: Schematic representation of the PBE cell

For the case at hand, the flow within the multi-stage screen-type static mixer can be considered as radially uniform because of the flat velocity profiles induced by the screens and the relatively small spacing between consecutive elements. To accommodate the large axial variation in turbulence intensity and energy dissipation rates depicted in Figure 2.1, the hydrodynamic performance of the static mixer was modeled by dividing it into very thin cells where uniform isotropic hydrodynamic conditions can be correctly assumed to exist (Figure 2.2).

In its most general form, the population balance for the uniform conditions present in the cell shown in Figure 2.2 can be written as,

$$\begin{bmatrix}\text{Rate of accumulation}\\ \text{of bubbles in control cell}\end{bmatrix} = \begin{bmatrix}\text{Net rate of transport into}\\ \text{the control cell by convection}\end{bmatrix} + \begin{bmatrix}\text{Net rate of generation}\\ \text{in control cell by}\\ \text{breakage and coalescence}\end{bmatrix} + \begin{bmatrix}\text{Net rate of generation in control cell by other means}\\ \text{e.g. chemical reaction, mass transfer...}\end{bmatrix} \quad (2.2)$$

Although bubble growth or dissolution is taken into account in the general PBE, it was neglected in the present analysis since the water used is already saturated with air which practically eliminates inter-phase mass transfer. That is supported by the recent findings of Laakkonen *et al.* (2006) who reported a negligible mass transfer growth term in the various sub-regions of a mechanically agitated tank when dry gas was dispersed in tap

water (where less than 1% growth in the mean bubble size was observed in the gas inlet sub-region where the dry gas became saturated with water).

For a cell moving under plug flow conditions the convection in and out of it can be neglected. Assuming that no heat and mass transfer takes place and neglecting the effect of chemical reactions, the rate of change of concentration of bubbles of diameter d with time can be expressed as a uni-dimensional PBE. For a locally isotropic turbulent field, this equation can be written as (Coulaloglou and Tavlarides, 1977),

$$\begin{aligned}\frac{\partial\left[N(t)A(d,t)\right]}{\partial t} &= N(t)\int_{d}^{d_{\max}}\beta(d',d)\cdot\nu(d')\cdot g(d')\cdot A(d',t)\,dd' \\ &\quad -N(t)\cdot g(d)\cdot A(d,t) \\ &\quad +\left[N(t)\right]^2\int_{0}^{d/2^{1/3}} h\left(\left(d^3-d'^3\right)^{1/3},d'\right) \\ &\qquad \times\lambda\left(\left(d^3-d'^3\right)^{1/3},d'\right)\cdot A\left(\left(d^3-d'^3\right)^{1/3},t\right)\cdot A(d')\,dd' \\ &\quad -\left[N(t)\right]^2\cdot A(d,t)\int_{0}^{\left(d^3_{\max}-d^3\right)^{1/3}} h(d,d')\cdot\lambda(d,d')\cdot A(d',t)\,dd'\end{aligned} \tag{2.3}$$

The first two terms on the right hand side respectively present the rate of formation and loss of bubbles of diameter d' due to breakage; where, $g(d')$ is the breakage frequency, $\nu(d')$ is the number of dispersed fluid entities formed from breakage of a bubble of size d', and $\beta(d',d)$ is the size distribution of daughter bubbles formed from breakage of a bubble of size d'. The following two terms represent the rate of formation and loss of bubbles of size d' due to coalescence. Here, $\lambda(d,d')$ is the coalescence efficiency between bubbles of size d and d', and $h(d,d')$ is the collision frequency between those of size d and d'.

This population balance representation is applicable to both gas-liquid and liquid-liquid dispersions provided that appropriate expressions for the various breakage and coalescence sub-processes are used. Such models have been presented by several authors,

many of which have been recently reviewed by Jakobsen *et al.* (2005) and Lasheras *et al.* (2002).

The phenomenological model developed by Coulaloglou and Tavlarides (1977) for describing breakage and coalescence processes in turbulently flowing liquid-liquid dispersions (and the associated breakage and coalescence kernels) was used in this investigation to describe the situation for gas-liquid systems. This is justified by the fact that this model is based on turbulent fragmentation and amalgamation where both phases are considered to be moving at the same mean velocity in a locally homogeneous and isotropic turbulence field, a condition that can be held valid in the current work. Further, this approach constituted the basis from which most of the gas-liquid breakage and coalescence models in turbulently flowing dispersions were derived (*e.g.* Lee *et al.*, 1987; Prince and Blanch, 1990; Luo and Svendsen, 1996).

2.2.2.1 Breakage sub-processes

The pressure fluctuations present in turbulent flows exerts shearing forces on bubbles that lead to their deformation and stretching. If the contact time between the turbulent eddy and the bubble is long enough, and if the energy of that turbulent eddy exceeds the surface energy of the bubble, it may result in its breakage to new smaller dispersed fluid entities. Therefore, a combination of the collision frequency between the bubbles and turbulent eddies as well as the probability that a collision leads to a successful breakage has been used to describe the breakage process.

For an isothermal system with no inter-phase mass transfer or reaction taking place, Coulaloglou and Tavlarides (1977) derived an equation for the breakage frequency assuming a locally isotropic turbulence field and that the size of fluid particles falls in the inertial sub-range. Based on the aforementioned considerations, the following function was derived,

$$g(d) = C_1 \cdot \frac{\varepsilon^{1/3}}{d^{2/3} \cdot (1+\phi)} \cdot \exp\left[-C_2 \cdot \frac{\sigma(1+\phi)^2}{\rho_d \cdot \varepsilon^{2/3} \cdot d^{5/3}} \right] \tag{2.4}$$

In addition to predicting the breakup frequency, the resulting size distribution of daughter bubbles and the number of fragments formed upon breakup must be specified to fully

describe the breakage process. However, despite the considerable amount of work spent on developing models for drop and bubble breakage in turbulent flows, little experimental data exist that can be used to validate these models.

In order to determine the probability at which bubbles of a certain size are formed as a result of a bigger bubble being broken up, it is necessary to identify the size distribution function of daughter bubbles. Coulaloglou and Tavlarides (1977) assumed that the daughter bubble density $\beta(d,d')$ function is a normally distributed and expressed as,

$$\beta(d,d') = \frac{4.6}{d'^3} \cdot \exp\left[-4.5 \cdot \frac{\left(2d^3 - d'^3\right)^2}{\left(d'^3\right)^2} \right] \tag{2.5}$$

While Hesketh *et al.* (1991) and more recently Andersson and Andersson (2006) concluded that an unequal-sized breakage is more probable in the case of gas bubbles, the experimental findings of Risso and Fabre (1998) indicate that equal-size daughter distribution is most commonly observed in the case of bubbles immersed in a turbulent field. The breakage functions proposed by Konno *et al.* (1980) and Martinez-Bazan *et al.* (1999) have a daughter distribution density function which yields a maximum probability for equally sized daughter fluid entities whereas that proposed by Luo and Svendsen (1996) depicts a very high probability for stripping infinitesimally small fragments. Several investigators criticized the latter distribution function (Kostoglou and Karabelas, 2005) but this deficiency was recently corrected by Lehr and Mewes (2001) who presented a daughter distribution function that predicts a maximum probability for equi-sized breakage when the mother bubble is small.

The number of daughter bubbles represented by breakage term, $\nu(d')$, is usually assumed to be two (i.e. binary breakage) which is in agreement with the observations of Andersson and Andersson (2006) who reported a very high probability (> 95%) for the occurrence of binary breakage in gas-liquid systems.

2.2.2.2 Coalescence sub-processes

Coalescence occurs when two (or more) bubbles collide with sufficient energy to overcome the interfacial tension between these dispersed fluid entities and the

surrounding liquid, and the contact time is long enough to allow drainage and rupture of the film separating the two colliding entities (Coulaloglou and Tavlrarides, 1977; Ni *et al.*, 2002). Although only bubble coalescence resulting from turbulent interactions between the continuous and dispersed phase is considered in this investigation, several other collision mechanisms exist. These include buoyancy-driven (that is collisions due to the difference in rise velocities of bubbles of different size) and collisions due to laminar shear occurring when bubbles follow the continuous fluid streamlines (Prince and Blanch, 1990); however, the relative importance of these mechanisms can be neglected under the highly turbulent conditions present in screen-type static mixers.

The binary coalescence rate between bubbles is usually expressed as the product of collision frequency and coalescence efficiency terms. In a locally isotropic field, the collision frequency of drops was modeled by Coulaloglou and Tavlarides (1977) in analogy with the collision of molecules as described in the kinetic theory of gases. The collision frequency of drops of diameter d and d' can thus be written as,

$$h(d,d') = C_3 \cdot (d+d')^2 \cdot \left(d^{2/3} + d'^{2/3}\right)^{1/2} \cdot \frac{\varepsilon^{1/3}}{(1+\phi)} \tag{2.6}$$

The expression given in Equation (2.6) is slightly different from the originally published one as it incorporates a small algebraic error identified by Hsia and Tavlarides (1980). In this model, the presence of the dispersed phase was assumed to dampen the intensity of turbulence in the continuous phase with the extent of this effect being larger at high dispersed phase volume fractions, ϕ. The introduction of this factor was partially driven by the observed formation of coarser drops at higher dispersed phase holdup but was also necessitated by the inability of the model to simulate the experimental data generated over a wide range of dispersed phase holdups ($0.025 \leq \phi \leq 0.15$). However, there is very little direct indication of turbulence dampening in liquid-liquid dispersion while there is a growing body of experimental and theoretical investigations suggesting that turbulence intensity can be enhanced in gas-liquid systems where large bubbles (2 – 12 mm) can generate high slip velocities. In the present investigation, the expressions containing the $(1+\phi)$ dependency will be retained because of the absence of detailed information about

that issue for the very small bubble sizes encountered in screen-type static mixers (0.1 – 1.2 mm).

Coulaloglou and Tavlarides (1977) also presented an expression for the coalescence efficiency term which is based on the film drainage between colliding dispersed phase entities which is applicable to the case of deforming entities with immobile interfaces. It assumes that turbulence causes the two entities to collide and holds them together for a definite time while the intervening film thins under a constant force applied by turbulence. Coalescence will therefore only occur when the contact time of the bubbles is longer than the time required for draining the film entrapped in between them.

$$\lambda(d,d') = \exp\left[-C_4 \cdot \frac{\mu_c \cdot \rho_c \cdot \varepsilon}{\sigma^2 \cdot (1+\phi)^3} \cdot \left(\frac{d \cdot d'}{d+d'}\right)^4\right] \tag{2.7}$$

The initial film thickness and the critical thickness for film rupture are assumed to be constant and lumped into the value of the parameter C_4. However, it is well known that the presence of surfactants or other contaminants in the system reduces coalescence rates because of their dramatic effect on the film thinning time. This is attributed to the observation that the surface tension gradient resulting from the thinning of the interface results in an immobilization of that interface which, in turn, requires longer contact times between the bubbles in order for a successful coalescence event to occur, a condition that does not always exist in turbulently flowing dispersions.

2.3 Testing and Validating the Turbulent Bubble Breakage and Coalescence Models

2.3.1 Numerical Solution of PBE

An accurate, stable, and robust algorithm for solving the integro-differential PBE obtained by considering batch or plug flow systems, where uniform energy dissipation conditions can be correctly assumed, was developed by Al Taweel *et al.* (2002). It was further modified to account for flow through systems with spatial variation of local energy dissipation rate and used to model turbulent drop breakup and coalescence in static mixers. This algorithm was found to accurately predict experimental liquid-liquid

dispersion data generated under the well controlled hydrodynamic conditions observed in screen-type static mixers (Azizi, 2004; Azizi and Al Taweel, 2005).

The aforementioned algorithm uses the size distribution sampling approach proposed by Sovova and Prochazka (1981) and combines it with cubic spline interpolation if information in between sampling points is needed. At any particular time, the value of the birth and death terms are determined by integrating over the size domain (using Simpson's rule) and the resulting ODE is numerically solved using the 4^{th} order Runge-Kutta method. Solution stability was enhanced by using a moving grid technique where insignificantly large bubbles were cut off from the bubble size domain while occasionally re-adjusting the distribution to ensure volume conservation. Higher solution accuracy was obtained by adopting such an approach which was able to achieve numerical solutions within 7% using 10 sampling points whereas the error obtained when the bubble size distribution is represented by 10 discrete classes was found to be as high as 29% (Al Taweel *et al.*, 2002). A high degree of accuracy (1.8%) and improved solution stability was achieved in the current work by using 40 sampling points within the self adjusting bubble size domain.

The ability of this approach to track the variation of the bubble size distribution as a function of the local energy dissipation rates along the length of the reactor can best be illustrated by following the temporal variation of the Sauter mean diameter as the immiscible dispersion flows through the static mixer (Figure 2.3). It can be clearly discerned that bubble diameter undergoes a sharp reduction in the high energy dissipation regions adjacent to the screen before the fine bubbles formed in these regions start to coalesce as they migrate to regions of lower energy dissipation rates further downstream. This observation is similar to those reported by Turunen and Haario (1994) and Andersson *et al.* (2004) who used different types of commercially available static mixers to promote dispersion. The results obtained clearly show that, under the conditions investigated in Figure 3, quasi-steady state conditions are expected to be reached after 2–3 stages.

The algorithm used to solve the PBE is attached in Appendix A. Furthermore, additional and more detailed descriptions of the methodology used to numerically solve the PBE, as

well as a slightly modified version of the algorithm used to solve it are provided in Chapter 4.

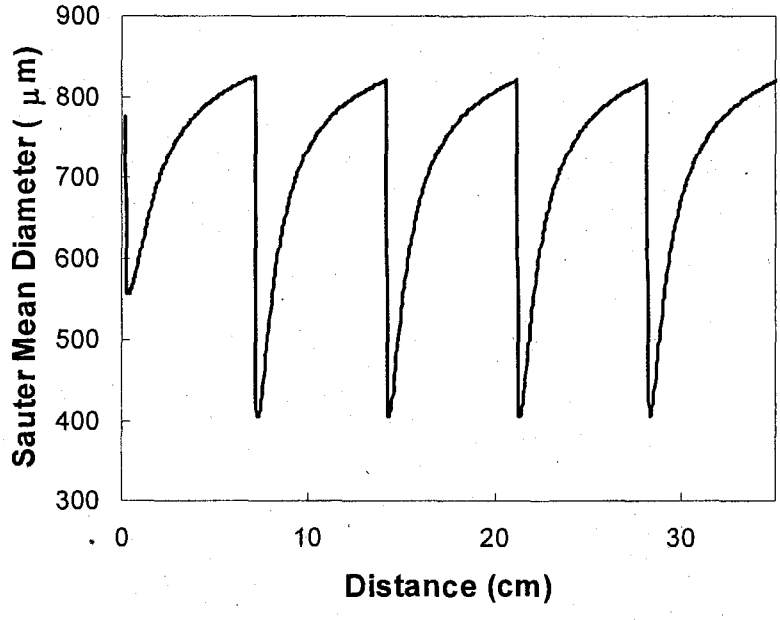

Figure 2.3: Predicted spatial variation of the Sauter mean diameter along the length of the contactor/reactor ($U = 1$ m/s; $\phi = 7\%$; $\alpha = 0.27$)

2.3.2 Experimental Determination of Gas-Liquid Contacting in Screen-type Static Mixers

The effectiveness of gas-liquid dispersions in screen-type static mixers has been experimentally investigated by Chen and Al Taweel (2007) using the setup depicted in Figure 2.4. The aqueous continuous phase and air were metered and introduced to a 2 m long vertical mixing section where dispersion is induced using a series of six equally spaced screens placed within a 25.4 mm ID precision bore Pyrex tube.

Table 2.1: Experimental conditions investigated

Inter-screen spacing	70 mm
Superficial velocity, U,	1.0 to 2.3 m/s
Screen fraction open area, α,	0.27
Dispersed phase holdup, ϕ	0.01 - 0.07
Concentration of SDS	0 – 10 ppm
Average energy dissipation rate, ε,	2.85 to 32.8 W/kg
Maximum energy dissipation rate	220 to 2680 W/kg

The stainless steel woven wire screen elements were soldered onto a set of slotted brass spacers which were used to adjust the distance between consecutive screens; however, a distance of 70 mm was maintained throughout this investigation. The laser-based light attenuation technique developed by Kasireddy and Al Taweel (1990) was used to measure the interfacial area of contact across the diameter of the flow section and the slots enabled for the measurement of the interfacial area of contact at various axial distances downstream from each screen.

The system investigated was tap water-air in which trace quantities of Sodium Dodecyl Sulphate (SDS) were added to simulate the breakage/coalescence behaviour of industrial streams containing amphiphilic materials such as alcohols, organic acids, electrolytes, amines, glycols, and proteins. Table 2.1 summarizes the range of experimental operating conditions used in this study.

The size of bubbles formed in different locations along the reactor's length, and the average interfacial area of contact, was found to depend on the operating and design conditions as well as the interfacial characteristics of the system with local interfacial areas of contact as high as 2700 m^2/m^3 being achieved. In general, screen mixing elements were found to be up to 20 times more energy efficient than tanks agitated by Rushton-type impellers (based on the same rate of power consumption per unit mass of the liquid processed) and can generate at least 3 times more interfacial area when compared with other commercially available static mixers. This advantage and the subsequent impact on inter-phase mass transfer, reaction selectivity, and inherent safety clearly show the advantages that can be gained by intensifying gas-liquid contacting through the judicious application of turbulence intensity.

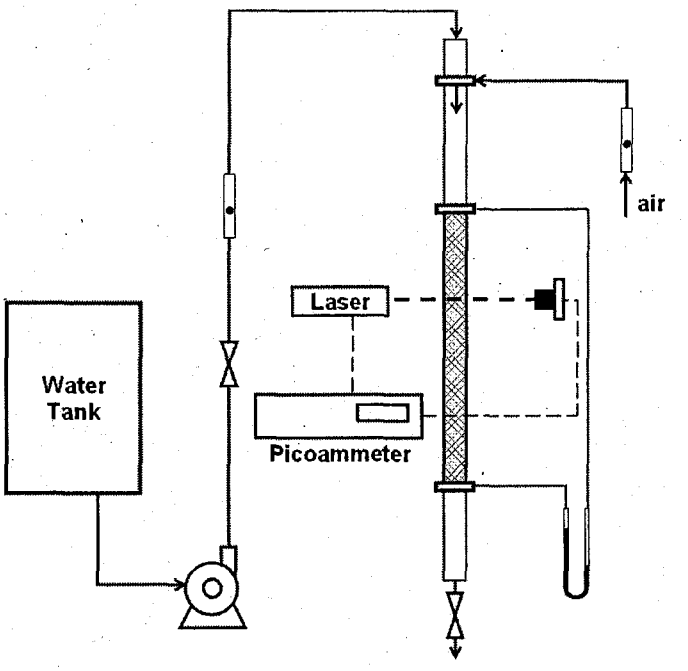

Figure 2.4: Experimental setup (Chen and Al Taweel, 2007)

2.3.3 Comparison with Experimental Results

Because of the non-linear dependency of the PBE on the various constants present in Equations (2.4), (2.6) and (2.7), the Levenberg-Marquardt non-linear optimization algorithm was used to identify the best estimates for the value of the constants C_1–C_4 and minimize the χ^2 (sum of squared errors) value while simultaneously varying all 4 parameters. The use of good initial estimates of the various parameters was found to significantly affect the fitting process; an initial fitting process was therefore undertaken in order to find reasonable estimates of these constants before using them as inputs to the Levenberg-Marquardt algorithm. To obtain the best estimates and reach acceptable global minima (in the multidimensional space), a stringent criterion of 2.5×10^{-4} relative change in the sum of squared residuals was applied to stop the fitting process.

It is well known that the acceleration and deceleration of a bubble in a liquid dictates a similar behaviour for a part of its surrounding continuum. This generates an additional force contribution to the general equation of momentum which is often referred to as the "added" or "virtual mass" force. The effect of the virtual mass force is expected to be more pronounced for gas in liquid dispersions because of the very high relative density ratio. Unfortunately, this effect is often neglected while modeling gas-liquid dispersions

although recent findings suggest that it is a very important parameter particularly when considering the response of bubbles to turbulent fluctuations (Mudde and Simonin, 1999; Joshi, 2001).

The effect of virtual mass is usually accounted for using the following expression,

$$\text{sum of forces} = (\rho_d \times \text{particle volume} + C_{vm} \times \rho_c \times \text{particle volume}) \times \text{acceleration} \quad (2.8)$$

where the coefficient of virtual mass, C_{vm}, is known to vary with the shape of the bubble and its size as well as the dispersed phase holdup (Kamp *et al.*, 2001). In the present investigation, the commonly used inviscid value of $C_{vm} = 0.5$ was applied throughout. This is tantamount to changing the dispersed phase density (which only appears in the breakage frequency sub-process) to reflect the effect of the "entrained liquid",

$$\rho_d = C_{vm} \times \rho_c \quad (2.9)$$

By accounting for the effect of virtual mass in the breakage kernel, it was possible to match the interfacial area maxima encountered immediately downstream of the screen.

This finding provides a partial explanation of the observations reported by Lasheras *et al.* (2002) who compared the Coulaloglou and Tavlarides breakage frequency term with other commonly used expressions for gas-liquid systems, and suggested that the dispersed phase density term be substituted by that of the continuous phase but provided no theoretical foundation for that recommendation. Furthermore, it is interesting to note that the virtual density of the bubbles are expected to approach that of the continuous phase at higher dispersed phase holdups and larger bubble diameters where C_{vm} can reach values as high as 0.8 (Kamp *et al.*, 2001).

In order to determine the numerical values for the empirical constants in the models, the spatial variation of the Sauter mean diameter was fitted against the experimentally measured values. Figure 2.5 shows the axial variation of the Sauter mean diameter along the length of the reactor after estimating the various model constants using the non-linear optimization approach, and Table 2.2 shows the value of these constants. The hydrodynamic conditions presented in Figure 2.5 can be considered as typical for those experimentally investigated and the values of the model constants derived thereof should be independent of the operating conditions and/or the design parameters of the mixer.

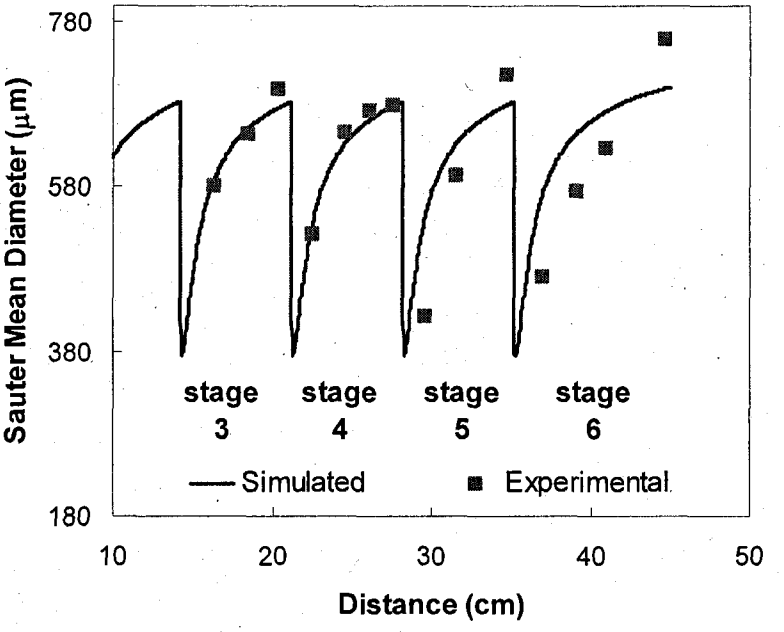

Figure 2.5: Spatial variation of the Sauter mean diameter along the reactor/contactor length (U = 1.3 m/s; ϕ = 7%; C_{SDS} = 0 ppm)

Table 2.2: Values of the model constants

Model Parameter	*0 ppm SDS*
C_1	60.2±3.6
C_2	1.40±0.1
C_3	14.7±1.1
C_4 (m^{-2})	$2.3\pm0.1\times10^{12}$

Neglecting the effect of virtual mass would have resulted in a breakage rate constant (C_2) that is several orders of magnitude smaller than that reported in Table 2 and the development of PB solutions that are incapable of predicting the high interfacial area peaks in the immediate vicinity of the screen (i.e. under-predicting the observed maximum breakage rates). It is also interesting to note that the value of the breakage rate constants (C_1 and C_2) obtained using the virtual mass effect are of the same order of magnitude as those reported for turbulently flowing liquid-liquid systems (Azizi and Al Taweel, 2005). This is in line with some of the recently published models that do not

require any adjustable parameters and can be assumed to be applicable to both gas-liquid and liquid-liquid systems (Luo and Svendsen, 1996; Lehr and Mewes, 2001).

Figure 2.6 clearly shows the effect of changing the operating conditions on the Sauter mean bubble diameter prevalent through stage 6 where quasi-steady state conditions are considered to be reached. The average equilibrium diameter was thus found to decrease with increasing superficial velocity mainly because of the enhanced energy dissipation rates in the regions downstream of the screens which, in turn, results in increasing the bubble breakage rate. The higher average energy dissipation levels encountered further down stream result in higher coalescence rates but the net effect is that of generating finer bubbles particularly in the presence of surfactants which retard coalescence.

However, the effect of increasing gas holdup (or gas-to-liquid flow ratios) shows an opposite trend where the average bubble diameter clearly increases as the gas holdup in raised from 1 to 7 %. This is mainly caused by the larger bubble population densities encountered at higher gas holdups and the subsequent increase in bubble collision and coalescence rates. As can be seen from Figure 2.6, the breakage and coalescence model used in this investigation can accurately predict the effect of varying the hydrodynamic conditions (gas holdup, residence time, and local turbulence intensities) on the average bubble size.

The presence of amphiphilic surfactants or contaminants in the gas-liquid system alters its interfacial characteristics and changes both the breakage and coalescence rates. A significant reduction in bubble breakage rate was observed (a factor of about 1.5) which is independent of surfactant concentration for the range of 2 to 10 ppm. This resulted in the value of C_1 being reduced from 60 to 10 whereas C_2 decreased from 1.4 to 0.9. This observation is very similar to that reported by Prince and Blanch (1990) who attributed this phenomenon to the Marangoni effect induced by the diffusion and adsorption of the amphiphilic molecules to the newly created interface generated during bubble breakup processes.

The situation is however more complex in the case of bubble coalescence where the presence of cationic surfactants, such as SDS, can affect both bubble collision rates (due to the development of positively charged bubbles) as well as bubble coalescence

efficiencies. The effect on coalescence efficiency is expected to be more pronounced since the presence of amphiphilic materials is known to increase the time required for the film entrapped between the colliding bubbles to drain (Chaudhari and Hofmann, 1994). An 18-fold decrease in the coalescence rate was thus observed when 2 ppm of SDS were introduced to the system followed by a slower monotonic reduction with increasing surfactant concentration (coalescence rate were reduced by a factor of about 2 as the surfactant concentration is doubled).

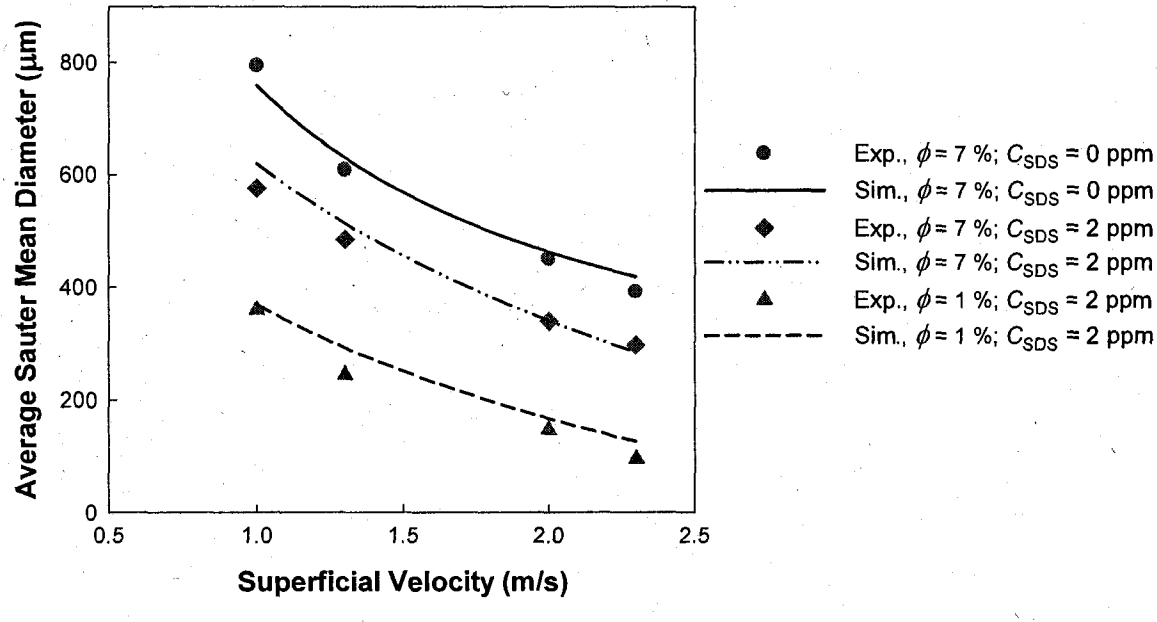

Figure 2.6: Effect of varying the superficial velocity and holdup on the equilibrium Sauter mean diameter in stage 6

The impact surfactants have on the bubble breakage and coalescence processes can best be understood by monitoring the axial variation of the interfacial area of contact as the gas-liquid dispersion passes through the consecutive high energy dissipation regions generated by the screens (Figure 2.7). Whereas quasi-steady conditions were typically obtained after 2–3 stages in the case of the air-water system, the interfacial elasticity induced by the presence of surfactants resulted in significantly reducing the breakage and coalescence rates and in shifting the point at which quasi-steady state is reached further downstream where no measurements were conducted. Although the model used in this investigation did not accurately predict the first two stages well, it accurately predicted

the spatial variation of the interfacial area throughout the remainder of the contactor. This difficulty is most probably caused by the fact that the model developed in this investigation takes into account neither the effect of interfacial elasticity nor bubble breakage by cutting action, a mechanism that is expected to play a large role when the bubbles are much bigger than the screen mesh size. The tendency of bubbles to shed microbubbles in the presence of surfactants could also have contributed to the deviation.

As can be seen from Figure 2.8, the model can predict the effect of surfactants on the average Sauter mean diameter quite well (with interfacial area of contact as high as 2100 m^2/m^3 being observed at high flow velocities). It however under predicts the effect of surfactant concentration in the case of lower velocities (1.3 m/s), a situation that is most

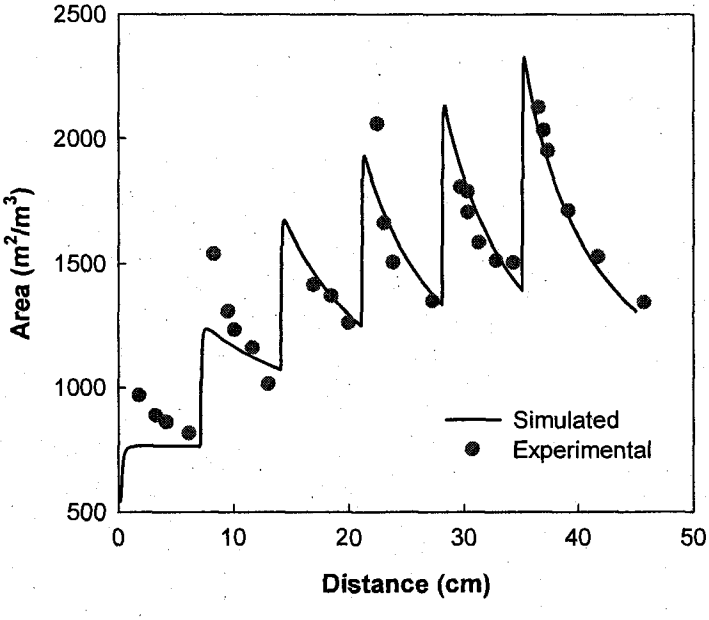

Figure 2.7: Effect of surfactants on the interfacial area of contact
($U = 2$ m/s; $\phi = 7$ %; $C_{SDS} = 5$ ppm)

probably caused by the fact that interfacial elasticity is known to increase with increasing surfactant concentration within the concentration range investigated, and that within the surface ages encountered during bubble collisions (order of milliseconds) the elasticity is essentially a linear function of the surface age. The effect of interfacial elasticity on bubble breakage and coalescence is therefore expected to be minimal at lower surfactant

concentrations and at higher superficial velocities where the characteristic bubble breakage and coalescence times are expected to be shorter.

The ability of the current model to accurately predict the changes in the operating conditions and the interfacial characteristics of turbulently flowing gas-liquid dispersions can be taken advantage of to predict the mass transfer performance of gas-liquid contactors/reactors equipped with screen-type static mixers. Using Higbie's penetration theory in combination with the surface renewal approach proposed by Kawase and Moo-Young, interphase mass transfer coefficients as high as 15 s^{-1} are expected to be achieved even at moderate gas holdups. Such high mass transfer rates can play an important role in enhancing the selectivity of multiphase chemical reactions.

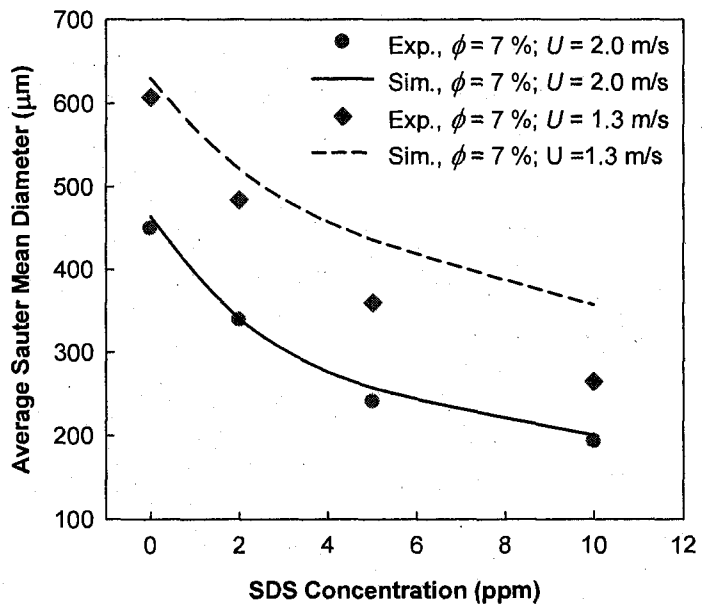

Figure 2.8: Effect of SDS concentration on average Sauter mean bubble size in stage 6

The raw data used in the present analysis, in addition to other graphs, are included in Appendix A.

2.4 Conclusions

From the aforementioned findings, one can conclude that the turbulent dispersion/coalescence of gas-liquid systems can be accurately predicted by incorporating the effect of virtual mass into the phenomenological model developed by Coulaloglou

and Tavlarides (1977) for liquid-liquid dispersions. In this study, a population balance model utilizing this kernel was developed and used to assess its ability to accurately simulate the gas-liquid contacting performance achieved in screen-type static mixers where nearly-isotropic turbulent plug flow conditions prevail.

The predicted spatial variation of the interfacial area of contact and Sauter mean diameter as well as the average Sauter mean diameter (when quasi-steady state conditions were assumed to be reached) were compared with experimental results and good agreement was obtained at different superficial velocities, dispersed phase volume fractions and interfacial characteristics of the system.

The successive exposure of the flowing dispersion to breakage-dominated and coalescence dominated regions (where local energy dissipation ratios as high as 400 can be achieved) provided very stringent conditions for testing and validating the model and for the development of accurate model parameters that may be used for simulating other more complex gas-liquid contacting conditions such as those encountered in MAT.

Acknowledgement

The financial support of NSERC, ACOA/BDP, and Dalhousie University is gratefully acknowledged.

2.5 Nomenclature

$A(d,t)$	Probability density of a bubble of diameter d at time t	[$m^{-3}.s^{-1}$]
b	Wire diameter	[m]
C	Turbulence decay equation constant	[–]
$C_{1,\ldots,4}$	Empirical constants	[–]
C_{SDS}	Concentration of SDS in the continuous phase	[ppm]
C_{vm}	Coefficient of virtual mass	[–]
d	Bubble diameter	[m]
$g(d')$	Breakage frequency of bubbles of diameter d'	[s^{-1}]
$h(d,d')$	Collision frequency of bubbles of diameter d and d'	[s^{-1}]
M	Screen mesh size	[m]
$N(t)$	Total number of bubbles in volume V	[–]

U	Superficial velocity	[m.s^{-1}]
x	Distance downstream of the screen	[m]
x_o	Virtual origin of turbulence decay	[m]

Greek Letters

α	Fraction open area of the screen	[–]
$\beta(d,d')$	Daughter bubble size distribution	[–]
ε	Energy dissipation rate	[m^2.s^{-3}]
$\lambda(d,d')$	Coalescence efficiency	[–]
μ	Dynamic viscosity	[kg.m^{-1}.s^{-1}]
$\nu(d)$	Number of daughter bubbles formed by breakage of bubble d	[–]
ρ	Density	[kg.m^{-3}]
σ	Static surface tension	[N.m^{-1}]
ϕ	Dispersed phase volume fraction	[–]

Subscripts

c	continuous phase
d	dispersed phase

2.6 References

Al Taweel, A.M, Chen, C., "Novel static mixer for the effective dispersion of immiscible liquids", Chem. Eng. Res. Des., **74**, 445-450 (1996).

Al Taweel, A.M., Li, C., Gomaa, H.G., Yuet, P, "Intensifying mass transfer between immiscible liquids: Using screen-type static mixers". Chem. Eng. Res. Des., **85**, 760-765 (2007).

Al Taweel, A.M., Madhavan, S., Podila, K., Koksal, M., Troshko, A., and Gupta, Y.P., "CFD simulation of multiphase flow: closure recommendations for fluid-fluid systems", Proc. of 12th European Conference on Mixing, Bologna, Italy, 495-502 (2006).

Al Taweel, A.M., Webber, J.R., Devavarapu, R.C., Gupta, Y.P., Elsayed, A.S.I., "An algorithm for accurately solving population balance problems", Alexandria Eng. J., **41**, 1069-1075 (2002).

Al Taweel, A.M., Yan, J., Azizi, F., Odedra, D., Gomaa, H.G., "Using in-line static mixers to intensify gas-liquid mass transfer processes", Chem. Eng. Sci., **60**, 6378-6390 (2005).

Azizi, F., "Intensification of the Fuels Desulfurization Processes", M.A.Sc. Thesis, Dalhousie University, Canada (2004).

Alexopoulos, A.H., Maggioris, D., Kiparissides, C., "CFD analysis of turbulence non-homogeneity in mixing vessels a two-compartment model", Chem. Eng. Sci., **57**, 1735-1752 (2002).

Andersson, R., Andersson, B., Chopard, F., Noren, T., "Development of a multi-scale simulation method for design of novel multiphase reactors", Chem. Eng. Sci., **59**, 4911-4917 (2004).

Andersson, R.., Andersson, B., "On the breakup of fluid particles in turbulent flows", AIChE J., **52**, 2020-2030 (2006).

Azizi, F., Al Taweel, A.M., "Reliable Design of Industrial Multiphase Contactors/Reactors", Paper presented at the North American Mixing Forum, Mixing XX; Parksville, BC, Canada, (2005).

Bourne, J. R.; Lips, M., "Micromixing in grid-generated turbulence. Theoretical analysis and experimental study", Chem. Eng. J. Biochem. Eng. J., **47**, 155-162 (1991).

Briassulis, G., Agui, J.H., Andreopoulos, Y., "The structure of weakly compressible grid-generated turbulence", J. Fluid Mech., **432**, 219-283 (2001).

Chaudhari, R.V., Hofmann, H., "Coalescence of gas bubbles in liquids", Rev. Chem. Eng., **10**, 131–190 (1994).

Chen, C., Al Taweel, A.M., "An experimental investigation of gas-liquid contacting in screen-type static mixers", in preparation (2007).

Coulaloglou, C.A., Tavlarides, L.L., "Description of interaction processes in agitated liquid-liquid dispersions", Chem. Eng. Sci., **32**, 1289-1297 (1977).

Groth, J., Johansson, A.V, "Turbulence reduction by screens", J. Fluid Mech., **197**, 139-155 (1988).

Hesketh, R.P., Etchells, A.W., Russell, T.W.F., "Experimental observations of bubble breakage in turbulent flows". Ind. Eng. Chem. Res., **30**, 831–845 (1991).

Hsia, M. A.; Tavlarides, L. L., "Simulation Model for Homogeneous Dispersions in Stirred Tanks", Chem. Eng. J. Biochem. Eng. J., **20**, 225-236 (1980).

Jakobsen, H.A., Lindborg, H., Dorao, C.A., "Modeling of bubble column reactors: progress and limitations", Ind. Eng. Chem. Res., **44**, 5107-5151 (2005).

Joshi, J.B., "Computational flow modelling and design of bubble column reactors", Chem. Eng. Sci., **56**, 5893-5933 (2001).

Kamp, A.M., Chesters, A.K., Colin, C., Fabre, J., "Bubble coalescence in turbulent flows: A mechanistic model for turbulence-induced coalescene applied to microgravity bubbly pipe flow", Int. J. Multiphas. Flow, **27**, 1363-1396 (2001).

Kang, H. S.; Chester, S.; Meneveau, C., "Decaying turbulence in an active-grid-generated flow and comparisons with large-eddy simulation", J. Fluid Mech., 129-160 (2003).

Kasireddy, V.K., Al Taweel, A.M., "An improved light attenuation technique for measuring large interfacial areas", Can. J. Chem. Eng., **68**, 690-693 (1990).

Konno, M., Matsunaga, Y., Arai, K., Saito, S., "Simulation model for breakup process in an agitated tank", J. Chem. Eng. Japan, **13**, 67-73 (1980).

Kostoglou, M., Karabelas, A.J., "Toward a unified framework for the derivation of breakage functions based on the statistical theory of turbulence", Chem. Eng. Sci., **60**, 6584-6595 (2005).

Laakkonen, M., Alopaeus, V., Aittamaa, J., "Validation of bubble breakage, coalescence and mass transfer models for gas-liquid dispersion in agitated vessel", Chem. Eng. Sci., **61**, 218-228 (2006).

Lasheras, J.C., Eastwood, C., Martinez-Bazan, C., Montanes, J.L., "A review of statistical models for the break-up an immiscible fluid immersed into a fully developed turbulent flow", Int. J. Multiphas Flow, **28**, 247-278 (2002).

Lee, C.K., Erickson, L.E., Glasgow, L.A., "Bubble breakup and coalescence in turbulent gas-liquid dispersions", Chem. Eng. Comm., **59**, 65-84 (1987).

Lehr, F., Mewes, D., "A transport equation for the interfacial area density applied to bubble columns", Chem. Eng. Sci., **56**, 1159-1166 (2001).

Luo, H., Svendsen, H.F., "Theoretical model for drop and bubble breakup in turbulent dispersions", AICHE J., **42**, 1225-1233 (1996).

Martinez-Bazan, C.; Montanes, J.L.; Lasheras, J.C., "On the breakup of an air bubble injected into a fully developed turbulent flow. Part 2. Size PDF of the resulting daughter bubbles", J. Fluid Mech., **401**, 183 (1999).

Mudde, R.F., Simonin, O., "Two- and three-dimensional simulations of a bubble plume using a two-fluid model", Chem. Eng. Sci., **54**, 5061-5069 (1999).

Ni, X., Mignard, D., Saye, B., Johnstone, J.C., Pereira, N., "On the evaluation of droplet breakage and coalescence rates in an oscillatory baffled reactor", Chem. Eng. Sci., **57**, 2101-2114, (2002).

Prince, M.J., Blanch, H.W., "Bubble coalescence and break-up in air-sparged bubble columns", AICHE J., **36**, 1485-1499 (1990).

Risso, F., Fabre, J., "Oscillations and breakup of a bubble immersed in a turbulent field", J. Fluid Mech., **372**, 323 (1998).

Sovova, H., Prochazka, J., "Breakage and coalescence of drops in a batch stirred vessel - 1. comparison of continuous and discrete models", **36**, 163-171 (1981).

Thakur, R.K., C. Vial, K.D.P. Nigam, E.B. Nauman and G. Djelveh, "Static Mixers in the Process Industries - a Review", Chem. Eng. Res. Des., **81**, 787-826 (2003).

Turunen, I. and H. Haario, "Mass Transfer in Tubular Reactors Equipped with Static Mixers", Chem. Eng. Sci., **49**, 5257-5269 (1994).

Chapter 3.
Hydrodynamics of Liquid Flow Through Screens and Screen-Type Static Mixers

F. Azizi and A.M. Al Taweel*

Department of Process Engineering and Applied Sciences, Dalhousie University, Halifax NS Canada B3J 2X4

Submitted for publication in:
Chemical Engineering Communications
July, 2008

Abstract

An approach for predicting the spatial variation of the energy dissipation rate downstream of a screen is proposed in this paper. It is based on extending the use of the homogeneous and isotropic turbulence decay equation to the very thin anisotropic region adjacent to the screen. Whereas the decay exponent and origin were kept constant in conformity with other previous investigations; the decay coefficient was slightly altered.

This approach was found to be capable of predicting the experimental energy dissipation data obtained using liquid flow through screens and screen-type static mixers reasonably well over a wide range of design and operating conditions.

Keywords:
Screen, wire mesh, pressure drop, drag coefficient, energy dissipation, turbulence decay.

3.1 Introduction

Over the past years, there has been a growing interest in the use of tubular reactors equipped with static mixers as they present an attractive alternative to conventional agitation due to their inherent advantages whereby similar or better performance can be achieved at lower capital and operating costs (Thakur et al., 2003). Recently, a new type

of static mixing element was introduced in which screens or grids are used to repetitively superimpose an adjustable uniformly-distributed turbulence field on the nearly plug flow conditions encountered in high velocity pipe flows. This characteristic made them particularly effective in processing multiphase systems (Al Taweel and Chen, 1996, Azizi and Al Taweel, 2008). Moreover, the very high turbulence intensities generated in the regions adjacent to the screens resulted not only in the formation of fine dispersed phase entities (bubbles and/or drops) but also considerably enhanced the value of the interphase mass transfer coefficient (Al Taweel et al., 2005 and 2007). The relatively uniform energy dissipation rates prevalent in the downstream regions behind screens offer ideal conditions for investigating bubble and drop breakup and coalescence under turbulent conditions and the assessment/screening of the various models proposed for such processes. In addition, the quasi-isotropic turbulence generated by grids was taken advantage of to study the effect of turbulent mixing on the evolution of chemical reactions (Bennani et al., 1985) and served as a medium for testing the applicability of micromixing models (Bourne and Lips, 1991).

Previous investigations have shown that a radially uniform velocity profile would be attained downstream of a screen in a tubular contactor even at low superficial velocities. In addition, screens were utilized to reduce axial and radial dispersion making plug flow conditions more easily attainable (Ziolkowski and Morawski, 1987); a favourable situation when designing tubular chemical reactors. Screen catalyst beds are also often used for very fast reactions such as the oxidation of ammonia into nitric oxide in the production of nitric acid (Farrauto and Lee, 1990).

The ability of screen-type static mixers to promote contact between immiscible liquids was found to be about 5-fold more energy efficient than mechanically agitated tanks equipped with Rushton-type impellers (Al Taweel and Chen, 1996). This factor, combined with the high inter-phase mass transfer coefficients achievable behind screens, resulted in inter-phase mass transfer coefficients as high as 13 s^{-1} being achieved in the case of liquid-liquid dispersions, and enables for 99% of the equilibrium conditions to be achieved in less than 1 s (Al Taweel et al., 2007). Similarly, the use of multi-stage screen-type contactors to promote gas-liquid contacting resulted in interfacial areas as high as 2700 m^2/m^3 being efficiently generated in the case of gas-liquid systems (Chen, 1996)

while oxygen transfer efficiencies as high as 4.2 kg/kWh were achieved even in the presence of surfactants (Al Taweel et al., 2005).

Screens have long been used to modify fluid motion for the production or reduction of turbulence scales and intensity, and to remove or create mean velocity non-uniformities (Oshinowo and Kuhn, 2000). Consequently, a relatively large body of knowledge is available concerning the nature of grid-generated turbulence and how it is affected by the nature of flow as well as by the characteristics of the wire mesh used (Gad-El-Hak and Corrsin, 1974; Groth and Johansson, 1988; Lance and Bataille, 1991; Briassulis et al., 2001; Kang et al., 2003). In most of these studies, which pertain to the use of screens for flow conditioning in wind tunnels, attention was focused on the various aspects of the spatial decay of turbulence and its governing laws, but none addressed the spatial distribution of the energy dissipation rate caused by the presence of grids/screens.

Since the rate at which turbulent energy is dissipated greatly affects breakage and coalescence processes, knowledge of the spatial distribution of the local rate of turbulent energy dissipation, ε, is of paramount importance for the study of multiphase flows through screens, and consequently the design and optimization of multiphase contactors/reactors utilizing wire meshes to modify flow conditions and/or intensify contact between the phases.

Preliminary investigations (Groth and Johansson, 1988; Bourne and Lips, 1991; Chen, 1996) suggest that a very rapid decay of the turbulent energy dissipation takes place in the very thin layers located immediately after the screen, and that bubble/drop breakup is therefore expected to dominate in this high-energy dissipation region. On the other hand, coalescence becomes significant further downstream where low turbulent energy dissipation rates prevail. These findings highlight the importance of accurately determining the spatial variation of the energy dissipation rate if the simulation results of multiphase flows are to bear a close resemblance to those actually occurring.

The objective of the current investigation is to develop a simulation approach to be used for predicting the spatial variation of the energy dissipation rate downstream of a screen. This is to be accomplished by balancing the average energy dissipation rate predicted

from the spatial variation of ε behind the screens with those experimentally determined from pressure drop measurements.

3.2 Pressure Drop for Liquids Passing Through Screens

The interaction between a screen or grid and the fluid passing through it at relatively high velocities, results in the turbulent dissipation of energy which is directly proportional to the pressure drop across the screen. The local value of the turbulent energy dissipation rate decays rapidly downstream of the screen; where, the eddy or length scales increases as one moves away from the screen (Oshinowo and Kuhn, 2000). Accurate information concerning the pressure drop across a screen is therefore necessary in order to validate the predictions of the energy dissipation rate downstream of the screen.

The pressure drop across the screen is caused by the contribution of both viscous and inertial resistances. The viscous resistance usually dominates in the laminar flow region where the pressure drop is attributed to the viscous drag (i.e. skin friction at the surface of the screen wires). At higher flow rates, the effect of the viscous forces become relatively unimportant and the total inertial pressure losses result mainly from the turbulent vortices and pressure drops caused by sudden enlargement and sudden contraction around the wire mesh screen.

In this section, expressions for estimating the drag coefficient for screens will be developed and compared with experimental results obtained using liquids passing through tubular contactors equipped with screen-type static mixers. This information will then be used in Section 3.3 to accurately estimate the energy dissipation rate and the parameters required to describe its spatial decay.

3.2.1 Predicting the Drag Coefficient of a Screen

In a fashion similar to flow past submerged objects, flow across screens can be analyzed using one of the many drag coefficient expressions proposed by several authors (Gad-El-Hak and Corrsin, 1974; Ehrhardt, 1983; Groth and Johansson, 1988; Chen, 1996). On the other hand, the pressure drop across screens was also treated analogously to that of flow through orifices by other investigators (Chhabra and Richardson, 1985) where the loss coefficient was analyzed as a function of the Reynolds number.

To express the magnitude of the screen pressure drop, the drag coefficient, Ψ, is defined as:

$$\Psi = \frac{\Delta P}{\frac{1}{2} \cdot \rho \cdot U^2} \tag{3.1}$$

The drag coefficient was found to be a function of the percentage open area of the screen, the wire Reynolds number, $\left(\mathrm{Re}_b = \frac{\rho U b}{\mu} \right)$, and the Mach number. However, for incompressible flow, this resistance coefficient becomes independent of the Mach number (Laws and Livesey, 1978; Ehrhardt, 1983; Groth and Johansson, 1988).

Ehrhardt (1983) proposed a commonly used expression for calculating the drag coefficient of screens which was found to be in close agreement with the results obtained using different approaches to model the pressure drop (Chhabra and Richardson, 1985). He investigated several liquids flowing through a large number of different types of wire meshes and proposed an empirical correlation for the drag coefficient as a function of the wire diameter, flow rate, and the physical properties of the liquid, which is applicable for $\mathrm{Re}_b = 0.5–1{,}000$ and $\alpha = 0.25–0.68$.

$$\Psi = \left(0.72 + \frac{49}{\mathrm{Re}_b / \alpha} \right) \cdot \left(\frac{1-\alpha}{\alpha^2} \right) \tag{3.2}$$

Groth and Johansson (1988) adopted the expression proposed by Pinker and Herbert (1967) and Laws and Livesey (1978) to express the drag coefficient of a screen as a function of wire Reynolds number and the screen open area:

$$\Psi = f\left(\mathrm{Re}_b\right) \cdot \frac{1-\alpha^2}{\alpha^2} \tag{3.3}$$

They reported that the function $f(\mathrm{Re}_b)$ approached a constant value of 0.45 at high Re_b but increased dramatically as Re_b decreased below 100. This compares well with the constant value of 0.52 reported by Pinker and Herbert (1967).

Based on an experimental investigation conducted using a wide range of screen porosities ($\alpha = 0.27–0.73$) and smaller wire diameters, Chen (1996) used an approach similar to that of Ehrhardt (1983) and achieved an improved correlation of the experimental data using the following expression:

$$\Psi = \frac{21}{\left(\mathrm{Re}_b / \alpha\right)^{0.46}} \cdot \left(\frac{1-\alpha}{\alpha^2}\right) \qquad (3.4)$$

It should be noted that the screens utilized in that investigation were made of smaller wire diameters (wire diameter smaller than 2 mm as compared to sizes larger than 2 mm utilized in the work of Ehrhardt (1983)).

3.2.2 Experimental Determination of the Drag Coefficient of Woven Screens

With the exception of the investigations conducted by Ehrhardt (1983) and Chhabra and Richardson (1985), all other studies were conducted using gases flowing through grids and screens because of the relevance of this situation to wind tunnels whereas few investigators addressed the turbulence characteristics in the case of oscillating or moving grids used to generate turbulence without mean shear flow (Bache and Rasool, 1996, 2001; Kang et al., 2003; Barry and Ivey, 2003; Schulz et al., 2006). Furthermore, most liquid investigations were carried out using coarse grids with large percentage open area and rare were the investigations reporting measurements of pressure drop even though such information is of paramount importance to the chemical process industry.

Hence, the effect of single phase flow velocity on the pressure drop across screen-type mixing elements has been experimentally investigated by Chen (1996) and El-Ali (2001) using the setup schematically depicted in Figure 3.1. Water was metered and pumped to a mixing section equipped with equally spaced screen-type static mixers and the pressure drop across the screen set (the number and characteristics of which was altered over a wide range) was measured using a water-on-mercury manometer and/or a differential pressure transmitter. A relatively large number (6-9) of screen elements was used in order to minimize the errors resulting from slight variations in screen construction but adequate inter-screen spacing was maintained to eliminate interaction between the screens. Table 6.3 summarizes the range of experimental and operating conditions used in these studies whereas Figure 3.2 shows a schematic representation of the geometry of the screen elements whose characteristics are summarized in Table 3.2 (Screens are generally characterized by their mesh size, M, wire/bar size, b, and the fractional open area, α);

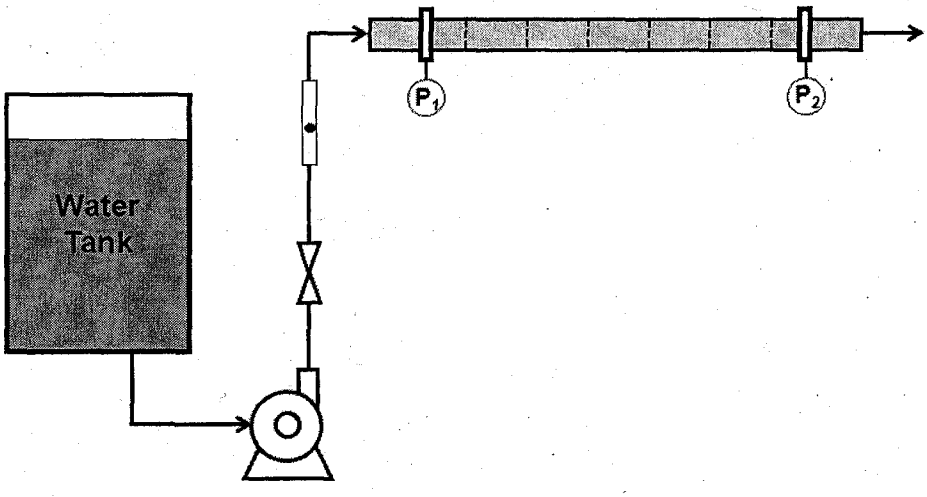

Figure 3.1: Schematic representation of the setup used to study the hydrodynamics of flow through screens.

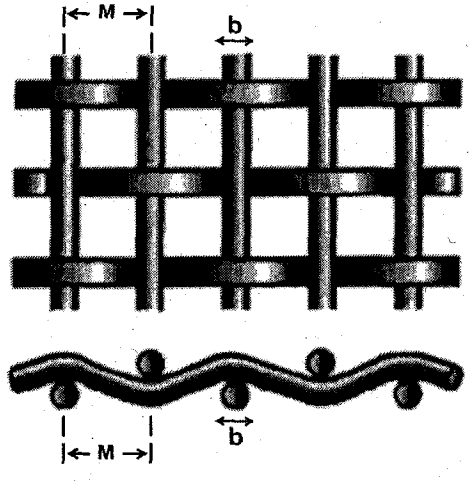

Figure 3.2: Geometry of the woven screen elements used in this investigation.

Table 3.1: Experimental conditions investigated (Chen, 1996; El-Ali, 2001)

Pipe ID, D	21; 25.4 mm
Inter-screen spacing	10; 70 mm
Superficial velocity, U,	0.5 – 2.63 m/s
Screen fraction open area, α,	0.27; 0.31; 0.41; 0.484
Wire Reynolds number, Re_b	45 –1680
Pressure drop across one screen	0.3 to 12.3 kPa

Table 3.2: Characteristics of the woven screens investigated (Chen, 1996; El-Ali, 2001).

Screen No.	Wire Size, b (mm)	Mesh Size, M (mm)	Open Area, α (%)
I	0.508	1.058	27
II	0.152	0.362	33
III	0.305	0.845	41
IV	0.640	2.117	48.4

The measured total pressure drop in the tubular reactor/contactor equipped with screen type static mixers used in this investigation stems from the frictional losses associated with fluid flow through the pipe in addition to the losses due to the flow through the screens. Consequently, the pressure drop across an empty pipe (caused by the combined effect of the frictional losses as well as the entrance and exit effects) were separately determined in the absence of screens and subtracted from the overall pressure drop data in order to determine the drag coefficient. However, these deviations were found to constitute only a small fraction of the total pressure drop (less than 5%).

3.2.3 Comparison with Experimental Results

The aforementioned experimental results were used to test the various expressions available for predicting the drag coefficient [Eqs. 3.2-3.4]. The expression proposed by Groth and Johansson (1988) was not included since no analytical expression for $f(\mathrm{Re}_b)$ was provided. The normalized drag coefficient, $\Psi[\alpha^2/(1-\alpha)]$ was then used for comparison purposes in order to account for the entire set of experimental results (obtained using a wide range of screen geometries), and to isolate the dependency of the drag coefficient, Ψ, on the screen open area, α,. The normalized wire Reynolds number, Re_b/α, was used instead of the conventional Reynolds number for the same reason.

As can be clearly seen from Figure 3.3, the correlation proposed by Ehrhardt (1983), was found to yield drag coefficient values that decreased with increasing Re_b values (ultimately reaching a quasi-constant value for $\mathrm{Re}_b > 250$). It under-predicted the experimentally determined drag coefficients obtained at low wire Reynolds numbers but over-predicted those obtained at higher ones. On the other hand, the expression proposed

by Chen (1996) predicts a continuously decreasing drag coefficient over the range of Re_b values investigated, and achieves much better fit to the experimental data.

The importance of using the right drag coefficient expression is clearly evident when one considers the ability of both expressions to predict the pressure drop across screens. As can be seen from Figure 3.4, both the Ehrhardt (1983) and Chen (1996) correlations yield good agreement with the experimental data at relatively low pressure drops (i.e. low superficial velocities and small percentage open area). On the other hand, whereas the Chen's correlation yields good agreement with the experimental values at pressure drops as high as 12.3 kPa per screen (less than 19 % error), errors as high as 110 % occur when the Ehrhardt (1983) correlation is used at such high pressure drop values.

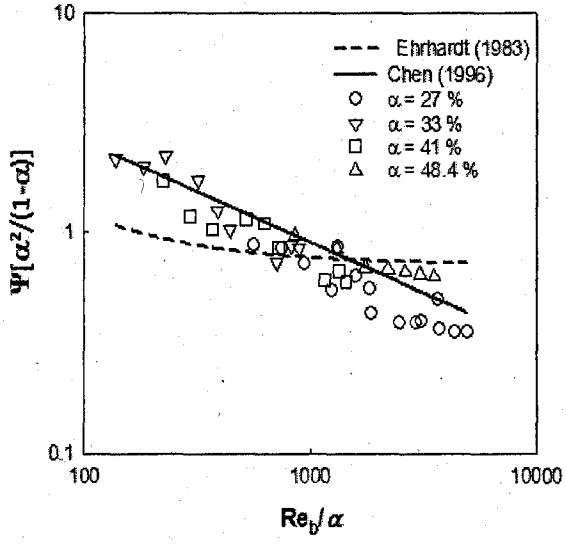

Figure 3.3: Comparison between the various correlations used to calculate the drag coefficient and the experimental results used in this study.

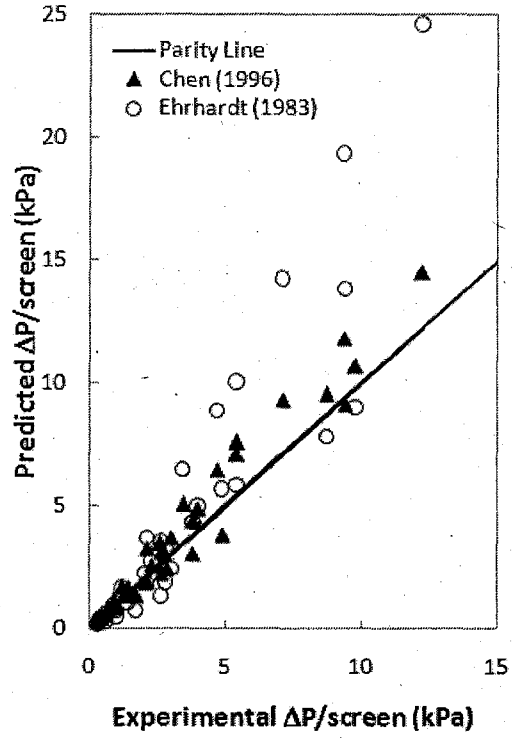

Figure 3.4: Parity plot of simulated values of pressure drop per screen against experimental results

The raw data used to generate this parity plot are included in Appendix B.

3.3 Energy Dissipation Rate behind Grids and Screens

The flow behind screens can be considered as a closely-packed set of jets that approach each other as they move downstream, finally coalescing into what may be considered an essentially uniform flow (Figure 3.5). The flow through a grid may thus be subdivided into three regions (Baines and Peterson, 1951): a) the free stream region well ahead of the screen; b) a region at which the jets emerging from the openings are expanding but are still essentially un-coalesced; c) a free stream region well behind the screen. Recently, Briassulis et al. (2001) subdivided the turbulence profile for the flow behind a grid into three characteristic regions. First is the developing region close to the grid where rod wakes are merging and the production of turbulent kinetic energy takes place. This region is followed by one where the flow is nearly homogeneous and isotropic but where appreciable energy transfer from one wave number to another occurs. This region is best described by the power-law decay of velocity fluctuations. The third or final region of

decay is farthest downstream of the grid and is dominated by strong viscous effects acting directly on the large energy-containing eddies. The interaction among those three regions makes it difficult to accurately predict the flow behind screens. Consequently, although extensive information concerning the nature of grid-generated turbulence is available in the literature (Gad-El-Hak and Corrsin, 1974; Groth and Johansson, 1988; Lance and Bataille, 1991; Briassulis et al., 2001; Kang et al., 2003), none of the previous investigator addressed or formulated an approach for modeling the spatial decay of the energy dissipation rate in the entire downstream region behind grids/screens. Such information is of critical importance for the design of multiphase contactors/reactors as the rate of energy dissipation within the mixer plays a crucial role in determining the drop/bubble size distribution of the flowing dispersion as well as the rate at which heat and mass is transferred between the phases.

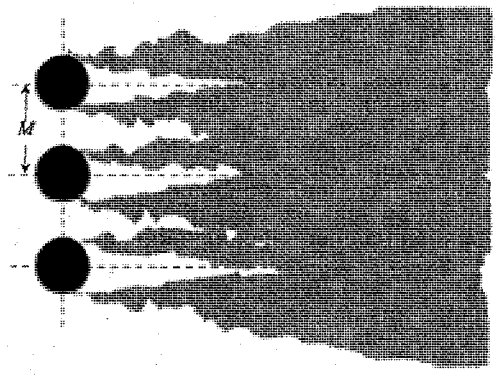

Figure 3.5: Incompressible shear layer flow behind a grid (Briassulis et al., 2001).

An approach describing the spatial decay of the rate of energy dissipation behind the screen is therefore proposed in the following section. It is then validated by comparing the experimentally-determined volume average energy dissipation rate in the system, with the spatial average rate obtained using the proposed simulation approach.

3.3.1 Modeling the Rate of Energy Dissipation in Screens

The turbulence structure generated downstream of the screen is controlled by the upstream superficial velocity as well as by the screen characteristics such as its mesh size, M, wire/bar/rod size b, and the fractional open area α. It is also well known that the local value of ε downstream from screens undergoes dramatic variation along the axis of

flow with the maximum value being encountered in the immediate vicinity of the screen (Groth and Johansson, 1988; Lance and Bataille, 1991). Whereas the turbulence generated up to 10-20 M from the centre of the screen depicts anisotropic characteristics, the vortex trails formed give way to a radially homogeneous and nearly isotropic turbulence which gradually decays. In the latter region (i.e. when $x > 10\ M$), the decay of grid-generated turbulence can be described by power laws such as (Bourne and Lips, 1991; Stewart and Huq, 2006):

$$\left(\frac{u'}{U}\right)^2 = \frac{1}{C}\left[\frac{x}{M} - \left(\frac{x}{M}\right)_0\right]^{-n} \tag{3.5}$$

where C is the decay coefficient, $(x/M)_0$ is the virtual origin of the turbulence decay, and n is the decay exponent. Because these power laws are based on experimental observation obtained using various grid geometries, the value of these parameters vary significantly in the literature (Groth and Johansson, 1988; Mohamed and LaRue, 1990; Kang et al., 2003).

Table 3.3: Range of the turbulence decay equation constants

Open area, α	n	C	$\left(x/M\right)_0$	Authors
0.56 – 0.69	1.15 – 1.33	7.1 – 35	2 – 5	Comte-Bellot and Corrsin (1966)
0.63	1.28 – 1.32	13.2 – 15	0	Gad-El-Hak and Corrsin (1974)
0.56 – 0.71	1 – 1.34	25.2	0 – 6	Groth and Johansson (1988)
0.56, 0.66	0.95 – 1.42	12.7 – 109.5	0 – 6	Mohamed and LaRue (1990)
0.64	1.1	28.5	3	Stewart and Huq (2006)

In their study, Mohamed and LaRue (1990) analyzed data from their experimental results and other previous studies, and concluded that a decay exponent value of $n = 1.30$, and a virtual origin value of $x_0 = 0$, are recommended for use for all values of Reynolds number, mesh size, open area and rod shape. But, the value of the decay coefficient, C, was found to vary as a function of these conditions. These results are in accordance with the findings of Groth and Johansson (1988) who found a decay exponent of $n = 1.32$ is needed when all data beyond $0.8M$ are to be included in the decay law, which in turn was in agreement with the works of Comte-Bellot and Corrsin (1966), and Warhaft and

Lumley (1978). However, as can be seen from Table 3.3, the various constants used in Equation (3.5) vary over a wide range although they were obtained using a relatively narrow open area range (α = 56–71%), and no investigations addressed the small α values of interest to the design of screen-type static mixers.

A large part of the discrepancy in the reported values of the various decay equation parameters can be attributed to the possibility that there may not be a universal self-preserving state. One other possible reason for such variations can be attributed to inconsistencies in performing the data analysis. Thus whereas the data obtained in the close vicinity of the grid (where the flow is anisotropic) is accounted for in some studies; such data were opted out of the analysis in other investigations. In addition, the virtual origin of decay was never determined in a consistent and objective manner (Mohamed and LaRue, 1990).

To overcome these inconsistencies, and to facilitate the design of screen-type catalytic reactors, flow modifiers and multiphase contactors/reactors, a novel approach capable of accurately predicting local energy dissipation rate for flow through screens was developed. It represents an improvement over the monotonic decay function recently used to simulate bubble breakup and coalescence in screen-type static mixers (Azizi and Al Taweel, 2007) which was found to be incapable of fully accounting for the total pressure drop across screens. In the present approach, constant energy dissipation rate is assumed to prevail in the very small distance between the center of the screen and point A which represents the virtual origin of the region where the micro-jets formed by the screen coalesce and turbulence decay begins (Figure 3.6).

3.3.2 Determination of the Turbulence Decay Parameters

For isotropic turbulence where the kinetic energy of turbulence is given by, $k = 3u'/2$, the equation used to determine the rate of turbulent energy dissipation and its spatial rate of decay behind screens can be derived from Equation (3.5) yielding the following expression,

$$\varepsilon = -\frac{dk}{dt} = \frac{3 \cdot n \cdot U^3}{2 \cdot M \cdot C} \cdot \left[\frac{x}{M} - \left(\frac{x}{M} \right)_o \right]^{-(n+1)} \tag{3.6}$$

As mentioned in section 3.1, the value of the parameters used in this equation (the decay coefficient, C; the virtual origin of the turbulence decay, $(x/M)_0$; and the decay exponent, n) vary significantly in the literature. The present approach is based on the use of well accepted values of n and $(x/M)_0$ whereas the decay coefficient was slightly altered to fit the experimental data. Consequently, in agreement with the recommendations of Mohamed and LaRue (1990), Groth and Johansson (1988), Warhaft and Lumley (1978), and Comte-Bellot and Corrsin (1966), the use of a zero virtual origin (i.e. $x_0 = 0$) and a decay exponent of $n = 1.32$ was adopted to describe the spatial variation of ε for $x > 0.8M$. To ensure continuity, the value of ε in the initial anisotropic region was taken to be equal to that calculated at the start of the decay (at $x = 0.8M$).

Accurate estimates of the remaining parameter, namely the decay coefficient C, are therefore needed in order to represent the spatial variation of the energy dissipation rate accurately. To accomplish this, the spatial average energy dissipation rate for fluids passing through screens, obtained using Equation (3.7), should closely match with the volume-average energy dissipation rate behind screens calculated using Equation (3.8).

$$\bar{\varepsilon}_{sim} = \frac{1}{L}\int_0^L \varepsilon \cdot dx \tag{3.7}$$

$$\bar{\varepsilon}_{\exp} = \frac{U \cdot \Delta P_{screen}}{\rho \cdot L} \tag{3.8}$$

where, L is the inter-screen spacing in the contactor in question and ΔP_{screen} is the pressure drop across the screen.

In the current study, the value of C is considered to be a function of the screen geometry only and does not depend on the flow velocity or Reynolds number. This contrasts with the approach adopted by most investigators, where the value of C is allowed to vary with the flow velocity, thus reducing the level of empiricism while simplifying computational effort without affecting the ability to accurately fit the experimental data within the range investigated. The values of the decay coefficient C that best fitted the experimental results are presented in Table 3.4. As can be seen from Figure 3.7, the value of C does not change much with α at small percentage open area; however, it begins to increase significantly for α values larger than 33%. This suggests that

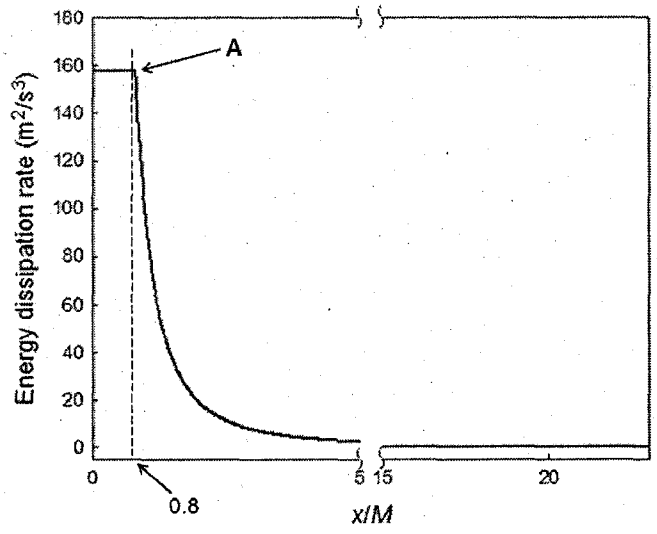

Figure 3.6: Rate of energy dissipation as a function of location downstream of a screen (α = 0.41, U = 0.5 m/s).

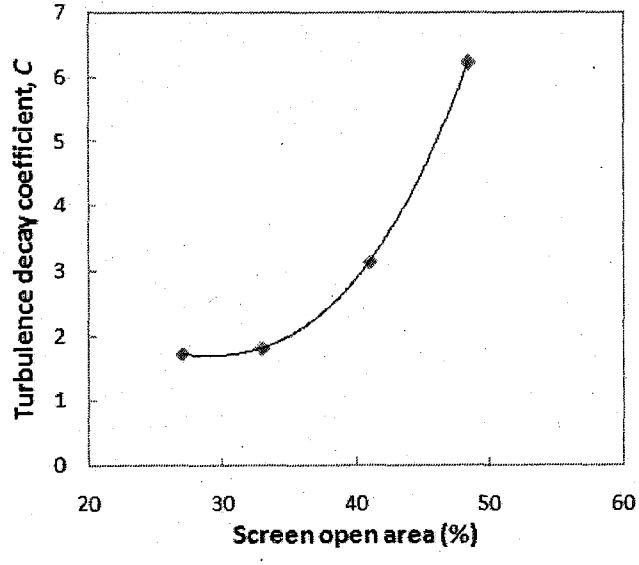

Figure 3.7: Effect of the percentage open area on the value of the turbulence decay coefficient.

the use of screens with small open area will result in the generation of high turbulent energy dissipation rates that dissipate slowly whereas the of screens with smaller solidity will result in lower energy dissipation rates that has a faster decay rate.

The raw data used to calculate the individual values of the decay constant, are included in Appendix B.

Table 3.4: Values of the decay coefficient *C*.

Screen No.	Open area α, (%)	Decay coefficient, *C*
I	27	1.72
II	33	1.82
III	41	3.15
IV	48.4	6.22

As can be seen from the parity plot shown in Figure 3.8, the proposed modelling approach presented in this investigation can accurately predict the average energy dissipation rate experimentally obtained over the wide range of operating and design conditions given in Table 3.1and Table 3.2.

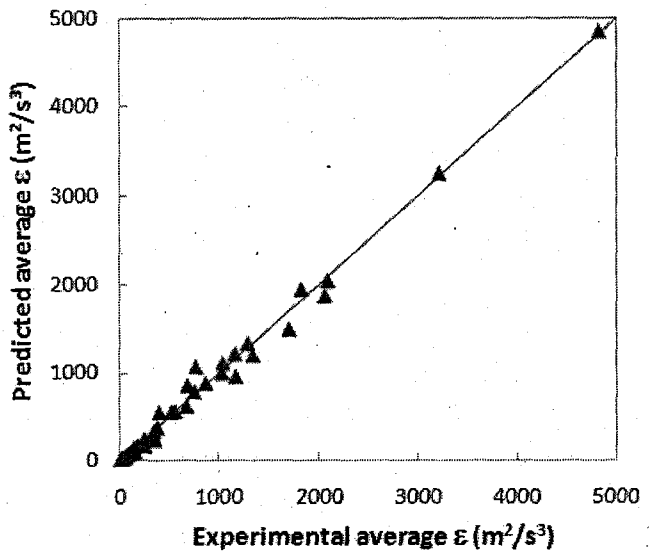

Figure 3.8: Parity plot of simulated and experimental average values of the energy dissipation rate (averaged over 1 cm behind a screen).

Figure 3.6 clearly shows that fluids passing through screens are exposed to a region of constant high energy dissipation rates the thickness of which is controlled by the screen mesh size. However, the value of ε to which the fluid is exposed to is dramatically reduced as the fluid flows further downstream from the screen (with up to 160-fold

variation in ε being observed within a $7M$ distance downstream of the screen). The residence time within the region of high energy dissipation, and the maximum level of local energy dissipation rates encountered in these regions, are therefore a function of the screen characteristics and the superficial velocity of the fluid passing through them (Figure 3.9).

Even though very high values of local energy dissipation rates can be achieved by passing fluids through screens (up to 40,000 W/kg), the corresponding residence time under such conditions is very short (as low as 150 μs) unless multiple screens are used. The ability of appropriately selected screens to focus energy dissipation rates within a very small volume that is uniformly distributed across the flow direction can thus result in significant enhancement in micro-mixing and inter-phase mass transfer without substantial demands in terms of total energy consumption rates (Al Taweel et al. 2008).

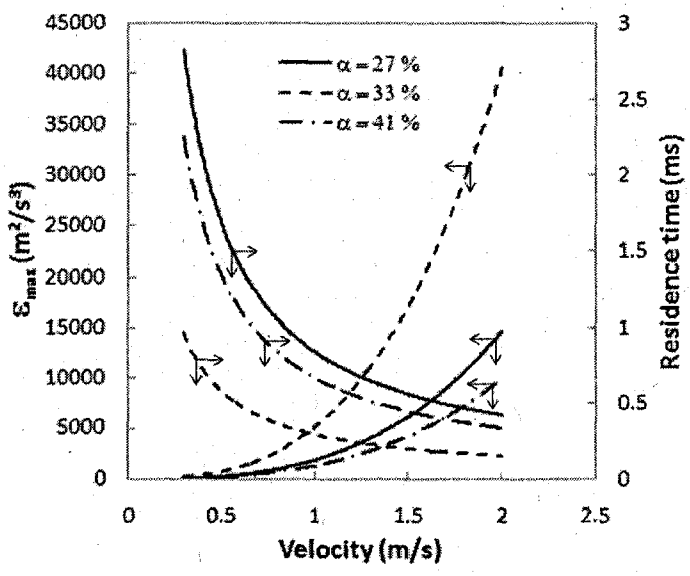

Figure 3.9: Effect of superficial velocity on the maximum energy dissipation rate and the residence time in the high energy dissipation region.

As can be seen from Figure 3.9, the maximum energy dissipation rate reached for the flow through a 33 % open area screen is significantly larger than that attained using a screen of 27 % open area (about 2.8-fold higher at a velocity of 2 m/s). This apparent contradiction to the aforementioned conclusions is attributed to the fact that the 33 % open area screen used in this investigation has a smaller wire diameter and mesh spacing; which, according to Equation (3.6) results in higher turbulent energy dissipation rates.

The importance of accurately predicting the rate of energy dissipation for flow through screens can best be illustrated by considering the effect it has on the drop breakup encountered as an immiscible dispersion is passed through screens. The results depicted in Figure 10 (which were obtained using the well known drop breakage and coalescence model of Coulaloglou and Tavlarides (1977) to predict the drop size distribution in tubular contactors equipped with a 9-stage screen-type static mixers) clearly show that the formation of finer dispersion is predicted when the high energy dissipation region

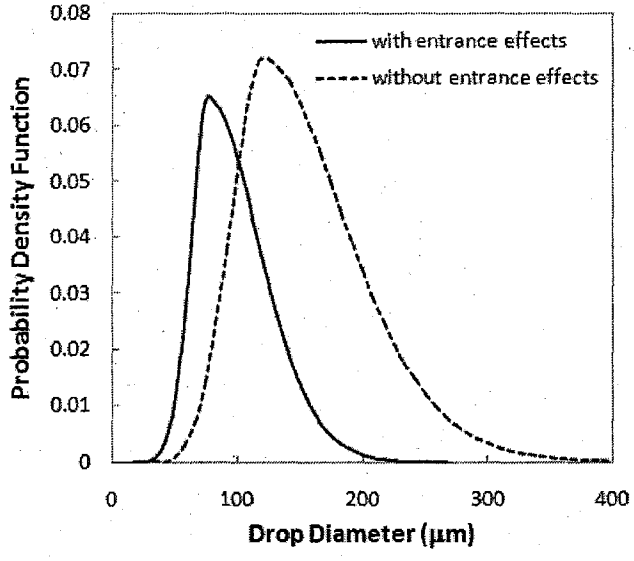

Figure 3.10: Effect of accurate modeling of local energy dissipation rate on the predicted drop size distribution (9 screens, $\alpha = 27$ %, $U = 1$ m/s)

present near the center of the screen is taken into account. Conversely, the predicted Sauter mean diameter was found to be significantly larger when only the energy dissipation rate present in the turbulently decaying region is taken into account. These findings draw attention to the need for accurately simulating the local energy dissipation rates near the tip of the Rushton-type impellers commonly used for dispersing immiscible liquids. Although the approach recently used by many investigators (in which the energy dissipation in the region surrounding the impeller is averaged over 2-3 times the volume swept by the impeller) represents a significant improvement over earlier efforts in which the spatial variation in energy dissipation rates was not taken into account, better resolution of the spatial variation of local energy dissipation (in a fashion similar to that adopted in the present investigation) is needed if one is to be able to accurately simulate

the complicated drop breakage and coalescence processes and predict the drop size distribution achievable in industrial units. This is particularly true in the presence of surfactants which retard the coalescence of the fine drops formed in regions of high local energy dissipation rates.

3.4 Conclusions

An approach for modelling the spatial variation of the energy dissipation rate behind a grid was proposed in this paper. It is based on extending the use of the homogeneous and isotropic turbulence decay equation to the anisotropic region of the flow. In accordance with the findings of previous investigators, the turbulence decay origin and decay exponent were kept constant and independent of the screen geometry and operating conditions. However, the screen-specific turbulence decay coefficient could be determined by balancing the volume average energy dissipation rate, obtained from pressure drop measurements or estimations, with the estimated spatial average energy dissipation rate.

The proposed turbulence decay profile behind a grid was divided into two regions: a) a region of constant high energy dissipation rate prevalent over a certain distance downstream of the grid, and b) a region of fast decay where the homogenous isotropic turbulence decay equation applies. Using this representation for modeling the spatial variation of the energy dissipation rate, all energy sources for the flow through screens were accounted for and the calculated values matched the experimentally determined volume average ε data quite well.

Even though energy dissipation rates as high as 40,000 W/kg could be reached in the first region, the corresponding residence times are as low as 150 μs. Therefore, micro-mixing and inter-phase mass transfer can be significantly enhanced at low total energy consumption rates.

Acknowledgement

The financial support of the Natural Sciences and Engineering Research Council of Canada (NSERC), and Dalhousie University is gratefully acknowledged.

3.5 Nomenclature

b	Wire diameter	[m]
C	Turbulence decay equation constant	[–]
k	Kinetic energy	[$m^2.s^{-2}$]
L	Distance between two consecutive screens	[mm]
M	Screen mesh size	[m]
n	Turbulence decay equation exponent	[–]
Re_b	Wire Reynolds number	[–]
t	Time	[s]
U	Mean velocity	[$m.s^{-1}$]
x	Distance down the screen	[m]
x_o	Virtual origin of turbulence decay	[m]

Greek Letters

α	Fraction open area of the screen	[–]
ΔP	Pressure drop	[$N.m^{-2}$]
ε	Energy dissipation rate	[$m^2.s^{-3}$]
μ	Viscosity	[$kg.m^{-1}.s^{-1}$]
ρ	Density	[$kg.m^{-3}$]
Ψ	Drag coefficient of the screen	[–]

Subscripts

exp	experimental data
sim	simulated data

3.6 References

Al Taweel, A.M., Azizi, F., Uppal, A., "Using static mixers to intensify diesel desulphurization reaction/operation", Paper presented at the International Symposium on Mixing in Industrial Processes VI, Niagara-on-the-Lake, Ontario, Canada (2008).

Al Taweel, A. M.; Chen, C., "Novel static mixer for the effective dispersion of immiscible liquids", Chem. Eng. Res. Des., **74**, 445-450 (1996).

Al Taweel, A. M.; Li, C.; Gomaa, H. G.; Yuet, P, "Intensifying mass transfer between immiscible liquids: Using screen-type static mixers". Chem. Eng. Res. Des., **85**, 760-765 (2007).

Al Taweel, A.M., Yan, J., Azizi, F., Odedra, D., Gomaa, H.G., "Using in-line static mixers to intensify gas-liquid mass transfer processes", Chem. Eng. Sci., **60**, 6378-6390 (2005)..

Azizi, F., Al Taweel, A.M., "Population balance simulation of intensified gas-liquid contacting", Chem. Eng. Sci., **62**, 7436-7445 (2007).

Baines, W.D., Peterson, E.G., "Investigation of flow through screens", Am. Soc. Mech. Engrs – Trans., **73**, 467-477 (1951).

Bennani, A., Gence, J.N., Mathieu, J., "Influence of a grid-generated turbulence on the development of chemical reactions", AIChE J., **31**, 1157-1166 (1985).

Bourne, J. R.; Lips, M., "Micromixing in grid-generated turbulence. Theoretical analysis and experimental study", Chem. Eng. J. Biochem. Eng. J., **47**, 155-162 (1991).

Briassulis, G., Agui, J.H., Andreopoulos, Y., "The structure of weakly compressible grid-generated turbulence", J. Fluid Mech., **432**, 219-283 (2001).

Chen, C., "Dispersion and coalescence in static mixers", Ph.D thesis, Dalhousie University, Canada (1996).

Chhabra, R.P., Richardson, J.F., "Flow of liquids through screens: relationship between pressure drop and flow rate", Chem. Eng. Sci., **40**, 313-316 (1985).

Comte-Bellot, G., Corrsin, S., "Use of contraction to improve isotropy of grid-generated turbulence", J. Fluid Mech., **25**, 657-682 (1966).

Coulaloglou, C.A., Tavlarides, L.L., "Description of interaction processes in agitated liquid-liquid dispersions", Chem. Eng. Sci., **32**, 1289-1297 (1977).

Ehrhardt, G., "Flow measurements for wire gauzes", Int. Chem. Eng., **23**, 455-465 (1983).

El-Ali, M., "Performance characteristics of a novel liquid-liquid contactor", Ph.D thesis, Dalhousie University, Canada (2001)..

Gad-el-hak, M., Corrsin, S., "Measurements of the nearly isotropic turbulence behind a uniform jet grid", J. Fluid Mech., **62**, 115-143 (1974).

Groth, J., Johansson, A.V, "Turbulence reduction by screens", J. Fluid Mech., **197**, 139-155 (1988).

Farrauto, R.J., Lee, H.C., "Ammonia oxidation catalysts with enhanced activity", Ind. Eng. Chem. Res., **29**, 1125-1129 (1990).

Kang, H. S.; Chester, S.; Meneveau, C., "Decaying turbulence in an active-grid-generated flow and comparisons with large-eddy simulation", J. Fluid Mech., 129-160 (2003).

Lance, M., Bataille, J., "Turbulence in the liquid phase of a uniform bubbly air-water flow", J. Fluid Mech., **222**, 95-118 (1991).

Laws, E.M., Livesey, J.L., "Flow through screens", Ann. Rev. Fluid Mech., **10**, 247-266 (1978).

Mohamed, M.S., LaRue, J.C., "Decay power law in grid-generated turbulence", J. Fluid Mech., **219**, 195-214 (1990).

Oshinowo, L., Kuhn, D.C.S., "Turbulence decay behind expanded metal screens", Can. J. Chem. Eng., **78**, 1032-1039 (2000).

Pinker, R.A., Herbert, M.V., "Pressure loss associated with compressible flow through square-mesh wire gauzes", J. Mech. Eng. Sci., **9**, 11-23 (1967).

Stewart, E.J., Huq, P., "Dissipation rate correction methods", Exp. Fluids, **40**, 405-421 (2006).

Thakur, R.K., C. Vial, K.D.P. Nigam, E.B. Nauman and G. Djelveh, "Static Mixers in the Process Industries - a Review", Chem. Eng. Res. Des., **81**, 787-826 (2003).

Warhaft, Z., Lumley, J.L., "Experimental study of the decay of temperature fluctuations in grid-generated turbulence", J. Fluid Mech., **88**, 659-684 (1978).

Ziolkowski, D., Morawski, J., "Flow characteristics of the liquid streams inside a tubular apparatus equipped with static mixing elements of a new type", Chem. Eng. Proc., **21**, 131-139 (1987).

Chapter 4.

Algorithm for the Accurate Numerical Solution of PBE for Drop Breakup and Coalescence under High Shear Rates

F. Azizi and A.M. Al Taweel*

Multiphase Mixing and Separations Research Lab, Department of Process Engineering and Applied Sciences, Dalhousie University, Halifax NS, Canada B3J 2X4 (Al.Taweel@Dal.Ca)

Submitted for publication in:
Chemical Engineering Science
October 2008

Abstract

Multiphase flows play an important role in the chemical and process industries and significant strides have recently been achieved in the design of such systems using the population balance models. However, some uncertainties still remain concerning the stability and accuracy of the numerical solution of such integro-differential equations.

This paper proposes a new methodology for solving the discretized population balance equation by minimizing the finite domain errors that often arise while discretizing the drop size domain. It relies on the use of the size distribution sampling approach combined with a moving grid technique. In addition, an enhanced solution stability algorithm was proposed and which relies on monitoring the onset of errors in the various birth and death terms encountered in PBE. It consequently allows for corrective action to be undertaken before the errors propagate in an uncontrollable fashion, and was found to improve the stability and robustness of the solution method even under very high shear rate conditions.

The proposed algorithm was tested using the model of Coulaloglou and Tavlarides under breakage and coalescence dominated conditions in low, moderate and high energy

dissipation regions, and was found to provide a stable solution that accurately predicts the quasi-equilibrium Sauter mean diameter.

Keywords: Population balance equations, Numerical solution, Stability, Size distribution, Breakage, Coalescence, Flocculation.

4.1 Introduction

Systems containing bubbles, drops are encountered in a wide range of industrial and environmental operations such as the production, storage and transport of oil and gas resources, oil sand extraction and processing, power generation, biotechnology, mineral and metal processing, water and waste water treatment, soil remediation, as well as various operations encountered in the chemical process industry. Unfortunately, design information concerning processing units handling multi-fluid system is traditionally obtained using experimental, semi-theoretical, and simplified mathematical methods; a practice that conceals many of the hydrodynamic details and non-idealities. Consequently, many of the equipment designs presently in use are based on the experience of experts applying rules of thumb and processes that are sensitive to local phenomena and reactant concentrations are therefore difficult to design or scale-up because the design correlations do not usually take scaleup into account. The consequent use of excessive safety margins results in inefficient performance and excessive capital expenditures.

The complex interaction of the various mechanisms involved in multiphase mixing processes makes it very difficult to scale-up and design multiphase contactors/reactors from experimental data (Marchisio et al., 2003). Consequently, most of the units presently used are inefficiently designed with subsequent adverse effects on the reaction yield and selectivity and/or the mass transfer performance. The design of multiphase contactors/reactors thus requires not only a knowledge of the dynamic properties of the dispersion, such as drop/bubble size distributions and residence time, but also the rate of drop/bubble breakup and coalescence.

A detailed description of the dispersed phase characteristics can be obtained by using the population balance models [PBE] that were introduced in the mid-60s to simulate chemical engineering operations. PBE have since become a well established tool that is

widely used for simulating dispersed phase operations because it has the advantage of being able to describe drop/bubble breakage and coalescence processes in terms of identifiable physical parameters and operational conditions.

However, the biggest uncertainty associated with the use of PBE to simulate multi-fluid processing (i.e. immiscible liquid-liquid and gas-liquid dispersions) remains the identification of the breakage and coalescence kernels that can accurately describe what happens in turbulent flows. This arises from the fact that single particle interactions, for example agglomeration or breakage of fluid particles, can be described by a plethora of different models with a varying degree of detail and complexity (Motz et al, 2004). Furthermore, the complexity of the birth and death rate functions used to represent breakage and coalescence in real physical situations dictated the use of numerical or statistical solution methods to obtain accurate solutions since analytical solutions are rare and include major simplifying assumptions that may not be met in practice (Jairazbhoy and Tavlarides, 2000). Sufficiently stable and accurate computational methods are therefore needed in order to solve the complex mathematical structures arising from the use population balance based modeling approach.

Over the years, several numerical techniques (e.g. method of moments, method of weighted residuals, method of lines, finite difference or discretization method, orthogonal collocation, finite element methods in combination with collocation procedures, stochastic methods) have been used to solve the PBE describing dispersed phase behaviour in multiphase contactors with varying degrees of accuracy (Venneker et al., 2002; Dorao and Jakobsen, 2006; Schmidt et al., 2006; Alopaeus et al., 2007). Such techniques have been reviewed and compared by various investigators, resulting in a wide array of contradicting conclusions and a common general recommendation still remains elusive (Vanni, 2000; Jairazbhoy and Tavlarides, 2000; Ramkrishna, 2000; Motz et al., 2002; Attarakih et al., 2004, Balliu et al., 2004). This results from the fact that many solution methods were developed for specific cases which limits their application to other situations. For example, the method of moments is considered as an efficient method to solve the PBE at the expense of a slower convergence as compared to the method of weighted residuals (Jairazbhoy and Tavlarides, 2000), but its solution gives no information about the shape of the distribution. However, if required, additional

algorithms can be used to reconstruct the distribution from the calculated moments by performing inverse transformations (Diemer and Olsen, 2002). On the other hand, its application under conditions that require the coupling of one moment with higher-order moments becomes impossible. To mitigate this problem, the quadrature method of moments was proposed; nevertheless, its application is also limited to situations where no more than a few moments are required (Dorao and Jakobsen, 2006).

In many instances, the computed dynamic behaviour was found to depict a strong dependence on the selected numerical method, which consequently affects the identification of model parameters from experimental data (Motz et al., 2002). Nevertheless, no systematic evaluation of the errors involved in such approaches has been undertaken, and the results obtained using present algorithms and models are often not very sensitive to the models assumed. This could be attributed to the questionable reliability of the different solution methods since their accuracy was often determined by comparing each numerical solution to itself (Dorao and Jakobsen, 2006). In addition, the discrimination between the many expressions used to describe the sub-processes involved in the breakage and coalescence models cannot be properly undertaken because of the lack of experimental results obtained under well-known and controlled hydrodynamic conditions.

Starting with the work of Valentas and Amundson (1966), the method of discretization of the continuous PBE has emerged as an attractive alternative to the various other numerical methods of solutions (Kumar and Ramkrishna, 1996 a,b; Balliu et al., 2004) and has been successfully employed to provide accurate numerical solutions of the PBE (Chen et al., 2005; Schmidt et al., 2006; Azizi and Al Taweel, 2007; Podila et al., 2007; Laakkonen et al., 2007).

Using this approach, Al Taweel et al. (2002) proposed an algorithm for the solution of the PBE based on reducing the error resulting from discretization in the drop size domain while maintaining optimum drop size integration ranges to describe the population. This algorithm was successfully employed to describe multiphase operations (Azizi and Al Taweel, 2005, 2007); however, it was found to be unstable under high shear conditions. This was attributed to the very high breakage and coalescence frequencies that are

expected to dominate in such regions, which caused a divergent solution to be encountered in many cases. The objective of the current work is therefore to develop a stable and robust algorithm for numerically solving the population balance equation. This algorithm is based on a more accurate representation of the drop size distribution, in addition to a sub-process control scheme to manage the stability of the solution.

The importance of this work becomes evident when one considers the very high local energy dissipation rates encountered in a variety of chemical reactors/contactors such as: rotor stators, impinging jet reactors, ultrasonic dispersers, colloid mills, liquid whistles, high pressure and narrow-gap homogenizers as well as in screen-type static mixers. This situation also appears in the commonly used mechanically agitated tanks in the regions adjacent to the impeller (i.e. the trailing vortex).

4.2 The General Population Balance Equation

Population balance equations describe the temporal variation in dispersed phase characteristics (e.g. size, mass, temperature, age, and species concentration) where the dispersed phase is considered as an assembly of drops/bubbles whose individual identities are being continually destroyed and recreated by the dynamic processes occurring within the system. The extent of drop/bubble breakup and coalescence in turbulently flowing liquid-liquid, or gas-liquid, mixtures thus governs the evolution of the drop/bubble size distribution in the dispersion, and consequently the interfacial area of contact between the phases. Under such conditions, the hydrodynamics and the interfacial forces are the major factors affecting the changes in the interfacial area of contact between the phases. Consequently, breakage and coalescence processes take place simultaneously until a quasi-equilibrium state is reached, where the dispersion and coalescence rates become comparable and no net changes in drop/bubble size and drop/bubble size distribution are observed.

The use of PBE to model these processes leads to an integro-partial-differential equation for which there exists very limited analytical solutions (usually obtained at the expense of assuming unrealistic major simplifications). Venneker et al. (2002) presented the PBE given by Ramkrishna (1985) in its most general form as,

$$\frac{\partial n(x,r,t)}{\partial t}+\nabla_x\cdot\dot{x}n(x,r,t)+\nabla_r\cdot u_p n(x,r,t)=B(x,r,Y,t)-D(x,r,Y,t) \qquad (4.1)$$

in which, $n(x,r,t)$ is the number density probability of the property under consideration as a function of the property vector x, the physical position of the particle r, and the time t. In this expression $\dot{x}$ is the growth rate of the particle due to processes other than interaction with other particles, and u_p is the velocity of the particle. The continuous phase variables which may affect the particle property, are represented by the vector, $Y(r,t)$. On the right hand side, $B(x,r,Y,t)$ represents the birth rate or production by either breakage of larger bubbles or coalescence of smaller bubbles, while $D(x,r,Y,t)$ represents the death rate or destruction by breakage into smaller bubbles and by coalescence into larger ones of particles of a particular state (x,r) at time t.

Such a complex formulation thus requires a discretization scheme in the drop size domain to transform the partial differential equation into a set of ordinary differential equations which are easier to solve numerically. Therefore, assuming that no heat and mass transfer takes place and neglecting the effect of chemical reactions, and the convection in and out of the system, the rate of change of concentration of drops/bubbles of diameter d with time can be expressed as a univariate PBE. For a locally isotropic turbulent field, this equation can be written as (Coulaloglou and Tavlarides, 1977),

$$\begin{aligned}\frac{\partial[N(t)A(d,t)]}{\partial t} &= B_b(d,t)-D_b(d,t)+B_c(d,t)-D_c(d,t)\\ &= N(t)\int_d^{d_{max}}\beta(d',d)\cdot\nu(d')\cdot g(d')\cdot A(d',t)\,dd'\\ &\quad -N(t)\cdot g(d)\cdot A(d,t)\\ &\quad +[N(t)]^2\int_0^{d/2^{1/3}} h\left(\left(d^3-d'^3\right)^{1/3},d'\right)\\ &\qquad \times\lambda\left(\left(d^3-d'^3\right)^{1/3},d'\right)\cdot A\left(\left(d^3-d'^3\right)^{1/3},t\right)\cdot A(d')\,dd'\\ &\quad -[N(t)]^2\cdot A(d,t)\int_0^{\left(d^3_{max}-d^3\right)^{1/3}} h(d,d')\cdot\lambda(d,d')\cdot A(d',t)\,dd'\end{aligned} \qquad (4.2)$$

where B_b, D_b, B_c, and D_c are the birth rate by breakage, death rate by breakage, birth rate by coalescence, and death rate by coalescence, respectively. The first two terms on the right hand side respectively represent the rate of formation and loss of drops/bubbles of diameter d' due to breakage; where, $g(d')$ is the breakage frequency, $\nu(d')$ is the number of dispersed fluid entities formed from breakage of a bubble of size d', and $\beta(d',d)$ is the size distribution of daughter drops/bubbles formed from the breakage of a drop/bubble of size d'. The following two terms represent the rate of formation and loss of drops/bubbles of size d' due to coalescence. Here, $\lambda(d,d')$ is the coalescence efficiency between drops/bubbles of size d and d', and $h(d,d')$ is the collision frequency between those of size d and d'.

This population balance representation is applicable to both gas-liquid and liquid-liquid dispersions provided that appropriate expressions for the various breakage and coalescence sub-processes are used. Such models have been presented by several authors, many of which have been recently reviewed by Jakobsen et al. (2005) and Lasheras et al. (2002).

4.2.1 Numerical Sources of Errors in Solving PBE

Because of their simplicity and flexibility, numerical methods are the technique commonly used by many investigators (Valentas and Amundson, 1966; Hounslow et al., 1988; Ramkrishna, 2000; Campos and Lage, 2003; Attarakih et al., 2004, Dorao and Jakobsen, 2006, Laakkonen et al., 2007; Qamar et al., 2008) and is thus the focus of the present investigation. However, little is known about the factors affecting the accuracy and stability of numerical solutions, as well as the computational demands associated with this approach. One of the problems associated with the use of the numerical solution approach is the fact that no prior knowledge about the time at which steady state conditions are approached is available to the user. This is a very important point, since significant errors, and/or solution instabilities, may be introduced if the numerical solution is extended beyond the point where the evolution of drop-size distribution practically ceases.

In general, the numerical approach for solving the one dimensional PBE is based on describing continuously changing variables by discretized functions. This discretization

takes place in both the time and the drop size domains and introduces a multitude of errors the magnitude of which depends on the discretization technique used. On the other hand, the round-off error arises from the finite nature of the computing machine (which cannot deal with infinitely represented numbers); nevertheless it is used to simulate a number system which uses infinitely long representations. The round off error accumulates as the number of calculations increases and becomes relatively more significant as the numbers of primary concern are small. The solution may blow up if the round-off errors are accumulated in one direction, or may come from a single operation (e.g. the greatest loss in significant numbers occurs when two numbers of about the same magnitude are subtracted so that most of the leading digits cancel out). Unless care is taken in advance, this can happen frequently during an extended computational operation. Calculations should therefore be conducted using a sufficiently large number of significant figures, to prevent the accumulated round-off errors from becoming too large.

The use of discretization in the drop size domain gives rise to two additional sources of error. The first is the inherent finite domain error (FDE) which is an inevitable result of trying to use a finite internal droplet coordinate to approximate an infinite one (Sovova and Prochazka, 1981; Attarakih et al., 2001). The second source of error stems from the method used to describe the drop size distribution [DSD] and to calculate the corresponding birth and death rates.

The use of numerical integration to solve the differential equations in the time domain introduces another discretization error which is often referred to as the truncation, or time-domain discretization error (Press et al., 2002). This results from truncating the Taylor series expansion describing a continuous function of time. In the case of the ordinary-differential-equation integrator used in this work (adaptive stepsize control for Runge-Kutta integration), the truncation error is in the order of $(\delta t)^6$, where δt is the time-step-size. The truncation error can therefore be reduced by minimizing the time-step-size. Unfortunately, this approach will also increase the number of time increments needed to reach the final integration time and situations can arise where the round off error resulting from the use of exceedingly small time intervals can be higher than the benefits accrued by decreasing discretization/truncation error. A balance should therefore

be struck between both truncation and round off errors while integrating PBE in the time domain.

Another problem that is associated with the numerical integration of PBE is the feedback or input error. As its name implies, this problem is generated when the numbers produced at one computational stage are fed back as initial values to be processed again. If errors are thus encountered at one stage, such a feedback loop would lead to error propagation throughout the solution trajectory. This situation could be encountered during the numerical solution of PBE where information concerning the DSD at time t is used as the new input for calculating the DSD at time $t+\delta t$. The presence of these computational feedback loops can destabilize the solutions obtained using such algorithms unless care is employed for minimizing the generation of errors and keeping them bounded within reasonable tolerances.

The method chosen to solve the PBE numerically is strongly dictated by the characteristics of the problem being solved. The application of a numerical method that is inappropriate to a particular system can thus lead to gross inefficiencies, or even to spurious results when applied to a radically different system. Appreciating that aspect of the solution procedure and the issues of round-off-errors, errors in initial values, truncation errors, and the impact they have on solution stability is therefore vital for the accurate solution of the PBE.

4.3 Algorithm for the Accurate Solution of PBE

An algorithm for solving the integro-differential PBE obtained by considering batch or plug flow systems, where uniform energy dissipation conditions can be correctly assumed, was developed by Al Taweel et al. (2002). This algorithm was found to accurately predict experimental liquid-liquid dispersion data genèrated under well controlled hydrodynamic conditions prevailing at low to moderate shear rates. However, under the conditions encountered in a multitude of high shear mixing devices, as well as in the trailing vortex present near rotating impellers, the onset of numerical instabilities that caused the solution to diverge were observed. The earlier algorithm was therefore restructured to incorporate more stringent stability measures.

In a fashion similar to that used by Al Taweel et al. (2002), the current algorithm uses the sampling approach proposed by Sovova and Prochazka (1981) for characterizing the drop size distribution and combines it with cubic spline interpolation if information in-between the sampling points is needed. At any particular time, the value of the birth and death terms are determined by integrating over the appropriate drop/bubble size domain (using Simpson's rule) and the resulting ODE is numerically integrated in the time domain using the adaptive time step-size version or the 5^{th} order Runge-Kutta. The solution stability was enhanced by using a moving grid technique where insignificantly large drops/bubbles were cut off from the size domain while occasionally re-adjusting the distribution to ensure volume conservation. The advantage of using the sampling technique over the conventionally used class approach is demonstrated by the observation that the average equilibrium drop size predicted by the numerical solution were within 7% of the analytical solution obtained by Rod and Misek (1982) when 10 sampling points were used (whereas the error obtained was found to be as high as 29% when the drop/bubble size distribution is represented by 10 discrete classes/bins). Improved solution stability and a higher degree of accuracy (maximum error of 1.8%) were achieved by using 40 sampling points within the self adjusting drop/bubble size domain (Al Taweel et al., 2002) whereas the error was still at 9% when the drop/bubble size was represented by 40 classes.

The aforementioned algorithm worked very well for wide range of breakage and coalescence kernels at average energy dissipation rates up to 30 W/kg (where local values as high as 2,680 W/kg were encountered for very short durations (Azizi and Al Taweel, 2007)). However, depending on the type of kernels used, the algorithm started showing some problems when applied to the case of higher ε values. Whereas it yielded very stable and accurate solutions (within 1.8 %) when the Rod and Misek kernels were used, instabilities were observed to occur when more realistic aggregation and disaggregation models were used (Al Taweel et al., 2008a). This is most probably caused by the fact that whereas the coalescence kernels used by Rod and Misek do not depict any dependence on drop/bubble diameter (a simplification necessitated by the desire to develop an analytic solution), the kernels used by Coulaloglou and Tavlarides (1977) to describe drop coalescence depict a strong dependence on the drop/bubble diameter (exponents of

approximately $d^{2.3}$ in the collision frequency term) whereas the floc aggregation kernel is typically represented with kernels that depict even stronger dependence on floc diameter.

This strong dependence on drop diameter is expected to result in a much faster rate of aggregation as well as a much higher sensitivity to variations in operating conditions. In addition, the stronger dependence of the Coulaloglou and Tavlarides model on the local energy dissipation rate, where the breakage term is proportional to $\varepsilon^{1/3}\exp(-\varepsilon^{-2/3})$ while the coalescence term is proportional to $\varepsilon^{1/3}\exp(-\varepsilon)$, plays an added role that further magnifies the sensitivity of the model. The energy dissipation rate is implicitly accounted for in the Rod and Misek (1982) model, where the ratio of the coalescence to breakage model constants dictates the equilibrium mean diameter. Therefore, the change in mean diameters between the initial and final stages gives an indication of the extent of energy dissipation in the system.

Consequently, the algorithm developed by Al Taweel et al. (2002) had to be modified in order to enhance its stability and allow for its use to numerically solve PBE at ε values as high as 40,000 W/kg encountered in screen-type static mixers (Chapter 3). The overall structure used in developing the improved algorithm for solving PBE, and calculating the transient DSD and mean diameter, is depicted in Figure 4.1. This PB algorithm was developed in a fashion that allows it to be applicable to all breakage, and coalescence kernels and initial drop/bubble distributions. The robustness of the new algorithm was demonstrated by its ability to yield stable solutions that simulate very high flocculation rates (Al Taweel et al., 2008a).

All the information required for initializing the PBE solution (e.g. physical properties of the two phases, initial drop/bubble size distribution, hydrodynamic and interfacial parameters, computational parameters, and the flags necessary to select appropriate/desired coalescence and breakage models) are first inputted into the program. Based on these initial conditions, the various breakage and coalescence rates, and the net rates of change of number density, are calculated for all sample points. Using suitable integration subroutines, the new DSD predicted to occur at $t+\delta t$ is calculated. This process is repeated until the maximum integration time is reached. Information

concerning the DSD is periodically sampled in order to determine the temporal variation in DSD, the interfacial area of contact and the value of the various mean diameters.

The success of the new algorithm in accurately solving PBE is based mainly on its ability to accurately represent drop/bubble size distributions and to identify their upper and lower limits.

4.3.1 Accurate Representation of Drop/Bubble Size Distribution

One of the major factors affecting the stability and accuracy of the PBE numerical solution is the method used to describe the drop/bubble size distributions encountered in the system. Most investigators use a limited number of fixed drop size intervals and the drops present within that interval are represented by an appropriately selected class average (arithmetic, geometric, or logarithmic mean). Significant errors are introduced through the use of classes and inappropriate selection of the average value representing a class (Calabrese et al., 1995). Using this approach, it was necessary to use up to 200 classes in order to achieve stable and accurate numerical solutions, a feat that was achieved at the expense of excessively large computational efforts particularly when low residual errors are required. On the other hand, as shown in the following sections, highly accurate and rapid numerical solutions could be obtained at lower computational effort when the DSD is described as a continuous function that is sampled at regular intervals in conjunction with the use of a moving grid approach.

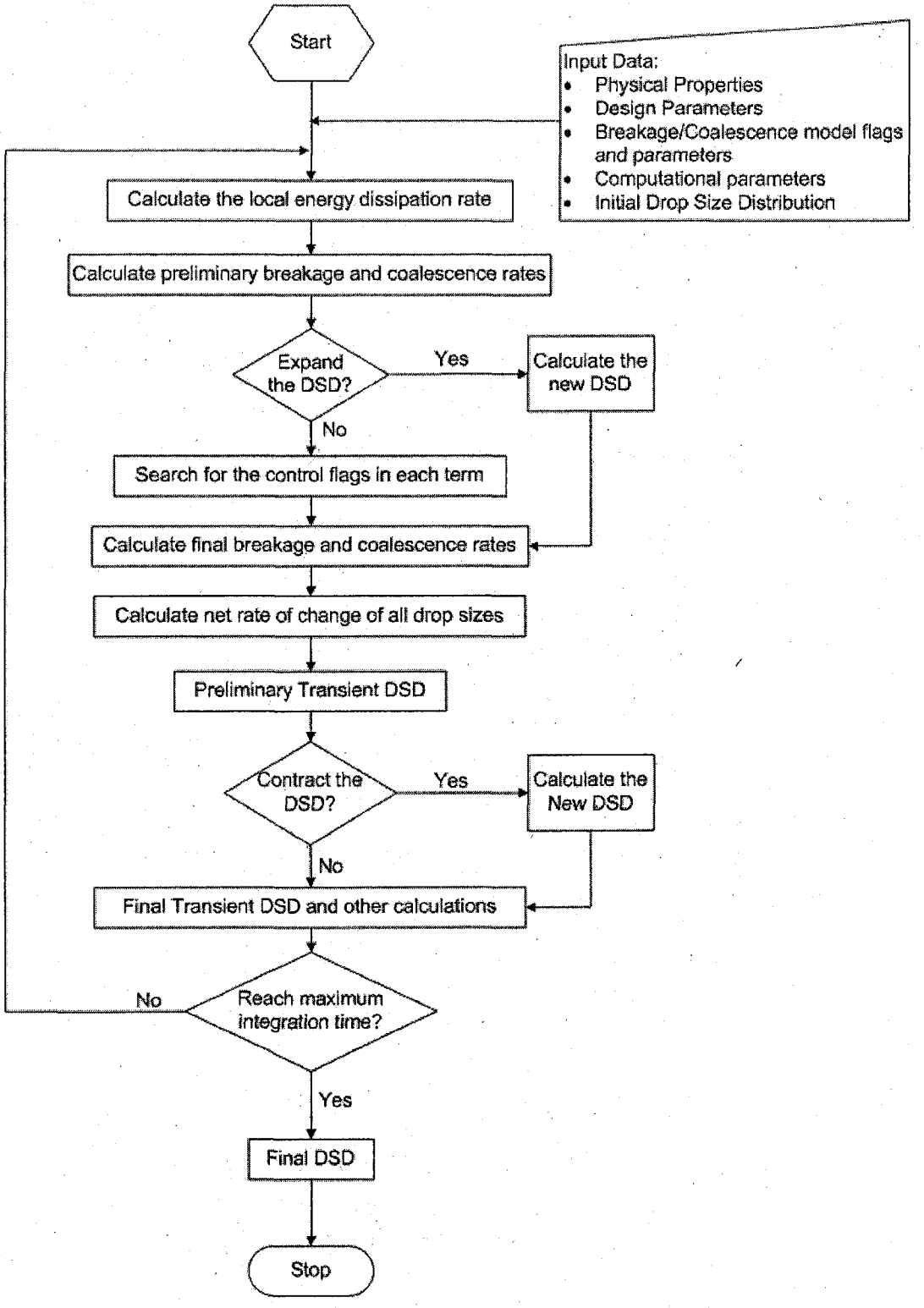

Figure 4.1: Overall algorithm for solving the PBE

4.3.1.1 *The sampled drop size distribution approach*

To achieve higher accuracy while numerically solving PB equations, the approach proposed by Sovova and Prochazka (1981) was used. In this approach, the DSD is treated as a continuous function that is discretized at a finite number of sampling points (Figure 4.2a). The breakage and growth rates at each of those sampling points are calculated by integration over the appropriate portion of the drop size domain.

A comparative evaluation of the two methodologies used to describe the DSD, namely, the method of classes and sampling, indicated that both yielded reasonably accurate and stable solutions under conditions where there is limited interaction in between the various sources of error (e.g. relatively slow rates of change, using a large number of classes/sampling-points to characterize the DSD, using small integration time intervals). On the other hand, the use of the sampled DSD approach was found to yield a more accurate, stable, and robust solution under conditions where there is strong interaction between the sources of error (e.g. rapid variations in drop size, using a small number of classes/sampling-points to describe the DSD, using relatively large integration time intervals). The sampled DSD methodology was thus found to allow for the use of relatively small number of discretization intervals without significant reduction in accuracy or stability (Polprasert et al., 2002).

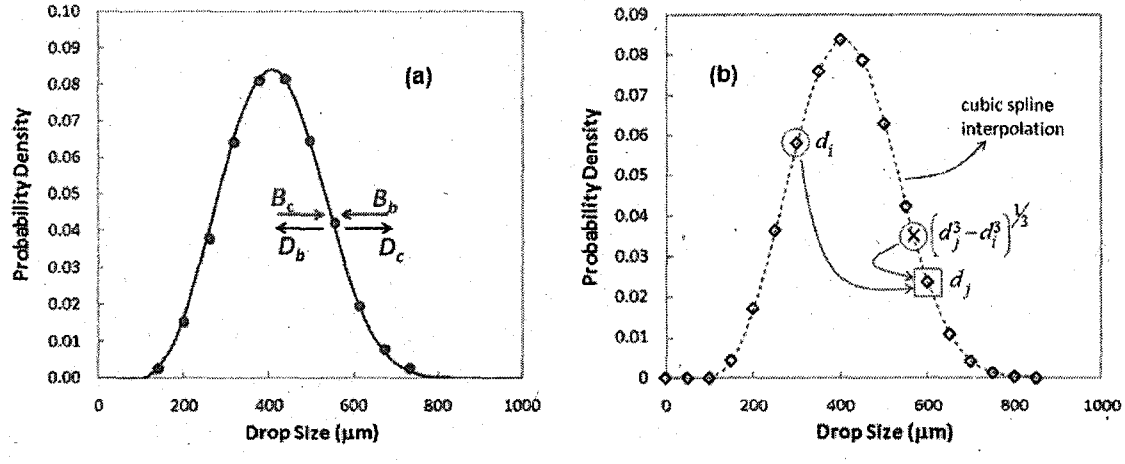

Figure 4.2: Schematic diagram representing the sampled DSD methodology used for calculating drop/bubble breakup and growth rates. a) Sampled drop size distribution; b) Cubic spline approach used to estimate non-sampled points while calculating the coalescence terms.

An additional source of uncertainty arises when classes or pivots are used to characterize the DSD while numerically solving the discretized PBE (where all the bubbles/drops present in a certain size range are assigned to a pivotal size). The main difficulty that arises is that aggregation or breakage of the dispersed phase entities usually leads to the formation of particles whose property does not exactly coincide with one of the existing grid representative diameters or pivots (Nopens et al., 2005). The example that best describes this problem is by considering three drops/bubbles classes with volumes $1v$, $2v$, and $4v$; the coalescence of a drop/bubble with volume $1v$ with another of size $2v$ will result in a drop/bubble with a volume of $3v$. This resulting drop/bubble now has to be distributed in fractions over the two neighbouring classes, in this case $2v$ and $4v$. The approaches employed to solve this issue varied from splitting the volume of the resultant drop/bubble in half between the two classes (Batterham et al., 1981) to the most common solution proposed by Kumar and Ramkrishna (1996a,b) which distributes the resulting entity between the two nearest categories in a fashion that assures the conservation of two arbitrary moments of the distribution. Whereas the most commonly conserved moments are the zeroth and third moments (i.e. conservation of number density and volume), a large variation in the moments selected was observed and are often problem specific; (Attarakih et al., 2004; Chen et al., 2005; Laakkonen et al., 2006). For example, Venneker et al. (2002) conserved the third (volume) and second (surface area) moments of the distribution since the latter was of importance to the case of mass transfer. Alopaeus et al. (2006) recently developed a high-order moment conserving method (that conserves the first six moments of the distribution) which was found to yield several orders of magnitude higher accuracy than the commonly used low-order moment conserving method of Kumar and Ramkrishna (1996a,b).

On the other hand, this problem does not exist in the sampled DSD methodology used in this investigation. For example, the rate of formation of a drop of size d_j by coalescence is determined by considering the coalescence rate of a sampled drop size $d_{i\,=\,1\ldots(j-1)}$ coalescing with a drop of size $\left(d_j^3 - d_i^3\right)^{1/3}$ where the number density of the latter drop size is determined using cubic spline interpolation between the points (Figure 4.2b). The same approach is used to compute the various rate terms included in the death by

coalescence. By using this methodology, the DSD approaches a continuous function which yields higher numerical accuracy and stability while simultaneously providing a more sound physical interpretation of the process.

4.3.1.2 The moving grid approach

Although it is well known that the DSD changes significantly as the coalescence and/or breakage processes take place, most of the algorithms previously used for numerically solving PB models utilize a fixed range (i.e. a fixed grid) in the drop size domain over which computations are performed. However, improper selection of the computational drop size range can give rise to excessive errors and can occasionally destabilize the solution particularly when the DSD undergoes very significant changes. This problem is mathematically known as an ill-posed boundary condition and was extensively discussed by Kumar and Ramkrishna (1996a) and Attarakih et al. (2003).

The use of fixed grids in the drop size domain gives rise to significant finite domain and discretization errors. The finite domain error thus becomes significant as the mean drop size approaches the upper limit of the range where the DSD taken into consideration while calculating breakage and growth terms can be severely truncated by improper selection of d_{max} (Figure 4.3a). On the other hand, significant discretization errors can be introduced by using a fixed grid containing a limited number of classes/samples to characterize the DSD over the whole size range. This stems from the fact that in most real situations the DSD present at any particular instant occupies only a small fraction of the total drop size domain. Consequently, the effective number of classes/samples used to describe the bulk of the DSD is reduced to a small fraction of that used to describe the whole range (Figure 4.3b), giving rise to a significant increase in the discretization error.

The aforementioned sources of error were virtually eliminated by limiting the computational drop size range to an optimal range that covers the major part of the dispersed phase volume (i.e. the moving grid technique depicted graphically in Figure 4.3c). The number of classes/sampling-points used to characterize the DSD within the computational domain was kept at its optimum value in order to enhance the accuracy and stability of the solution while keeping the computational demands low. This

approach eliminates the need for computations outside the representative drop size domain.

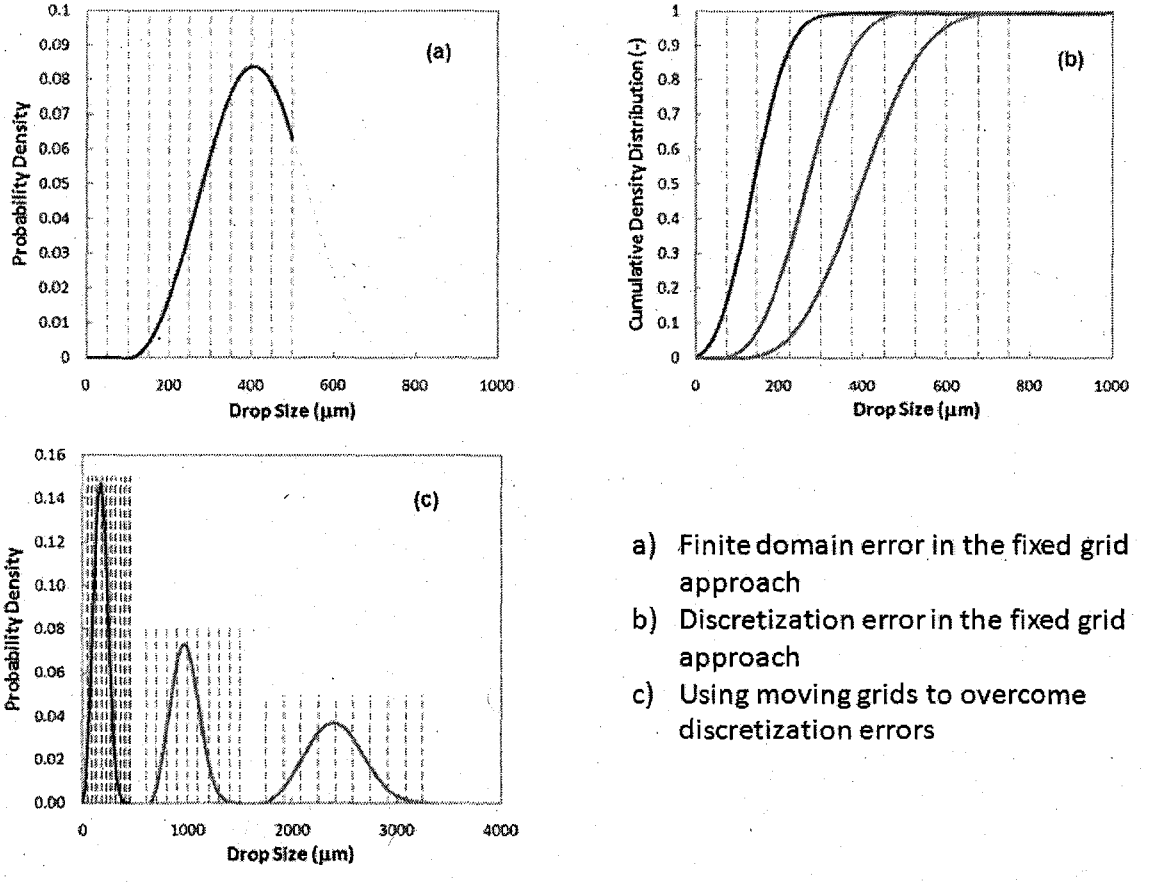

Figure 4.3: Schematic representation of the fixed and moving grid techniques for solving PB equations.

By applying the aforementioned algorithms to the case of growth-dominated situations, the self-adjusting grid was found to progressively expand in order to include the larger drops formed. On the other hand, the self-adjusting grid contracted to a narrower DSD in the case of breakage-dominated situations. Consequently, the major part of the dispersed phase volume is characterized by the desired number of sampling-points (Figure 4.3c). Using the class/pivot approach, this technique was applied by Litster et al, 1995; Kumar and Ramkrishna (1996b), Attarakih et al. (2003) and achieved higher accuracy than those obtained using fixed grid discretization while using the same number of classes/pivots. Conversely, it was possible to reduce the number of intervals (hence reducing the

computational effort) while maintaining the same degree of accuracy (Nopens et al., 2005).

4.3.1.2.1' Identifying the upper limit of the distribution

In addition to the aforementioned benefits associated with the use of the moving grid technique, its use was found to eliminate one of the most important error sources that cause numerical instabilities. These errors arise from the fact that the value of the net rate of change of drop/bubble numbers is determined by the difference between two much larger parameters, namely the death and birth rates resulting from drop/bubble breakup and growth (Figure 4.4). As can be seen from Figure 4.5a, the round-off errors associated with such operations can be easily overlooked, particularly at low local energy dissipation rates where the absolute value of the death and birth rates are relatively small. On the other hand, a careful examination of the regions where no apparent changes exist (Figure 4.5b), clearly shows the onset of oscillatory error in the net rate term. Although the magnitude of this error can be easily neglected when compared to the peak net rate term, its presence was found to trigger oscillatory behaviour in the transient DSD and can destabilize the numerical solution particularly at high ε values. Figure 4.6a shows the transient DSD at two consecutive time steps and whereas no apparent difference exists between the two, a closer look at the tail of the distribution (Figure 4.6b) shows how the numerical errors are amplified at each time step and eventually lead to a non-converging solution if no remediation steps were implemented. This observation may well explain the oscillatory behaviour in the "no-go" region reported by Hounslow (1990) for the case of flocculating micron-sized particulate matter. This phenomenon was attributed to an increased finite domain error in that region and used for selecting the minimum diameter while discretizing the PBE.

The aforementioned problems could be eliminated by switching from a fixed grid solution methodology into a self-adjusting grid the limits of which are selected using optimal truncation methods. However, although the problem of selecting the limits of the distribution while solving the PBE is commonly encountered and well acknowledged in the literature, little attention has been paid to the development of a systematic method of selecting appropriate limits of the domain. On the other hand, it is well known that the

selection of unnecessarily large values of d_{max} renders the problem computationally expensive, if not difficult to converge, because of the very small density values that can be attained at large particle sizes and their vulnerability to large round-off errors (Nicmanis and Hounslow, 1998).

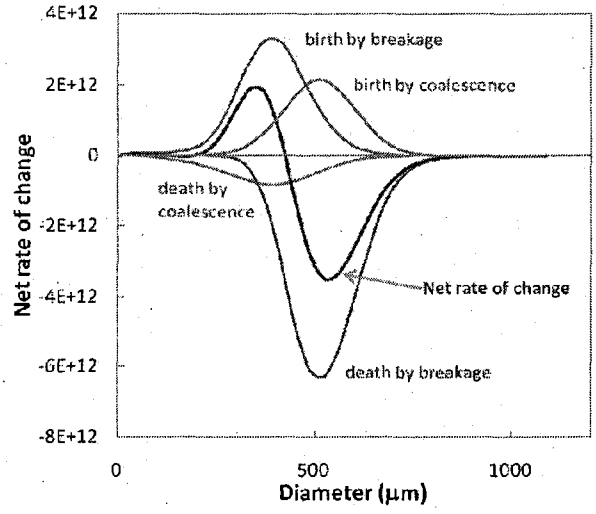

Figure 4.4: Illustrative example of the effect of drop size on the birth and death terms, and the net rate of change.

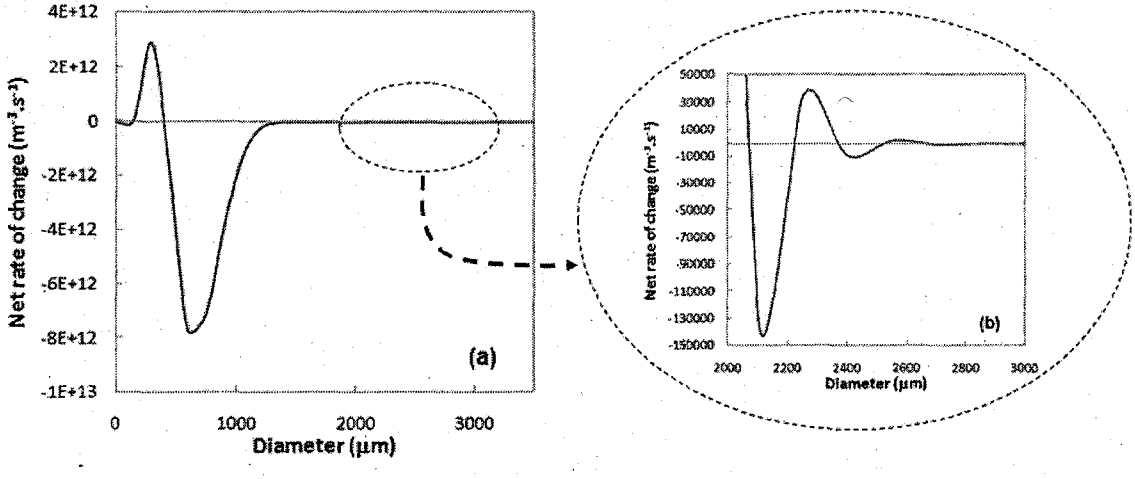

Figure 4.5: Development of oscillatory numerical instabilities in the net rate of change.

Based on the work of Gelbard and Seinfeld (1978), Hounslow and Nicmanis (1998) proposed an approach for determining the upper limit of the domain. However, this approach remains unreasonable for simulation purposes since it relies on a visual inspection of the distribution in order to determine an order of magnitude estimate of the

upper limit. Attarakih et al. (2003) developed an optimal moving grid technique by preserving two integral properties of the distribution and forcing the residuals at the upper and lower limits to be equal at each time step. By doing so, a path that must be followed by the grid is specified and the domain boundaries are defined as a function of time. However, such a description of the boundaries could not be applied to the case of continuous systems where the constant feed distribution made it difficult for the upper distribution limit to move in case of a breakage dominated situation. This necessitated the development of an optimal fixed grid which relies on minimizing the time-averaged finite domain errors. On the other hand, Alexopoulos et al. (2004) relied on obtaining a satisfactory resolution of the time-varying particle size distribution in order to determine the limits of their finite domain.

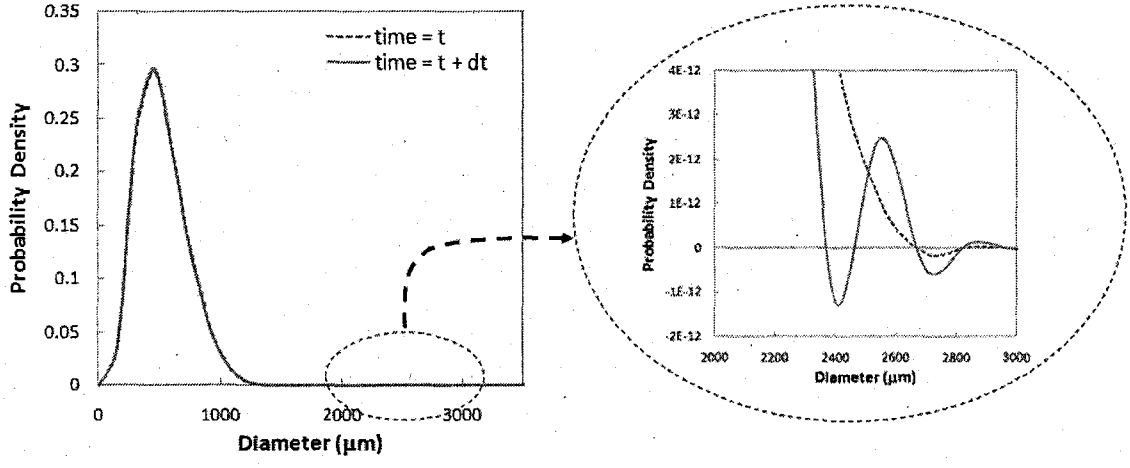

Figure 4.6: Development of oscillatory numerical instabilities in the transient DSD.

To conclude, there presently exists no method for the determination of the upper and lower limits of the size domain that is neither computationally or time consuming. For this purpose a method for determining the size domain boundaries is proposed. It is based on monitoring the drop/bubble size distribution at every time step during the solution process in order to determine the limit of the domain by using optimal truncation parameters. In this way, more than 99.99% of the particulate mass is accounted for within the upper and lower size bounds while eliminating outlying regions which contribute to the onset of the oscillatory errors.

Four algorithms that can be used to identify the upper and lower bounds of the drop/bubble size domain over which the PB equations can be integrated were assessed. They included:

- limiting the integration range at the drop size where the net rate of change is less than 0.01% of the maximum net rate, or
- limiting the integration range at the drop size where the number density is less than 0.01% of the maximum number density, or
- limiting the integration range at the drop size where the net rate of change starts to oscillate,
- limiting the integration range at the drop size where the number density starts to oscillate.

When a large number of intervals was used (e.g. M >40), all methods gave almost the same degree of accuracy; whereas in the case of small number of sampling points (e.g. M = 10), the least error was achieved by limiting the integration range at the drop size where the number density is less than 0.01% of the maximum number density.

In this investigation, the upper boundary of the drop/bubble size domain was therefore identified as being the smaller of two diameters: that above which the number density becomes insignificant as compared to the DSD mode (a relative number density of 10^{-4} was used as the cut-off criterion), or the drop size where the number density starts to oscillate.

In cases where large spatial variation in the value of the local energy dissipation rate exists, the minimum drop diameter needed to accurately represent the size distribution of the dispersed phase can vary dramatically between regions of high and low energy dissipation rates (reaching values as low as 1 μm). Because of this, the lower limit of the DSD was kept unchanged in the current work. For cases where the DSD shows oscillatory instabilities at the lower drop sizes such as those described by Hounslow (1990) a similar approach to that described for the identification of the upper bound of the drop size domain could be applied at those lower boundaries. However, instead of cutting off the distribution at the point where oscillations start, a general extrapolation technique was applied to ensure the continuity and smoothness of the distribution.

In order to keep the finite domain error to a minimum, grid refinement was continuously undertaken whenever the maximum drop/bubble diameter was relocated to a new value. Since it was desirable to maintain the number of sample points at the preselected value, the location of the sampling points was changed by re-adjusting the size of the interval at which they are selected.

4.3.2 Concurrent Conservation of Drop Volume and Mass

Discretization of the DSD is expected to introduce minor errors with regard to the dispersed phase volume, but the cumulative effect of this error increases in significance with integration time; corrective measures need to be applied in order to ensure that the principle of volume conservation is not violated. The situation becomes more complex when PB are used to simulate particle aggregation processes where, in addition to the aforementioned problem, it is necessary to simultaneously meet the mass and volume conservation requirements for solid particles where the larger aggregates might have a density that changes with the aggregate volume (Al Taweel et al, 2008). In this investigation, attention is focused on bubbles and drops where the density of all the dispersed phase entities remains constant, and volume and mass conservation was mathematically maintained by continuously monitoring the total volume of the dispersed phase present within the integration domain and comparing it with that originally present in the dispersion. Whenever the dispersed phase mass deviated by more than 0.01% of its initial value, the difference was distributed over the whole set of sample points present within the upper and lower bounds in accordance to the volume fraction at each point.

4.4 Algorithm Validation

Whereas it is relatively easy to test the stability of the numerical solution algorithm, it is necessary to test the numerical solution results against analytical or known solutions of the PB equations in order to determine the accuracy of the proposed algorithm. Unfortunately, analytical solutions are rare and include major simplifying assumptions that are not met in practice and do not truly reflect the complex mathematical structures encountered in PBE when realistic breakage and growth kernels are used. Consequently, the accuracy and stability of the algorithm developed in this investigation was tested

using the kernels developed by Rod and Misek (1982) as well as those of Coulaloglou and Tavlarides (1977).

4.4.1 Modeling Drop/Bubble Breakage and Coalescence in Turbulently Flowing Dispersions

In their attempt to describe immiscible liquid dispersion in mechanically agitated tanks, Rod and Misek (1982) developed a set of simplified breakage and coalescence kernels given by,

$$g(d) = K_b \cdot d^{3(p+1)} \tag{4.3}$$

$$\beta(d,d') = 3\frac{d^2}{d'^3} \tag{4.4}$$

$$h(d,d') = K_c \cdot \left(d^3 + d'^3\right)^p \tag{4.5}$$

The simplified kernels adopted in their study, and the assumption that the DSD follows a normal distribution, enabled for the development of an analytical solution (for the case of $p = 0$ only) that yields the temporal variation of the mean drop size as well as the quasi-steady-state equilibrium value. Although the breakage functions (Eq. (4.3) and (4.4)) account for the drop diameter for the case of $p = 0$, the simplified coalescence expression used by them (Eq. (4.5)) depicts no dependency on drop diameter when $p = 0$.

The impact of using the complex mathematical structures encountered in realistic breakage and growth kernels on the stability and accuracy of the proposed algorithm was investigated using the phenomenological model of Coulaloglou and Tavlarides (1977). This model assumes that both phases are moving at the same mean velocity in a locally homogeneous and isotropic turbulence field, a condition that is encountered in many real situations. Furthermore, this approach constituted the basis from which most of the gas-liquid and liquid-liquid breakage and coalescence models in turbulently flowing dispersions were derived (e.g. Lee et al., 1987; Prince and Blanch, 1990; Luo and Svendsen, 1996).

4.4.1.1 Breakage sub-processes

For an isothermal system with no inter-phase mass transfer or reaction taking place, the breakage frequency of fluid particles the size of which lies in the inertial sub-range is given by,

$$g(d) = C_1 \cdot \frac{\varepsilon^{1/3}}{d^{2/3} \cdot (1+\phi)} \cdot \exp\left[-C_2 \cdot \frac{\sigma(1+\phi)^2}{\rho_d \cdot \varepsilon^{2/3} \cdot d^{5/3}} \right] \tag{4.6}$$

In addition, the number of daughter drops/bubbles represented by breakage term, $v(d')$, is usually assumed to be two (i.e. binary breakage) which is also in agreement with the observations of Andersson and Andersson (2006) who reported a very high probability (> 95%) for the occurrence of binary breakage in gas-liquid systems, while stating that such an assumption remains a reasonable one for liquid-liquid systems. This is also in accordance with the work of Maass et al. (2007) who reported that binary breakage has the highest probability of occurrence for drops with sizes smaller than 1 mm in liquid-liquid systems. However, this issue remains unsettled for the case of liquid-liquid systems where contradicting conclusions can often be found in the literature. This is due to the fact that the viscosity of the dispersed phase has a large impact in determining the number of daughter drops/bubbles born in a single breakage event (Podgorska, 2006; Tcholakova et al., 2007).

Furthermore, the size distribution of the fragments formed upon breakup must be specified to fully describe the breakage process and several probability density functions have been used for that purpose. In this investigation, the following beta distribution function proposed by Hsia and Tavlarides (1980) was used instead of the normal distribution originally proposed by Coulaloglou and Tavlarides (1977) because of the ability of the former to completely account for the total volume of the fragments within the upper and lower bounds.

$$\beta(d,d') = 90 \cdot \frac{d^2}{d'^3} \cdot \left(\frac{d^3}{d'^3} \right)^2 \cdot \left(1 - \frac{d^3}{d'^3} \right)^2 \tag{4.7}$$

This distribution produces a zero probability for the formation of infinitely small daughter bubbles/drops and a high probability for the evolution of equi-sized bubbles/drops. Other distributions, such as those proposed by Tsouris and Tavlarides (1994) or Luo and Svendsen (1996), were not used as they predict that the probability of breaking the parent particle into a very small particle and a complementary large particle is larger than the probability of equal-size breakage. This is in contradiction with the experimental observations of Risso and Fabre (1998) who reported that the probability of equi-sized breakage is highest for gas-liquid systems. The contradictory experimental observations reported in the literature dealing with liquid-liquid dispersions (Podgorska, 2006; Maass et al., 2007; Tcholakova et al., 2007) indicate that further experimental investigation is needed in order to reliably determine the factors affecting the number of daughter drops formed under turbulent breakage conditions and the probability distribution functions of such daughter drops.

4.4.1.2 Coalescence sub-processes

The binary coalescence rate between drops/bubbles entrained in turbulent flows is usually expressed as the product of collision frequency and coalescence efficiency terms. In a locally isotropic field, the collision frequency of drops was modeled by Coulaloglou and Tavlarides (1977) in analogy with the collision of molecules as described in the kinetic theory of gases. The collision frequency of drops of diameter d and d' and their coalescence efficiency can thus be written as,

$$h(d,d') = C_3 \cdot (d+d')^2 \cdot \left(d^{2/3} + d'^{2/3} \right)^{1/2} \cdot \frac{\varepsilon^{1/3}}{(1+\phi)} \tag{4.8}$$

$$\lambda(d,d') = \exp\left[-C_4 \cdot \frac{\mu_c \cdot \rho_c \cdot \varepsilon}{\sigma^2 \cdot (1+\phi)^3} \cdot \left(\frac{d \cdot d'}{d+d'} \right)^4 \right] \tag{4.9}$$

where the initial film thickness and the critical thickness for film rupture in the efficiency term are assumed to be constant and lumped into the value of the parameter C_4.

4.4.1.3 Estimating quasi-steady state mean diameter

In order to have confidence in the algorithm developed and test its validity, it is necessary to determine the errors arising from a comparison with known analytical solutions. Unfortunately, there are very few analytical solutions for the PBE and they are usually obtained at the expense of major simplifying assumptions. The few solutions that exist are usually derived for special cases (typically, a batch stirred vessel in which either breakage or coalescence dominates; Scott, 1968; Bajpai and Ramkrishna, 1976; Ziff and Mcgrady, 1985), with even fewer ones in which both breakage and coalescence were simultaneously considered (e.g. Rod and Misek, 1982; Patil and Andrews, 1998). In order to eliminate ambiguity that might arise from the use of such case specific solutions, and because of the need to minimize and eliminate any additional sources of errors, it was important to keep conformity with the model selected for testing the validity of the algorithm; namely, the aforementioned Coulaloglou and Tavlarides model.

By assuming the DSD to be monodispersed and setting coalescence and breakage rates as equal, Alopaeus et al. (1999) were able to reach an estimate of the quasi-equilibrium Sauter mean diameter using the Coulaloglou and Tavlarides model breakage and coalescence terms. An estimate of the Sauter mean diameter can be obtained by solving the following equation.

$$\ln\left(10.8308\cdot\phi\cdot\frac{C_3}{C_1}\right)=C_4\cdot\frac{\mu_c\cdot\rho_c\cdot\varepsilon}{\sigma^2\cdot(1+\phi)^3}\cdot\left(\frac{d_{32,e}}{2}\right)^4-C_2\cdot\frac{\sigma\cdot(1+\phi)^2}{\rho_d\cdot\varepsilon^{2/3}\cdot d_{32,e}^{5/3}} \qquad (4.10)$$

In the absence of analytical solutions, this estimate of d_{32} was used to provide an indication about the accuracy of the numerical solution, and will be referred to hereafter as the estimated d_{32}, and denoted, $d_{32,\,e}$. Under given hydrodynamic conditions and system properties, and for any set of model constants, there exists one real solution to the aforementioned polynomial equation (Eq. (4.10)); thus, the value of $d_{32,\,e}$ can be calculated independently of the PBE solution using any polynomial root-finding algorithm or commercial software.

4.4.2 Identifying the Stability and Accuracy Limits of the Previous Algorithm

Preliminary investigations using the algorithm previously developed by Al Taweel et al. (2002) indicated that, whereas it yields stable and accurate solutions at relatively low energy dissipation rates, instabilities and inaccuracies are introduced at higher energy dissipation rates. The extent to which these errors are introduced was found to depend on the breakage and aggregation kernels used and the hydrodynamic conditions investigated. A systematic investigation of this issue was therefore undertaken using the behaviour of a turbulently flowing liquid-liquid dispersion (the characteristics of which are given in Table 4.1) which is suddenly exposed to a step change in local energy dissipation rate. Both breakage-dominated and coalescence-dominated conditions were investigated while assuming the turbulence to be locally homogeneous and isotropic. The model parameters encountered in Eq. (4.6), (4.8) and (4.9) were allocated the values shown in Table 4.2 which are typical for liquid-liquid dispersions flowing through regions where the energy dissipation rate fluctuates between drastically high and low values.

Table 4.1: Experimental conditions

Property	*Value*	*Units*
Continuous phase density, ρ_c	1000	kg/m^3
Dispersed phase density, ρ_d	810	kg/m^3
Continuous phase viscosity, μ_c	0.001	kg/m.s
Interfacial tension, σ	19	mN/m
Dispersed phase hold-up, ϕ	0.5, 5	(%)
Energy dissipation rate, ε	10 to 1,000	W/kg

Under breakage-dominated conditions, Figure 4.7 clearly shows that there were no problems while using the algorithm developed by Al Taweel et al. (2002) for solving the PBE at low to moderate energy dissipation rates (ε = 100 W/kg). However, under high shear rates, e.g. ε = 1,000 W/kg, the temporal evolution of the numerical solution was found to depend heavily on the breakage distribution function. The solution obtained using the normal distribution function proposed by Coulaloglou and Tavlarides (1977) showed an erroneous behaviour before reaching quasi-steady state. This problem was

however eliminated by using the beta distribution function of Hsia and Tavlarides (1980). The beta distribution was therefore adopted hereafter while describing the breakage processes. It is also interesting to note that the Sauter mean diameter estimate of Alopeaus et al. (1999) provided a very reasonable indication of the quasi-equilibrium drop size value obtained under the different hydrodynamic conditions and daughter drop size distributions favouring equi-sized breakage.

Table 4.2: Values of the various model constants

Description	Symbol	Value
First breakage frequency constant	C_1	1.0
Second breakage frequency constant – *embedded in the exponential term*	C_2	4.1
Collision frequency constant	C_3	0.1
Coalescence efficiency constant	C_4	1×10^9

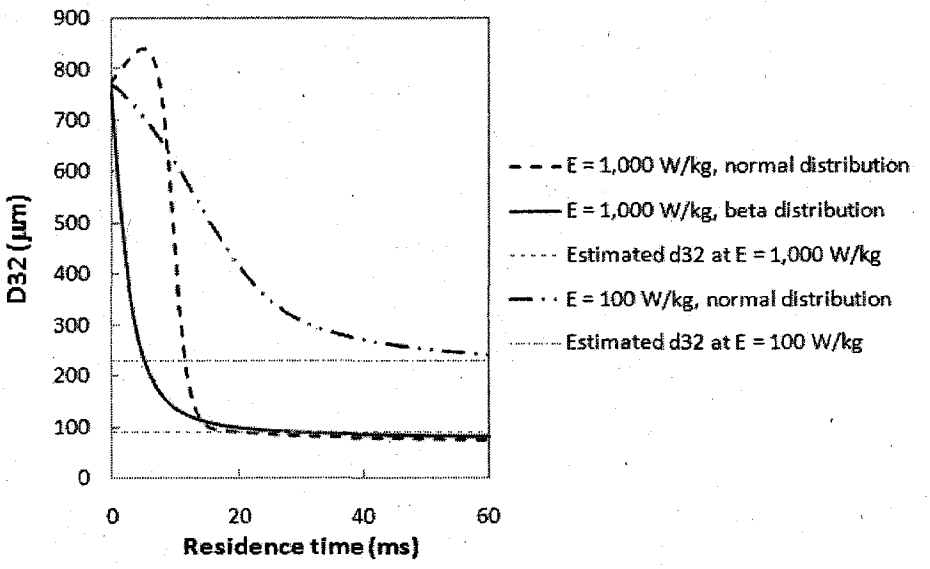

Figure 4.7: Temporal variation of the Sauter mean diameter under breakage dominated conditions (obtained using the algorithm of Al Taweel et al. (2002), $\phi = 0.5\%$).

In order to study the coalescence dominated regime, the model constants depicted in Table 4.2 were kept unchanged; however, the dispersed phase volume fraction was

increased by 10-fold where the resulting higher drop population densities significantly increase drop collision and coalescence rates.

Similarly, it was found that the algorithm developed by Al Taweel et al. (2002), rendered a stable solution at low and moderate turbulent intensities under coalescence-dominated conditions (Figure 4.10). However, the solution did not converge under high energy dissipation rates; this could be attributed to the control algorithm used where only the relative number density was employed to determine the DSD boundaries. These findings clearly indicated the need for having a better criterion for identifying the DSD limits.

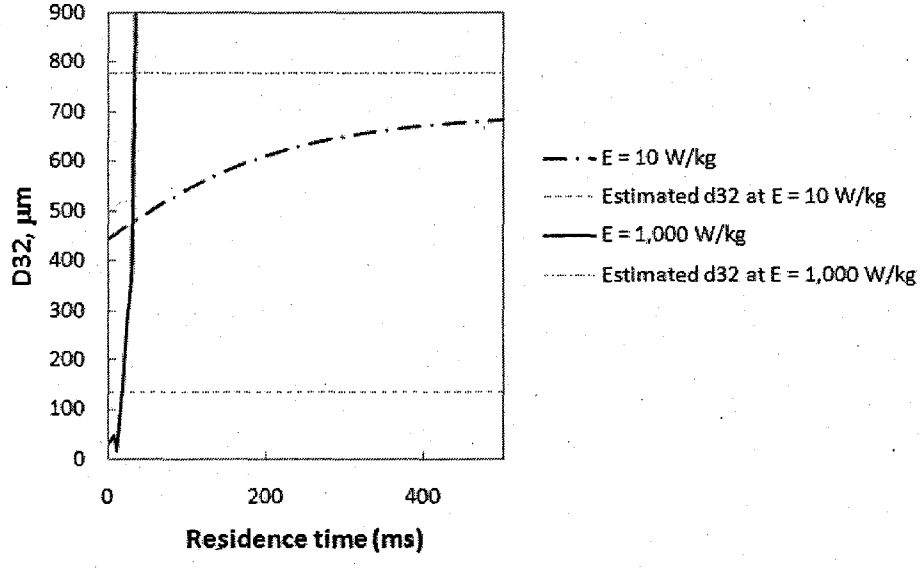

Figure 4.8: Temporal variation of the Sauter mean diameter under coalescence dominated conditions (obtained using only the relative drop number density approach for determining the upper limit, ϕ=5%).

4.4.3 Causes of the Numerical Instabilities

As previously discussed, the numerical solution of the discretized PBE is prone to errors of various sources; namely, truncation, round-off, feedback, and finite domain errors. If no remediation steps are implemented, such errors will propagate and amplify as time progresses, leading to a non-converging solution. Using the algorithm relying on the relative number density as the sole criterion for controlling the drop size domain was found to generate stable and accurate numerical solutions at energy dissipation rates as high as 100 W/kg (quite a feat considering that very few if any of the previously

developed algorithms and methods of solutions have been tested under such intense and demanding conditions). In spite of this, this algorithm failed under the extreme conditions of very high energy dissipation rates (ε = 1,000 W/kg) where the solution suffered from convergence problems.

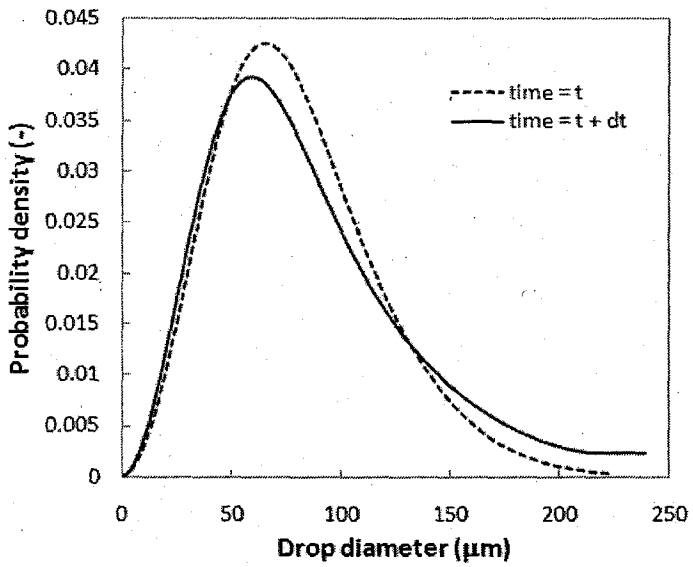

Figure 4.9: Typical temporal evolution of the DSD under coalescence dominated conditions at ε = 1,000 W/kg (using only the relative drop number density approach for determining the upper limit of the size domain).

The source of this difficulty was identified by carefully evaluating the temporal evolution of the DSD (Figure 4.9) where an unexplainable inflection in the drop probability density curves was found to take place. This instability was magnified at a rate that is much faster than what the algorithm relying on the relative number density as the sole criterion for controlling the drop size domain, could control. In order to alleviate this problem, its root causes were identified by monitoring the individual birth and death terms in the PBE and determining means by which such problems can be mitigated.

Figure 4.10a illustrates an example of such source of error which is encountered when the relative drop number density approach is used as the sole criterion for determining the upper limit of the size domain. Thus whereas the rate of bubble/drop formation by birth is supposed to asymptotically approach the value of zero at the upper and lower bounds of the drop size distribution, the presence of an inflection point is clearly evident at large drop diameters with an accelerating birth rate being predicted for drop diameters larger

than where the inflection takes place. Figure 4.10b shows similar behaviour for the case of death by coalescence terms; however, in this case, the tail drops back to zero at the largest drop diameter simply because it is an imposed boundary condition where it is assumed that the maximum drop diameter do not coalesce with smaller diameters. The combined effect of these two factors is responsible for the slight inflection observed in the DSD shown in Figure 4.9 where erroneously high concentrations of large diameter entities are predicted. This error is further propagated and amplified with every successive time step, leading the solution to diverge.

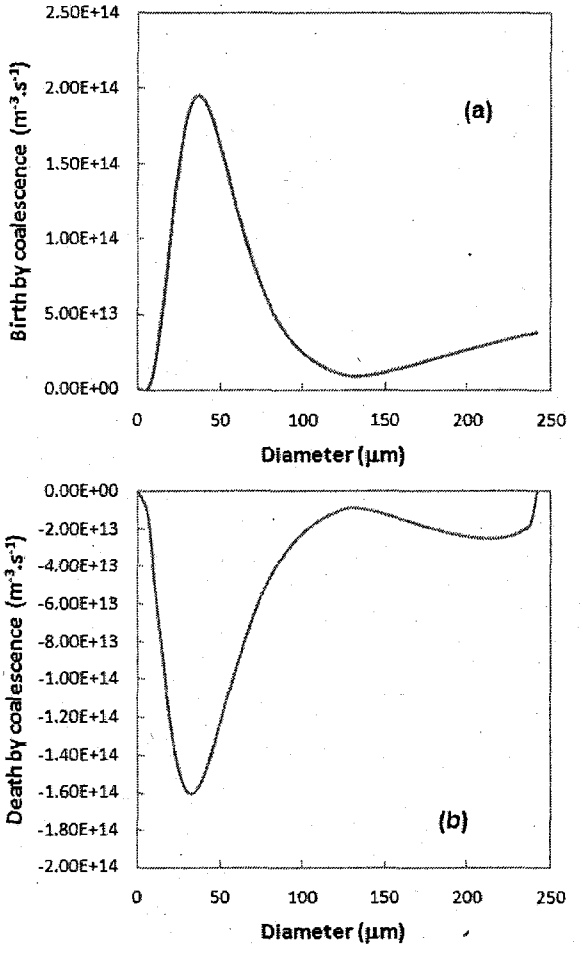

Figure 4.10: Typical birth and death by coalescence rates obtained at ε = 1,000 W/kg (using only the relative drop number density approach for determining the upper limit of the size domain).

4.4.3.1 Algorithm for enhanced stability

These aforementioned finite domain errors are inherent to the solution method adopted in this work, namely, the moving grid technique, where the upper limit of the size domain is

continuously changing with time. This problem is omnipresent when the grid does not adjust itself fast enough to accommodate the increase in large diameter entities. However, such problems should not be looked at as specific to the algorithm proposed in this work since they are encountered in most discretization solution techniques such as the fixed or moving grid techniques (Kumar and Ramkrishna, 1996 a,b; Attarakih et al., 2003, Alopaeus et al., 2008); where, the finite domain used to describe the drop size distribution, if not carefully selected and adjusted, will propagate these errors at a fast rate especially under coalescence dominated conditions.

To mitigate such problems, a more advanced stability and control algorithm is needed for the highly demanding conditions discussed in this investigation. This was accomplished using the algorithm depicted in Figure 4.11 which is based on a preliminary calculation of all the birth and death terms in the PBE. Every rate term (birth by breakage, death by breakage, birth by coalescence, and death by coalescence) is treated as a separate function and used to identify the onset of any instabilities/oscillations as well as to determine whether the drop size distribution needs to be expanded or not. This is accomplished by scanning the distribution of each rate term in order to identify its maximum value and ensuring that the drop size domain is large enough in order to minimize the introduction of errors and instabilities.

If the value of any of the four rate terms corresponding to the large diameters in the domain, does not fall below 1 % of its maximum value, the drop size domain needs to be expanded to accurately account for all birth and death terms. In order to keep the finite domain errors to a minimum by avoiding an unnecessary increase of the drop size domain, a 5% increase was applied whenever an expansion was required. The resulting expansion of the DSD domain will not affect the present one (which will retain its original shape) but adds new drop size samples to the computation domain that did not exist before. On the other hand, the consequent ability to fully account for the birth and death terms will reduce the introduction of instabilities and the finite domain errors to the solution.

Once the drop size domain requirements are met, and if no expansion was required, the algorithm also scans the four rate distributions to identify the presence of inflection

points at which any of the four rate terms start to change its slope at a diameter that is larger than the mode. The diameter at which this error source is observed is referred to as the "control point" and corrective action needs to be applied to the various birth and death terms in order to prevent this error source from propagating as integration proceeds. In the present investigation, this was accomplished by forcing the various rate distribution functions to asymptotically approach the value of zero at the upper bound of the drop size distribution. A cubic spline extrapolation is thus used to reconstruct the rate distribution for the region between the "control point" and the maximum drop diameters. The example qualitatively depicted in Figure 4.12 clearly shows how the birth and death rates by coalescence are successfully changed to meet the primary requisite of asymptotically approaching the value of zero at D_{max}.

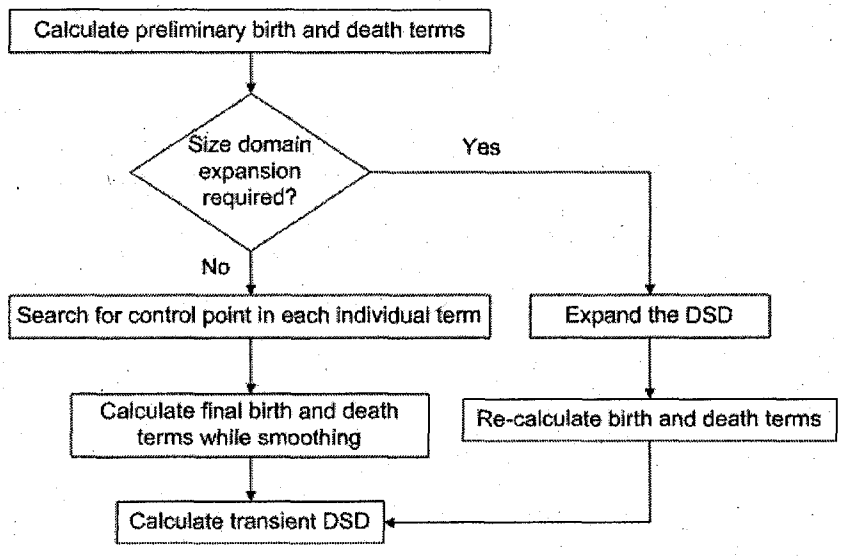

Figure 4.11: Algorithm for controlling instabilities in the individual birth and death terms

4.4.4 Effectiveness of the Proposed Stability Algorithm

The new algorithm introduced in this investigation relies on monitoring the onset of errors in the various birth and death terms encountered in PBE rather than monitoring the DSD as was the case of Al Taweel et al. (2002). It thus provides a much more sensitive indication of the numerical errors that can be introduced and allows for corrective action to be undertaken before the errors propagate in an uncontrollable fashion.

To test the validity and effectiveness of the proposed stability algorithm it is important to test this approach under conditions similar to those presented in the previous section. It was therefore tested using the case of a turbulently flowing liquid-liquid dispersion (the characteristics of which are analogous to those presented in Table 4.1) under breakage- and coalescence-dominated conditions. As shown in Figure 4.13, the numerical solution obtained by applying the new algorithm to breakage-dominated conditions yields a stable solution that is not significantly

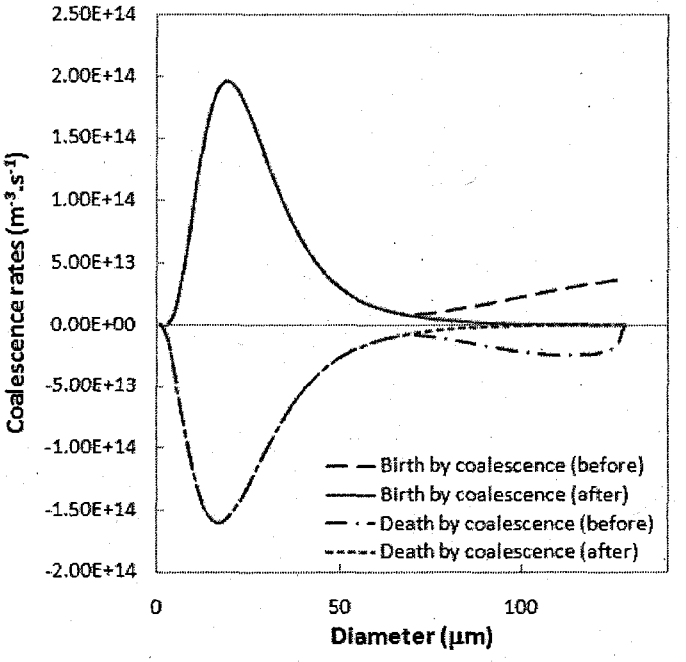

Figure 4.12: Location of the control point and smoothing of the birth and death rates

different from that obtained using the algorithm proposed by Al Taweel et al. (2002) even at energy dissipation rates as high as 1,000 W/kg. The calculated quasi-equilibrium Sauter mean diameters are also very close to the estimates proposed by Alopaeus et al. (1999).

The main advantage of using the new algorithm is, however, clearly evident when it is applied at high energy dissipation rates under coalescence-dominated conditions. As can be seen from Figure 14, the proposed algorithm yields stable solutions that converges smoothly to the quasi-equilibrium Sauter mean diameter which was reached within 50 milliseconds in the case where ε = 1,000 W/kg. This is a dramatic contrast with the results obtained using the algorithm proposed by Al Taweel et al. (2002) which resulted

in the development of unstable solutions at such high energy dissipation rates (Figure 4.8). Additional benefits of using the new algorithm are clearly illustrated in

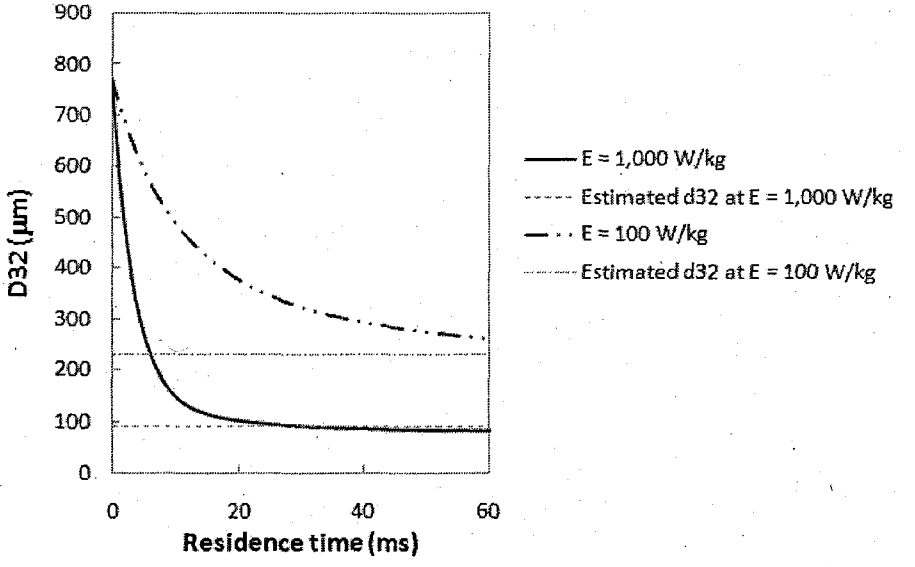

Figure 4.13: Temporal variation of the Sauter mean diameter under breakage dominated conditions using the enhanced solution stability algorithm ($\phi = 0.5$ %).

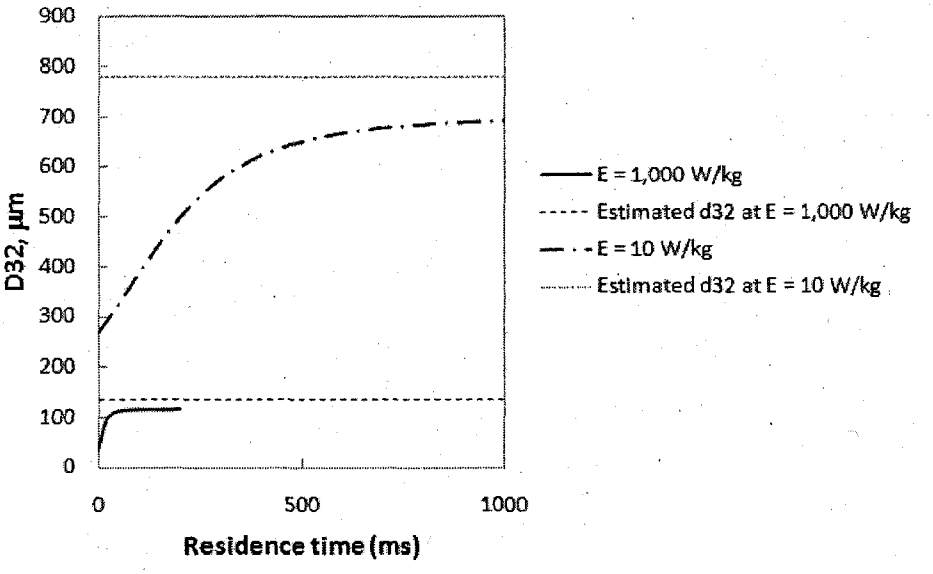

Figure 4.14: Temporal variation of the Sauter mean diameter under coalescence-dominated conditions using the enhanced solution stability algorithm ($\phi = 5\%$)

Figure 4.15 which shows that, under the coalescence-dominated conditions encountered at ε = 1,000 W/kg due to the sudden increase in dispersed phase concentration, the initial

drop size distribution evolves into a much coarser one with the mean diameter increasing by a factor of almost 3 in that case.

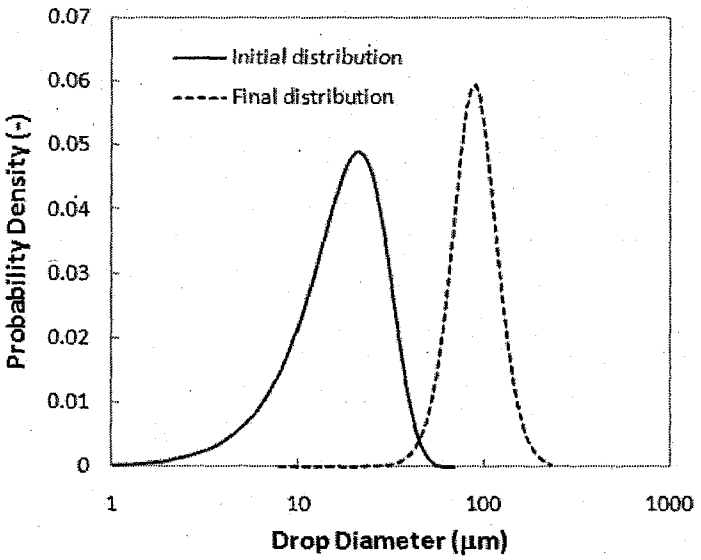

Figure 4.15: Temporal evolution of the DSD under coalescence dominated conditions at high ε (ε = 1,000 W/kg) using the enhanced solution stability algorithm.

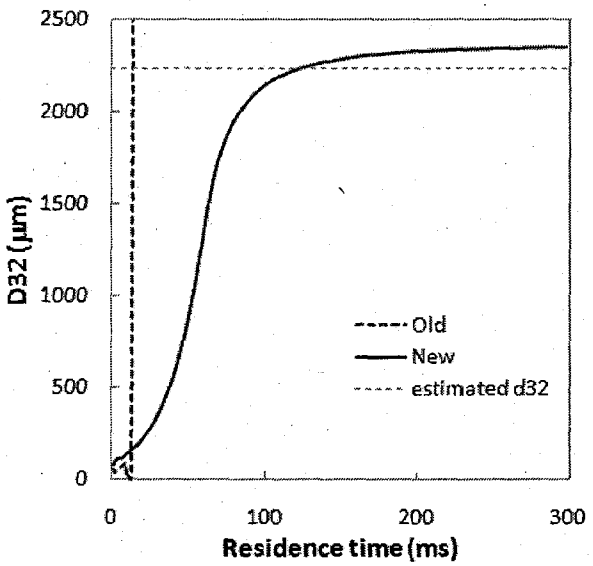

Figure 4.16: Comparison between the temporal variations of the Sauter mean diameter under coalescence dominated conditions using the different solution methods (ε = 1 W/kg, coalescence frequency increased by 3 orders of magnitude, C_3 = 100).

The advantage of using the new algorithm is further illustrated by its ability to predict even larger changes in the mean diameters under coalescence-dominated conditions. For

example, in the case of rapidly coalescing systems (simulated by increasing the value of the coalescence rate constant C_3 from 0.1 to 100), a 30-fold increase in the value of the equilibrium Sauter mean diameter was predicted using the new algorithm (Figure 4.16). On the other hand, the previous algorithm became numerically unstable under such high coalescence rates.

The ability of the new algorithm to cope with the numerical demands encountered when the dispersion is exposed to sudden changes in the local energy dissipation is clearly illustrated in Figure 4.17 where the new algorithm accurately predicted a 23-fold reduction in the value of d_{32} when the flowing dispersion is suddenly exposed to a very high shear rate region where ε = 10,000 W/kg. Under such severe conditions, even the previously stable algorithm developed by Al Taweel et al. developed numerical instabilities and failed to converge.

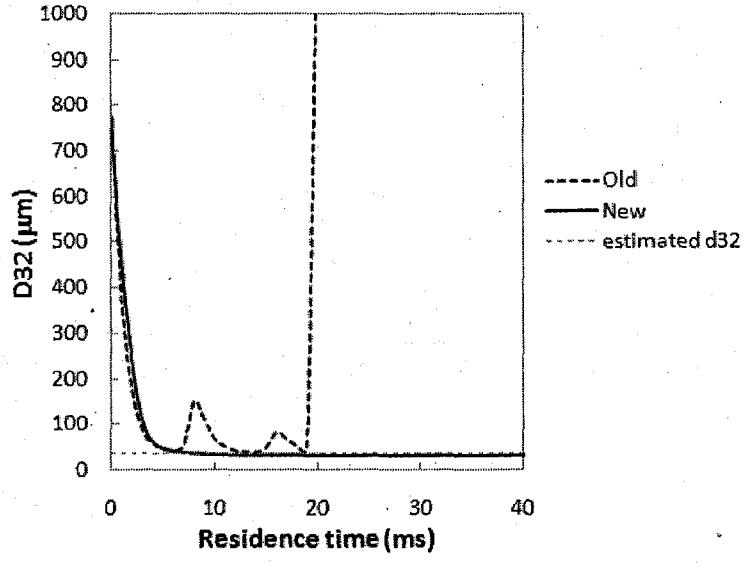

Figure 4.17: Effect of the numerical algorithm on the temporal variations of the Sauter mean diameter under breakage-dominated conditions (ε = 10,000 W/kg).

The raw data used in the present analysis, in addition to other related curves, are included in Appendix C.

4.5 Conclusions

A methodology for solving the discretized population balance equation was developed in this work. This method is built on the algorithm developed by Al Taweel et al. (2002) and is based on the use of the size distribution sampling approach proposed by Sovova and

Prochazka (1981) combined with a moving grid technique. Using this approach for solving the PBE, the finite domain errors resulting from discretization were reduced if not eliminated while maintaining optimum drop size integration ranges to describe the population. The resulting partial-integro differential equation was subsequently evaluated using commonly available integration schemes while simultaneously conserving mass and volume. In addition, an enhanced solution stability algorithm was proposed and which relies on monitoring the onset of errors in the various birth and death terms encountered in PBE. It consequently provides a much more sensitive indication of the numerical errors that can be introduced and allows for corrective action to be undertaken before the errors propagate in an uncontrollable fashion.

This method was tested under breakage and coalescence dominated conditions and was found to render a highly stable solution under low, moderate and high shear rate conditions. It should be stressed that while the solution methodology proposed by Al Taweel et al. (2002) was found unstable under very high turbulence intensity conditions, that method has proven itself stable, robust and accurate under conditions of low to moderate energy dissipation rates.

Acknowledgment

The authors would like to acknowledge the financial support of the Natural Science and Engineering Research Council of Canada (NSERC).

4.6 Nomenclature

$A(d,t)$	Probability density of a drop/bubble of diameter d at time t	$[m^{-3}.s^{-1}]$
B_b	Rate of particle generation by breakage per unit volume	$[m^{-3}.s^{-1}]$
B_c	Rate of particle generation by coalescence per unit volume	$[m^{-3}.s^{-1}]$
$C_{1\text{-}3}$	Empirical constants	[–]
C_4	Coalescence efficiency constant	$[m^{-2}]$
d	Drop/bubble diameter	[m]
D_b	Rate of particle destruction by breakage per unit volume	$[m^{-3}.s^{-1}]$
D_c	Rate of particle destruction by coalescence per unit volume of a parent particle	$[m^{-3}.s^{-1}]$

$g(d')$	Breakage frequency of drops of diameter d'	$[s^{-1}]$
$h(d,d')$	Coalescence intensity of drops of diameter d and d'	$[s^{-1}]$
n	number density probability	$[m^{-4}]$
$N(t)$	Total number of drops/bubbles	[–]
r	Radial coordinate	[m]
t	Residence time	[s]
u_p	Particle velocity	$[m.s^{-1}]$
x	drop/bubble diameter	[m]

Greek Letters

$\beta(d,d')$	Probability that a drop of size d' is formed when a drop d breaks	[–]
ε	Energy dissipation rate	$[m^2.s^{-3}]$
$\lambda(d,d')$	Coalescence efficiency	[–]
μ	Dynamic viscosity	$[kg.m^{-1}.s^{-1}]$
$\nu(d)$	Number of daughter drops formed by breakage of drop d	[–]
ρ	Density	$[kg.m^{-3}]$
σ	Static surface tension	$[N.m^{-1}]$
ϕ	Dispersed phase volume fraction	[–]

Subscripts

c	continuous phase
d	dispersed phase

4.7 References

Al Taweel A.M., F. Azizi, K. Podila and A. Speers, "In-Line Processing for the Production of Large Compact Flocs", Technical report submitted to the Energy Technology Centre, CANMET, Devon Alberta (2008).

Al Taweel, A.M., Webber, J.R., Devavarapu, R.C., Gupta, Y.P., Elsayed, A.S.I., "An algorithm for accurately solving population balance problems", Alexandria Eng. J., **41**, 1069-1075 (2002).

Alexopoulos, A.H. , Roussos, A.I., Kiparissides, C., "Part I: Dynamic evolution of the particle size distribution in particulate processes undergoing combined particle growth and aggregation", Chem. Eng. Sci., **59**, 5751–5769 (2004).

Alopaeus, V., Koskinen, J., Keskinen, K.I., "Simulation of the population balances for liquid-liquid systems in a nonideal stirred tank. Part 1. Description and qualitative validation of the model", Chem. Eng. Sci., **54**, 5887-5899 (1999).

Alopaeus, V., Laakkonen, M., Aittamaa, J., « Solution of population balances with breakage and agglomeration by high-order moment-conserving method of classes", Chem. Eng. Sci., **61**, 6732-6752 (2006).

Alopaeus, V., Laakkonen, M., Aittamaa, J., "Solution of population balances with growth and nucleation by high order moment-conserving method of classes", Chem. Eng. Sci., **62**, 2277-2289 (2007).

Alopaeus, V., Laakkonen, M., Aittamaa, J., "Solution of population balances by high order moment-conserving method of classes: reconstruction of a non-negative density distribution", Chem. Eng. Sci., **63**, 2741-2751 (2008).

Andersson, R.., Andersson, B., "On the breakup of fluid particles in turbulent flows", AIChE J., **52**, 2020-2030 (2006).

Attarakih, M., Fara, D.A., Sayed, S., "Dynamic modeling of a packed-bed glycerol - Water distillation column", Ind. Eng. Chem. Res., **40**, 4857-4865 (2001).

Attarakih, M.M., Bart, H., Faqir, N.M., "Numerical solution of the spatially distributed population balance equation describing the hydrodynamics of interacting liquid-liquid dispersions", Chem. Eng. Sci., **59**, 2567-2592 (2004).

Attarakih, M.M., Bart, H.-., Faqir, N.M., "Optimal moving and fixed grids for the solution of discretized population balances in batch and continuous systems: Droplet breakage". Chem. Eng. Sci., **58**, 1251-1269 (2003).

Azizi, F., Al Taweel, A.M., "Reliable Design of Industrial Multiphase Contactors/Reactors", Paper presented at the North American Mixing Forum, Mixing XX; Parksville, BC, Canada, (2005).

Azizi, F., Al Taweel, A.M., "Population balance simulation of intensified gas-liquid contacting", Chem. Eng. Sci., **62**, 7436-7445 (2007).

Azizi, F., Al Taweel A.M., "Hydrodynamics of liquid flow through screens and screen-type static mixers", Submitted for publication in Chem. Eng. Comm. (2008).

Bajpai, R.K., Ramkrishna, D., Prokop, A., "A coalescence redispersion model for drop-size distributions in an agitated vessel", Chem. Eng. Sci., **31**, 913-920 (1976).

Balliu, N.E., Cameron, I.T., Newell, R., "A comparative study of numerical methods for solving continuous population balance models for aggregation processes", Dev. Chem. Eng. Min. Proc., **12**, 277-291 (2004).

Batterham, R.J., Hall, J.S., Barton, G., "Pelletizing kinetics and simulation of full-scale balling circuits". Proceedings of the 3rd International Symposium on Agglomeration, Nurnberg, Germany, A136 (1981).

Campos, F.B., Lage, P.L.C., "A numerical method for solving the transient multidimensional population balance equation using an Euler-Lagrange formulation", Chem. Eng. Sci, **58**, 2725-2744 (2003).

Chen, P., Sanyal, J., Dudukovic, M.P., "Numerical simulation of bubble columns flows: Effect of different breakup and coalescence closures", Chem. Eng. Sci., **60**, 1085-1101 (2005).

Calabrese, R.V.; Cheng, S.-H.; Lin, J.-C.; Gentry, J.W., "Effect of kernel on aggregation of coalescence of large clusters", Part. Sci. Tech., 13, (1995).

Coulaloglou, C.A., Tavlarides, L.L., "Description of interaction processes in agitated liquid-liquid dispersions", Chem. Eng. Sci., **32**, 1289-1297 (1977).

Diemer, R.B., Olson, J.H., "A moment methodology for coagulation and breakage problems: Part 2-Moment models and distribution reconstruction", Chem. Eng. Sci., **57**, 2211-2228 (2002).

Dorao, C.A., Jakobsen, H.A., "A least squares method for the solution of population balance problems", Comp. Chem. Eng., **30**, 535-547 (2006).

Gelbard, F., Seinfeld, J.H., "Numerical solution of the dynamical equation for particulate systems", J. Comp. Phy., **28**, 357–375 (1978).

Hounslow, M.J., "Discretized population balance for continuous systems at steady state", AICHE J., **36**, 106-116 (1990).

Hsia, M. A.; Tavlarides, L. L., "Simulation Model for Homogeneous Dispersions in Stirred Tanks", Chem. Eng. J. Biochem. Eng. J., **20**, 225-236 (1980).

Jairazbhoy, V., Tavlarides, L.L., "Numerical technique for the solution of integrodifferential equations arising from balances over populations of drops in turbulent flows", Comp. Chem. Eng., **23**, 1725-1735 (2000).

Jakobsen, H.A., Lindborg, H., Dorao, C.A., "Modeling of bubble column reactors: progress and limitations", Ind. Eng. Chem. Res., **44**, 5107-5151 (2005).

Kumar, S., Ramkrishna, D., "On the solution of population balance equations by discretization - I. A fixed pivot technique", Chem. Eng. Sci., **51**, 1311-1332 (1996a).

Kumar, S., Ramkrishna, D., "On the solution of population balance equations by discretization - discretization - II. A moving pivot technique", Chem. Eng. Sci., 51, 1333-1342 (1996b).

Laakkonen, M., Alopaeus, V., Aittamaa, J., "Validation of bubble breakage, coalescence and mass transfer models for gas-liquid dispersion in agitated vessel", Chem. Eng. Sci., **61**, 218-228 (2006).

Laakkonen, M., Moilanen, P., Alopaeus, V., Aittamaa, J., "Modelling local bubble size distributions in agitated vessels", Chem. Eng. Sci., **62**, 721-740 (2007).

Lasheras, J.C., Eastwood, C., Martinez-Bazan, C., Montanes, J.L., "A review of statistical models for the break-up an immiscible fluid immersed into a fully developed turbulent flow", Int. J. Multiphas Flow, **28**, 247-278 (2002).

Lee, C.K., Erickson, L.E., Glasgow, L.A., "Bubble breakup and coalescence in turbulent gas-liquid dispersions", Chem. Eng. Comm., **59**, 65-84 (1987).

Litster, J.D., Smit, D.J., Hounslow, M.J., "Adjustable discretized population balance for growth and aggregation", AICHE J., **41**, 591-603 (1995).

Luo, H., Svendsen, H.F., "Theoretical model for drop and bubble breakup in turbulent dispersions", AICHE J., **42**, 1225-1233 (1996).

Maaß, S., Gäbler, A., Zaccone, A., Paschedag, A.R., Kraume, M., "Experimental investigations and modeling of breakage phenomena in stirred liquid/liquid systems", Chem. Eng. Res. Des., **85**, 703-709 (2007).

Marchisio, D.L., Fox, R.O., "Solution of population balance equations using the direct quadrature method of moments". J. Aerosol Sci., **36**, 43-73 (2005).

Marchisio, D.L., J.T. Pikturna, R.O. Fox, R.D. Vigil and A.A. Barresi, "Quadrature Method of Moments for Population-Balance Equations", AICHE J., **49**, 1266-1276 (2003).

Motz, S., Mannal, S., Gilles, E., "Integral approximation - an approach to reduced models for particulate processes", Chem. Eng. Sci., **59**, 987-1000 (2004).

Motz, S., Mitrovic, A., Gilles, E., "Comparison of numerical methods for the simulation of dispersed phase systems". Chem. Eng. Sci., **57**, 4329-4344 (2002).

Nicmanis, M., Hounslow, M.J., "A finite element method for the steady state population balance equation", AIChE J., **44**, 2258–2272 (1998).

Nopens, I., Beheydt, D., Vanrolleghem, P.A., "Comparison and pitfalls of different discretised solution methods for population balance models: A simulation study", Comp. Chem. Eng., **29**, 367-377 (2005).

Patil, D.P., Andrews, J.R.G., "An analytical solution to continuous population balance model describing floc coalescence and breakage — A special case", Chem. Eng. Sci., **53**, 599-601 (1998).

Podila, K., Al Taweel, A.M., Koksal, M., Troshko, A., Gupta, Y.P., "CFD simulation of gas-liquid contacting in tubular reactors", Chem. Eng. Sci., 62, 7151-7162 (2007).

Podgorska, W., "Modelling of high viscosity oil drop breakage process in intermittent turbulence", Chem. Eng. Sci., **61**, 2986-2993 (2006).

Polprasert, G., Al Taweel, A.M.,Webber, J., Gupta, P., Elsayed, A.S.I., "Improving the stability and accuracy of population balance numerical solutions: I- methods of describing drop size distribution", Alexandria Eng. J., **41**, 1059-1067 (2002).

Press, W.H., Teukolsky, S.A., Vetterling, W.T., Flannery, B.P., "Numerical recipes in C: the art of scientific computing, Cambridge University Press, Cambridge (2002).

Prince, M.J., Blanch, H.W., "Bubble coalescence and break-up in air-sparged bubble columns", AICHE J., **36**, 1485-1499 (1990).

Qamar, S., Ashfaq, A., Angelov, I., Elsner, M.P., Warnecke, G., Seidel-Morgenstern, A., "Numerical solutions of population balance models in preferential crystallization", Chem. Eng. Sci., **63**, 1342-1352 (2008).

Ramkrishna, D., "Status of population balances", Rev. Chem. Eng., **3**, 49-95 (1985).

Ramkrishna, D., "Population Balances: Theory and Applications to Particulate Processes in Engineering", Academic Press, New York, NY (2000).

Risso, F., Fabre, J., "Oscillations and breakup of a bubble immersed in a turbulent field", J. Fluid Mech., **372**, 323 (1998).

Rod, V., Misek, T., 'Stochastic modelling of dispersion formation in agitated liquid-liquid systems", Trans. IChemE, **60**, 48-53 (1982).

Schmidt, S. A.; Simon, M.; Attarakih, M. M.; Lagar G., L.; Bart, H., "Droplet population balance modelling - Hydrodynamics and mass transfer", Chem. Eng. Sci., **61**, 246-256 (2006).

Scott, W.T., "Analytic studies of cloud droplet coalescence", J. Atm. Sci., **25**, 54-65 (1968).

Sovova, H., Prochazka, J., "Breakage and coalescence of drops in a batch stirred vessel - 1. comparison of continuous and discrete models", **36**, 163-171 (1981).

Tcholakova, S., Vankova, N., Denkov, N., Danner, T., "Emulsification in turbulent flow : 3. Daughter drop-size distribution", J. Col. Int. Sci., 310, 570-589 (2007).

Valentas, K.J., Amundson, N.R., "Breakage and coalescence in dispersed phase systems", Ind. Eng. Chem. Fund., **5**, 533-542 (1966).

Vanni, M., "Approximate Population Balance Equations for Aggregation–Breakage Processes", J. Col. Int. Sci., **221**, 143-160 (2000).

Venneker, B. C. H.; Derksen, J. J.; Van den Akker,Harrie E.A., "Population balance modeling of aerated stirred vessels based on CFD", AICHE J., **48**, 673-685 (2002).

Ziff, R.M., McGrady, E.D., "The kinetics of cluster fragmentation and depolymerisation", J. Phys. A: Mathematical and General, **18**, 3027-3037 (1985).

Chapter 5.
Turbulently Flowing Liquid-Liquid Dispersions. Part I: Drop Breakage and Coalescence

F. Azizi and A.M. Al Taweel*

Multiphase Mixing and Separation Research Lab, Department of Process Engineering and Applied Sciences, Dalhousie University, Halifax NS, Canada B3J 2X4 (Al.Taweel@Dal.Ca)

Submitted for publication in:
Chemical Engineering Science.
January 2009

Abstract

A successful attempt to simulate turbulently flowing liquid-liquid dispersions was undertaken in this work where the turbulent dispersion/coalescence of drops was accurately predicted over a wide range of operating conditions using the model developed by Coulaloglou and Tavlarides (1977). Experimental data obtained from an intensified liquid-liquid reactor/contactor in which screen-type static mixers were used to superimpose an adjustable uniformly-distributed turbulence field on the nearly plug flow conditions encountered in high velocity pipe flows were used to validate the model predictions.

Drop size distribution and the Sauter mean diameter (when quasi-steady state conditions were assumed to be reached) were compared with the experimental results measured by photographic techniques and good agreement was obtained at different flow velocities and diverse screen geometries.

The use of mutli-stage screen-type static mixers where alternating breakage-dominated and coalescence dominated regions exist allowed the development of accurate model

parameters that may be used for simulating other more complex liquid-liquid contacting conditions such as those encountered in MAT.

5.1 Introduction

Despite the extensive literature dealing with both the hydrodynamic and interface science aspects, the dispersion of immiscible liquids remains one of the most difficult and least understood mixing problems, where minor changes in the chemical composition of the system would drastically affect its performance (Paul et al., 2003). Consequently, the majority of the liquid-liquid contactors/reactors presently used are inefficiently designed with subsequent adverse effects on the reaction yield and selectivity and/or the mass transfer performance.

Stirred vessels, rotor–stator mixers, static mixers, valve or jet homogenizers, and extraction columns, are an example of industrial process equipments used to contact liquid–liquid systems. Due to the very complex hydrodynamic conditions prevalent in most of these commercially available contactors/reactors, designing such units is very difficult without an extensive employment of empiricism. However, the widespread use of empirical correlations poses several limitations as they conceal many of the hydrodynamic details and non-idealities (Bakker et al., 2001). Consequently, such results cannot be used over parameter ranges not included in the original measurement data set without the incorporation of excessive safety margins, thus requiring an extensive amount of pilot-scale testing. Therefore, a detailed understanding of the mixing process combined with the ability to accurately predict the volumetric mass transfer coefficient in such units can help in optimizing the performance, economy, and safety of these industrial systems.

Stirred tank reactors/contactors are the most commonly used in the chemical process industries, however, the operating conditions, the agitator and vessel geometry, as well as the positions of the inlet and outlet streams have direct impact on the tank's performance as they determine the hydrodynamics and turbulence intensities in the vessel. Nevertheless, these types of reactors suffer from many drawbacks as they lack uniformity, where mixing, drop size distributions, hold-up, and temperature profiles have large local variations (Andersson et al., 2004).

On the contrary, plug flow reactors serve as a better choice in order to understand the complex phenomena taking place as well as providing better performance and control over the mixing, breakage and coalescence of drops, as well as heat and mass transfer. Moreover, tubular reactors equipped with static mixers have been gaining strong momentum in the chemical industries as they present an attractive alternative to conventional agitation since similar and sometimes better performance can be achieved at lower cost (Thakur et al., 2003). A common feature of these reactors is that turbulence is continuously produced and dissipated along the reactor. The turbulence is more homogeneous and nearly isotropic compared to a stirred tank reactor where most turbulence is produced and dissipated in the impeller region. They also provide large interfacial area of contact, effective radial mixing and narrow residence time distribution (Turunen and Haario 1994; Al Taweel et al., 2003; Andersson et al., 2004). In addition, the mass transfer efficiency can be easily adjusted according to the requirements of the reaction. For example, using mixers that provide high energy dissipation allow the formation of small drop diameters which favours the processes with high reaction rates since they require large interfacial area of contact between the phases. Similar results can also be achieved by operating under high flow velocities. On the other hand, if the reaction is slow; lower interfacial areas and flow velocities would be sufficient. Likewise, inter-mixer spacing play also an important role in determining the extent of the reactions since they allow the control of the breakage and coalescence processes taking place where longer spaces favours the coalescence of the dispersion and shorter ones enhance the drop breakage.

Recently, a new type of static mixing element was introduced in which screens or grids are used to repetitively superimpose an adjustable uniformly-distributed turbulence field on the nearly plug flow conditions encountered in high velocity pipe flows. This characteristic made them particularly effective in processing multiphase systems and their ability to promote contact between immiscible liquids was found to be about 5-fold more energy efficient than mechanically agitated tanks equipped with Rushton-type impellers (Al Taweel and Chen, 1996). The very high turbulence intensities generated in the regions adjacent to the screens result not only in the formation of fine dispersed phase entities but also considerably enhance the value of the interphase mass transfer

coefficient. The combined effect of these two factors resulted in inter-phase mass transfer coefficients as high as 13 s^{-1} being achieved in the case of liquid-liquid dispersions (Al Taweel et al., 2007) and allow for 99% of equilibrium conditions to be achieved in less than 1 s. Furthermore, such high performance allowed for orders of magnitude reduction in the reactor volume when applied to desulfurization processes (Al Taweel et al., 2008b).

While phenomenological interpretations of the role that turbulence has on multiphase contacting, led to such performance improvements; the use of mathematical models that can accurately predict the temporal evolution of drop size distributions is essential to further optimize the performance of such multiphase contactors/reactors. This necessitates the use of population balance equations, PBE, to handle drop breakage and coalescence within various regions of the contactor, and the identification of the breakage/coalescence kernels that can accurately describe these processes.

The widespread use of PBE as a tool to describe dispersed phase operations emerged from its capability to describe drop breakage and coalescence processes in terms of identifiable physical parameters and operational conditions. However, the ultimate success of this approach relies on the ability of PBE to yield realistic and accurate description of the overall drop breakage/coalescence processes.

The objective of this work is to explore the possibility of using PBE to accurately simulate drop breakage and coalescence processes in turbulently flowing liquid-liquid dispersions taking place in multi-stage screen-type static mixers (where alternating breakage-dominated and coalescence dominated regions exist).

Furthermore, since the hydrodynamic conditions prevailing in screen-type static mixers closely approach those of isotropic homogeneous turbulence, the drop breakage/coalescence kernels identified in this investigation are expected to apply to other more complex hydrodynamic conditions (such as those encountered in MAT) provided that the contactor/reactor volume is subdivided into a large number of segments where isotropic homogeneous turbulence can be correctly assumed to prevail.

5.2 Drop Breakage and Coalescence in Turbulently Flowing Liquid-Liquid Dispersions

Information concerning the temporal variation of the dispersed phase characteristics (e.g. size, mass, temperature, age, and species concentration) can be obtained using the population balance equations, where the dispersed phase is considered as an assembly of drops whose individual identities are being continually destroyed and recreated by the dynamic processes occurring within the system. Under such conditions, the change in the interfacial area of contact between the phases is mainly affected by the hydrodynamics and the interfacial forces. In a two-phase turbulent flow, breakage and coalescence processes take place simultaneously until a quasi-equilibrium state is reached, where the dispersion and coalescence rates become comparable and no net changes in drop size and drop size distribution are observed.

Even though most of the breakage and coalescence models were developed using sound thermo-, and hydro-dynamical theories, most of their validation was conducted using data obtained in mechanically-agitated tanks where the complex hydrodynamics encountered in such units were often over-simplified by assuming perfectly mixed conditions with uniform energy dissipation rates. This deficiency was recently mitigated by sub-dividing the contactor volume into 2–24 compartments (Alopaeus et al., 1999; Alexopoulos et al., 2002; Wells and Ray, 2005; Laakkonen et al., 2006; Schmelter, 2008) where, different, but uniform value of the turbulent energy dissipation rate is assumed to exist in each compartment. The errors introduced from such a discretization approach are practically eliminated when CFD is used where the contactor volume is divided into a very large number of sub-regions. Unfortunately, most CFD tests used to test pertinent PB kernels suffer from the uncertainties associated with the use of incomplete inter-phase momentum closures, and turbulence modulation relations, needed to accurately describe the interaction between the phases in the Eulerian-Eulerian approach (Al Taweel et al., 2006).

In addition, the discrimination between the many expressions used to describe the sub-processes involved in the breakage and coalescence models cannot be properly

undertaken because of the lack of experimental results obtained under well-known and controlled hydrodynamic conditions (Eastwood et al., 2004, Laakkonen et al., 2007).

Conversely, most of the aforementioned hydrodynamic modeling difficulties are eliminated under the flow conditions encountered in multi-stage screen-type static mixers developed by Al Taweel and Chen (1996). The residence time distributions are very narrow (essentially plug flow) and the characteristics of the turbulence generated in the region downstream from each consecutive screen are well known. These mixers therefore offer a good alternative to conventional MAT mixers for developing and testing the various hydrodynamic models as they overcome the difficulties associated with the high spatial variations of the energy dissipation rates as well as flow recirculation non-uniformities. In addition, the nearly plug flow conditions present in the multi-stage screen-type contactor allow for the direct integration of the non-linear integro-differential equations obtained by applying the PBE, thereby eliminating any computational uncertainties and errors introduced through the use of CFD.

In the following sections, the hydrodynamic conditions prevalent in screen type static mixers are discussed with an emphasis on the models used for simulating drop breakage and coalescence in turbulent flows.

5.2.1 Modelling Energy Dissipation Rates in Screen Type Static Mixers

The rate of energy dissipation within the static mixer plays a crucial role in determining the drop size distribution of the emerging dispersion. The volume-average energy dissipation rate in the mixer can be calculated from the pressure drop using the following expression,

$$\varepsilon = \frac{U \cdot \Delta P}{\rho_c \cdot L_M} \tag{5.1}$$

However, it is well known that the local value of ε downstream from screens undergoes dramatic variation along the axis of flow with the maximum value being encountered in the immediate vicinity of the screen (Groth and Johansson, 1988; Briassulis et al., 2001). Screens can be characterized by their mesh size (M); bar size (b) (or wire diameter); and the fractional open area (α). Where, the turbulence structure generated downstream of the screen is controlled by the upstream superficial velocity as well as by those parameters. A relatively large body of knowledge is available concerning the nature of grid-generated

turbulence and how it is affected by the nature of flow as well as the wire mesh used (Gad-El-Hak and Corrsin, 1974; Groth and Johansson, 1988; Lance and Bataille, 1991; Zwart et al., 1997; Briassulis et al., 2001; Kang et al., 2003). However, the most distinctive characteristic of flow through screens is the generation of nearly isotropic turbulence in the downstream flow. Further, the decay of grid-generated turbulence is described by power laws such as:

$$\left(\frac{u'}{U}\right)^2 = \frac{1}{C}\left[\frac{x}{M} - \left(\frac{x}{M}\right)_0\right]^{-n} \tag{5.2}$$

Where C is the decay coefficient, $(x/M)_0$ is the virtual origin of turbulence decay, and n is the decay exponent.

The hydrodynamic factors affecting the performance of screen type static mixers were recently analyzed by Azizi and Al Taweel (Chapter 3) who proposed that the turbulence decay profile behind a grid be divided into two regions, a region of constant high energy dissipation rate prevalent over a certain distance downstream of the grid, and a region of

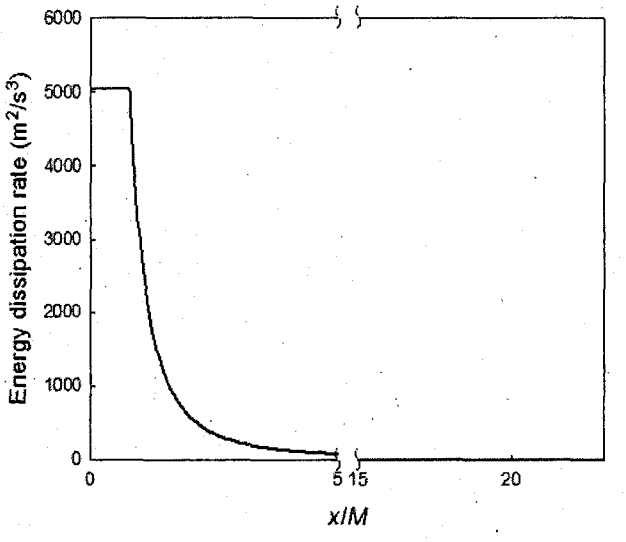

Figure 5.1: Rate of energy dissipation as a function of location downstream of a screen (U = 1.0 m/s, M = 362 μm, α = 0.33).

fast decay where the homogenous isotropic turbulence decay equation applies. Using this representation for modeling the spatial variation of the energy dissipation rate (Figure 5.1), all energy sources for the flow through screens were accounted for and the

calculated values matched the experimentally determined volume average ε data quite well.

The introduction of screens into the pipe flow will therefore create regions with very high energy dissipation the thickness of which depends on the screen characteristics (mesh size). However, the value of ε to which the fluid is exposed to is dramatically reduced as it flows further downstream from the screen (with up to 160-fold variation in ε being observed within a $7M$ distance downstream of the screen). The residence time within the region of high energy dissipation, and the maximum level of local energy dissipation rates encountered in these regions, are therefore a function of the screen characteristics and the superficial velocity of the fluid passing through them. Figure 5.2 shows such an example, whereas very high values of local energy dissipation rates can be achieved by passing fluids through screens (up to 15,000 W/kg for this example of a screen with 27 % open area), the corresponding residence time under such conditions is very short (as low as 420 μs) unless multiple screens are used.

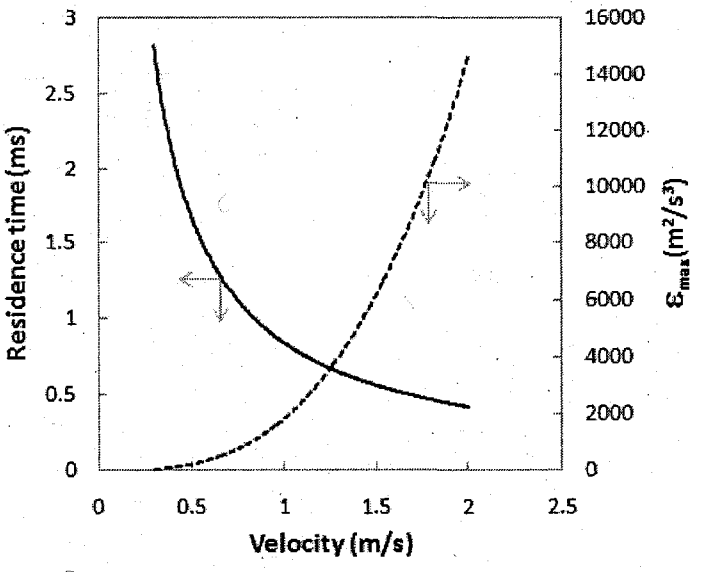

Figure 5.2: Effect of superficial velocity on the maximum energy dissipation rate and the residence time in the high energy dissipation regions (M = 1058 μm, α = 0.27).

Additional information concerning the values of these various parameters and the proposed approach for predicting the spatial variation of the energy dissipation rate downstream of a screen are reported elsewhere (Chapter 3).

5.2.2 Modelling of Breakage and Coalescence in Screen-type Static Mixers

A variety of processes taking place in turbulently flowing dispersions induces continuous changes in the internal properties of the dispersed phase droplets (e.g. size, concentration and age) which consequently lose their identities. For the case of a flowing dispersion exposed to regions of high and low energy dissipation rates, the drops undergo breakage in the regions of high turbulence intensity whereas they coalesce into coarser drops while circulating in low shear regions.

Generally, drop breakage results from the interaction of a single droplet and the turbulent continuous phase eddies; therefore, if the energy gained is enough to compensate for the surface energy increase due to the expansion of the droplet surface area, then break-up occurs. Further, coalescence occurs when two drops (or more) join together into one entity. Typically, this amalgamation process consists of three successive steps. First, drops have to collide, trapping a small amount of liquid between them, the second step involves drainage of the liquid out of the film trapped between the adjacent drop surfaces, while the third and final step is the rupture of the film, after reaching a critical thickness, leading to coalescence (Venneker et al., 2002). For a flowing dispersion, as time progresses, the breakage and coalescence rates change until reaching equilibrium where the rate of both processes become virtually equal. These phenomena describing the evolution of the dispersed phase drop size distribution (DSD) can best be expressed using the population balance approach.

In its most general form, the continuous PBE is a dynamic transport equation that describes the temporal evolution of population density as a result of four particulate mechanisms, namely, nucleation, growth, aggregation and breakage as well as transport due to the flow field (Rigopoulos and Jones, 2003). The resulting equations are often partial integro-differential equations with integral boundary conditions that rarely admit analytical solutions; therefore the use of numerical techniques is necessary for obtaining a solution (Mahoney and Ramkrishna, 2002; Attarakih et al., 2004; Azizi and Al Taweel, 2008b). Consequently, the method of discretization of the continuous PBE has emerged as an attractive alternative to the various other numerical methods of solutions (Kumar and Ramkrishna, 1996 a,b; Balliu et al., 2004) and has been successfully employed, starting with the work of Valentas and Amundson (1966), to render accurate numerical

solutions of the PBE (Alopaeus et al., 2002; Schmidt et al., 2006; Azizi and Al Taweel, 2007; Laakkonen et al., 2007).

For the case at hand, the flow within the multi-stage screen-type static mixer can be considered as radially uniform because of the flat velocity profiles induced by the screens and the relatively small spacing between consecutive elements. To accommodate the large axial variation in turbulence intensity and energy dissipation rates depicted in Figure 5.1, the hydrodynamic performance of the static mixer was modeled by dividing it into very thin cells where uniform isotropic hydrodynamic conditions can be correctly assumed to exist (Figure 5.3).

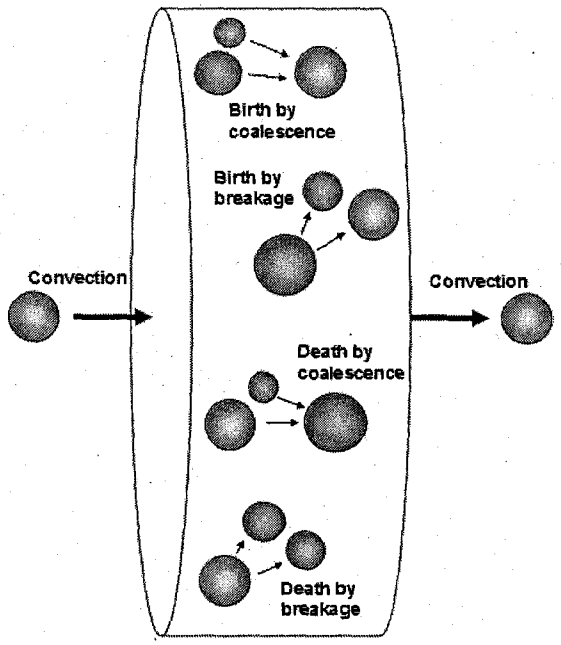

Figure 5.3: Schematic representation of the PBE cell

In the case of a well-mixed physical volume, in which there is no convection and no changes in temperature, concentration, and other internal variables are taking place, one is only concerned with dispersed phase breakage and coalescence occurrences in uniform spatial energy dissipation rate (Figure 5.3).

Under such conditions, the rate of change of concentration of drops of diameter d with time can be expressed as a uni-dimensional PBE. For a locally isotropic turbulent field, this equation can be written as,

$$\left.\frac{\partial N(d,t)}{\partial t}\right|_d = B_b(d,t) - D_b(d,t) + B_c(d,t) - D_c(d,t) \tag{5.3}$$

Where $N(d,t)$ is the number density of drop size d. B_b, D_b, B_c, and D_c are the birth rate by breakage, death rate by breakage, birth rate by coalescence, and death rate by coalescence, respectively. Further, the rates of drop birth and death by breakup can be expressed as (Coulaloglou and Tavlarides, 1977)

$$B_b(d,t) = \int_d^{d_{max}} \beta(d',d)\cdot\nu(d')\cdot g(d')\cdot N(d',t)\,dd' \tag{5.4}$$

$$D_b(d,t) = g(d)\cdot N(d,t) \tag{5.5}$$

where, $g(d')$ is the breakage frequency, $\nu(d')$ is the number of dispersed fluid entities formed from breakage of a bubble of size d', and $\beta(d',d)$ is the size distribution of daughter bubbles formed from breakage of a bubble of size d'.

In addition, the rates of drop birth and death by coalescence are written as:

$$B_c(d,t) = \int_0^{d/2^{1/3}} h\left(\left(d^3 - d'^3\right)^{1/3}, d'\right) \times \lambda\left(\left(d^3 - d'^3\right)^{1/3}, d'\right)\cdot N\left(\left(d^3 - d'^3\right)^{1/3}, t\right)\cdot N(d',t)\,dd' \tag{5.6}$$

$$D_c(d,t) = N(d,t)\int_0^{\left(d^3_{max} - d^3\right)^{1/3}} h(d,d')\cdot\lambda(d,d')\cdot N(d',t)\,dd' \tag{5.7}$$

Here, $\lambda(d,d')$ is the coalescence efficiency between bubbles of size d and d', and $h(d,d')$ is the collision frequency between those of size d and d'.

This population balance representation is applicable to both gas-liquid and liquid-liquid dispersions provided that appropriate expressions for the various breakage and coalescence sub-processes are used. Such models have been presented by several authors, many of which have been recently reviewed by Jakobsen *et al.* (2005) and Lasheras *et al.* (2002).

Coulaloglou and Tavlarides (1977) developed a phenomenological model to describe drop breakage and coalescence in turbulently flowing liquid-liquid dispersions. This

model assumes a locally isotropic turbulent field where both phases are moving at the same velocity. In addition, the system is considered isothermal with no interphase mass transfer or reactions are taking place, and that only turbulent fragmentation and amalgamation occur. Since all these aforementioned conditions can be held valid in this work, this model will therefore be used to describe breakage and coalescence phenomena.

In addition, this model seems to be the most widely used over the past few decades, because it has the ability to encompass the various physical and hydrodynamical properties of the system in the drop rate functions and provides a better physical understanding of the processes taking place. Further, this model constituted the basis from which most of the breakage and coalescence models in turbulently flowing dispersions for both gas-liquid and liquid-liquid systems were derived (e.g. Prince and Blanch, 1990; Luo and Svendsen, 1996).

A discussion of the various breakage and coalescence sub-processes employed in this work will thus be presented in the following sections.

5.2.2.1 Breakage frequency

Breakage models have been generally modeled using a combination of the collision frequency between the drops and turbulent eddies as well as the probability that a collision leads to a successful breakage. For drop sizes falling within the inertial sub-range, Coulaloglou and Tavlarides (1977) assumed that the fraction of drops breaking is proportional to the fraction of drops which have a total kinetic energy greater than a minimum value necessary to overcome the surface energy holding the drop intact. Moreover, the distribution of the total kinetic energy of the drops was considered proportional to the distribution of the kinetic energies of the turbulent eddies. Based on the aforementioned considerations, Coulaloglou and Tavlarides proposed the following breakage frequency function,

$$g(d) = C_1 \cdot \frac{\varepsilon^{1/3}}{d^{2/3} \cdot (1+\phi)} \cdot \exp\left[-C_2 \cdot \frac{\sigma (1+\phi)^2}{\rho_d \cdot \varepsilon^{2/3} \cdot d^{5/3}} \right] \tag{5.8}$$

5.2.2.2 *Number of daughter drops*

The average number of daughter drops, $v(d')$, formed upon the breakage of a parent drop of diameter d', generally depends on the forces applied on the parent drop, the interfacial tension of that drop and its diameter (Hsia and Tavlarides, 1980). However, this term is usually assumed to be two (i.e. binary breakage) which is considered as a valid assumption by Andersson and Andersson (2006) who found that the probability of binary breakage increases with an increase in the energy dissipation rate; a condition that is expected to hold true in the current work where very high energy dissipation rates are expected to prevail in tubular reactors/contactors equipped with screen-type static mixers. This is also in accordance with the work of Maaß et al. (2007) who reported that binary breakage has the highest probability of occurrence for drops with sizes smaller than 1 mm in liquid-liquid systems. However, this issue remains unsettled for the case of liquid-liquid systems where contradicting conclusions can often be found in the literature. This is due to the fact that the viscosity of the dispersed phase has a large impact in determining the number of daughter drops born in a single breakage event (Podgorska, 2006; Tcholakova et al., 2007).

Nonetheless, for the purpose of the current work, binary breakage will be assumed to take place, which according to Ruiz and Padilla (2004) is not a restrictive assumption as the breakage of a parent drop in any number of daughter drops can be simulated efficiently by a rapid sequence of binary breakage events.

5.2.2.3 *Breakage size distribution*

In addition to the knowledge of the breakage frequency function and the number of drops formed after a breakage, the size distribution of these daughter drops is required for a complete description of the breakage sub-process. This daughter size distribution determines the probability at which drops of a certain size are formed as a result of a bigger drop being broken.

Coulaloglou and Tavlarides (1977) utilized a purely statistical distribution to express the daughter size distribution, $\beta(d,d')$, by assuming that the function is normally distributed as reported by Valentas and Amundson (1966) and written as,

$$\beta(d,d') = \frac{4.6}{d'^3} \cdot \exp\left[-4.5 \cdot \frac{\left(2d^3 - d'^3\right)^2}{\left(d'^3\right)^2} \right] \tag{5.9}$$

However, the use of a more sophisticated beta distribution function to describe the daughter density function has been proposed by Hsia and Tavlarides (1980) and later adopted by several investigators (Bapat et al., 1983; Bapat and Tavlarides, 1985; Alopaeus et al., 1999). This beta distribution has the advantage over the normal distribution proposed by Coulaloglou and Tavlarides (1977) in that it produces a zero probability for the infinitely small daughter drops and the daughter drops equal to the size of the mother drop (Bapat et al., 1983). This beta function is expressed as,

$$\beta(d,d') = 90 \cdot \frac{d^2}{d'^3} \cdot \left(\frac{d^3}{d'^3} \right)^2 \cdot \left(1 - \frac{d^3}{d'^3} \right)^2 \tag{5.10}$$

In contrary to other models available in the literature (e.g. Tsouris and Tavlarides, 1994; Luo and Svendsen, 1996), this beta distribution avoids the zero probability for the evolution of equi-sized drops; which is in line with the observations of Maaß et al. (2007) and Andersson and Andersson (2006) who reported that the probability of equi-sized breakage is highest for liquid-liquid systems.

Furthermore, the use of the normal distribution for describing breakage processes was found to introduce erroneous behavior under high shear rates, e.g. $\varepsilon \geq 1{,}000$ W/kg, and the problem was eliminated by using the beta distribution function of Hsia and Tavlarides (1980) (Azizi and Al Taweel, 2008b). Since energy dissipation rates of the same order of magnitude or even higher are expected to prevail in tubular contactors/reactors equipped with screen-type static mixers, the beta distribution will therefore be adopted hereafter while describing the breakage processes.

5.2.2.4 Collision frequency

The collision between drops can be initiated by several different mechanisms. These include buoyancy-driven (that is collisions due to the difference in rise velocities of drops of different size), and collisions due to laminar shear occurring when drops follow the continuous fluid streamlines (Prince and Blanch, 1990), in addition to drop coalescence

resulting from turbulent interactions between the continuous and dispersed phase. However, only the latter coalescence mechanism will be considered in this investigation because the relative importance of the various mechanisms as compared to turbulence-induced collisions can be neglected under the highly turbulent conditions present in screen-type static mixers.

Coulaloglou and Tavlarides (1977) derived a turbulent collision frequency model (assuming binary collisions) for drops with immobile interfaces by postulating that the mechanism of collision is analogous to collisions between molecules as described in the kinetic theory of gases. The collision frequency of drops of diameter d and d' can thus be written as,

$$h(d,d') = C_3 \cdot (d+d')^2 \cdot \left(d^{2/3} + d'^{2/3} \right)^{1/2} \cdot \frac{\varepsilon^{1/3}}{(1+\phi)} \tag{5.11}$$

The expression given in Equation (5.11) is slightly different from the originally published one as it incorporates a small algebraic error identified by Hsia and Tavlarides (1980).

5.2.2.5 Coalescence efficiency

Coulaloglou and Tavlarides (1977) also presented an expression for the coalescence efficiency term which is based on the film drainage between colliding dispersed phase entities which is applicable to the case of deforming entities with immobile interfaces. It assumes that turbulence causes the two entities to collide and holds them together for a definite time while the intervening film thins under a constant force applied by turbulence. Coalescence will therefore only occur when the contact time of the bubbles is longer than the time required for draining the film entrapped in between them. Therefore, the coalescence efficiency was expressed as,

$$\lambda(d,d') = \exp\left[-C_4 \cdot \frac{\mu_c \cdot \rho_c \cdot \varepsilon}{\sigma^2 \cdot (1+\phi)^3} \cdot \left(\frac{d \cdot d'}{d+d'} \right)^4 \right] \tag{5.12}$$

In the current work, the initial film thickness and the critical thickness for film rupture are assumed to be constant and lumped into the value of the parameter C_4.

5.3 Results and Discussion

5.3.1 Numerical Solution of PBE

An accurate, stable, and robust algorithm for solving the discretized PBE, where uniform energy dissipation conditions can be correctly assumed, was recently developed by Azizi and Al Taweel (2008b). This algorithm is based on minimizing the finite domain errors that often arise while discretizing the drop size domain and includes an enhanced solution stability algorithm which relies on monitoring the onset of errors in the various birth and death terms encountered in PBE. It consequently allows for corrective action to be undertaken before the errors propagate in an uncontrollable fashion, and was found to improve the stability and robustness of the solution method even under very high shear rate conditions.

This algorithm was further modified to account for flow through systems with spatial variation of local energy dissipation rate and thus will be used in the current work to model turbulent drop breakup and coalescence in static mixers. It uses the size distribution sampling approach proposed by Sovova and Prochazka (1981) and combines it with cubic spline interpolation if information in between sampling points is needed. It also employs a moving grid technique where insignificantly large drops are cut off from the drop size domain while occasionally re-adjusting the distribution to ensure volume conservation. At any particular time, the value of the birth and death terms are determined by integrating over the size domain (using Simpson's rule) and the resulting ODE is numerically solved using the adaptive step-size control for Runge-Kutta (5^{th} order Runge-Kutta).

This algorithm was developed with the ability of using general forms of the breakage and coalescence kernels and can therefore be used to describe both liquid-liquid and gas-liquid dispersions. Further, it has the ability to predict the transient drop size distribution and the temporal variation of the various dispersed phase characteristic sizes.

In the current work, 60 sampling points were used to describe the drop size domain at every time step. For further information on the method of solution, its stability and robustness, the reader is referred to Chapter 4.

5.3.2 Experimental Determination of Liquid-Liquid Contacting in Screen-type Static Mixers

The operational characteristics of screen-type static mixers were investigated using dilute liquid-liquid dispersions flowing in a 25.4 mm ID pipe (El-Ali and Al Taweel, 2008). The setup, shown in Figure 5.4, consisted of a vertical mixing section that incorporated a set of static mixing elements whose characteristics are given in Table 5.1. The drop size distribution obtained at different design and operating conditions was recorded using a video camera with very short exposure times (2 μs). An adjustable intensity light source was used to provide the high intensity illumination necessary for imaging the dispersion at the very short exposure times necessary to freeze the images of the moving drops. The resulting images were analyzed using semi-automated image analysis software for measuring the sizes of the drops present in the dispersion. The resulting dispersions were characterized using various mean diameters (d_{10}, d_{20}, d_{30}, d_{32} and d_{43}), the number-, and volume-density distributions, as well as the variance around the Sauter mean diameter, d_{32}.

Table 5.1: Characteristics of the woven screens investigated.

No.	Wire Size, b, (mm)	Mesh Size, M, (mm)	Open Area, a, (%)
I	0.508	1.058	27
II	0.152	0.362	33
III	0.305	0.845	41

The system investigated was a dispersion of Bayol Oil in tap water, the physical properties of which are listed in Table 5.2.

Table 5.2: Physical properties of the phases at 25 °C

Phase	Density, ρ, (kg/m^3)	Viscosity, μ, (kg/m.s)	Interfacial Tension, σ, (mN/m)
Water	997	1.0×10^{-3}	-
Bayol Oil	792	2.26×10^{-3}	19

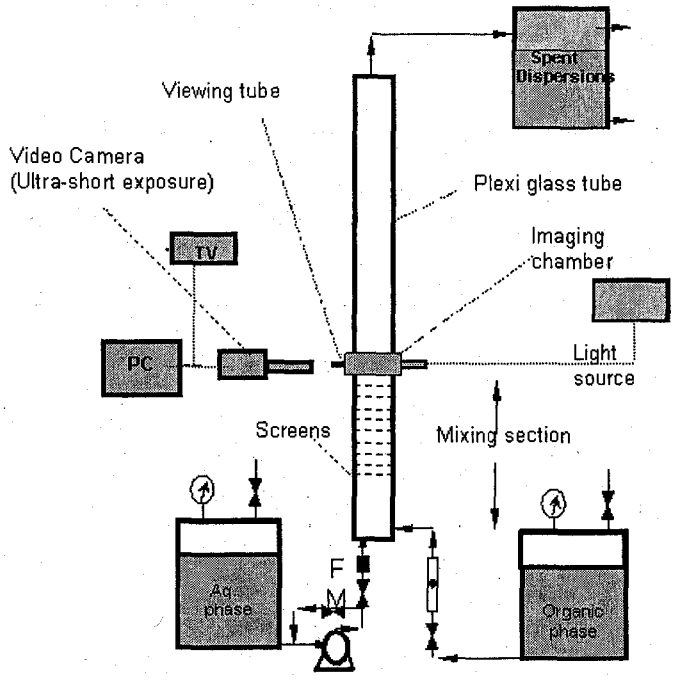

Figure 5.4: Schematic representation of the experimental setup.

A small quantity of salt (500 ppm) was added to the water in order to compensate for the uncontrolled variation in the composition of the tap water. Table 5.3 summarizes the range of experimental conditions investigated in this study.

Table 5.3: Experimental Conditions:

Number of Screen elements	9
Inter-screen spacing	10 mm
Superficial velocity, U	0.85 to 1.94 (m/s)
Screen open area, α	27 to 41 %
Dispersed phase hold-up, ϕ	0.5 %
Pipe Reynolds numbers	21,000 to 50,000

5.3.3 Comparison with Experimental Results

5.3.3.1 Determining the model constants

The experimental data represent a good case for validating the current work since it provides a large set of experimental results obtained under a wide range of design and operating conditions. Contrary to data obtained in mechanically-agitated tanks (MAT)

where highly non-uniform hydrodynamic conditions are encountered, these results were obtained under radially uniform turbulence conditions. The fact that turbulence in a thin slice behind screens closely approximates homogeneous isotropic conditions can be used to predict the evolution of DSD as the liquid-liquid dispersion flows through the static mixer.

In order to simulate the behaviour of turbulently flowing dispersions using the Coulaloglou and Tavlarides (1977) model the empirical constants used in the drop breakage/coalescence rate functions (Equations (5.8), (5.11) and (5.12)) need to be first identified. To accomplish this, attempts to fit the quasi-steady state Sauter mean diameters against the experimentally measured ones while minimizing the sum of squared errors as well as achieving reasonable fits of the DSD were undertaken. This is clearly presented in Figure 5.5 which shows the variation of the quasi-equilibrium Sauter mean diameter with the superficial flow velocity after estimating the various model constants in addition to the drop volume density distribution using screen I. It is evident that the model predictions match the experimentally determined values with a very good accuracy. The best fit to the experimental data was obtained using the values of the empirical constants shown in Table 4.2.

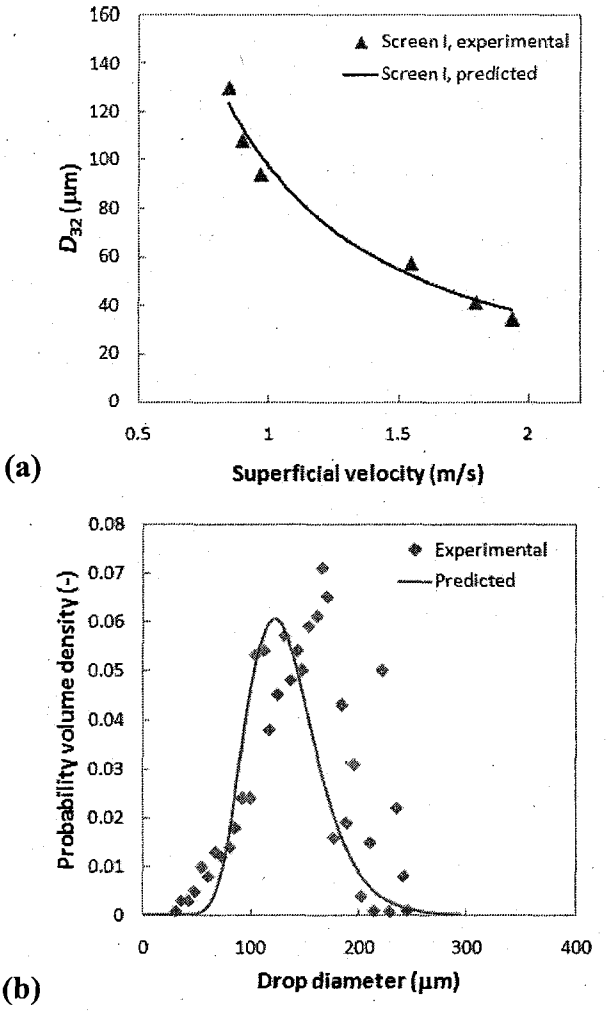

Figure 5.5: (a) Variation of the Sauter mean diameter with the superficial velocity ($\alpha = 27\%$; $\phi = 0.5\%$); (b) Probability volume density distribution ($\alpha = 27\%$; $U = 0.85$ m/s; $\phi = 0.5\%$)

Table 5.4: Values of the various model constants

Description	*Symbol*	*Value*
First Breakage Frequency Constant	C_1	0.86
Second Breakage Frequency Constant – *embedded in an exponential term*	C_2	4.1
Collision Frequency Constant	C_3	0.04
Coalescence Efficiency Constant	C_4	1×10^{10}

5.3.3.2 Simulation results

The ability of the current approach to track the variation of the drop size distribution as a function of the local energy dissipation rate along the length of the reactor can best be illustrated by following the temporal variation of the Sauter mean diameter as the immiscible dispersion flows through the static mixer (Figure 5.6). As can be seen from Figure 5.6, the relatively coarse drops introduced to the tubular contactor/reactor undergo a progressive reduction in the Sauter mean diameter as the dispersion passes through successive static mixing elements. A quasi-steady condition is asymptotically reached beyond which the DSD does not undergo significant changes with increasing number of mixing elements. In addition, it can be clearly discerned that the drop diameter undergoes a sharp reduction in the high energy dissipation regions adjacent to the screen before the fine bubbles formed in these regions start to coalesce as they migrate to regions of lower energy dissipation rates further downstream. This observation is similar to those reported by Turunen and Haario (1994) and Andersson et al. (2004) who used different types of commercially available static mixers to promote dispersion.

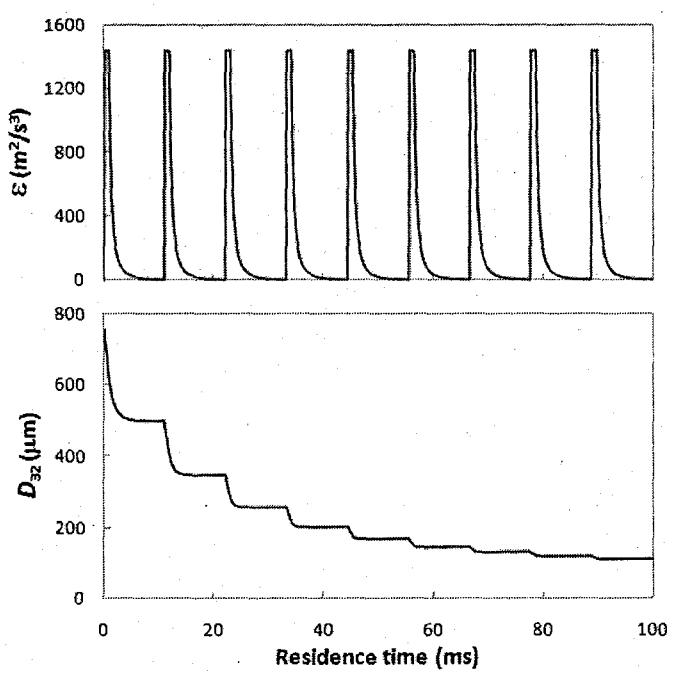

Figure 5.6: Predicted spatial variation of the local energy dissipation rate and the Sauter mean diameter along the length of the contactor/reactor
($U = 0.9$ m/s; $\phi = 0.5$ %; $\alpha = 0.27$)

The hydrodynamic conditions presented in Figure 5.5a, encompass those experimentally investigated and the values of the model constants derived thereof should be independent of the operating conditions and/or the design parameters of the mixer. Furthermore, to eliminate any effect the selection of the initial drop size distribution might have on the solution, and to maintain consistency in the study, a normal distribution ranging from 0 to 1500 μm with a Sauter mean diameter of 750 μm was selected as the initial condition in all the simulation runs.

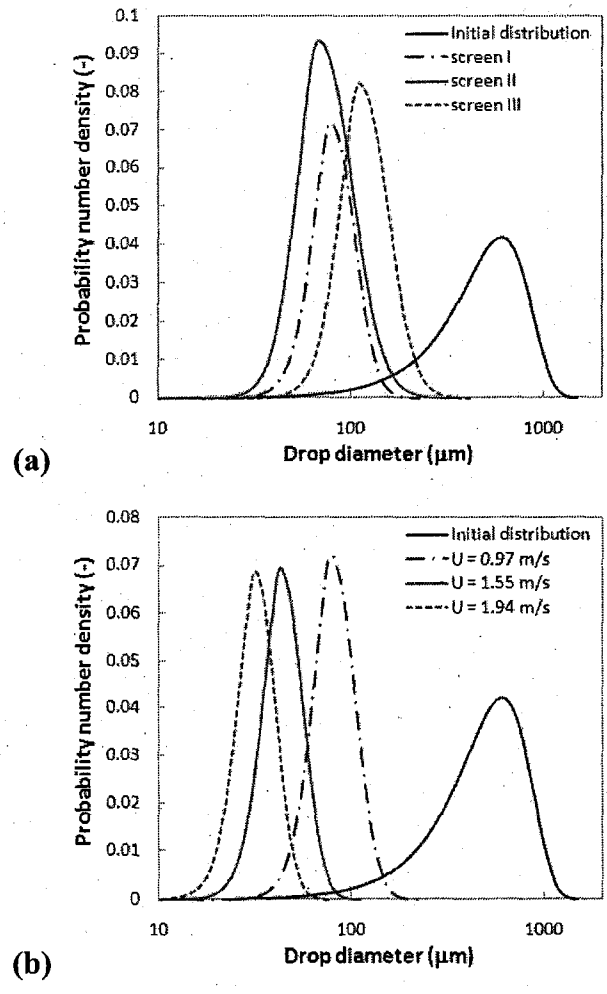

Figure 5.7: Effect of varying design and operating conditions on the quasi-equilibrium DSD at $\phi = 0.5$ %. (a) Effect of screen design at $U = 0.97$ m/s; (b) Effect of velocity for $\alpha = 27$ %

In addition, the ability of the simulation program to account for the variations in the operating or design conditions is clearly evident in Figure 5.7 where the quasi-steady

state DSD are plotted against the initial distribution. The case where the operating conditions were kept unchanged while varying the screen geometry is plotted in Figure 5.7a, while that highlighting the effect of the superficial velocity on the quasi-equilibrium DSD is given in Figure 5.7b for a type I screen. It is evident that the changes in the hydrodynamics of the system are well accounted for while retaining a very good resolution of the predicted DSD. This elucidates the importance of the moving grid technique used in the current work and its ability to keep the finite domain errors to a minimum by cutting insignificantly large drops from the size domain, and focus the computational efforts in the regions of most significance.

5.3.3.3 Matching model predictions with experimental data

The model constants derived in the previous section and listed in Table 5.4 should be a function of the physical properties of the system but independent of the operating conditions and/or the design parameters of the mixer. Therefore, these values are considered universal and will be kept unchanged throughout this investigation. However, the values of these constants were found to be several orders of magnitude larger than those obtained by previous authors who used the same model to simulate liquid-liquid dispersions using MATs (Coulaloglou, 1975; Ross et al., 1978; Hsia, 1981; Bapat and Tavlarides, 1985; Ribeiro et al., 1995). The discrepancy depicted in Table 5.5, is most probably due to the simplifying assumptions used by these authors in which they assumed a uniform local energy dissipation rate throughout the entire volume of the MAT.

Furthermore, to highlight the difference between the various sets of constants, the cumulative number densities estimated using both the old and the new sets of model parameters were plotted against the experimentally determined values in Figure 5.8. Since the older sets are of a similar magnitude, those obtained by Ribeiro et al. (1995) were chosen for the purpose of this comparison. The large discrepancy between the two simulation results is clearly shown in Figure 5.8 where the constants obtained in the current study predict the experimental results very well while the old constants failed to fall within the same order of magnitude as the mean diameter. This higher accuracy of the current set of constants emphasizes the importance of accounting for the spatial variation

in the energy dissipation rates while estimating the model parameters. This unmistakably illustrates the danger of assuming simplified hydrodynamic conditions and estimating the breakage and coalescence processes under conditions that do not truly apply.

Table 5.5: Numerical values of the empirical constants in the drop rate functions.

Proposed by	C_1	C_2	C_3	C_4
Coulaloglou (1975)	0.00487	0.0552	2.17×10^{-4}	2.28×10^{13}
Ross et al. (1978)	0.00487	0.08	2.17×10^{-4}	3×10^{12}
Hsia (1981)	0.01031	0.06354	4.5×10^{-4}	1.891×10^{13}
Bapat and Tavlarides (1985)	0.00487	0.08	1.9×10^{-3}	2×10^{12}
Ribeiro et al. (1995)	0.00481	0.0558	1.65×10^{-3}	4.74×10^{12}
Current work	**0.86**	**4.1**	**0.04**	$\mathbf{1 \times 10^{10}}$

In an attempt to characterize breakage and coalescence phenomena for droplets in rotating disc contactors, Schmidt et al. (2006) employed only the coalescence functions of Coulaloglou and Tavlarides (1977) along with a different breakage kernel. When the model parameters were determined as independent of the hydrodynamic conditions prevailing in the system, they obtained a set of constants for the coalescence kernel that are very similar to those obtained in the current work (C_3 = 0.036 and C_4 = 1.152 $\times 10^{10}$ m^{-2}). However, these results were found dependent on the chemical system used. Whereas the system exhibiting an interfacial tension comparable to the one employed in this work (σ = 14 mN/m compared to 19 mN/m in this work) resulted in very comparable sets of constants, other chemical systems with larger interfacial tensions required the use of a different set of constants to be accurately predicted.

This however does not completely justify the order of magnitude difference in the model constants, since changes in the interfacial characteristics of the system are not expected to induce such large variations in their values. However, it is important to add that the model parameters used by Ribeiro et al. (1995) for example were derived for two different systems whose interfacial tensions ranged from 9 to 32 mN/m. Therefore, even

though the interfacial characteristics of the system play an important role in determining the extent of the model parameters, the importance of an accurate representation of the energy dissipation rate while characterizing breakage and coalescence processes remains imperative.

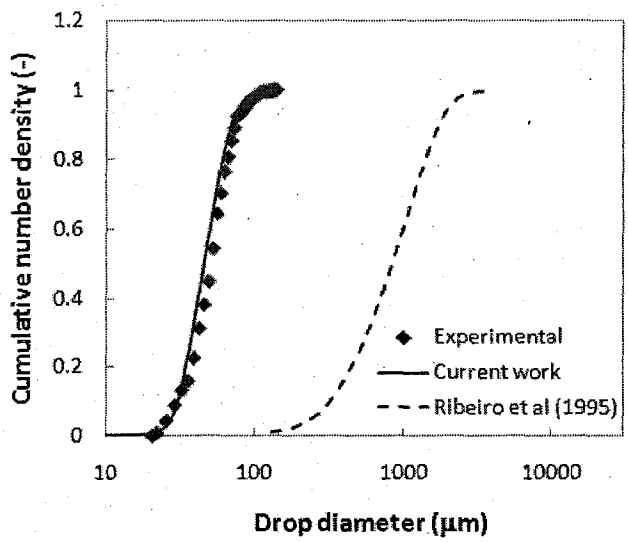

Figure 5.8: Comparison between old and new constants
($\alpha = 41$ %; $U = 1.94$ m/s; $\phi = 0.5$ %)

Figure 5.9 clearly shows the effect of changing the operating conditions on the Sauter mean drop diameter prevalent after the ninth screen element where quasi-steady state conditions are considered to be reached. The average equilibrium diameter was thus found to decrease with increasing the superficial velocity while decreasing with an increase in the screen open area. It is well known that the superficial velocity is one of the major factors governing liquid-liquid dispersion processes as it controls the kinetic energy in the micro-jets formed by the screens, and hence the turbulent breakup and coalescence processes. In the case at hand, the superficial velocity affects both the local rate of energy dissipation, ε, as well as the residence time of the fluid elements within the region of high local energy dissipation rate. Moreover, screens with lower open area are expected to produce higher velocity jets and hence higher local energy dissipation rates in the regions immediately downstream from the screens. Consequently, finer dispersions are expected as the screen open area decreases.

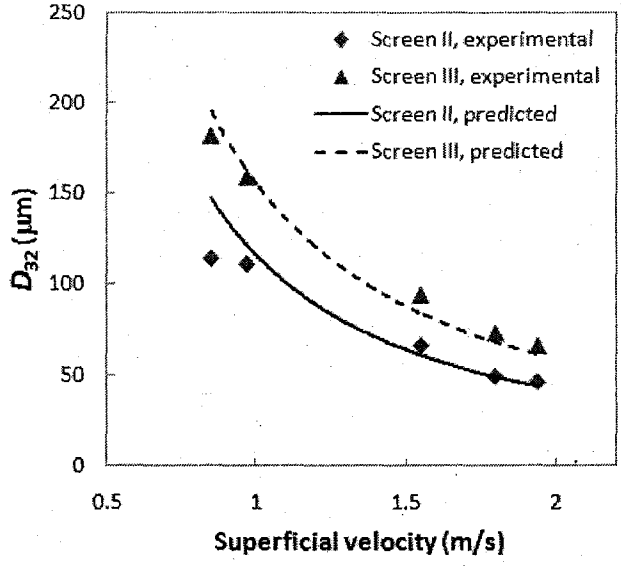

Figure 5.9: Effect of screen geometry on the variation of the Sauter mean diameter with the superficial velocity ($\phi = 0.5\%$)

The fact that the model predicts the experimental observations with high accuracy is an additional indication that the hydrodynamic model responsible for predicting the spatial variation of the energy dissipation rate (Azizi and Al Taweel, 2008a) throughout the contactor works quite well and yields good estimates of ε since good agreements between simulations and experimental data are also to a large extent based on good predictions of the turbulent energy dissipation rate (Andersson et al., 2004).

The ability of the model to render accurate estimates of the DSD under a wide range of operating and design conditions is further shown in Figure 5.10 where the experimental and simulation results are plotted for three different screen geometries and varying superficial velocities. Even though small deviations from the experimental values are apparent, it is clear that the simulation algorithm predicts the distributive effect with a good accuracy.

The raw data used in this study, in addition to all distributive and cumulative distributions covering the full range of operating and design conditions investigated, are given in Appendix D.

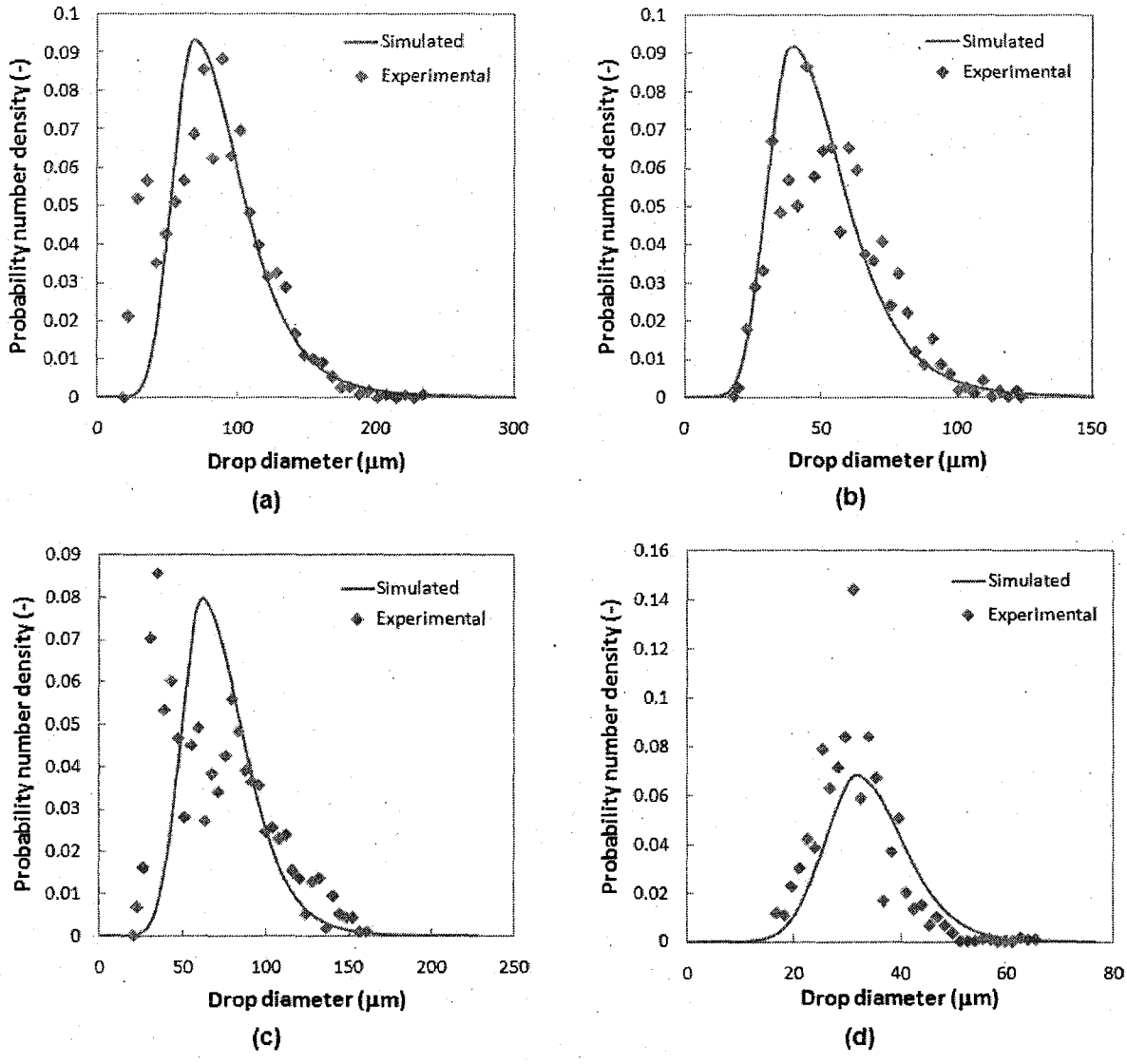

Figure 5.10: Effect of varying operating and design conditions on the probability number density distributions at $\phi = 0.5\%$: (a) $\alpha = 33$ % at $U = 0.97$ m/s; (b) $\alpha = 33$ % at $U = 1.55$ m/s; (c) $\alpha = 41$ % at $U = 1.55$ m/s; (d) $\alpha = 27$ % at $U = 1.94$ m/s.

5.4 Conclusion

From the aforementioned findings, one can conclude that the turbulent dispersion/coalescence of liquid-liquid systems can be accurately predicted using the phenomenological model developed by Coulaloglou and Tavlarides (1977). In this study, a population balance model utilizing this kernel was developed and used to assess its ability to accurately simulate the liquid-liquid contacting performance achieved in screen-type static mixers where nearly-isotropic turbulent plug flow conditions prevail.

The predicted drop size distribution as well as the Sauter mean diameter (when quasi-steady state conditions were assumed to be reached) was compared with experimental results measured by photographic techniques and good agreement was obtained at different flow velocities and diverse screen geometries.

The successive exposure of the flowing dispersion to breakage-dominated and coalescence dominated regions provided very stringent conditions for testing and validating the model and for the development of accurate model parameters that may be used for simulating other more complex liquid-liquid contacting conditions such as those encountered in MAT.

In addition to generating very uniform hydrodynamic conditions, the major advantage of using this type of reactor is that it allows an easy optical access to each mixing element. This would be of great importance in experimentally determining breakage and coalescence processes under well controlled and well characterized turbulent conditions.

Acknowledgment

The authors would like to acknowledge the financial support of the Natural Science and Engineering Research Council of Canada (NSERC).

5.5 Nomenclature

a	Interfacial area of contact between the phases	$[m^{-1}]$
b	Wire diameter	[m]
B_b	Rate of particle generation by breakage per unit volume	$[m^{-3}.s^{-1}]$
B_c	Rate of particle generation by coalescence per unit volume	$[m^{-3}.s^{-1}]$
C	Turbulence decay equation constant	[–]
$C_{1,\ldots,4}$	Empirical constants	[–]
d	Drop diameter	[m]
D_b	Rate of particle destruction by breakage per unit volume	$[m^{-3}.s^{-1}]$
D_c	Rate of particle destruction by coalescence per unit volume of a parent particle	$[m^{-3}.s^{-1}]$
$g(d')$	Breakage frequency of drops of diameter d'	$[s^{-1}]$
$h(d,d')$	Coalescence intensity of drops of diameter d and d'	$[s^{-1}]$

L	Distance between 2 consecutive screens	[mm]
L_M	Total mixer length	[m]
M	Screen mesh size	[m]
n	Turbulence decay equation exponent	[–]
$N(d,t)$	Number density function	[m^{-3}]
u'	Root mean square velocity fluctuation	[$m.s^{-1}$]
U	Mean velocity	[$m.s^{-1}$]
v	Droplet volume	[m^3]
x	Distance down the screen	[m]
x_o	Virtual origin of turbulence decay	[m]

Greek Letters

α	Fraction open area of the screen	[–]
$\beta(d,d')$	Probability that a drop of size d' is formed when a drop d breaks	[–]
ΔP	Pressure drop	[$N.m^{-2}$]
ε	Energy dissipation rate	[$m^2.s^{-3}$]
$\lambda(d,d')$	Coalescence efficiency	[–]
σ	Interfacial tension	[N/m]
μ	viscosity	[$kg.m^{-1}.s^{-1}$]
$\nu(d)$	Number of daughter drops formed by breakage of drop d	[–]
ϕ	Dispersed phase volume fraction	[–]
ρ_c	Continuous phase density	[$kg.m^{-3}$]

5.6 References

Al Taweel, A. M.; Chen, C., "Novel static mixer for the effective dispersion of immiscible liquids", Chem. Eng. Res. Des., **74**, 445-450 (1996).

Al Taweel, A.M., M. El-Ali, F. Azizi, B. Liekens, D. Odedra, A. Uppal and H.G. Gomaa, "In-Line Processing for Intensifying Multi-Phase Contacting Operations", Proceedings of the 5th Inter. Conf. Proc. Int. **5**, 59-73 (2003).

Alopaeus, V., J. Koskinen and K.I. Keskinen, "Utilization of Population Balances in Simulation of Liquid-Liquid Systems in Mixed Tanks", Chem. Eng. Comm. **190**, 1468-1484 (2003).

Alves, S. S.; Maia, C. I.; Vasconcelos, J. M. T. Gas-liquid mass transfer coefficient in stirred tanks interpreted through bubble contamination kinetics. Chem. Eng. Proc. **43**, 823-830 (2004).

Andersson, R., Andersson, B., Chopard, F., Noren, T., "Development of a multi-scale simulation method for design of novel multiphase reactors", Chem. Eng. Sci., **59**, 4911-4917 (2004)..

Attarakih, M.M., H. Bart and N.M. Faqir, "Solution of the Droplet Breakage Equation for Interacting Liquid-Liquid Dispersions: A Conservative Discretization Approach", Chem. Eng. Sci. **59**, 2547-2565 (2004).

Azizi, F., "Intensification of the fuels desulfurization processes", Dalhousie University, Halifax, N.S. (2004).

Bakker, A., A.H. Haidari and L.M. Oshinowo, "Realize Greater Benefits from CFD", Chem. Eng. Prog. **97**, 45-53 (2001).

Bapat, P.M. and L.L. Tavlarides, "Mass Transfer in Liquid-Liquid CFSTR", AICHE J. **31**, 659-666 (1985).

Bischof, F., M. Sommerfeld and F. Durst, "Mass transfer from bubbles under the influence of surface active agents", Chem. Ing. Tech **65**, 1365-1367 (1993).

Brucato, A., M. Ciofalo, F. Grisafi and R. Tocco, "On the Simulation of Stirred Tank Reactors Via Computational Fluid Dynam", Chem. Eng. Sci., **55**, 291-302 (2000).

Coulaloglou, C.A., "Dispersed Phase Interactions in an Agitated Flow Vessel", PhD Thesis, Illinois Institute of Technology, Chicago, IL (1975).

Coulaloglou, C.A., Tavlarides, L.L., "Description of interaction processes in agitated liquid-liquid dispersions", Chem. Eng. Sci., **32**, 1289-1297 (1977).

Davies, J.T., "Turbulence Phenomena", Academic Press, New York (1972).

Harris, C.K., D. Roekaerts, F.J.J. Rosendal, F.G.J. Buitendijk, P. Daskopoulos, A.J.N. Vreenegoor and H. Wang, "Computational Fluid Dynamics for Chemical Reactor Engineering", Chem. Eng. Sci., **51**, 1569-1594 (1996).

Hsia, M.A., "The Modeling of Liquid-Liquid Extraction in Stirred Tanks by a Simulation Approach", Ph.D. Thesis, Illinois Institue of Technology, Chicago, IL (1981).

Kostoglou, M. and A.J. Karabelas, "On the Attainment of Steady State in Turbulent Pipe Flow of Dilute Dispersions", Chem. Eng. Sci., **53**, 505-513 (1998).

Mahoney, A.W. and D. Ramkrishna, "Efficient Solution of Population Balance Equations with Discontinuities by Finite Elements", Chem. Eng. Sci., **57**, 1107-1119 (2002).

Marchisio, D.L., J.T. Pikturna, R.O. Fox, R.D. Vigil and A.A. Barresi, "Quadrature Method of Moments for Population-Balance Equations", AICHE J., **49**, 1266-1276 (2003).

Rigopoulos, S. and A.G. Jones, "Finite-Element Scheme for Solution of the Dynamic Population Balance Equation", AICHE J. **49**, 1127-1139 (2003).

Agitated Dispersion – 2. Measurement and Interpretation of Mixing Experiments", Ind. Eng. Chem. Fund., **17**, pp. 101-108 (1978).
Ross, S.L., F.H. Verhoff and R.L. Curl, "Droplet Breakage and Coalescence Processes in an

Sahu, A.K., P. Kumar, A.W. Patwardhan and J.B. Joshi, "CFD Modelling and Mixing in Stirred Tanks", Chem. Eng. Sci., **54**, 2285-2293 (1999).

Sommerfeld, M. and S. Decker, "State of the Art and Future Trends in CFD Simulation of Stirred Vessel Hydrodynamics", Chem. Eng. Tech., **27**, 215-224 (2004).

Thakur, R.K., C. Vial, K.D.P. Nigam, E.B. Nauman and G. Djelveh, "Static Mixers in the Process Industries - a Review", Chem. Eng. Res. Des., **81**, 787-826 (2003).

Turunen, I. and H. Haario, "Mass Transfer in Tubular Reactors Equipped with Static Mixers", Chem. Eng. Sci., **49**, 5257-5269 (1994).

Vasconcelos, J.M.T., S.P. Orvalho and S.S. Alves, "Gas-Liquid Mass Transfer to Single Bubbles: Effect of Surface Contamination", AICHE J. **48**, pp. 1145-1154 (2002).

Vazquez, G., G. Antorrena and J.M. Navaza, "Influence of Surfactant Concentration and Chain Length on the Absorption of CO_2 by Aqueous Surfactant Solutions in the Presence and Absence of Induced Marangoni Effect", Ind. Eng. Chem. Res., **39**, 1088-1094 (2000).

Vazquez, G., M.A. Cancela, R. Varela, E. Alvarez and J.M. Navaza, "Influence of Surfactants on Absorption of CO_2 in a Stirred Tank with and without Bubbling", Chem. Eng. J. **67**, 131-137 (1997).

Venneker, B. C. H.; Derksen, J. J.; Van den Akker,Harrie E.A., "Population balance modeling of aerated stirred vessels based on CFD", AICHE J., **48**, 673-685 (2002).

Walter, J.F. and H.W. Blanch, "Bubble break-up in gas-liquid bioreactors: break-up in turbulent flows", Chem. Eng. J. Biochem. Eng. J., **32**, 7-17 (1986).

Chapter 6.
Turbulently Flowing Liquid-Liquid Dispersions. Part II: Inter-Phase Mass Transfer

F. Azizi and A.M. Al Taweel*

Multiphase Mixing and Separation Lab, Department of Process Engineering and Applied Science, Dalhousie University, Halifax NS, Canada B3J 2X4

Submitted for publication in:

Industrial and Engineering Chemistry Research

January 2009

Abstract

A model for estimating the dispersed phase mass transfer coefficient was developed using Higbie's penetration theory combined with Kawase's surface renewal approach for the turbulent exposure time, and the effect of surface contamination on interfacial mobility. This model was then incorporated in a Population Balance algorithm capable of accurately predicting drop size distribution in various parts of the contactor and used to calculate the local mass transfer coefficients in regions of varying turbulent energy dissipation rates.

This model was found to be capable of predicting the experimental data, obtained using screen-type static mixers, reasonably well over a wide range of design and operating conditions. While the rigid and laminar circulation models significantly under-predicted the experimental results, the turbulent internal surface renewal model provided a hydrodynamic justification for the commonly used effective diffusivity correction factor which is reported to vary between 1 and 50.

Topical Heading: Fluid mechanics and transport phenomena

Keywords: Mass transfer, turbulent flows, surface contamination, static mixers, population balance, drops.

6.1 Introduction

The dispersion of immiscible liquids is one of the most difficult and least understood mixing problems despite the extensive literature dealing with both the hydrodynamic and the surface science aspects of the problem (Paul et al., 2004). Consequently, the majority of the liquid-liquid contactors/reactors presently used are inefficiently designed with subsequent adverse effects on the reaction yield and selectivity and/or the mass transfer performance. Furthermore, the large inventories of hazardous materials present in conservatively-designed contactors/reactors pose unnecessarily safety hazards and excessive amounts of energy are wasted while promoting contact between the phases as it is estimated that the efficiency by which energy is utilized to generate and maintain the interfacial area of contact between the phases is less than 2%.

Due to the very complex hydrodynamic conditions prevalent in most of the commercially available contactors/reactors handling immiscible dispersions, designing such units is very difficult without the employment of empirical knowledge and experience and an extensive amount of pilot-scale testing. However, a detailed understanding of the mixing process combined with the ability to accurately predict the volumetric mass transfer coefficient in such units can help in optimizing the performance, economy, and safety of these industrial systems.

The value of the local volumetric mass transfer coefficient, Ka, is affected by both the interfacial area of contact between the phases, a, and the overall mass transfer coefficient, K. Knowledge concerning how these parameters vary within the contactor/reactor volume is therefore essential for the rational design of a variety of liquid-liquid contactors (Botello-Alvarez et al., 2004; Dehkordi, 2002). To achieve such a goal, mathematical models capable of accurately predicting drop size and motion within the contactor/reactor in question as well as the mass transfer coefficient at various locations within the contactor, are needed.

A detailed description of the dispersed-phase characteristics can be achieved by using the population balance models that were introduced to the chemical engineering field in the mid-60s. Population balance equations, PBE, have since become a well-established tool that is widely used for simulating dispersed phase operations because it has the advantage

of being able to describe drop/bubble breakage and coalescence processes in terms of identifiable physical parameters and operational conditions. The biggest uncertainty associated with the use of PBE to simulate multi-fluid processing (*i.e.* immiscible liquid-liquid and gas-liquid systems) remains the identification of the breakage and coalescence kernels that can accurately describe what happens in turbulent flows. Most of the models developed over the past several decades were verified using experimental data obtained in mechanically agitated tanks in which the dispersed phase holdup, drop size distribution, and energy dissipation rate are assumed to be uniformly distributed throughout the volume of the mixing vessel. The fact that such units exhibit a broad residence time distribution, and that drops periodically circulate between the regions of high and low energy dissipation rates present in the mixing tank (where the local energy dissipation rates can vary by a factor of more than 10,000) are usually overlooked.

Computational fluid dynamics, CFD, can presently be used to simulate the hydrodynamic performance of mechanically agitated tanks handling immiscible liquids provided that one can accurately predict drop breakage/coalescence processes taking place in the various parts of the vessel. Armed with such knowledge - and a model that can account for the effect of drop size, turbulence intensity, and interfacial characteristics on the inter-phase rate of mass transfer - the mass transfer performance of mechanically agitated tanks may then be simulated. Unfortunately, no such capabilities have been reported yet, most probably because of the complex hydrodynamic conditions prevalent in MAT (*e.g.* large spatial variation in circulation patterns, dispersed phase holdup, and local energy dissipation rates), uncertainties surrounding the choice of appropriate breakage and coalescence kernels, and the lack of a reliable model that can be used to predict the inter-phase rate of mass transfer under highly turbulent conditions.

The objective of this work is to develop a model for predicting the dispersed phase mass transfer coefficient under conditions where the turbulence intensity in the continuous phase plays an important role. To accomplish this objective, Higbie's (Higbie, 1935) penetration theory was combined with Kawase's (Kawase et al., 1987) approach for calculating exposure time at different energy dissipation rates and the effect of interfacial mobility, which plays a big role in industrial systems, was taken into account using an approach similar to that proposed by West et al. (1951). This mass transfer model was

then incorporated into the recently developed PBE-based hydrodynamic model describing drop breakage and coalescence in turbulent flows (Chapter 4). The predictions of this model were then compared with those obtained using more traditional approaches as well as the experimental results for the overall inter-phase mass transfer obtained under well known and controlled hydrodynamic conditions prevalent in screen-type static mixers.

6.2 Modelling Inter-Phase Mass Transfer in Turbulently Flowing Liquid-Liquid Dispersions

The transfer of a component from one phase to another is governed by a wide array of complex processes such as concentration gradients, molecular diffusivities, mixing conditions, bulk and interfacial rheology, chemical reactions, temperature, and pressure. Mass transfer effectiveness is usually expressed by means of the volumetric mass transfer coefficient, Ka where the effect of the aforementioned variables (with the exception of the concentration gradients and the interfacial area of contact) is reflected in the value of the mass transfer coefficient, K. While the interfacial area of contact is controlled by the hydrodynamic and interfacial forces that determine breakage and coalescence rates, the value of the mass transfer coefficient is dependent on the hydrodynamics of the continuous phase, size of the drops, mobility of the interface, slip velocity and the physical properties of the system. Unfortunately, the complex hydrodynamic conditions encountered in most of the contactors/reactors investigated led to the development of a large number of equipment-, and system-specific mass transfer correlations which apply to very narrow and particular conditions.

Because of the big concern about inappropriately describing the hydrodynamics involved, many investigators recommended the separation of the two parameters, K and a, while estimating the volumetric mass transfer coefficient (Botello-Alvarez, et al., 2004; Alves et al., 2004; Vasquez and Bautista, 1997). It is only recently that the large spatial variation in average flow, and local turbulent energy dissipation rates, were taken into consideration and reasonably good agreement with experimentally-determined drop/bubble size distributions was achieved by incorporating dispersed phase population balances into multi-block, or CFD, representation of the multiphase contactor/reactor for

dispersed phase hold-ups as high as 5% (Andersson et al., 2004; Laakkonen, et al., 2006; Venneker, et al. 2002).

Most of the aforementioned hydrodynamic modeling difficulties are eliminated under the flow conditions encountered in multi-stage screen-type static mixers developed by Al Taweel and Chen (1996). The residence time distributions are very narrow (essentially plug flow) and the characteristics of the turbulence generated in the region downstream from each consecutive screen are well known. These mixers therefore offer a good alternative to conventional MAT mixers for developing and testing various hydrodynamic and mass transfer models as they overcome the difficulties associated with the high spatial variations of the energy dissipation rates as well as flow/recirculation non-uniformities. In addition, they fulfill the need for plug flow conditions by offering narrow residence time distributions and allowing both phases to move concurrently through the contactor with little or no axial dispersion. Finally, the use of plug flow contactors instead of stirred tank contactors eliminates the need to monitor the rapidly changing concentrations at various locations of the contactor and replaces it with steady state measurements of concentration at different locations along the axis of the flow.

6.3 Development of a Model for Predicting Drop Side Mass Transfer Coefficient in Turbulent Flows

The volumetric mass transfer coefficient is a key parameter in the characterization and design of stirred and non-stirred industrial liquid-liquid contactors/reactors. In order to achieve a better understanding of the effect various hydrodynamic and interfacial forces have on this transfer phenomenon, it is recommended to separately consider the mass transfer coefficient, K, and the interfacial area of contact, a, in order to isolate the contributions of the design/operating conditions and the physical properties of the phases on each of these parameters (Botello-Alvarez, et al., 2004; Bouaifi et al., 2001). To date, the problem of estimating the mass transfer coefficients for liquid drops in a turbulent medium is not well understood and the values predicted using the many empirical and theoretical models presented in the literature can be significantly different from those determined experimentally.

Several investigators reviewed the hydrodynamic and interfacial factors affecting the continuous and dispersed phase mass transfer coefficients (Vasquez and Bautista, 1997; Henschke and Pfennig, 1999; Kumar and Hartland, 1999; Bart, 2003). These clearly show that much of the recent understanding of inter-phase mass transfer was obtained from single drop experiments usually conducted using relatively large drops moving within stagnant or slowly moving continuous phase. Although the models and correlations stemming from such an approach may be suitable for the relatively mild agitation intensities encountered in spray and rotating disc extraction columns, they do not apply to the case of high intensity contactors/reactors used in industry (such as MAT, impinging jets, in-line rotors, stators, ultrasonic dispersers, colloid mills, high pressure and narrow-gap homogenizers as well as screen-type static mixers).

The overall mass transfer coefficient, K, is controlled by the resistance offered by both the dispersed and continuous phases as well as any interfacial resistance to mass transfer. For the cases where the film resistance is much larger than the interfacial resistance, the Whitman two-film theory can be expressed as,

$$\frac{1}{K} = \frac{m}{k_c} + \frac{1}{k_d} \tag{6.1}$$

where, m is the distribution coefficient between the phases ($m = C_{d,eq}/C_{c,eq}$).

For cases where the solute exhibits very high affinity to the continuous phase (*i.e.* where m is very small), the overall mass transfer coefficient becomes controlled by the dispersed phase resistance and the sensitivity of the experimental results to variations in the continuous-phase resistance is, therefore, significantly reduced (Camurdan et al., 1989; Noh and Baird, 1984). This observation is very relevant considering the fact that it was found to be the factor controlling inter-phase mass transfer in many industrial operations particularly where the viscosity of the dispersed phase is higher than that of the continuous one (Bart, 2003; Henschke and Pfennig, 1999). Consequently, attention will be focused on the various models available for predicting the dispersed phase mass transfer coefficient and how it is affected by the various hydrodynamic and interfacial factors.

6.3.1 Previous Work

Mass transfer in the dispersed phase is generally affected by a combination of molecular diffusion, and natural/forced convection within the drop. A large number of mechanisms and models have therefore been proposed for laminar and creeping flows within stagnant, circulating, or oscillating drops with the majority being focused on diffusive mass transfer and hydrodynamically-induced convective mass transfer. Newman (1931) developed a model for rigid drops which describes mass transfer by unsteady molecular diffusion. This model was further expanded by Kronig and Brink (1950) to account for laminarly circulating drops where an enhancement factor of up to 2.5 is obtained with a fully mobile interface. Many researchers (Handlos and Baron, 1957; Johnson and Hamielec, 1960; Steiner, 1986; Slater, 1995) attributed the experimentally observed high mass transfer coefficient values by assuming turbulent conditions inside the drop and applied the eddy diffusivity approach to quantify that impact. In this approach, an overall effective diffusivity, D_{oe}, is used to replace D_d in the rigid drop model with the ratio of the two values expressed as an enhancement factor, R, the value of which may vary between 1 and 50 and is experimentally determined from (Steiner, 1986).

$$k_d = \frac{2\pi^2}{3} \times \frac{D_{oe}}{d} = R \times \frac{2\pi^2}{3} \times \frac{D_d}{d} \tag{6.2}$$

In order to account for the effect of contaminants on inter-phase mass transfer, West et al. (1951) applied the Higbie penetration theory to the case of single drops rising in stagnant liquids and assumed the exposure time to be that needed for the drop to rise a distance equal to its own diameter. Using this assumption, they could predict the experimental results of Sherwood et al. (1939) reasonably well but were not as successful with their own data; this discrepancy was then attributed to the difference in solvent purities and physical properties as well as the construction material used in the experiments.

Few investigators attempted to account for the destabilizing effect induced by mass transfer, a factor which can significantly affect the value of k_d for relatively large drops. In their recent investigation, Henschke and Pfennig (1999) observed that for large drops (d > 1.5 mm) the measured mass transfer coefficients are often much larger than those

predicted by the theory of laminar circulation inside drops and discarded the hydrodynamic reasoning for turbulent transfer. They credited the enhancement to the onset of mass-transfer-induced turbulence within the drop which drives the correction factor above the limiting value of 2.5 predicted for laminar circulation with a fully mobile interface.

However, all the aforementioned efforts did not address the impact that continuous phase turbulence has on the value of k_d in spite of its relevance to many industrial situations. Although the dispersed phase mass transfer coefficient, k_d, for liquid drops moving within turbulently flowing liquids, may be estimated using the penetration theory of Higbie combined with an accurate estimate of the exposure time, few investigators adopted this approach in their analysis of the factors affecting the value of k_d. The recent review by Jajuee et al. (2006) provides a detailed analysis of the efforts directed towards the development of surface renewal concepts and models for estimating the inter-phase mass transfer coefficient in agitated liquid-liquid and gas liquid systems under conditions where the external mass transfer coefficient is controlling. Unfortunately, all the models discussed yield a single average value for the exposure time that changes with the average turbulence intensity within the contactor but does not truly reflect the effect of spatial variation of energy dissipation rate within it. The findings are thus not of fundamental nature, as they apply only to the specific conditions investigated and can not be easily translated to other contactor sizes and configurations.

In their analysis of the continuous phase mass transfer coefficient, Skelland and Lee (1981) clearly identified that the assumption of equal degree of turbulence at various locations in MAT does not apply. They presented a more realistic approach to the hydrodynamic conditions in which drops circulate between the high energy dissipation regions around the impeller, and the much lower energy dissipation rates prevalent in other parts of the mixing vessel. A model containing periodically varying rates of surface renewal was therefore proposed on the basis of the average time drops take to circulate within the vessel. Although this model is based on a more realistic representation of the hydrodynamic conditions within the vessel, it violates the fundamental concept that the surface renewal rate must be determined by the hydrodynamic parameters prevalent in the regions surrounding the drop and not the average value prevalent throughout the

contactor. Their model also does not take into account the temporal variation of drop sizes as they undergo periodic breakup and coalescence and overlooks the fact that monodisperse drops are rarely encountered in industrial operations.

On the other hand, many of the aforementioned deficiencies have been recently overcome by some investigators who applied penetration theory to the case of gas liquid dispersions where the continuous phase resistance dominates the rate of inter-phase mass transfer. Using the single phase flow patterns predicted by CFD simulations, Bakker and van Den Akker (1994) calculated the transport of gas throughout mechanically agitated tanks using an in-house finite difference code. Higbie's penetration theory was then used to predict the local and overall continuous phase mass transfer coefficients in the tank and good agreement between the predicted overall volumetric mass transfer coefficient and their experimental findings was obtained for gas holdups < 5%. However, attempts to use the same approach and solution scheme failed to predict the inter-phase mass transfer coefficient in mechanically agitated tanks handling pseudo-plastic fluids mainly because of the inability to accurately predict the gas holdup profiles and bubble size distributions (Venneker et al., 2002). A similar approach was adopted by Laakkonen et al. (2006) who subdivided the tank into 22 sub-regions each of which has a particular value of ε, ϕ, and d. Using single phase flow patterns predicted by CFD simulations, a discretized population balance code, and Higbie's penetration theory, good agreement between the predicted oxygen concentrations and their experimental results on absorption and desorption of oxygen were only possible after adjusting a parameter in the liquid film mass transfer equation.

In summary, proper understanding of the various factors affecting the dispersed phase mass transfer coefficient is still incomplete and the need for phenomenological models that account for the various physicochemical and hydrodynamic conditions on the dispersed-phase mass transfer coefficient is evident. A model capable of predicting the drop side mass transfer coefficient in turbulently flowing liquid-liquid dispersions was therefore developed by combining Higbie's penetration theory with Kawase's surface renewal approach for the turbulent exposure time, and accounting for the effect of surface contamination on interfacial mobility.

6.3.2 Model Development

According to Higbie's penetration theory, the dispersed phase mass transfer coefficient can be expressed as,

$$k_d = \frac{2}{\sqrt{\pi}} \cdot \sqrt{\frac{D_d}{t_e}} \tag{6.3}$$

where, t_e, is referred to as the exposure time and represents the mass transfer surface renewal time. Accurate estimation of this parameter and its variation under different hydrodynamic conditions plays a paramount role in correctly predicting the value of the mass transfer coefficient. Two commonly used approaches were suggested for solving this problem. The first one, proposed by Higbie himself (Higbie, 1935) relates the contact time to the bulk liquid flow around the entity, assuming that,

$$t_e = \frac{d}{v_s} \tag{6.4}$$

where, d is the drop diameter and v_s is the steady state slip velocity between the phases. Substituting Equation (6.4) in Equation (6.3), the dispersed phase mass transfer coefficient can now be described as:

$$k_d = \frac{2}{\sqrt{\pi}} \cdot D^{1/2} \cdot \sqrt{\frac{v_s}{d}} \tag{6.5}$$

Equation (6.5) is mainly referred to as a "slip velocity" model, and has been extensively used for describing continuous-phase mass transfer coefficients in gas-liquid and liquid-liquid applications (Steiner, 1986; Saien and Barani, 2005; Alves et al., 2006) especially under low turbulent intensity conditions where large diameter bubbles/drops having large slip velocities dominate. It predicts a strong dependence of the mass transfer coefficient on the bubble/drop diameter but does not account for the effect of turbulence in the continuous phase.

The second approach, which will be adopted in the formulation of the current model, is based on the surface renewal due to the interaction of drops with turbulent eddies. It is based on the observation that whereas the interaction of drops with the low-frequency large scale eddies will result in the drops being mainly carried along with the eddies, the

interaction with the high-frequency small-scale eddies will result in the formation of shear stresses that trigger surface renewal and shape deformations. The rate of mass transfer within a drop that is exposed to a highly turbulent flow field can thus be assumed to be largely controlled by the interactions between the drops and the high-frequency small-scale eddies. Based on this understanding, Kawase et al. (1987) suggested that for the case of gas-liquid systems with fully mobile interface, the contact time can be considered to be of the order of the characteristic time of an eddy given by Kolmogorov's isotropic turbulent flow theory,

$$t_e = \left(\frac{\nu}{\varepsilon}\right)^{1/2} \tag{6.6}$$

The relative density between the continuous and dispersed phases is much higher in the case of gas liquid dispersions than is the case of liquid-liquid dispersions. However, the effect of virtual mass experienced by dispersed phase entities accelerating/decelerating in turbulent flows tends to minimize such differences (Azizi and Al Taweel, 2007). Consequently, it is possible to assume that in the case of immiscible liquid-liquid systems with fully mobile interface, the contact time can similarly be considered to be of the order of the characteristic time of an eddy as given by Equation (6.6).

Combining Equations (6.6) and (6.3), the dispersed-phase mass transfer coefficient in turbulently flowing liquid-liquid dispersions can be written as:

$$k_d = \frac{2}{\sqrt{\pi}} \cdot D_d^{1/2} \cdot \left(\frac{\varepsilon}{\nu}\right)^{1/4} \tag{6.7}$$

provided that the interface between the phases is fully mobile. This equation fits into the category generally referred to as an "eddy" model in the field of multiphase mass transfer. It predicts a decisive influence of the turbulent energy dissipation on k_d which is independent of drop diameter (as long as the relative contribution of the slip velocity to the mass transfer is limited).

Further, the presence of contaminants at the interface between the phases is known to reduce interfacial mobility with the extent of reduction being a function of the nature and concentration of the contaminant. This can exert a significant adverse effect on inter-

phase mass transfer, a situation that is encountered in industrial systems where the presence of amphiphilic constituents is known to play an important role. To account for that effect in the present model, the exposure time, t_e, is modified by the introduction of a correction factor, f_c, that represents the square root of the ratio of the vertical velocity of the interface to that of the continuous phase, both taken with respect to the drop center. Its value decreases from 1 for fully mobile surfaces and approaches zero for rigid surfaces where no internal turbulent diffusion takes place.

The turbulent internal surface renewal model, can now be written as follows,

$$k_d = \frac{2}{\sqrt{\pi}} \cdot f_c \cdot D_d^{1/2} \cdot \left(\frac{\varepsilon}{\nu}\right)^{1/4} \tag{6.8}$$

where f_c is the correction factor for the surface mobility of the drop and is formulated along the line adopted by West et al. (1951) who studied single drops rising in stagnant liquids.

This model is expected to apply at the high power inputs encountered in mixing tanks and other efficient contactor/reactors where small droplets are formed rather than for the drop sizes encountered in extraction columns (1,500 – 5,000 μm) where mild turbulence intensities prevail.

It is important to note that the model presented by Equation (6.8) can be used to predict drop side mass transfer coefficient in any contactor/reactor configuration provided that its volume is subdivided into elements sufficiently small that the assumption of uniform hydrodynamic conditions within each can be reasonably well met. It should also be applicable to clean systems where the interface is mobile as well as for industrial systems where the presence of amphiphilic materials can result in immobilizing the interface to various degrees.

6.4 Testing and Validating the Turbulent Mass Transfer Model

As previously mentioned, the hydrodynamic conditions encountered in most investigations dealing with interphase mass transfer in turbulently-flowing immiscible liquids are not well known and can therefore not be easily used to test and validate theoretical models because of the large spatial variation in circulation patterns, dispersed

phase holdup, and local energy dissipation rates. On the other hand, the recent introduction of screen type static mixers offers the possibility of conducting mass transfer studies under well controlled hydrodynamic conditions (approaching plug flow) in which the turbulence characteristics are well known.

In the following sections, the hydrodynamic conditions prevalent in screen-type static mixers are discussed with an emphasis on the recently developed model for drop breakage and coalescence in turbulent flows and its ability to predict drop size distributions achieved in screen-type static mixers by numerically solving the resulting population balance equations. The newly developed mass transfer model (Equation(6.8)) was then incorporated into the hydrodynamic model and used to estimate the local and volume-average interphase mass transfer coefficients. These predictions were then compared with those obtained using more traditional approaches and with the experimental results for the overall inter-phase mass transfer obtained in screen-type static mixers.

6.4.1 Modelling Energy Dissipation Rates in Screen-Type Static Mixers

The rate of energy dissipation within the mixer plays a crucial role in determining the drop size distribution of the flowing dispersion as well as the rate at which mass is transferred between the phases. A relatively large body of knowledge is available concerning the nature of grid-generated turbulence and how it is affected by the nature of flow as well as by the characteristics of the wire mesh used (Kang et al., 2003; Briassulis et al., 2001). The most distinctive characteristic of flow through screens is the generation of nearly isotropic turbulence in the downstream flow.

Furthermore, the hydrodynamic factors affecting the performance of screen type static mixers were recently analyzed by Azizi and Al Taweel (2008a) who proposed that the turbulence decay profile behind a grid be divided into two regions; namely, a region of constant high energy dissipation rate prevalent over a certain distance downstream of the grid, and a region of fast decay where the homogenous isotropic turbulence decay equation applies. As shown in Figure 6.1, the local turbulent energy dissipation rate downstream from the screens undergoes dramatic variation along the axis of flow with the maximum value being encountered in the immediate vicinity of the screen. This

behaviour can be described using the following power law expression (Bourne and Lips, 1991):

$$\varepsilon = \frac{3 \cdot n \cdot U^3}{2 \cdot M \cdot C} \cdot \left[\frac{x}{M} - \left(\frac{x}{M} \right)_o \right]^{-(n+1)} \tag{6.9}$$

where C is the decay coefficient, M is the mesh spacing and x is the distance downstream from the screen. For the screen used in this investigation (b = 152 μm; M = 362 μm) C was equal to 1.82, n was set to 1.32 and x_o = 0. Additional information concerning the values of these various parameters and the proposed approach for predicting the spatial variation of the energy dissipation rate downstream of a screen are reported elsewhere (Chapter 3).

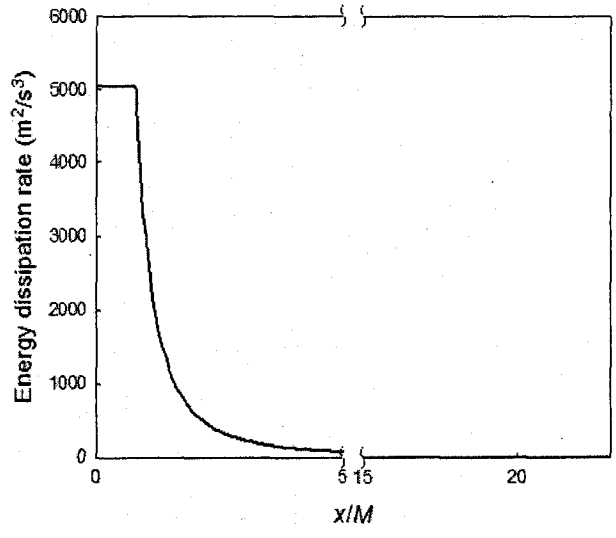

Figure 6.1: Rate of energy dissipation as a function of location downstream of a screen (U = 1.0 m/s, M = 362 μm, α = 0.33).

6.4.2 Simulating Drop Breakage and Coalescence in Screen-Type Static Mixers

The aforementioned large axial variation in local energy dissipation rate behind screens results in the drops present in the dispersion passing through the screen undergoing very rapid breakage in the regions of high energy dissipation rates adjacent to the screen. They will however progressively coalesce into coarser drops as they migrate into the regions of lower energy dissipation rates further downstream. This phenomenon can best be simulated using population balance equations (PBE).

Population balance equations are generally used to simulate the generation of dispersions because they allow a detailed description of the two rate processes that occur in the system; namely, drop breakage and coalescence. Rigorous modeling of these processes leads to formation of an integro-partial-differential equation known as the population balance equation. Analytical solutions of the PBE in its most general form are rare with the few reported instances involving major simplifying assumptions that may not be easily met in practice. The PBE are therefore generally discretized to transform the partial differential equations into ordinary differential equations, rendering their numerical solution easier.

In its most general form, the population balance for a well mixed control volume can be written as:

$$\begin{bmatrix}\text{Rate of accumulation}\\ \text{of particles}\\ \text{in the control volume}\end{bmatrix} = \begin{bmatrix}\text{Net rate of transport into}\\ \text{the control volume by convection}\end{bmatrix} + \begin{bmatrix}\text{Net rate of generation}\\ \text{in the control volume by}\\ \text{breakage and coalescence}\end{bmatrix} + \begin{bmatrix}\text{Net rate of generation in the control volume by other means}\\ \text{e.g. chemical reaction, mass transfer...}\end{bmatrix}$$

The relative contribution of the mass transfer to the dispersed phase volume fraction (the third term on the R.H.S) can be neglected for dilute solutions, a situation that is analogous to the findings of Laakkonen et al. (2006) for gas-liquid systems.

Radially uniform turbulence conditions that approach the ideal situation of isotropic turbulence are encountered in the flow within screen-type static mixers. In order to accommodate the large axial variation in turbulence intensity reported for this contactor (Equation (6.9)), its hydrodynamic performance was modeled by dividing it into very thin control cells where uniform isotropic hydrodynamic conditions can be correctly assumed to exist. The population balance approach was then applied to each cell using the breakage and coalescence kernels developed by Coulaloglou and Tavlarides (1977). The resulting equations (listed in Table 6.1) incorporate the small algebraic corrections identified by Hsia and Tavlarides (1980), in addition to their proposed daughter size distribution which was used instead of that originally reported by Coulaloglou and Tavlarides (1977). These integro-differential eq uations were then numerically solved using an accurate and robust algorithm developed for such purposes (Chapter 4).

Table 6.1: Coulaloglou and Tavlarides Breakage and Coalescence kernels

Sub-process	***Equation***
Breakage frequency	$g(d) = C_1 \cdot \frac{\varepsilon^{1/3}}{d^{2/3} \cdot (1+\phi)} \cdot \exp\left[-C_2 \cdot \frac{\sigma \cdot (1+\phi)^2}{\rho_d \cdot \varepsilon^{2/3} \cdot d^{5/3}} \right]$
Number of daughter drops	$v(d) = 2$
Size distribution of daughter drops	$\beta(d,d') = 90 \cdot \frac{d^2}{d'^3} \cdot \left(\frac{d^3}{d'^3} \right)^2 \cdot \left(1 - \frac{d^3}{d'^3} \right)^2$
Coalescence frequency	$h(d,d') = C_3 \cdot \frac{\varepsilon^{1/3}}{(1+\phi)} \cdot (d+d')^2 \cdot \left(d^{2/3} + d'^{2/3} \right)^{1/2}$
Coalescence efficiency	$\lambda(d,d') = \exp\left[-C_4 \cdot \frac{\mu_c \cdot \rho_c \cdot \varepsilon}{\sigma^2 \cdot (1+\phi)^3} \cdot \left(\frac{d \cdot d'}{d+d'} \right)^4 \right]$

Although the various sub-processes modeled by Coulaloglou and Tavlarides are based on sound theoretical foundations that have been validated by very recent findings, the approach used by them to quantify the model parameters C_1 - C_4 is fundamentally flawed as it is based on over simplified postulations in which MAT are assumed to be perfectly mixed with a spatially uniform energy dissipation rate. The value of the constants derived from such an approach can therefore not be used to predict the spatial variation in drop size distribution within MAT or any other contactor for that matter.

The data generated under the plug flow conditions encountered in screen-type static mixers under a wide range of hydrodynamic conditions were recently used by Azizi and Al Taweel (Chapter 4) to test the ability of PBE to accurately predict drop size distributions under conditions of isotropic turbulence. They found that the breakage and coalescence kernels developed by Coulaloglou and Tavlarides can accurately predict the Sauter mean diameter and drop size distribution over a wide rage of hydrodynamic conditions provided that a new set of model parameters is used (Figure 6.2). By using that new set of model parameters, the Coulaloglou and Tavlarides model can be used to describe the various breakage and coalescence sub-processes taking place in turbulently flowing liquid-liquid dispersions (*i.e.* within any contactor configuration) since the new

values of the parameters were obtained taking into consideration the spatial variation of the energy dissipation rate.

The new values of the model constants shown in Table 6.2 were found to be several orders of magnitude different from those commonly used in the literature, which were derived assuming homogeneous energy dissipation rates. The errors introduced by applying the wrong model parameters is evident from Figure 6.2 where they predict a mean drop diameter that is 17-fold larger than that experimentally observed.

The suggestion that the Coulaloglou and Tavlarides model can be used to describe the various breakage and coalescence sub-processes taking place in turbulently flowing liquid-liquid dispersions in a fashion that is independent of the contactor configuration is strengthened-by the observation that Schmidt et al. (2006) found it necessary to change the collision frequency and coalescence efficiency constants, C_3 and C_4, to a value that is close to that developed in Chapter 5 in order to achieve a simulation of drop breakage and coalescence in rotating disc extraction columns that is independent of the specific hydrodynamic conditions and/or column configuration.

Table 6.2: Values of the various model constants

Model Parameter	***Physical Meaning***	***Best Fit Value***	***Value reported by Ribeiro et al. (1995)***
C_1	First Breakage Frequency Constant	0.86	0.481×10^{-2}
C_2	Second Breakage Frequency Constant – *embedded in the exponential term*	4.1	0.558×10^{-1}
C_3	Collision Frequency Constant	0.04	0.165×10^{-2}
C_4 (m^{-2})	Coalescence Efficiency Constant	1×10^{10}	0.474×10^{13}

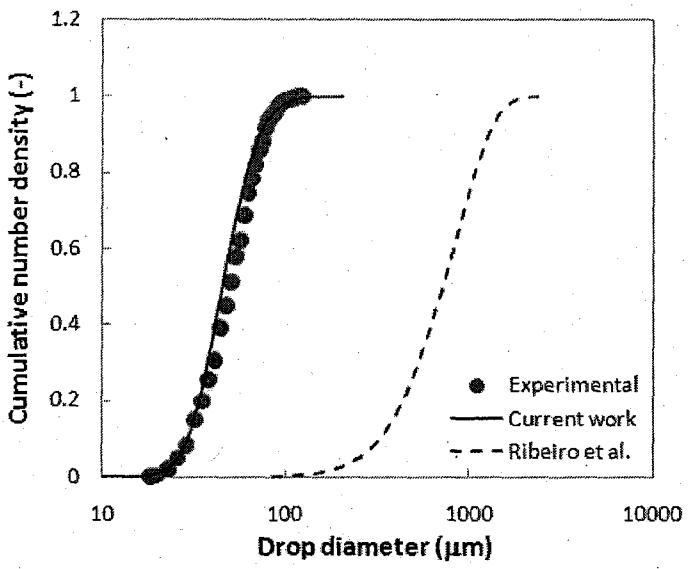

Figure 6.2: Effect of model parameters on predicted drop size distributions (α = 33 %; U = 1.55 m/s; ϕ = 0.5 %; L = 10 mm; $d_{32,\,exp}$ = 66 μm; $d_{32,\,sim}$ = 65.6 μm; $d_{32,\,Ribeiro}$ = 1103 μm)

6.4.3 Calculating the Local Volumetric Mass Transfer Coefficient

The value of the local volumetric mass transfer coefficient, Ka, is affected by both the interfacial area of contact between the phases, a, and the overall mass transfer coefficient, K. The magnitude of these two parameters varies significantly within the contactor/reactor volume as a result of the spatial variation in local energy dissipation rates.

To estimate the volumetric mass transfer coefficient, the PBE were first solved in order to determine the drop size distribution of the dispersed phase and its axial variation along the length of the static mixer. The resulting drop size distribution was then used to calculate the values of K for each drop sample which, in turn, allowed the estimation of the local Ka distributions using Equations (6.10) and (6.11). The average mass transfer coefficient at any particular point throughout the contactor was therefore calculated using the whole drop size distributions in order to avoid the errors associated with the use of the Sauter mean diameter as an average characteristic length for calculating K. A subsequent integration of the local Ka values over the entire reactor/contactor volume returned the overall volumetric mass transfer coefficient.

$$a_i = 6 \cdot \phi \cdot \frac{n_i \cdot d_i^2}{\sum_{j=1}^{m} n_j \cdot d_j^3} \tag{6.10}$$

$$Ka = \sum_{i=1}^{m} n_i \cdot K_i \cdot a_i \tag{6.11}$$

where, n_i is the probability density of a drop d_i, a_i is its corresponding surface area, and K_i is the mass transfer coefficient of that drop class/sample. Equation (6.10) renders the interfacial area of contact for an individual drop size sampled off the local distribution, whereas, Equation (6.11) describes the integration of the individual volumetric mass transfer coefficient of each drop size sample over the drop size domain in order to calculate the local volumetric mass transfer coefficient. In the current work, the models of Newman (1931), Kronig and Brink (1950), effective diffusivity (Equation (6.2)), slip model (Equation (6.5)) and the newly developed model (Equation (6.8)) were tested and used to calculate the local dispersed phase mass transfer coefficient.

The axial variation of the predicted volumetric mass transfer coefficient along the length of a reactor/contactor equipped with screen-type static mixers is depicted in Figure 6.3, where the mass transfer coefficient was calculated based on Equation (6.8) using a contamination factor value of 0.25. Very high mass transfer coefficients can be clearly observed in the regions of high energy dissipation rates adjacent to the screens with the peaks being more pronounced at high superficial velocities. These quickly decrease as the drops flow further downstream into the regions of low energy dissipation rates. Therefore, the remarkable mass transfer enhancement predicted near the screens can be mainly attributed to the effect of turbulence.

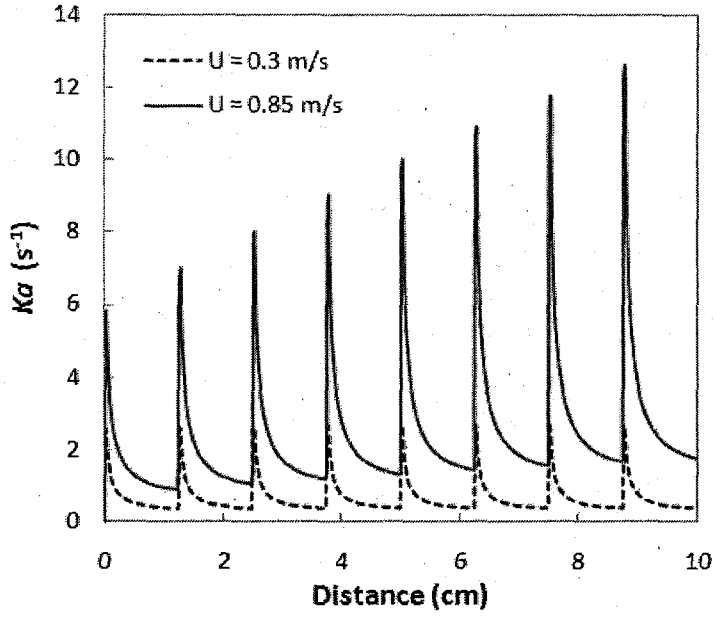

Figure 6.3 Axial variation of volumetric mass transfer coefficient in screen type static mixers using Equation (6.8) with $f_c = 0.25$ ($\phi = 30$ %; $\alpha = 33$ %; $L = 12.7$ mm)

The observations depicted in Figure 6.3 are remarkably analogous to the phenomenological concepts introduced by Skelland and Lee (1981) in which the rate of surface renewal vary periodically as the drops circulate between the regions of high and low energy dissipation rates. However, the main difference between the screen-type static mixers considered in this investigation and MAT is the fact that whereas the former exhibits well controlled flows, the latter conceals large spatial variation in circulation patterns, dispersed phase holdup, and local energy dissipation rates.

6.4.4 Experimental Determination of Mass Transfer in Screen-Type Static Mixers

The mass transfer characteristics of screen-type static mixers were recently investigated (Al Taweel et al., 2007) using the water/ acetic acid / diesel system where the value of the distribution constant is so low (m =0.004) that in accordance with Equation (6.1), the drop side mass transfer coefficient k_d dominates the inter-phase mass transfer operation. The volumetric mass transfer coefficients reported in that investigation were obtained under mainly isotropic homogeneous turbulent conditions and the results obtained offer an excellent opportunity to test the proposed model for dispersed phase mass transfer (Equation (6.8)) and to quantify the errors introduced by applying commonly used models. These results depict some of the highest inter-phase mass transfer coefficients

reported in the literature for liquid-liquid dispersions, and are an order of magnitude larger than the values obtained in the highly effective impinging jet reactors at identical power consumption per unit volume of organic phase (Al Taweel et al., 2007). This shows the advantages that can be gained by being able to intensify mass transfer by judicious application of turbulence intensity without excessive expenditure of energy.

An expanded set of the experimental results obtained in that investigation was used to test and validate the proposed drop-side mass transfer model and the range of the experimental conditions tested in the present work is given in Table 6.3.

Table 6.3: Experimental conditions tested

Inter-screen spacing	25.4 and 12.7 mm
Total superficial velocity, U,	0.18 to 1.1 m/s
Screen fraction open area, α,	0.33
Dispersed phase holdup, ϕ	0.1 - 0.48
Average energy dissipation rate, ε,	1.5 to 117 W/kg
Maximum energy dissipation rate	37 to 6267 W/kg

6.4.5 Testing and Validating the Turbulent Mass Transfer Model

Various models for predicting the dispersed phase mass transfer coefficient are available in the literature. It was therefore necessary to compare the prediction results of the model developed in this investigation against experimental findings as well as predictions from the other models. Therefore, the contamination factor of the proposed model needs to be determined in addition to the empirical constants in the other models to be tested. A base case will be selected for that purpose and the derived constants should be independent of the hydrodynamic conditions and therefore will be kept unchanged when testing and comparing the various models by studying the effect of holdup, velocity, and inter-screen spacing on the overall mass transfer coefficient.

As previously mentioned, the presence of contaminants at the interface between the phases reduces interfacial mobility with a consequent adverse impact on inter-phase mass transfer. This is accounted for in Equation (6.8) through the incorporation of the contamination factor, f_c, the value of which varies from 1 down to about zero. To identify

the value of the contamination factor applicable to the system at hand, the average overall volumetric mass transfer coefficient was fitted against the experimentally measured values. Therefore, a base case (ϕ = 30 %; α = 33 %; L = 25.4 mm), the hydrodynamic conditions of which can be considered as typical for those experimentally investigated, was selected to help identify the various parameters. Various simulation runs were then conducted using different values for f_c and the results obtained are compared to the experimental findings in Figure 6.4. The value of the contamination factor derived thereof should be independent of the operating conditions and/or the design parameters of the mixer.

As can be seen from Figure 6.4, the proposed expression for the drop-side mass transfer coefficient (Equation (6.8)) can accurately predict the effect of the superficial velocity on mass transfer. However, the assumption of a fully mobile interface (i.e. f_c = 1.0) results in overestimating the overall mass transfer coefficient, whereas it is severely underestimated by using the assumption of rigid interfaces (i.e. as $f_c \rightarrow 0.0$). A good match between the predicted values and those determined experimentally was obtained (R^2 = 0.98, σ^2 = 0.04) by using a contamination factor of f_c = 0.39. Although this parameter is expected to vary somewhat under different hydrodynamic and chemical environments, it was found to be capable of matching the experimental results reasonably well over the whole range of experimental conditions used in this investigation.

Similarly for the eddy diffusivity model (Equation (6.2)), an enhancement factor (R = 18.83) was found necessary to render a good fit of the same base case (R^2 = 0.99, σ^2 = 0.02).

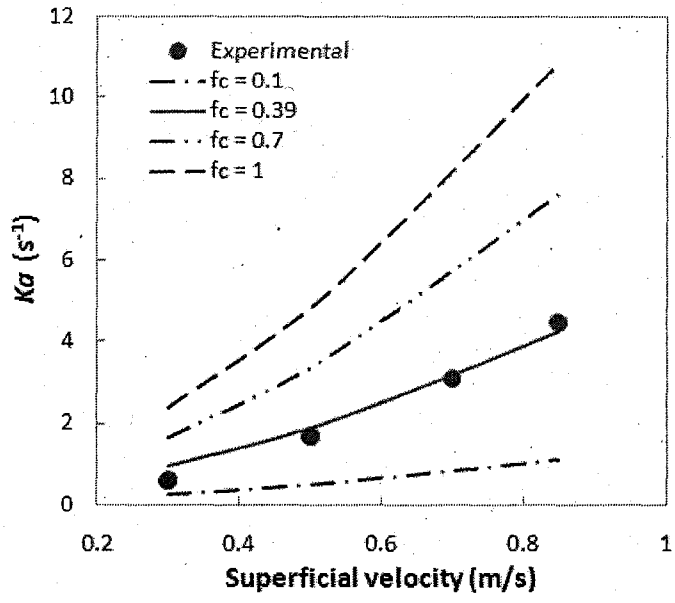

Figure 6.4: Effect of contamination factor on *Ka* predictions
($\phi = 30$ %; $\alpha = 33$ %; $L = 25.4$ mm)

The ability of both the hydrodynamic and mass transfer models developed in this investigation to accurately predict the volumetric mass transfer coefficient was further tested by comparing its predictions with the experimental results obtained at higher dispersed phase concentration ($\phi = 0.48$) and somewhat higher velocities where the effect of turbulence is more pronounced. The results obtained are presented in Figure 6.5 which also includes similar results obtained using commonly used models such as the Newman model (Newman, 1931), the Kronig and Brink model (Kronig and Brink. 1950), the eddy diffusivity model (Equation (6.2)), and the slip model (Equation (6.5)) (Higbie, 1935). The fact that all three models with the exception of the slip model follow the experimental trends and yield reasonably accurate order-of-magnitude analysis of the experimental values is an indication that the hydrodynamic model responsible for predicting drop breakage and coalescence throughout the contactor (used in conjunction with all models) works quite well and yields good estimates of the drop size distributions.

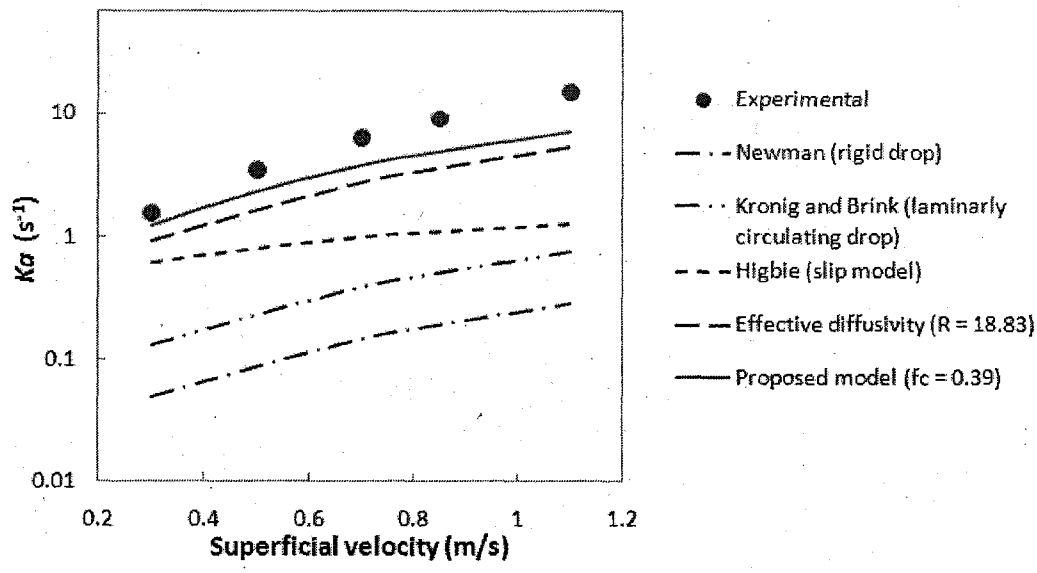

Figure 6.5: Comparative evaluation of the mass transfer models
($\alpha = 33$ %; $\phi = 48$ %; $L = 25.4$ mm)

However, as Figure 6.5 clearly shows, up to a 50-fold error in predicting the volumetric mass transfer coefficient can result through the use of inappropriate mass transfer models at high turbulence intensities. Thus, whereas the rigid, drop model of Newman (1931) predicted very small values, the predictions obtained using the model of Kronig and Brink (1950) (that neglects the effect of turbulence but assumes laminarly circulating drops with a mobile interface) underestimates the experimental findings by a factor of about 20.

Using the same value of the enhancement factor, R, the eddy diffusivity model failed to predict the experimental data (Figure 6.5) over the entire range of flow velocities. Nevertheless, the newly developed model yields better correspondence with the experimental values when a contamination factor value derived from the base case (i.e. $f_c = 0.39$) is used.

To further explore the ability of the model to accurately predict the overall mass transfer coefficient over a wide range of operating and design conditions, the results obtained under smaller inter-screen spacing were compared with model predictions in Figure 6.6. Generally speaking, a decrease in the inter-screen spacing will result in an increase of the average energy dissipation rate in the contactor/reactor (because of the more frequent occurrence of the energy dissipation peaks) and will thus result in enhanced Ka values.

The experimental results presented in Figure 6.6 confirm this tendency as the inter-screen spacing was reduced from 25.4 down to 12.7 mm. Although the Kronig and Brink mass transfer model was able to account for the effect of decreasing the screen spacing, it under-predicted the experimental mass transfer coefficient by an average value of about five. On the other hand, the newly developed model and the eddy diffusivity model in conjunction with the previously identified factors of $f_c = 0.39$ and $R = 18.83$, were found to yield good agreement with the experimental finding. This clearly proves the ability of the hydrodynamic model to properly describe the effect of varying the contactor/reactor design on drop size distribution and the consequent increase in interfacial area of contact.

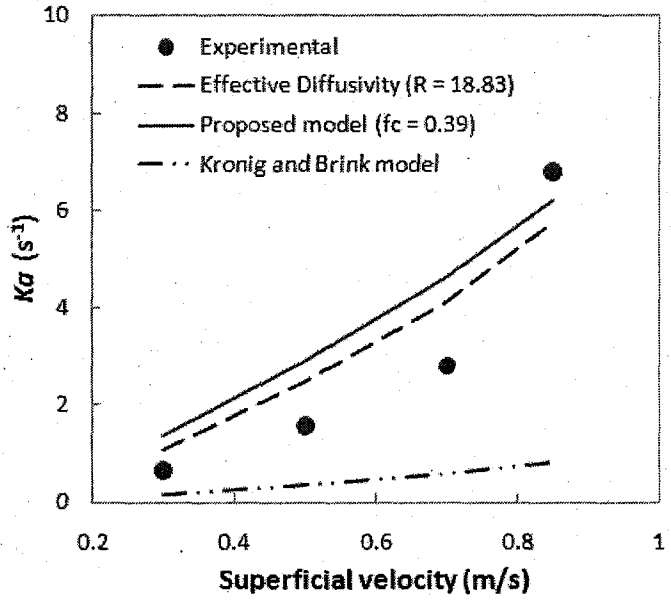

Figure 6.6: Effect of velocity on Ka at a smaller inter-screen spacing ($\alpha = 33$ %; $\phi = 30$ %; $L = 12.7$ mm)

However, at higher dispersed phase holdup and a similar inter-screen spacing ($\phi = 47\%$, $L = 12.7$ mm) the proposed model was found to provide better predictions of the experimental Ka values than the eddy diffusivity model. Increasing the holdup (or dispersed-to-continuous flow ratios) results in increasing the average drop diameter because of the larger drop population densities encountered and the subsequent increase in drop collision and coalescence rates. Therefore, the fact that the newly-developed model can better account for the effect of dispersed phase holdup (at different inter-screen spacing) can be explained by the inherent nature of these models. Whereas, the

effective diffusivity model predicts a strong dependence of the mass transfer coefficient on the drop diameter, the proposed model predicts a decisive influence of the turbulent energy dissipation on k_d while being independent of drop diameter.

Similar trends were obtained when the effect of dispersed phase holdup on the overall mass transfer coefficient was investigated (Figure 6.7) with the best fit being predicted using the proposed model. However, the eddy diffusivity model failed to predict the effect of changing the holdup, where even its ability to follow the experimental trends was not successful. The fact that the predicted Ka values for the case of the eddy diffusivity model decrease while increasing the holdup can be attributed to the aforementioned inherent nature of the model and its dependency on the drop diameter. An increase in the holdup would usually reflect an increase in the mean diameters, however the interfacial area of contact between the phases does not necessarily follow trend since the ratio of the changes in holdup to mean diameter is the decisive one. For the case of the eddy diffusivity model it is apparent that the decrease in the mass transfer coefficient, k_d, due to the increase in holdup and consequently the mean diameters was more pronounced than the apparent increase in the interfacial area of contact.

Even though the values predicted using $f_c = 0.39$ are in close agreement with the experimental observations, it appears that the contamination factor might vary slightly with holdup. This can be explained by the observation that the inter-phase shear stresses are enhanced at higher dispersed phase holdups with a consequent increase in the mobility of their surfaces. However, such a conclusion requires further investigation and experimental testing before correlations between the dispersed phase volume fraction and the contamination factor can be considered.

Henschke and Pfennig (1999) recently investigated the mass transfer to and from single drops and recognized the strong dependence of turbulent mass transfer coefficient on the drop diameter. They argued that for small drop diameters, the turbulent eddies within the drop will be smaller, and their influence will be increasingly damped by the viscosity of the dispersed phase as the drop become smaller. They also observed that for larger drops ($d > 1.5$ mm) the measured mass transfer coefficients are

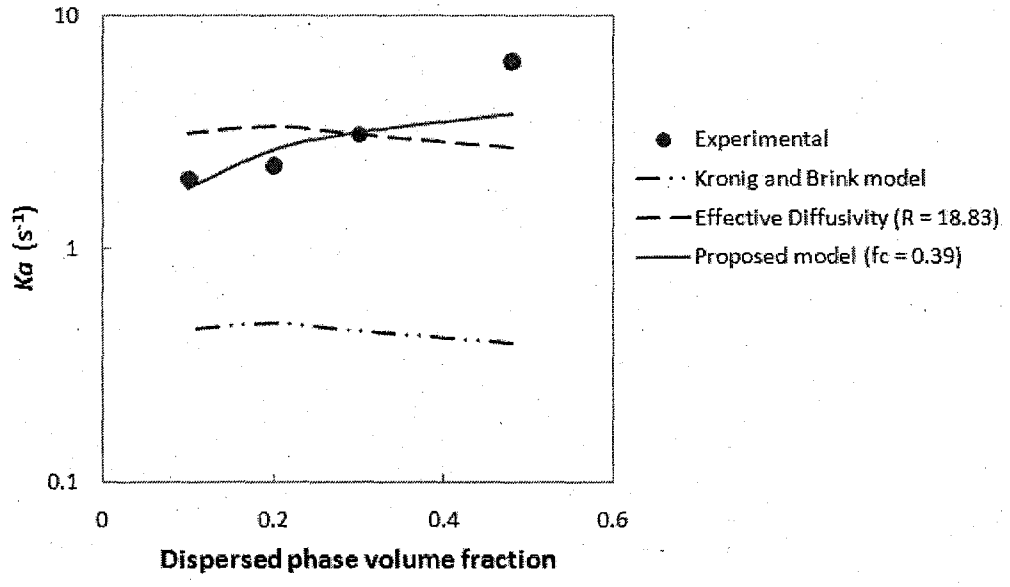

Figure 6.7: Effect of varying the holdup on Ka
(α = 33 %; U = 0.7 m/s; L = 25.4 mm)

often much larger than calculated with the theory of laminar circulation inside drops. While discarding the hydrodynamic reason for turbulent transfer that many investigators (Steiner, 1986; Slater, 1995) apply in the form of eddy diffusivity, Henschke and Pfennig attributed the onset of mass-transfer-induced turbulence to interfacial instabilities and accounted for it by using an instability parameter the magnitude of which is to be determined experimentally. They recommended that this correction factor be used only if the mass transfer coefficient exceeds that predicted by the model of Kronig and Brink. However, the experimental and modeling results presented in the current investigation (Figures Figure 6.5 to Figure 6.7) clearly show that the model of Kronig and Brink (1950) under-predicts the measured volumetric mass transfer coefficient, and since the drop sizes present in screen-type static mixers are expected to be much smaller than 1.5 mm, these results suggest that a significant portion of the dispersed phase mass transfer enhancement observed in turbulent flows can be attributed to hydrodynamic effects. The magnitude of the mass-transfer-induced turbulence proposed by Henschke and Pfennig is therefore expected to be much smaller in high shear contactors/reactors.

Finally, a parity plot is shown in Figure 6.8 for comparison of the experimental and calculated values of the overall volumetric mass transfer coefficient using the proposed

model and the eddy diffusivity model over the entire range of operating and design conditions, and the results clearly demonstrate the validity of the newly developed model.

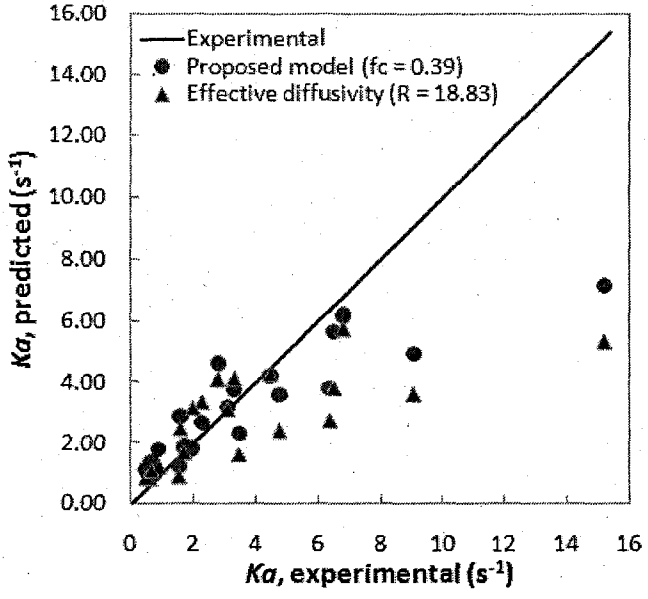

Figure 6.8: Parity plot of simulated values against experimental results

Additional graphs covering the remainder of the investigated operating and design conditions are given in Appendix E.

6.5 Conclusions

A new model capable of calculating the dispersed phase mass transfer coefficient in turbulently flowing dispersions was developed. It is based on Higbie's penetration theory combined with Kawase's surface renewal approach for the turbulent exposure time and can therefore account for the effect of turbulence in the continuous phase on the rate of surface renewal within the drop. The effect of surface contamination on the predicted turbulent mass transfer coefficient was also taken into account using a contamination factor the value of which reflects the degree of surface mobility of the drop.

This model was then incorporated in a population balance based simulation program capable of accurately predicting the drop size distributions obtained in screen-type static mixers, and used to estimate the local dispersed phase mass transfer coefficients under the well known and controlled hydrodynamic conditions present in tubular

contactors/reactors equipped with screen-type static mixers, and the average overall volumetric mass transfer coefficient obtained in such units. The value of the contamination factor, f_c, was determined by matching the predicted overall volumetric mass transfer coefficient with the experimental results.

Good correspondence between experimental and predicted values was obtained by using an f_c value of 0.39 for the system used in these experiments (water/ acetic acid / diesel). This is a reflection of the ability of the hydrodynamic model to accurately predict the drop size distribution, and the ability of the newly developed mass transfer model to predict the effect of turbulence on the drop side mass transfer coefficient. Using the constant value of the contamination factor, the validity of the turbulent drop side mass transfer model was tested over a wide range of dispersed phase holdup and local energy dissipation rates (*e.g.* $0.1 \leq \phi \leq 0.48$; $0.04 \leq \varepsilon \leq 6267$ W/kg) and good agreement between the experimental and predicted results was observed.

A comparative evaluation of the various models capable of predicting the drop side mass transfer coefficient, including the newly developed turbulent one, reveals that:

- The rigid drop model severely under-predicts the mass transfer coefficient achievable in turbulent flows with up to 50-fold error being observed in this investigation.
- Better agreement with the mass transfer data was obtained by using the Kronig and Brink (1950) model which accounts for the effect of laminar circulation within the drop. The predicted values are however still much lower than the experimentally determined values with errors as high as 20-fold being observed.
- The values predicted using an effective diffusivity correction factor of $R = 18.83$ were found to agree well with the base case data (obtained at $\phi = 0.30$ and $L = 25.4$ mm) and were able to correctly describe the variations in the hydrodynamic conditions; however they failed to predict the changes in the dispersed phase volume fraction.
- The dispersed phase mass transfer coefficients predicted by the newly developed model were found to agree well with the experimental data obtained under well

controlled hydrodynamic conditions. With a contamination factor of 0.39, the values predicted by Equation (6.8) are up to 27-fold those predicted by Newman's (Newman, 1931) rigid body model. The present analysis may therefore be providing a hydrodynamic explanation of the empirically determined effective diffusivity correction factor which is reported to vary between 1 and 50 (Slater, 1995).

- The proposed model provided a better fit of the entire experimental results than the eddy diffusivity model. Moreover, it accounted for the effect of changing the dispersed phase volume fraction in a better fashion than the other models as it predicts a decisive influence of the turbulent energy dissipation on k_d while being independent of drop diameter.

These findings suggest that the proposed turbulent mass transfer model may be used to estimate the overall volumetric mass transfer coefficient under more complex hydrodynamic conditions (*e.g.* those encountered in MAT and impinging jet reactors) provided that accurate representation of the bulk flow and the drop breakage/coalescence taking place within such units is achieved. However, the contamination factor applicable to the system under consideration should be known or experimentally determined.

Acknowledgement

The financial support of the Natural Sciences and Engineering Research Council of Canada (NSERC) and Dalhousie University is gratefully acknowledged.

6.6 Nomenclature

a	Interfacial area of contact between the phases	$[m^2.m^{-3}]$
b	Wire diameter	[m]
C	Turbulence decay equation constant	[–]
C_{1-3}	Empirical constants	[–]
C_4	Coalescence efficiency constant	$[m^2]$
D	Diffusivity	$[m^2.s^{-1}]$
D_{oe}	Overall effective diffusivity	$[m^2.s^{-1}]$
d	Drop diameter	[m]

f_c	Contamination factor	[–]
$g(d')$	Breakage frequency of drops of diameter d'	[s^{-1}]
$h(d,d')$	Coalescence intensity of drops of diameter d and d'	[s^{-1}]
k	Individual mass transfer coefficient	[$m.s^{-1}$]
K	overall mass transfer coefficient	[$m.s^{-1}$]
L	Distance between two consecutive screens	[mm]
m	Distribution coefficient	[–]
M	Screen mesh size	[m]
n	Turbulence decay exponent	[–]
n_i	Probability density	[–]
R	Enhancement factor (D_{oe}/D_d)	[–]
t_e	exposure time	[s]
U	Mean velocity	[$m.s^{-1}$]
v_s	slip velocity	[$m.s^{-1}$]
x	Distance down the screen	[m]
x_o	Virtual origin of turbulence decay	[m]

Greek Letters

α	Fraction open area of the screen	[–]
$\beta(d,d')$	Probability that a drop of size d' is formed when a drop d breaks	[–]
ΔP	Pressure drop	[$N.m^{-2}$]
ε	Energy dissipation rate	[$m^2.s^{-3}$]
$\lambda(d,d')$	Coalescence efficiency	[–]
μ	Viscosity	[$Pa.s^{-1}$]
$\nu(d)$	Number of daughter drops formed by breakage of drop d	[–]
ϕ	Dispersed phase volume fraction	[–]
σ	Interfacial tension	[$N.m^{-1}$]
ρ	Density	[$kg.m^{-3}$]

Subscripts

c	continuous phase

d dispersed phase

6.7 References

Al Taweel, A. M.; Chen, C., "Novel static mixer for the effective dispersion of immiscible liquids", Chem. Eng. Res. Des., **74**, 445-450 (1996).

Al Taweel, A. M.; Li, C.; Gomaa, H. G.; Yuet, P, "Intensifying mass transfer between immiscible liquids: Using screen-type static mixers". Chem. Eng. Res. Des., **85**, 760-765 (2007).

Alves, S. S.; Maia, C. I.; Vasconcelos, J. M. T. Gas-liquid mass transfer coefficient in stirred tanks interpreted through bubble contamination kinetics. Chem. Eng. Proc. **43**, 823-830 (2004).

Alves, S. S.; Vasconcelos, J. M. T.; Orvalho, S. P, "Mass transfer to clean bubbles at low turbulent energy dissipation", Chem. Eng. Sci., **61**, 1334-1337 (2006).

Andersson, R., Andersson, B., Chopard, F., Noren, T., "Development of a multi-scale simulation method for design of novel multiphase reactors", Chem. Eng. Sci., **59**, 4911-4917 (2004).

Azizi, F., Al Taweel, A.M., "Reliable Design of Industrial Multiphase Contactors/Reactors", Paper presented at the North American Mixing Forum, Mixing XX; Parksville, BC, Canada, (2005).

Azizi, F., Al Taweel, A.M., "Population balance simulation of intensified gas-liquid contacting", Chem. Eng. Sci., **62**, 7436-7445 (2007).

Azizi, F., Al Taweel A.M., "Hydrodynamics of liquid flow through screens and screen-type static mixers", submitted for publication in Chem. Eng. Comm. (2008a).

Azizi, F.; Al Taweel, A. M., "Algorithm for the accurate numerical solution of PBE for drop breakup and coalescence under high shear rates", submitted for publication in Chem. Eng. Sci. (2008b).

Bakker, A., A.H. Haidari and L.M. Oshinowo, "Realize Greater Benefits from CFD", Chem. Eng. Prog. **97**, 45-53 (2001).

Bart, H.J., "Reactive extraction in stirred columns - A review". Chem. Eng. Tech., **26**, 723-731 (2003).

Botello-Alvarez, E. J.; Navarrete-Bolanos, L. J.; Jimenez-Islas, H.; Estrada-Baltazar, A.; Rico-Martinez, R., "Improving mass transfer coefficient prediction in bubbling columns via sphericity measurements", Ind Eng Chem Res, **43**, 6527-6533 (2004).

Bouaifi, M.; Hebrard, G.; Bastoul, D.; Roustan, M., "Comparative study of gas hold-up, bubble size, interfacial area and mass transfer coefficients in stirred gas-liquid reactors and bubble columns", Chem. Eng. Proc., **40**, 97-111 (2001).

Bourne, J. R.; Lips, M., "Micromixing in grid-generated turbulence. Theoretical analysis and experimental study", Chem. Eng. J. Biochem. Eng. J., **47**, 155-162 (1991).

Briassulis, G., Agui, J.H., Andreopoulos, Y., "The structure of weakly compressible grid-generated turbulence", J. Fluid Mech., **432**, 219-283 (2001).

Camurdan, M. C.; Baird, I. M. H.; Taylor, P A., "Steady state hydrodynamics and mass transfer characteristics of a Karr extraction column", Can. J. Chem. Eng., **67**, 554-559 (1989).

Coulaloglou, C.A., Tavlarides, L.L., "Description of interaction processes in agitated liquid-liquid dispersions", Chem. Eng. Sci., **32**, 1289-1297 (1977).

Dehkordi, A., "Liquid-liquid extraction with chemical reaction in a novel impinging-jets reactor", AICHE J., 48, 2230-2239 (2002).

Handlos, A. E.; Baron, T., "Mass and heat transfer from drops in liquid-liquid extraction", AICHE J., **3**, 127-136, (1957).

Henschke, M.; Pfennig, A., "Mass-transfer enhancement in single-drop extraction experiments", AICHE J., **45**, 2079-2086 (1999).

Higbie, R., "The rate of absorption of a pure gas into a still liquid during a short time of exposure", Trans Amer Inst Chem Eng, **31**, 365 (1935).

Hsia, M. A.; Tavlarides, L. L., "Simulation Model for Homogeneous Dispersions in Stirred Tanks", Chem. Eng. J. Biochem. Eng. J., **20**, 225-236 (1980).

Jajuee, B.; Margaritis, A.; Karamanev, D.; Bergougnou, M. A., "Application of surface-renewal-stretch model for interface mass transfer", Chem. Eng. Sci., **61**, 3917-3929 (2006).

Johnson, A. I.; Hamielec, A. E., "Mass transfer inside drops", A.I.Ch.E. J., **6**, 145-149 (1960).

Kang, H. S.; Chester, S.; Meneveau, C., "Decaying turbulence in an active-grid-generated flow and comparisons with large-eddy simulation", J. Fluid Mech., 129-160 (2003).

Kawase, Y.; Halard, B.; Moo-Young, M., "Theoretical Prediction of Volumetric Mass Transfer Coefficients in Bubble Columns for Newtonian and Non-Newtonian Fluids", Chem. Eng. Sci., **42**, 1609-1617 (1987).

Kronig, R.; Brink, J. C., "On theory of extraction from falling droplets". App. Sci. Res., **A2**, 142-154 (1950).

Kumar, A.; Hartland, S. Correlations for prediction of mass transfer coefficients in single drop systems and liquid-liquid extraction columns. Trans. IChemE, **77**, 372-384 (1999).

Laakkonen, M., Alopaeus, V., Aittamaa, J., "Validation of bubble breakage, coalescence and mass transfer models for gas-liquid dispersion in agitated vessel", Chem. Eng. Sci., **61**, 218-228 (2006).

Newman, A. B., "The Drying of Porous Solids - Diffusion Calculations", Trans Amer Inst Chem Eng, **27**, 310, (1931).

Noh, H. S.; Baird, I. M. H., "Mass Transfer and Pressure Drop in a Cocurrent Reciprocating Plate Extraction Column", AICHE J., **30**, 120-127 (1984).

Paul, E. L.; Atiemo-Obeng, V. A.; Kresta, S. M., "Handbook of industrial mixing : science and practice", Wiley-Interscience: Hoboken, N.J., (2004).

Ribeiro, L.M.; Regueiras, P.F.R; Guimaraes, M.M.L.; Madureira, C.M.N.; Cruz-Pinto, J.J.C., "Dynamic behaviour of liquid-liquid agitated dispersions - I. The hydrodynamics", Comp.. Chem. Eng., **19**, 333-343 (1995).

Saien, J.; Barani, M., "A combined mass transfer coefficient model for liquid-liquid systems

Schmidt, S. A.; Simon, M.; Attarakih, M. M.; Lagar G., L.; Bart, H., "Droplet population balance modelling - Hydrodynamics and mass transfer", Chem. Eng. Sci., **61**, 246-256 (2006).

Sherwood, T. K.; Evans, J. E.; Longcor, J. V. A., "Extraction in spray and packed columns", Ind. Eng. Chem., **31**, 1144-1150 (1939).

Skelland, P. A. H.; Lee, J. M., "Drop Size and Continuous-Phase Mass Transfer in Agitated Vessels", AICHE J., **27**, 99-111 (1981).

Slater, M. J., "Combined model of mass transfer coefficients for contaminated drop liquid-liquid systems". Can. J. Chem. Eng., **73**, 462-469 (1995).

Steiner, L., "Mass Transfer Rates from Single Drops and Drop Swarms", Chem. Eng. Sci., **41**, 1979-1986 (1986).

under simultaneous effect of contamination and agitation", Can. J. Chem. Eng. **83**, 224-231 (2005).

Vasquez, V.; Bautista, R. G., "Mass transfer correlation coefficients for two-phase systems: A general review for liquid-liquid", Miner Process Extr Metal Rev, **17**, 239-255, 1997.

Venneker, B. C. H.; Derksen, J. J.; Van den Akker,Harrie E.A., "Population balance modeling of aerated stirred vessels based on CFD", AICHE J., **48**, 673-685 (2002).

West, F. B.; Robinson, P. A.; Morgenthaler, A. C.; Beck, T. R.; McGregor, D. K., "Liquid-Liquid Extraction from Single Drops", Ind. Eng. Chem., **43**, 234-238 (1951).

Chapter 7.
Intensifying Gas-Liquid Mass Transfer Operations

F. Azizi and A.M. Al Taweel*

Multiphase Mixing and Separation Lab, Department of Process Engineering and Applied Science, Dalhousie University, Halifax NS, Canada B3J 2X4

Technical report to be submitted for publication

Abstract:

An attempt to intensify gas-liquid mass transfer operations was undertaken in which the use of screen-type static mixers to promote inter-phase mass transfer was found to result in volumetric mass transfer coefficients as high as 4.08 s^{-1} at low specific energy consumption rates. Furthermore, k_La was found to increase with an increase in the gas volume fraction because of its subsequent effect in increasing the turbulent energy dissipation rate in the contactor. In addition, the effect of contaminants was studied in terms of adding varying quantities of SDS, where the increase in the interfacial area of contact between the phases due to coalescence retardation proved beneficial to compensate for the reduction in the mass transfer coefficient k_L.

In addition, compared to other commercially available units used for contacting gas-liquid systems, the reactor/contactor investigated showed a superior performance. The screen-type static mixers not only achieved volumetric mass transfer coefficients that are orders of magnitude higher than most contactors, but also a higher mass transfer coefficient per unit volume of the bubbles.

7.1 Introduction

Gas-liquid mass transfer is a commonly encountered rate-limiting step in many multiphase reactions. Gas–liquid contacting therefore emphasizes the enhancement of inter-phase mass transfer which is usually achieved by dispersing the gases into fine bubbles that possess large interfacial area of contact, and by enhancing the inter-phase mass transfer coefficient. Achieving high volumetric mass transfer coefficients, $k_L a$, thus allows for the use of smaller and safer reactors and can significantly increase the selectivity and yield of mass-transfer-controlled chemical reactions. Several contactor types (such as mechanically agitated tanks, plunging and impinging jets, static mixers, bubble and reciprocating plate columns, oscillatory flow reactors) are used for this purpose but the design of such units is very difficult without the employment of empirical knowledge and experience and the use of an extensive amount of pilot-scale testing. This is mainly caused by the very complex hydrodynamic conditions prevalent in these contactors/reactors with the local value of the mixing intensity, gas holdup, and bubble size distribution depicting large spatial variations (Andersson et al., 2004).

Lately, there has been a growing interest in the use of tubular reactors equipped with static mixers as they present an attractive alternative to conventional agitation due to their inherent advantages whereby similar or better performance can be achieved at lower capital and operating costs (Thakur et al., 2003).

Recently, a new type of static mixing element was introduced in which screens or grids are used to repetitively superimpose an adjustable uniformly-distributed turbulence field on the nearly plug flow conditions encountered in high velocity pipe flows. This characteristic made them particularly effective in processing multiphase systems and their ability to promote contact between immiscible liquids were found to be about 5-fold more energy efficient than mechanically agitated tanks equipped with Rushton-type impellers (Al Taweel and Chen, 1996). Interfacial areas as high as 2,200 m^2/m^3 could also be efficiently generated in the case of gas-liquid systems (Chen, 1996). The very high turbulence intensities generated in the regions adjacent to the screens result not only in the formation of fine dispersed phase entities (bubbles and/or drops) but also considerably enhance the value of the inter-phase mass transfer coefficient. The

combined effect of these two factors resulted in inter-phase mass transfer coefficients as high as 13 s^{-1} being achieved in the case of liquid-liquid dispersions (Al Taweel et al., 2007) and allow for 99% of equilibrium conditions to be achieved in less than 1 s.

Furthermore, most industrial liquids contain varying quantities of amphiphilic compounds (alcohols, organic acids, electrolytes, amines, glycols, proteins, finely divided particles and emulsions) the presence of which is known to strongly affect the hydrodynamics of gas/liquid contacting. The presence of these materials also adversely impacts the volumetric inter-phase mass transfer coefficient, k_La, in a fashion that is dependent on their concentration and interfacial activity as well as the type of contactor used (Al-Masry, 1999; Vazquez et al., 2000; Vasconcelos et al., 2002, Linek et al., 2005). This observation is mainly attributed to the reduction of the liquid phase mass transfer coefficient, k_L, due to the presence of contaminant at the interface, and the consequent suppression of internal circulation within the bubble (Rosso et al., 2006). The induced surface elasticity (the Marangoni effect) also dampens the bubble surface/volume oscillations which are known to play an important role in promoting inter-phase mass transfer. On the other hand, the presence of these compounds significantly reduces bubble coalescence rate (Camarasda et al., 1999; Zahradnik et al., 1999, Hébrard et al., 2008), a phenomenon that can be taken advantage of to intensify gas-liquid contacting by generating large interfacial area of contact at low energy consumption rates.

The effect of contaminants on the gas-liquid behaviour of industrial streams can be attributed to the observation that the bi-polar contaminant entities tend to adsorb at the interface and depict interfacial characteristics that are very similar to those of dilute surfactant-containing aqueous solutions, including the development of Marangoni elastic interfacial forces (Al Taweel et al., 2009). When the bubbles move relative to the surrounding liquid, the surface active contaminant entities get convected to the bubble's tailing end where they accumulate forming a stagnant cap. This reduces internal circulation and the value of the inter-phase mass transfer coefficient, k_L, decreases from that of a circulating bubble (Higbie's penetration theory) to that of a rigid sphere (Frössling Equation). This represents up to 7-fold reduction in the case of 1 mm bubbles (Vazquez et al., 2000; Vasconcelos et al., 2002; Alves et al., 2004). Additional reduction is caused by the ability of the Marangoni elasticity to dampen the hydrodynamic

disturbances near the gas-liquid interface (Kastánek et al., 1993; Walter and Blanch, 1986; Vazquez et al., 1997 and 2000), a factor that plays an important role in determining the magnitude of inter-phase mass transfer (Davies, 1972). The decrease in the mass transfer coefficient, k_L, was also attributed to the fact that the surfactants would create a new resistance to mass transfer due to a change in local diffusion at the boundary layer film (Painmanakul et al., 2005; Hébrard et al., 2008).

In a previous study, Al Taweel et al. (2005) found that inter-phase mass transfer can be considerably enhanced by inserting a screen-type static mixing element into the two-phase pipeline flow. In that study, emphasis was placed on achieving significant improvement in inter-phase mass transfer at low energy expenditures and the elements were therefore placed 375 to 1,175 mm apart. Although that arrangement resulted in significantly enhancing the volumetric mass transfer coefficient (particularly in the slowly-coalescent industrial systems and in the presence of surfactants), the value of k_La was limited to the value of 0.44 s^{-1} mainly because of the very low energy dissipation rates encountered throughout most of the reactor/contactor volume. Consequently, the objective of the present work is to investigate the possibility of using smaller inter-screen spacing to achieve very high volumetric mass transfer coefficients in gas-liquid systems while maintaining the plug flow characteristics associated with such design. These factors are crucial for enhancing the yield and selectivity of rapid gas-liquid reactions. Furthermore, the effect of the system's interfacial characteristics on the volumetric mass transfer coefficient in this novel gas-liquid contactor was determined in order to enhance the relevance of the findings to industrial situations.

7.2 Experimental

7.2.1 Experimental Setup

The continuous flow experimental setup used in this investigation is schematically depicted in Figure 7.1. The aqueous phase was prepared and stored in a 500 L agitated tank which was then fed to the static mixer loop using a variable speed centrifugal pump (MONARCH Industries, Model ACE-S20) and its flow rate measured using a paddle flow meter (SIGNET model: MK 309). The desired compressed air flow rate was

adjusted using the pressure regulator and the control valve connected to the mass flow meter. The liquid flow rate was manually varied from 0.4 to 0.96-L/s which yielded liquid superficial velocities, U_L, in the pipe ranging from 0.8 to 1.9 m/s.

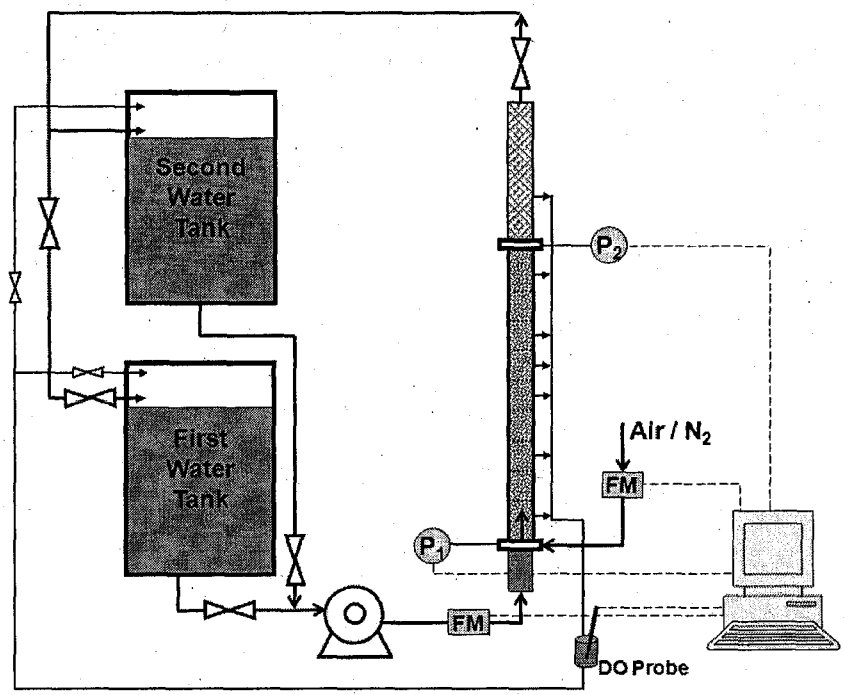

Figure 7.1: Schematic representation of the experimental setup

Gas-liquid contacting was conducted using a 25.4 mm ID vertical pipeline whose mixing section was 560 mm long. The vertical placement was chosen in order to eliminate the introduction of flow non-uniformities due to the action of gravity. In this study, the static mixing elements were made from stainless steel woven wire mesh placed between a set of polycarbonate cylindrical spacers within a 38.1 mm ID transparent polycarbonate pipe. These spacers (70 mm long with 25.4 mm ID hole) ensured that the screens remained perpendicular across the flow direction and maintained the screen interspacing at the desired value. A peripheral ring provided for withdrawing samples from four points around the circumference of the inner pipe, thereby ensuring better representation of the sample composition.

The characteristics of the stainless steel plain-weave wire cloth screens used in this investigation are given in Table 7.1. Screen-type static mixing elements were used in this investigation because of their ability to generate reasonably uniform hydrodynamic

conditions across the cross sectional area of the pipe and their ability to efficiently generate liquid dispersions (Azizi and Al Taweel, 2007; Al Taweel et al., 2007; Al Taweel and Chen, 1996).

Table 7.1: Characteristics of the investigated woven screen

Wire size, b (μm)	*Mesh Size, M* (μm)	*Open Area, α* (%)
165.1	362.8	29.8

The pressure at the inlet to the mixing section, as well as the pressure and temperature at the exit of the mixing section, were monitored and used to calculate the mass flow rate of gas necessary to achieve a certain gas holdup. This was accomplished using a National Instruments data acquisition board (AT-MIO-16E-10) and a specially developed LabVIEW program. Nitrogen was injected into the system through a 2 mm ID horizontal pipe placed 20 mm downstream of the first screen and its flow rate was controlled using a mass flow meter/controller. The oxygen depleted aqueous stream was discarded of directly, however, the option of returning it to a separate storage tank from which it could be recycled to the primary tank at the end of the experiments was available.

A physical technique for measuring the volumetric mass transfer coefficient (oxygen desorption method) was selected in order to eliminate the influence of the reagents needed for the various chemical techniques on bubble breakage and coalescence rates. To determine the value of $k_L a$, the oxygen content in the liquid entering the mixing section, and that in the flowing dispersion was measured using a sensitive dissolved oxygen probe (model OD 7685 supplied by B&C Electronics, with a response time of 0.5 s) at equal intervals of 140 mm which corresponds to the dispersion going through two consecutive screen mixers. This enabled for the continuous monitoring of the oxygen concentration in the water throughout the experiments. Additionally, the temperature was monitored using a thermocouple (Cole Parmer Instruments, Model: 08404-10) while the pressure at the inlet and the outlet of the column was measured using pressure transducers with a response time of 0.01 s (FP 2000 supplied by Honeywell Sensotec Sensors).

Although the setup is capable of operating in the recycle mode, all the experiments reported in this investigation were conducted using a once through approach. Under those conditions, the steady state oxygen concentrations in the feed stream were around 9.78 ± 0.25 ppm as the inlet water temperature was about 9 ± 0.5 °C.

7.2.1.1 Sources of error and reproducibility

The calculated average energy dissipation and energy consumption rates are subjected to errors rising from inaccuracies associated with pressure and flow rate measurements, which generate errors of ± 0.01 % and ± 1 % of full scale respectively. Similarly, the errors related to the volumetric mass transfer coefficient stem from those linked to the pressure drop and flow rate measurements, which would affect the calculations of the equilibrium oxygen concentration, and those of the dissolved oxygen probe, which is about ± 2 %.

For that purpose a reproducibility test was conducted at relatively low flow rates, where the errors are expected to be the highest (U_{mix} = 1 m/s; ϕ = 10 %; C = 0 ppm; ΔP = 32.52 kPa). Based on five replicate measurements, the reproducibility obtained was less than ± 4.2 % for the volumetric mass transfer coefficient (corresponding to less than ± 0.04 mg/L in oxygen concentration measurements) and ± 1 % for the average energy dissipation rate in the system. However, the data presented in this investigation are less prone to error because they were mostly obtained using the average of two replicate measurements.

7.2.2 System Investigated

In this investigation, the system air/tap water was used. However, small quantities of surface active agents (SAA) were added to the aqueous phase in order to simulate the behaviour of industrial streams as well as wastewaters in which SAA are present (Stenstrom and Gilbert, 1981; Wagner and Popel, 1996; Al Taweel et al., 2009). Minute quantities of SDS (supplied by Sigma Chemical Co.) were added to the tap water in order to simulate such coalescence retarding behaviour. This system was selected because it is commonly used to test the effect of interfacial properties on the performance of gas-liquid contactors and its static and dynamic interfacial characteristics are well known.

Three different surfactant concentrations were used in the experiments, namely: 0, 10, and 20 ppm (corresponding to 0, 3.472×10^{-5}, and 7.944×10^{-5} M of SDS respectively). These concentrations are much smaller than the critical micelle concentration of 8.39×10^{-3} M but were found to sufficiently alter the bubble breakage/coalescence processes. The static and dynamic interfacial characteristics, σ and σ_t of these solutions are summarized in Table 7.2. The range of experimental conditions investigated in this study is summarized in Table 7.3.

Table 7.2: Physical properties of systems investigated (Luo, 2002)

SDS Concentration		***Density,*** ρ_L	***Viscosity,*** μ_L	***Surface tension,*** σ	***Surface Pressure,*** Π	***Dynamic surface tension,*** σ_t
(ppm)	(mM)	(kg/m^3)	(cP)	N/m at 25°C	N/m	N/m
0	0	997	0.903	0.072	0	0.072
10	0.0347	997	0.903	0.0614	0.0106	$0.0609+10.1\times10^{-4}\times t^{-0.5}$
20	0.0693	997	0.903	0.0524	0.0196	$0.0471+11.4\times10^{-4}\times t^{-0.5}$

7.2.3 Method of Data Analysis

7.2.3.1 Volumetric mass transfer coefficient

The steady state oxygen desorption technique used in this investigation does not require the introduction of any extraneous chemicals which can alter the interfacial characteristics of the system and can thus provide very accurate results when used properly. However, it requires a good knowledge of the axial dispersion taking place in the contactor in order to accurately determine the value of k_La. Because of the radial uniformity of the hydrodynamic resistance offered by the screen elements and the large axial resistance offered by the screens, the flow conditions were found to be essentially plug flow in the case of closely spaced screen-type static mixers (Ziolkowski and Morawski, 1987).

The volumetric mass transfer coefficient was measured in an oxygen/nitrogen/water system, where gaseous nitrogen was fed to the reactor just before entering the mixing section (20 mm before the first static mixer element). The nitrogen-rich gaseous stream

Table 7.3: Range of experimental conditions investigated

Parameter	Operating Conditions
Number of screens elements	8
Inter-screen spacing, L_{screen}	70 mm
Screen open area, α	29.8 %
Length of the mixing section, L_M	560 mm
Total superficial velocity, U_{mix}	1.0 – 2.0 m/s
Liquid superficial velocity, U_L	0.8 – 1.9 m/s
Gas superficial velocity, U_G	0.05 – 0.4 m/s
Temperature in the contactor	9 ± 0.5 °C
Dispersed phase holdup, ϕ	0.05 – 0.2
Pipe Reynolds number, Re	~ 21,000 –54,000
ΔP across the column	28 – 90 kPa
Residence time in the mixing section, t	0.23 – 0.56 s
Average energy dissipation rate, ε	~ 40 – 217 W/kg
Maximum local energy dissipation rate, ε_{max}	4,970 – 39,775 W/kg
Residence time in high shear regions,	145.12 – 290.24 μs
SDS concentration	0.0 – 20 ppm

strips the oxygen from the liquid stream flowing through the static mixer (nitrogen is thus transferred from the gas bubbles into the liquid while, simultaneously, oxygen is transferred from the liquid into the gas bubbles). Under these conditions, the inter-phase rate of mass transfer can be expressed as,

$$\frac{\delta C_{O_2}}{\delta t} = k_L a\left(C_{O_2} - C^*_{O_2}\right) \tag{7.1}$$

Where $C^*_{O_2}$ is the oxygen concentration in the liquid phase at equilibrium with the gases present in the bubbles.

Assuming that the volumetric mass transfer coefficient, $k_L a$, to be constant throughout the contactor volume, Equation (7.1) yields the following expression upon integration,

$$\ln\left(C_{O_2} - C^*_{O_2}\right) = -k_L a \cdot t + \ln\left(C_{O_2,in} - C^*_{O_2,in}\right) \tag{7.2}$$

Where C_{O_2} is the oxygen concentration in the liquid at the sampling point while $C^*_{O_2,in}$ and $C_{O_2,in}$ represent the initial conditions at the reactor inlet. Since the value of the equilibrium oxygen concentration, $C^*_{O_2}$, varies with the location along the contactor/reactor length, its value at every sampling point was determined by a simple mass balance that takes into account the changes of the amount of oxygen present in both the liquid and gaseous streams. In order to calculate the equilibrium O_2 concentration, the total amount of transferred material was calculated from the measured O_2 concentration and the corresponding partial pressure of O_2 in the gas stream was then determined. Based on that information, $C^*_{O_2}$ in the liquid was then calculated using Henry's law. The Henry's constant for O_2 which equals to 769.2 L.atm/mol at 298 K was corrected for the current operating temperature of 282 K using a van't Hoff equation (Staudinger and Roberts, 2001). Depending on the volumetric flow rates of the aqueous and gaseous phases, the value of $C^*_{O_2}$ at the outlet was found to vary between 0.28 and 1.17 ppm.

If the assumption that the value of $k_L a$ remains constant throughout the contactor, a plot of $\ln\left(C_{O_2} - C^*_{O_2}\right)$ vs. time should therefore yield a straight line the slope of which is equal to the volumetric mass transfer coefficient. As can be seen from the typical results shown in Figure 7.2 this assumption holds true for the static mixer at hand and the approach used in this investigation allows for the accurate determination of the mass transfer coefficient (maximum deviation from the regression line being within ± 5 %) in a fashion that is far superior to that obtained using the two-point approach which relies solely on measuring the inlet and exit concentrations.

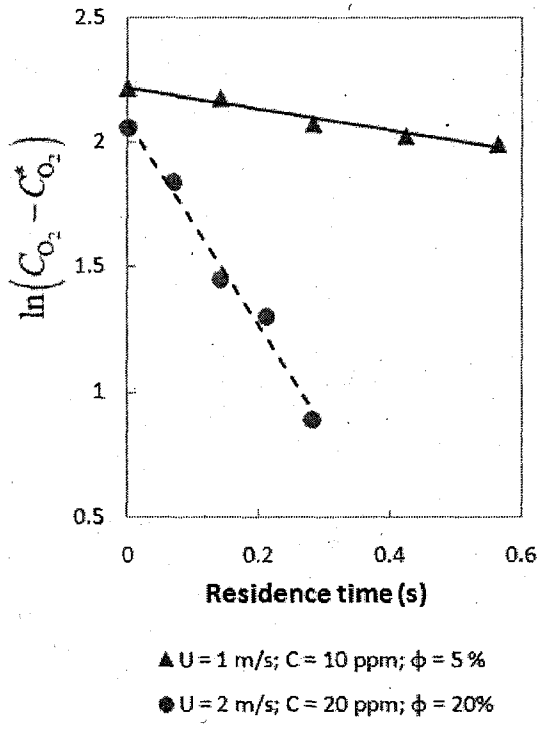

Figure 7.2: Typical experimental results

7.2.3.2 Energy dissipation and power consumption

The pressure drop is the most important design criterion for a static mixer as it is directly related to the energy dissipation rate and has a decisive role in estimating the energy efficiency of static mixers (Heyouni et al., 2002). It also plays a crucial role in determining the bubble size distribution of the emerging dispersion.

Three different sources contribute to the overall pressure drop in the reactor at hand; namely, pressure drop due to the friction at the pipe wall, pressure drop due to the difference in static head caused by the vertical orientation of the mixer, and the pressure drop caused by the flow across the screens. These, in turn, are affected by several operational and design parameters such as the liquid and gas flow rates, the contactor/reactor length, and the number and geometrical configuration of the screen elements used. However, under the highly turbulent conditions encountered in the current study, the pressure drop across the screens is the most dominant parameter where its contribution to the overall pressure drop in the system was found to vary between 70 to 90 % depending on the operating conditions.

The volume-average turbulent energy dissipation rate in the mixer was calculated from the measured pressure drop values using the following expression,

$$\varepsilon = \frac{Q_L \cdot \Delta P}{\rho_L \cdot V_L} \tag{7.3}$$

However, it is well known that the local value of ε downstream from the screen undergoes dramatic variation along the axis of flow with the maximum value being encountered in the immediate vicinity of the screen. Figure 7.3 clearly depicts this behaviour where up to 160-fold variation in ε could be observed within a $7M$ distance downstream of a screen (corresponding to about 2.5 mm for the screen geometry investigated in this work) (Azizi and Al Taweel, 2008).

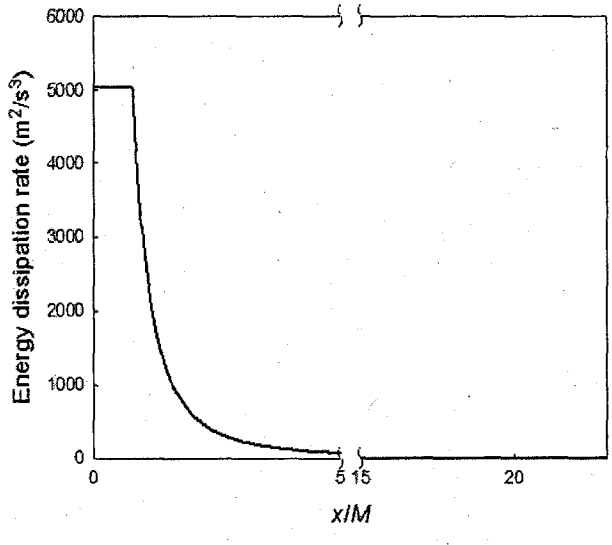

Figure 7.3: Axial variation of energy dissipation rate (U = 1.0 m/s, M = 362 μm, α = 0.33) (Azizi and Al Taweel, 2008).

Such knowledge of the spatial distribution of the local energy dissipation rate is of great importance when characterizing or designing multiphase contactors/reactors as it plays a crucial role in determining the extent of breakage and coalescence events.

There are alternative ways by which the energy input to a mixer (or the rate of energy dissipation) can be characterized. The first approach is related to the overall amount of energy supplied to the mixer per time unit, E. This term represents the power input of electric motors driving gas blowers or compressors, liquid pumps, or agitating devices.

For the case of in-line static mixers, the following simplified expression can be used for the energy consumption in the contactor/reactor,

$$E = \Delta P \cdot (Q_L + Q_G) \tag{7.4}$$

The second approach focuses on the rate of energy dissipated per unit time and unit mass in the region where the gas dispersion is formed. The whole dispersion volume is often used if mixing intensity is taken as essentially uniform throughout the contactors volume. This parameter is extensively used to characterize energy demands of various mixer types. In the case of in-line static mixers, the energy dissipation rate per unit reactor volume is given by,

$$E_V = \frac{E}{V} \tag{7.5}$$

while the energy dissipation rate per unit mass of the treated liquid can be written as,

$$E_m = \frac{E}{V \cdot \rho_{mix}} \tag{7.6}$$

However, these parameters do not truly reflect the energy that has to be provided while processing the immiscible dispersion since they do not take into account the residence time requirements for various mixer types, a factor which can significantly affect power consumption (Al Taweel et al., 2007). To overcome this difficulty, the concept of the energy needed to process a unit of the flowing mixture was applied by Koglin et al. (1981) and Al Taweel and Walker (1983) to the case of continuously flowing systems. This parameter has the advantage of representing the concerns of mixing equipment users rather than those of equipment designer and has recently been adopted by many investigators (Schubert and Engel, 2004; Kuzmin et al., 2005). It also allows for comparing the performance of mixing units with significantly different mixing times. The energy needed to process a unit of the dispersed phase was thus calculated from,

$$E_{spm} = \frac{E}{V \cdot \rho_{mix}} \times (\text{residence time}) \tag{7.7}$$

Alternatively, the overall amount of gaseous matter transferred to or from the liquid phase per unit energy consumed can be used instead of $k_L a$ to characterize energy effectiveness of inter-phase mass transport. This basic parameter E_t (kgO_2/kWh),

representing the amount of oxygen transported to or from liquid phase per unit of energy consumed, is extensively used in the field of water/wastewater treatment to characterize the effectiveness by which energy is utilized to facilitate interfacial mass transport.

The amount of oxygen transported from the gaseous matter to the liquid phase, M_{O_2}, is given by,

$$M_{O_2} = Q_L \cdot \left(C_{O_2,in} - C_{O_2,out}\right) \tag{7.8}$$

while the amount of oxygen transferred per unit power consumption, E_t, is given by,

$$E_t = \frac{M_{O_2}}{E} \tag{7.9}$$

7.3 Results and Discussion

In this investigation, the effect of various operational parameters as well as the system's interfacial characteristics were investigated with the objective of identifying their effect on energy dissipation in the mixer, the volumetric mass transfer coefficient achieved, and the efficiency by which energy is used to facilitate inter-phase mass transfer.

It should be noted that under the various operating conditions, especially at low liquid superficial velocities and high dispersed phase volume fraction, the gas-liquid dispersion remained in the bubbly regime. This was determined by visual observation. However, the dispersion got a "milky" appearance and turned more opaque with increasing the superficial velocity and/or the surfactant concentration. This is clearly evident from Figure 7.4 which shows the evolution of the dispersion (after the last screen element) from a clean system at low average superficial velocities (Figure 7.4-a) where the pipe appears to be clear; to that of a flowing dispersion in the presence of SDS (Figure 7.4-b) which looks "milkier" and of a more opaque appearance.

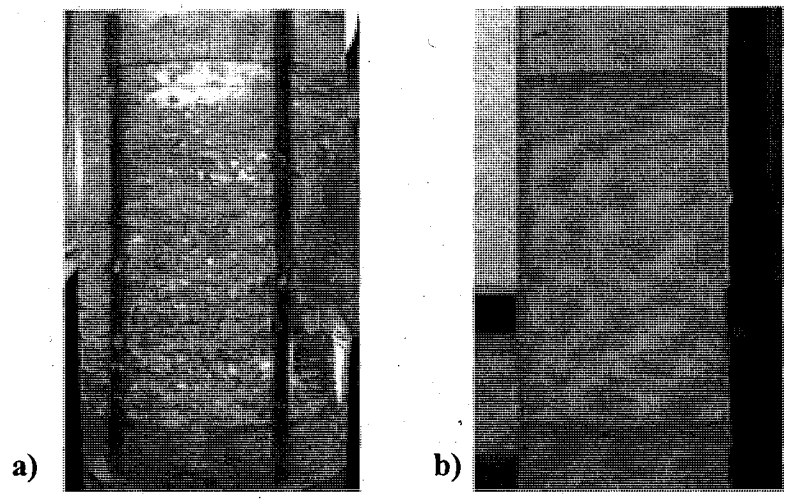

Figure 7.4: Effect of screen-type static mixing elements on the gas-liquid dispersion a) U_{mix} = 0.6 m/s; ϕ = 5 %, C = 0 ppm b)U_{mix} = 1.3 m/s; ϕ = 10 %, C = 10 ppm

7.3.1 Pressure Drop

As previously stated, the pressure drop is the most important criterion in characterizing static mixers as it controls the value of the energy dissipation rate. As can be seen from Figure 7.5a, the pressure drop in the screen-type static mixer increases as the total superficial velocity is increased. Typically, the pressure drop across the screen is caused by the contribution of both viscous and inertial resistances. The viscous resistance usually dominates in the laminar flow region where the pressure drop is attributed to the viscous drag (i.e. skin friction at the surface of the screen wires). At higher flow rates, the effect of the viscous forces become relatively unimportant and the total inertial pressure losses result mainly from the turbulent vortices and pressure drops caused by sudden enlargement and sudden contraction around the wire mesh screen. However, at any particular total superficial velocity the pressure drop across the contactor was found to decrease upon the introduction of the gaseous dispersed phase with the effect being more pronounced as the volume fraction of the gas is increased (Figure 7.5a). This is mainly caused by the lowering of dispersion density (which is essentially inversely proportional to the gas-to-liquid flow ratio) and the consequent reduction in the kinetic energy of the micro-jets formed by the screen (Azizi and Al Taweel, 2008). This, however, could not account for the full pressure reductions observed, and the remaining difference may be

attributed to the reduced drag coefficient observed in the presence of fine bubbles in the flowing stream (Chen, 1996), a phenomenon somewhat similar to that reported when a bubble blanket is used to reduce the drag on boat hulls (Amromin et al., 2006). The increased compressibility of the gas-liquid dispersion could also allow a higher recovery of the inertial losses when the two-phase mixture goes through the screens, thereby, decreasing the total pressure losses.

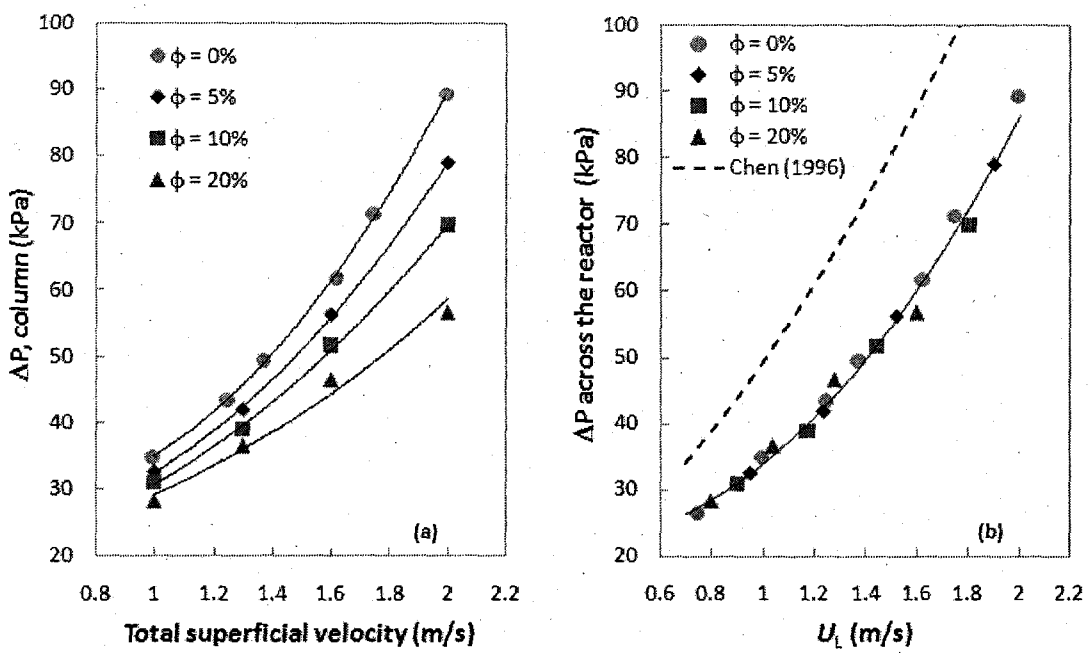

Figure 7.5: Effect of gas-to-liquid flow ratio on the pressure drop across a screen-type contactor/reactor

This is clearly evident from the results shown in Figure 7.6-a where the average turbulent energy dissipation rate, ε, was found to slightly increase with increasing gas holdup. Such a behaviour is expected to affect the volumetric mass transfer coefficient since the turbulence intensities in the continuous phase are considerably increased at higher gas holdups. A higher ε value would result in increasing bubble breakage frequency (hence a higher interfacial area of contact) while the mass transfer coefficient, k_L, would also be enhanced considerably as the rate of surface renewal, which is directly proportional to the rate of turbulent kinetic energy dissipation, is increased.

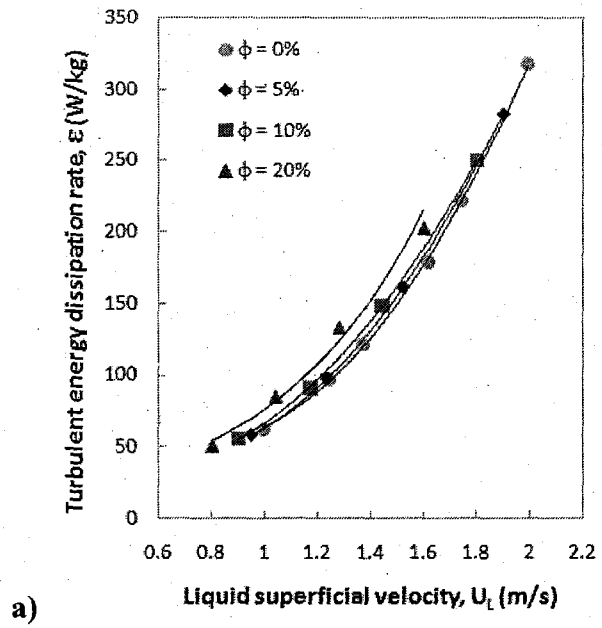

a)

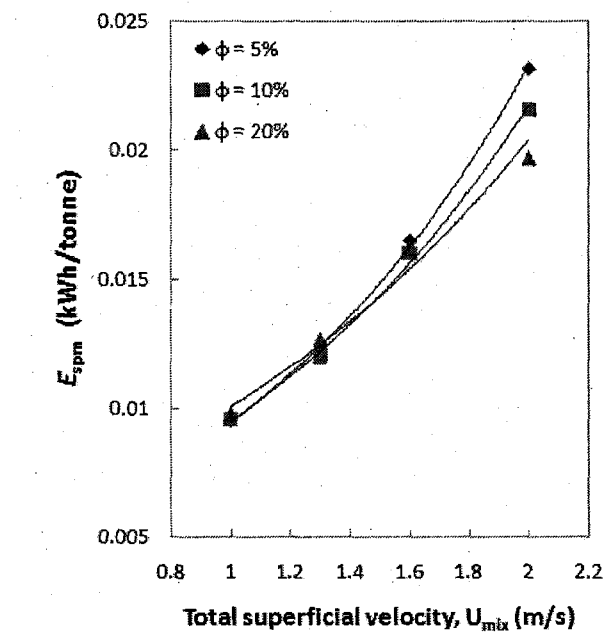

b)

Figure 7.6: Effect of gas holdup on the turbulent energy dissipation rate, ε and the specific energy consumption per unit mass processed (pressure drop averaged for various surfactant concentrations)

However, such increase in the turbulent energy dissipation does not necessarily reflect an increase in the power consumption rates. As can be seen from Figure 7.6-b, an increase in the dispersed phase volume fraction was found to reflect a decrease in the specific power

consumption per unit mass processed of the continuous phase. While such a decrease emanates from the apparent decrease in the total pressure drop with ϕ, the extent of reduction is however slower because of the consequent decrease in the processed mass.

As can be seen from Figure 7.5-b, the experimental pressure drops results obtained in this investigation are much smaller than those predicted by the correlation proposed by Chen (1996). This discrepancy can be attributed to the use of a much finer screen geometry in this investigation. Thus whereas most of the screens used by Chen were characterized by a larger mesh size (1.058 – 2.117 mm), the mesh size of the screen used in the current work is approximately three-fold smaller.

The pressure drop data obtained in this investigation (49 points) were correlated using Equation (7.10) and good agreement between predicted and experimental data was achieved (Figure 7.7a).

$$\Delta P = 36.23 \times U_L^{1.19} \times (1-\phi)^{0.231} \qquad \left(R^2 = 0.964\right) \tag{7.10}$$

To highlight the phenomenon of drag reduction encountered by bubbly two-phase flow through screens, the screen drag coefficient was correlated in a fashion similar to that proposed by Ehrhardt (1983) and Chen (1996) where the drag coefficient is given as a function of the screen open area, α, and the wire Reynolds number, Re_b, $\left(Re_b = \frac{b \cdot U \cdot \rho}{\mu}\right)$. However, the effect of the dispersed phase volume fraction was also taken into account to reflect the effect bubbles have on the drag coefficient. As can be seen from the parity plot depicted in Figure 7.7b, the drag coefficient correlation presented in Equation (7.11) yields good correspondence with the experimental results.

$$\Psi = \frac{21.76}{\left(Re_b / \alpha\right)^{0.514}} \cdot (1-\phi)^{1.16} \cdot \left(\frac{1-\alpha}{\alpha^2}\right) \qquad \left(R^2 = 0.82\right) \tag{7.11}$$

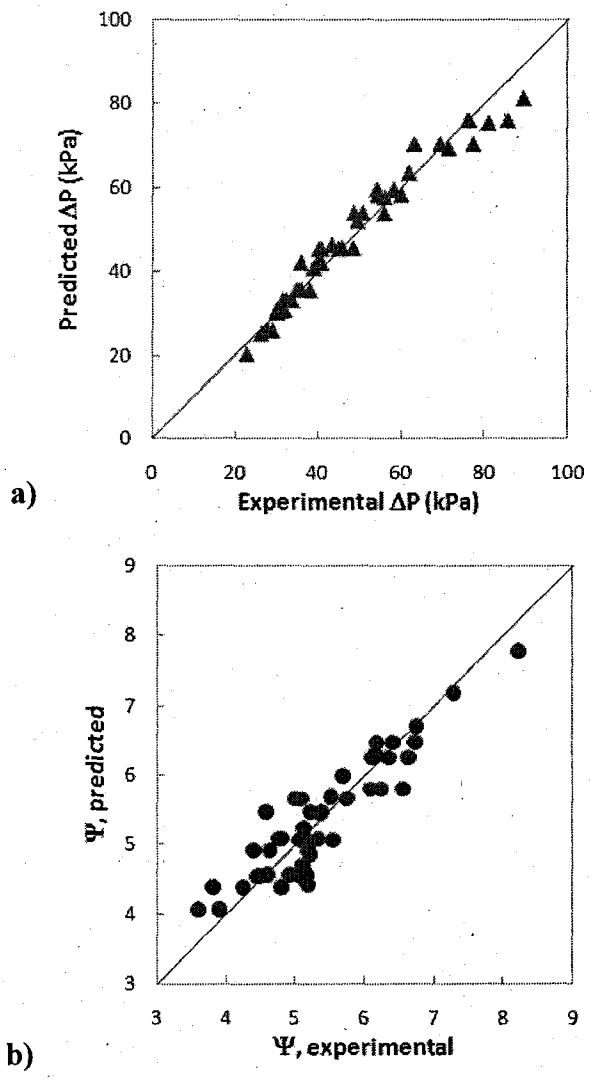

Figure 7.7 Parity plot of predicted values against experimental results for the pressure drop (a) and the drag coefficient of the screen (b).

7.3.2 Volumetric Mass Transfer Coefficient

In a previous study, Al Taweel et al. (2005) found that mass transfer is considerably enhanced by introducing a screen-type static mixing element into the two-phase pipeline flow. Although high energy utilization efficiencies were achieved by introducing one or two screen elements placed 375 to1,175 mm apart, the resulting volumetric mass transfer coefficient was limited to relatively low values (< 0.44 s^{-1}). Such contacting arrangement will therefore be most suitable for use in processing operations where energy expenditures are of primary importance (e.g. wastewater aeration and stripping of volatile compounds) or for conducting relatively slow multiphase chemical reactions where

reaction selectivity and/or process safety does not play a critical role (e.g. oxidation of trace compounds, disinfection by ozonation). On the other hand, the ability to achieve high volumetric mass transfer coefficients plays a significant role in enhancing the conversion, selectivity and inherent safety of fast multiphase reactions. The present investigation therefore focuses on the potential for achieving high volumetric mass transfer coefficients by using closely spaced screen-type static mixing elements. Attention was focused on the effect of superficial liquid velocity, the gas-to-liquid flow ratio, as well as the interfacial characteristics of the system.

7.3.2.1 Effect of superficial liquid velocity

The superficial liquid velocity controls the residence time of the dispersed phase in the mixer. It also controls the intensity of turbulence generated, its characteristic length, and the rate at which energy is dissipated. This applies to the turbulence generated by the pipe flow as well as that generated by the screen-type static mixing elements (Azizi and Al Taweel, 2008). All of these factors play an important role in determining, gas holdup, bubble size distribution and inter-phase rate of mass transfer.

As previously mentioned, an increase in the liquid superficial velocity results in increasing the pressure drop and the average turbulent energy dissipation rate, ε. For a gas-liquid dispersion flowing through regions of high energy dissipation rates, the bubbles undergo very rapid breakage into a fine dispersion that generates very large interfacial area of contact between the phases. Consequently, higher k_La values are expected to be achieved at higher velocities particularly since the value of the mass transfer coefficient, k_L, is expected to be enhanced by the highly turbulent regions generated by the screens. This is in line with the recent findings which showed that under high turbulent conditions, the mass transfer coefficient is independent of the bubble size but is a function of the turbulent kinetic energy dissipation rate (Lezhnin et al., 2003, Linek et al., 2004; Alves et al., 2006).

Figure 7.8a, clearly shows such behaviour where an increase in the total superficial velocity results in increasing the value of k_La. The importance of the turbulent energy dissipation rate is clearly shown in Figure 7.8b where larger k_La values were obtained at higher energy dissipation rates. This is particularly true at large gas-to liquid ratios where

the greater coalescence tendencies are counteracted by the higher shear stresses. Such behaviour was observed in the presence or absence of surface active agents in the system.

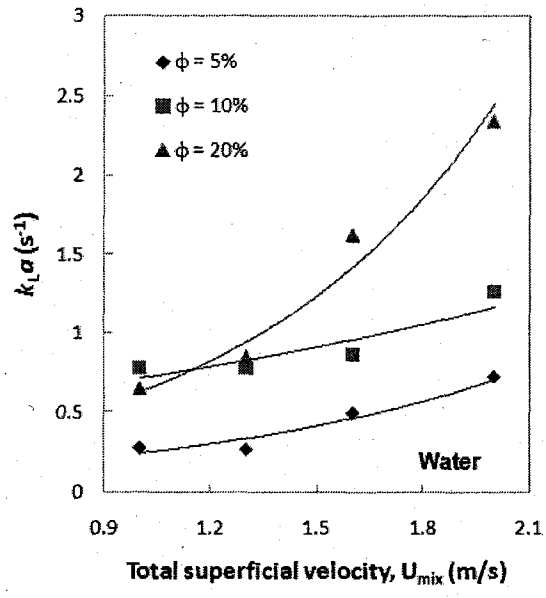

a)

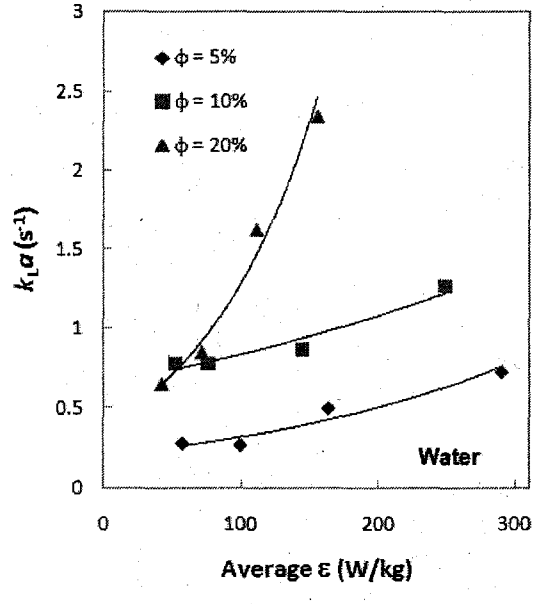

b)

Figure 7.8: Effect of the total superficial velocity and the turbulent kinetic energy dissipation rate on the volumetric mass transfer coefficient.

7.3.2.2 Effect of gas-to-liquid flow ratio

For the case of a gas-liquid dispersion with a constant energy dissipation rate, an increase in the holdup results in increasing the bubble population density which enhances bubble collision and coalescence rates and shifts the bubble breakage/coalescence equilibrium towards the formation of larger bubbles. Consequently, the interfacial area of contact between the phases does not necessarily increase in proportion to the gas holdup unless coalescence is completely suppressed. However, under conditions where coalescence can take place, the impact of increasing gas holdup depends on the two counteracting influences and is determined by the ratio between gas holdup and Sauter mean bubble diameter.

The effect of the gas-to-liquid flow ratio (which is essentially equal to the gas holdup, ϕ, for the very small bubbles encountered in the present investigation) on the average volumetric mass transfer coefficient was conducted at different SDS concentrations and some of the results obtained are shown in Figure 7.9. The dispersion gas holdup was found to exert a strong impact on the value of k_La which was found to increase with increasing gaseous volume fraction. This can be attributed to the observed enhancement in the turbulent energy dissipation rate when the dispersed phase volume fraction is increased.

This is in line with the experimental findings of Chen (1996) and the population balance simulations of Azizi and Al Taweel (2007), who reported an enhancement in the interfacial area of contact with an increase in the gas holdup for the case of turbulently flowing gas-liquid dispersions in screen-type static mixers. In addition, the increase in the turbulent energy dissipation rate is also known to increase the value of the mass transfer coefficient, k_L. Therefore, the substantial improvement in the value of k_La is due to the cumulative effect of both factors.

It is interesting to note that when the gas holdup increased from 5 to 10 %, the volumetric mass transfer coefficient almost doubled as well. However, as the dispersed phase volume fraction is further increased from 10 to 20 %, the value of k_La did not follow the trend, but increased by a value of about 80%. This could be attributed to either an

enhanced coalescence rate, which is not expected to play a major role in the presence of surfactants; or to the compressibility of the dispersed phase.

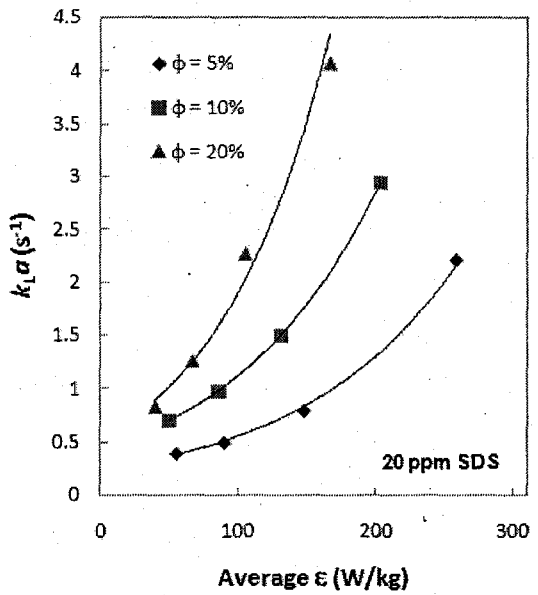

Figure 7.9: Effect of gas-to-liquid flow ratio on the volumetric mass transfer coefficient.

7.3.2.3 Effect of interfacial characteristics

Although the presence of small quantities of SDS is expected to somewhat decrease the maximum stable bubble size (due to the reduction of static surface tension), this tendency is counteracted by the tendency to impede bubble breakage due to the development of the Marangoni elastic forces (Walter and Blanch, 1986). On the other hand, bubble coalescence rate is strongly hindered by the presence of very small SDS concentrations (Majirova et al., 2004). Consequently, the fine bubbles generated at the screen-type mixing elements will be maintained for longer downstream distances, thereby yielding high specific interfacial areas which should enhance the value of the volumetric mass transfer coefficient. This was experimentally confirmed by Chen (1996) and by the population balance simulation results undertaken by Azizi and Al Taweel (2007). However, as mentioned previously, the presence of SDS negatively affects the liquid-phase mass transfer coefficient k_L. The effect of SDS concentration on the average volumetric mass transfer coefficient is therefore a function of the overall effect of these competing factors.

The results obtained in this investigation clearly show that in the case of closely placed screen-type static mixing elements, the value of $k_L a$ increases with an increase in the SDS concentration (Figure 7.10) with the magnitude of the increase being most prominent at higher surfactant concentrations and high energy dissipation rates. This observation suggests that under the conditions used in this investigation, the reduction in the value of the inter-phase mass transfer coefficient caused by the presence of the surfactants does not outweigh their ability to retard the coalescence rate and maintain the large interfacial area generated downstream from the screens for a long distance (thereby increasing the average interfacial area of contact between the phases). Similar observations have been reported by Jackson (1964) and Zlokarnik (1985). Furthermore, these findings are in line with those reported by Al Taweel et al. (2005) where one or two screen-mixing elements were introduced in a pipe flow to enhance the mass transfer performance of the contactor. However, in their study, the volumetric mass transfer coefficient was found to increase with an increase in the SDS concentration up to 10 ppm and then decreases with further additions. Such behaviour could well be attributed to the different hydrodynamic

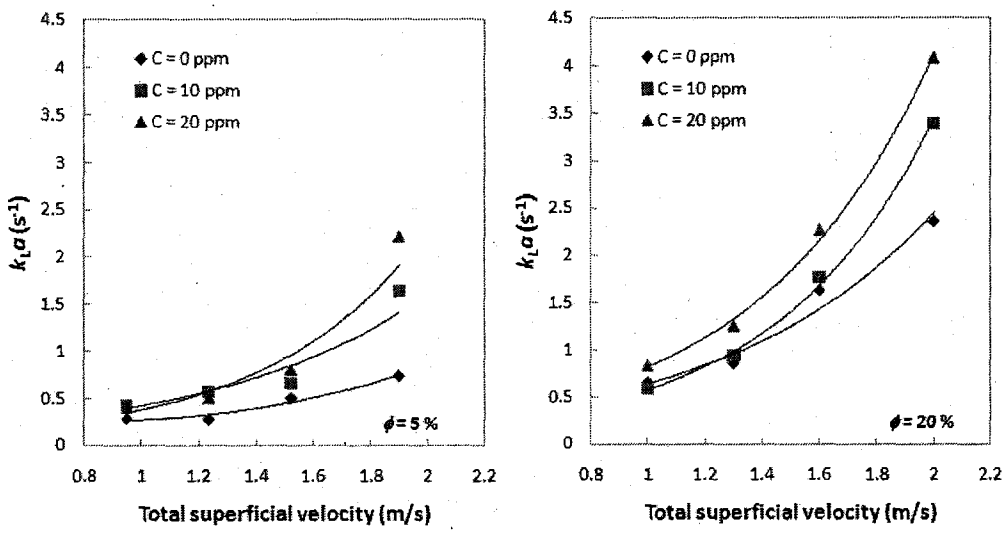

Figure 7.10: Effect of SDS concentration on the average volumetric mass transfer coefficient.

conditions encountered in the two contactors. Whereas the mixing elements were placed 70 mm apart in the current investigation with the purpose of intensifying the oxygen

transfer in the shortest distance, those in the study of Al Taweel et al. (2005) were placed at a much larger inter-screen spacing (700 to 1,200 mm apart).

As previously mentioned, the presence of contaminants at the interface between the phases reduces interfacial mobility and helps maintaining a finer dispersion for longer residence times without requiring additional energy input to the system. However, a further increase in the SDS concentration (from 10 to 20 ppm) at the same energy input would have resulted in a further suppression of k_L. This reduction in k_L thus outweighed the enhancement in the interfacial area of contact and resulted in the observed decrease in k_La. On the other hand, focusing the energy dissipation in a smaller volume proved beneficial to compensate for the suppression of the mass transfer coefficient in the presence of surfactants.

These observations stand in contrast to the findings of several investigators where the presence of anionic or cationic surfactants in the system was found to significantly reduce the value of the volumetric mass transfer coefficient (Koide et al., 1985; Kastánek et al., 1993; Vasconcelos et al., 2003; Painmanakul et al., 2005; Sardeing et al., 2006; Rosso et al., 2006). This is mainly attributed to the approach adopted in this investigation which focuses energy dissipation rate within a small volume and relying on the surfactants to retard coalescence rate in regions of low energy dissipation rates.

The impact of inter-screen spacing on interphase mass transfer can be best illustrated by the observation that whereas k_La values as high as 0.44 s^{-1} were observed in the work of Al Taweel et al. (2005) in the presence of 10 ppm SDS, volumetric mass transfer coefficients as high as 3 s^{-1} were observed in the current work for the same level of contamination and superficial velocities.

7.3.3 Energy Utilization Efficiency

The efficiency by which energy is utilized to promote mass transfer is one of the most important factors in evaluating the performance of gas-liquid contactors. This is often expressed using the parameter E_t, which represents the amount of oxygen transported to/or from the liquid phase per unit of dissipated energy ($kg(O_2)/kWh$). Thus, the value of E_t achieved using various gas-liquid contactors depends on the design particulars of the unit as well as the interfacial characteristics of the system (Stenstrom and Gilbert, 1981).

However, such aeration efficiency is usually reported at a standard temperature; while the temperature of 10 °C is used in Germany, 20 °C is the standard in the USA (Cancino et al., 2004). Since the data obtained in this investigation were at a temperature of 9±0.5 °C, the German standard will thus be used. Because the oxygen transfer rate from or to the liquid is the same, the aeration efficiency will be calculated using the following expression,

$$E_t = \frac{k_L a \cdot C^*_{O_2@10°C} \cdot V_L}{E} \tag{7.12}$$

Where $C^*_{O_2@10°C}$ is the saturation concentration of O_2 in the water at 1 atm and 10 °C and is equivalent to 11.29 ppm. Nonetheless, the value of the aeration efficiency can be easily adjusted to different temperatures by re-adjusting the value of the saturation concentration to that of the corresponding operating temperature. This is true if the assumption of a negligible effect of the temperature on the interfacial area of contact between the phases, and that no change in the concentration and/or diffusivity of the contaminants at the interface is induced by temperature changes, holds valid.

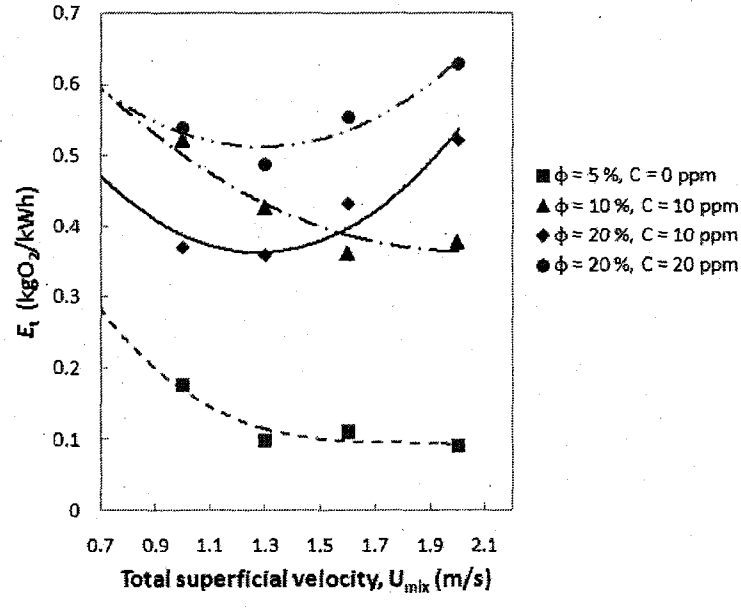

Figure 7.11: Effect of the total superficial velocity on the amount of oxygen transferred per unit energy input.

Consequently, the amount of oxygen transported per unit energy within the contactor/reactor varied between 0.09 and 0.63 kg(O_2)/kWh, depending on the operating conditions and interfacial characteristics of the system.

The effect of the total superficial velocity, U_{mix}, on the value of E_t is shown in Figure 7.11 from which it is clear that the energy utilization effectiveness in this type of contactor decreases with increasing the velocity where it becomes almost constant at higher total superficial velocities. However, at high dispersed phase volume fractions and in the presence of SDS, these trends were found to diverge from the common observation and start to increase after reaching a minimum at around U_{mix} = 1.3 m/s.

Moreover, the values of the oxygen transfer efficiency obtained in the present study are much lower than those reported by Al Taweel et al. (2005), where values as high as 5.7 kg(O_2)/kWh (values were adjusted for the current method of calculation) were reached. Such a large difference is mainly due to the inherent differences between these investigations. While the objective of the current work is to achieve high interfacial area of contact between the phases and consequently increase the volumetric mass transfer coefficients by intensifying the energy input to the system in a small reactor volume; the previous study emphasized achieving significant improvement in inter-phase mass transfer at low energy expenditures.

7.3.4 Correlating the Volumetric Mass Transfer Coefficient

The volumetric mass transfer coefficient was found to be affected by the energy input to the system, the gas-to-liquid flow ratio, and the interfacial characteristics of the system. Attempts were therefore made to correlate the overall volumetric mass transfer coefficient obtained in this investigation with the various operating conditions affecting the performance of screen-type static mixers.

The general correlation encompassing all three factors is listed in Equation (7.13) and the parity plot showing the good agreement between the predicted and experimental findings is depicted in Figure 3.4, where the data are within ± 25 %

$$k_L a = 1\times10^{-3}\cdot\sigma^{-1.61}\cdot\phi^{0.736}\cdot E_v^{0.86} \qquad (7.13)$$

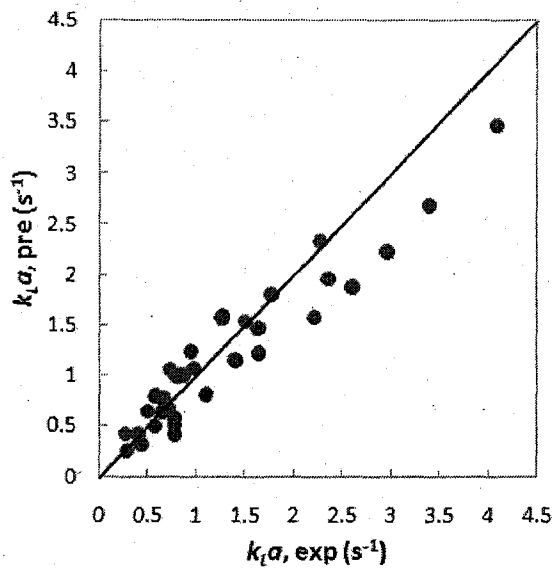

Figure 7.12: Parity plot of predicted values of k_La against experimental results.

7.3.5 Comparison with Other Types of Contactors

In multiphase reactions and mass transfer operations, the gas must be effectively and efficiently contacted with the liquid to achieve efficient absorption-desorption operation and to approach the inherent reaction rate. Conventionally, gas-liquid contacting has been performed using mechanically agitated tanks, bubble columns, air-lift reactors, and a variety of other mechanical units which are summarized in Table 7.4. This table also presents the mass transfer characteristics of such units where the range of achievable k_La values was collected from various sources in the literature and summarized.

A comparative evaluation of the present contactor with the various contactor types for which sufficient information are available clearly shows that the gas-liquid mass transfer performance of screen-type static mixers surpassed that of most conventional reactors/contactors with at least an order of magnitude difference in the reported k_La values. Furthermore, the high inter-phase mass transfer coefficients and the plug flow regime encountered in this contactor resulted in the ability to reach 98% equilibrium within residence times of less than one second (Figure 7.13) and, if necessary, shorter times can be reached by using an inter-screen spacing smaller than used in the present investigation (70 mm). This is orders of magnitude smaller than the residence times needed for mechanically agitated tanks and bubble columns and is expected to

significantly improve the yield, selectivity and inherent safety of multi-phase reactors. Such a superior performance can be attributed to the plug flow conditions encountered in

Table 7.4: Mass transfer characteristics of various gas-liquid contacting devices

Type of gas-liquid contactor	k_La (s^{-1})	*Source*
Air-lift reactors	0.005 – 0.021	Idhbeaa (2009)
Bubble columns	0.005 – 0.4	Middleton and Smith (2004)
Conventional air-lift reactors	0.001 – 0.0095	Vasconcelos et al. (2003)
Conventional impinging jet absorber	0.025 – 1.22	Tamir et al. (1990)
High intensity impinging jet reactor	1 – 14.2	Botes et al. (1999)
Horizontal pipeline contactors	0.02 – 0.24	Middleton and Smith (2004)
Hydrocyclones	0.02 – 0.15	Botes et al. (1999)
Mechanically agitated tanks	0.003 – 0.5	Middleton and Smith (2004)
Oscillatory flow reactors	0.003 – 0.017	Hewgill et al. (1993)
Oscillatory mesotubes	0.009 – 0.156	Reis et al. (2008)
Packed columns	0.0004 – 0.12	Middleton and Smith (2004)
Plate columns (counter- and co-current)	0.001 – 0.4	Botes et al. (1999)
Reciprocating plate columns	0.01 – 0.12	Al Taweel et al. (1979, 1996)
Static mixers	0.1 – 2	Heyouni et al., 2002
Submerged and plunging jet reactors	0.013 – 0.06	Sotiriadis et al. (2005)
Ultrasonic reactors	0.001 – 0.11	Kumar et al. (2004)
Venturi scrubbers	0.08 – 0.25	Botes et al. (1999)
Current work	**0.27 – 4.08**	–

the present contactor, and the ability to control the hydrodynamic conditions in order to generate fine gas-liquid dispersions in the high energy dissipation regions behind screens. Another major advantage of using screen-type static mixing elements is the virtual absence of deadzones, an important factor that can strongly affect reaction selectivity and inherent safety.

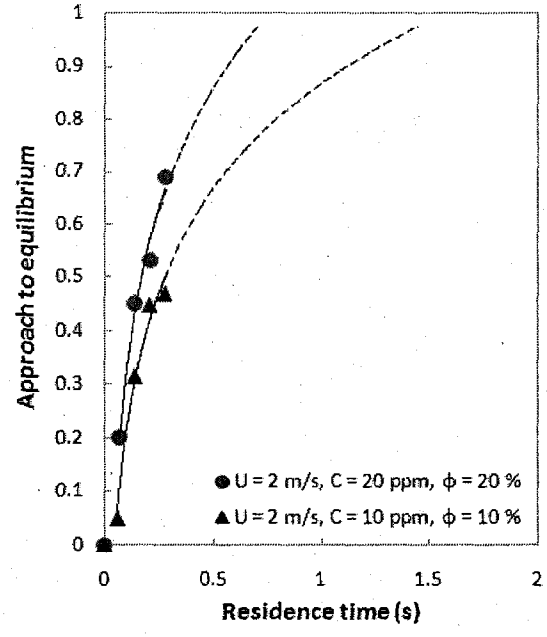

Figure 7.13: Effect of residence time on the approach to equilibrium

To facilitate comparison with the mass transfer performance of other contactors (which are mainly obtained using the air/water system), the data obtained in the absence of surfactants were correlated in a fashion similar to that used for stirred vessels where the mass transfer performance is correlated with the power input to the system. The following correlations were obtained for the water/air data only,

$$k_L a = 0.26 \cdot \left(E_m\right)^{0.603} \cdot \phi^{0.817} \qquad \left(R^2 = 0.86\right) \tag{7.14}$$

$$k_L a = 0.26 \cdot \left(E_V\right)^{0.608} \cdot \phi^{0.893} \qquad \left(R^2 = 0.86\right) \tag{7.15}$$

where, E_m is the power input per unit mass of the liquid expressed in W/kg, and E_v is the power input per unit of the reactor volume expressed in kW/m^3.

In a fashion similar to that of all other contactor types, the volumetric mass transfer coefficient was found to increase with increasing E_m or E_v where the dependency on the power input varied between 0.6 and 0.8 for–tubular reactors/contactors equipped with Lightnin, Kenics or Sulzer static mixers which also reported similar magnitude of $k_L a$ values (Heyouni et al., 2002; Zhu et al., 1992; Roes et al., 1984; Middleton, 1978). In addition, the dependency on the dispersed phase volume fraction was also found similar to those reported in the literature where it varied between 0.6 and 1.

The use of static mixers for gas liquid contacting suffered from the perception that the use of this contactor type results in excessive energy consumption rates. Whereas it is true that the average energy dissipation rate within static mixers is usually high (typically 20 – 1,000 W/kg), the energy needed to process a unit of liquid or gas mixture flowing through this contactor/reactor can be relatively low because of the very short residence times associated with the use of these units. The use of power input per unit mass, or per unit volume, as means for comparing the volumetric mass transfer coefficients achievable in various contactor types can be misleading as it does not take into account the impact of the residence time in the contactor. For example, the residence times used in the present investigation (230 – 560 ms) is much smaller than the 2–12 min typically reported for mechanically agitated tanks, a fact that can significantly impact the amount of energy consumed per unit of liquid or gas processed (determined using Equation (7.7)). Thus, while 320 W/kg were required to achieve the highest reported k_La value of 4.08 s^{-1}, the energy needed to process a unit mass of the continuous phase, E_{spm}, was 0.02 kWh/tonne (Figure 7.14).

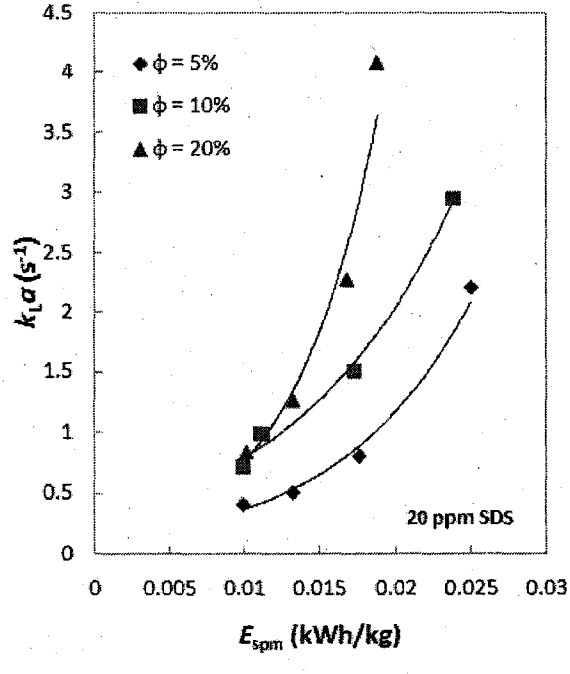

Figure 7.14: Effect of the specific power consumption on the volumetric mass transfer coefficient

Further, the mass transfer performance of the static mixer design that uses woven screens elements at an inter-screen spacing of 70 mm is smaller than that reported for the specialized high intensity jet reactor developed by Botes et al. (1999). Although a large gas holdup helps in enhancing the interfacial area of contact, it is not always desirable because the profitability of a reactor is largely controlled by the quantity of liquid it contains (Middleton and Smith, 2004). To take such a factor into account, many investigators compare the performance of the various contacting devices on the basis of the mass transfer coefficient per unit volume of bubbles present in the reactor, $k_L a/\phi$. For example, Roes et al. (1984) found that, in the case of co-current gas-liquid flow through gauze wire packing, the value of $k_L a/\phi$ increases from 0.1 to about 10 s^{-1} as the power consumption per unit mass of the dispersion is increased from 0.1 to 50 W/kg. However, up to 100 W/kg were required in the study of Heyouni et al. (2002) to achieve similar $k_L a/\phi$ (~10 s^{-1}) for the case of Lightnin static mixer. On the other hand, Botes et al. (1999) achieved a $k_L a/\phi$ value as high as 15.7 s^{-1} using a specialized high intensity jet reactor which resulted in an order of magnitude improvement over earlier versions of this type of contactor. Unfortunately, no data on the energy consumption in this high intensity jet reactor was provided and the complex technique used for evaluating the various performance parameters resulted in relatively large inaccuracies and uncertainty surrounding the results. Furthermore, the gaseous and liquid streams are expected to significantly deviate from the desirable plug flow characteristics. On the other hand, the $k_L a/\phi$ values obtained in the present investigation were found to vary between 3.26 and 14.6 s^{-1} as the power consumption per unit mass was changed from 63 to 320 W/kg.

In a fashion similar to that of Heyouni et al. (2002), the values of $k_L a$, achieved using the clean air-water system are graphically compared with those obtained for conventional reactors/contactors in Figure 7.15-a. While the screen-type static mixing elements clearly show a higher performance when compared to bubble columns and stirred tanks, the $k_L a$ values are of the same order of magnitude as those reported for other types of static mixers. However, if the data obtained in the presence of surface active agents are also taken into account, the performance of the screen-mixers exceeds that of the other commercially available static mixers (Figure 7.15-b), where a reduction in the volumetric mass transfer coefficient is usually reported in the presence of contaminants.

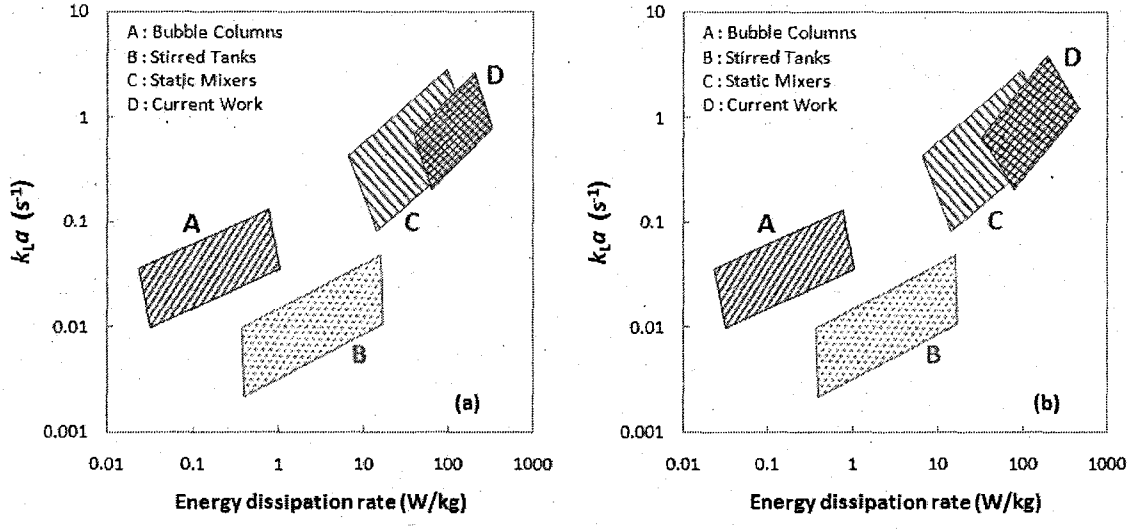

Figure 7.15: Comparison of the volumetric mass transfer coefficient achieved between the current work and other classical gas-liquid contactors (modified from the results of Heyouni et al.).

7.4 Conclusions

An attempt to intensify gas-liquid mass transfer operations was undertaken in this investigation, where the use of screen-type static mixers to promote inter-phase mass transfer was found to result in volumetric mass transfer coefficients as high as 4.08 s^{-1}. Such exceptional performance can be attributed to the ability to focus energy dissipation rates within a small region adjacent to the screen and the consequent generation of very high local energy dissipation rates. This provided the hydrodynamic conditions that are conducive for enhancing inter-phase mass transfer (micro-mixing) while resulting in the formation of fine dispersions that exhibit large inter-phase mass transfer coefficients and high interfacial area of contact.

However, for slow multiphase reactions where high energy utilization efficiencies are favoured, introducing a low number of screen elements with a very large inter-screen spacing is recommended. On the other hand, the ability to achieve high volumetric mass transfer coefficients by using the present mixer design, even in the presence of contaminants, plays a significant role in enhancing the conversion, selectivity and inherent safety of fast multiphase reactions.

While the volumetric mass transfer coefficient was found to increase with an increase in the energy input to the system, the value of k_La was also found to increase with

increasing gas holdups for slow and rapidly coalescent systems. Furthermore, the effect of contaminants in the system was investigated by means of adding SDS to the gas-liquid dispersion, where the value of k_La was found to increase with an increase in the concentration of SDS. Although the presence of SAA is known to decrease the value of the mass transfer coefficient, the increase in the interfacial area of contact between the phases, outweighed the decrease in the value of k_L.

Compared to other commercially available units used for contacting gas-liquid systems, the reactor/contactor investigated showed a superior performance. The screen-type static mixers not only achieved volumetric mass transfer coefficients that are orders of magnitude higher than most contactors, but also a higher mass transfer coefficient per unit volume of the bubbles.

Acknowledgement

The financial support of the Natural Sciences and Engineering Research Council of Canada (NSERC) and Dalhousie University is gratefully acknowledged.

7.5 Nomenclature

a	Interfacial area of contact	$[m^2/m^3]$
b	Screen wire diameter	[m]
C	Bulk surfactant concentration	[ppm]
$C^*_{O_2}$	Oxygen concentration in liquid phase at equilibrium	[ppm]
C_{O_2}	Oxygen concentration in liquid phase	[ppm]
D	Pipe diameter or tank diameter	[m]
E	Energy dissipation rate	[kW]
E_m	Energy dissipation per unit mass of the liquid	[W/kg]
E_v	Energy dissipation per unit of the reactor volume	$[kW/m^3]$
E_{spm}	Specific energy consumption rate	[kW/kg]
E_t	Amount of oxygen transported to/or from liquid phase per unit of energy dissipated	$[kgO_2/kWh]$
k_L	Mass transfer coefficient	$[m\ s^{-1}]$
k_La	Volumetric mass transfer coefficient	$[s^{-1}]$

L	Pipe length	[m]
L_M	Length of the mixing section	[m]
L_{screen}	Inter-screen spacing in the mixing section	[m]
M	Wire mesh size	[m]
M_{O2}	Amount of oxygen transported from liquid phase to the gas	[kg/h]
Q	Volumetric flow rate	[m^3/s]
Re	Pipe Reynolds number	[s]
t	Residence time	[s]
U	Superficial velocity	[m/s]
V	Volume	[m^3]

Greek symbols

α	Porosity or percentage open area of screen	
ΔP	Pressure drop in the pipe ,	[Pa]
ε	Turbulent kinetic energy dissipation rate	[W/kg]
ρ	Density	[kg/m^3]
σ	Static (equilibrium) surface tension	[N/m]
μ	Viscosity	[cP]
ϕ	Volumetric fraction of dispersed phase	[-]
Π	Surface pressure	[mN/m]

Subscript

L	Liquid
G	Gas
mix	mixture

7.6 References

Al Taweel A. M. and Walker, L. D., "Liquid dispersion in-line mixers", Can. J. Chem. Eng., **61**, 527-533 (1983).

Al Taweel A.M. and C. Chen, "A novel static mixer for the effective dispersion of immiscible liquids", Trans. Inst. Chem. Eng., **74**, 445- 450 (1996).

Al Taweel, A. M.; Li, C.; Gomaa, H. G.; Yuet, P, "Intensifying mass transfer between immiscible liquids: Using screen-type static mixers". Chem. Eng. Res. Des., **85**, 760-765 (2007).

Al Taweel, A.M., Landau, J., Picot, J.J.C., "Oxygen transfer in reciprocating plate columns", AIChE Symposium Series, **75**, 217-224 (1979).

Al Taweel, A.M., Yan, J., Azizi, F., Odedra, D., Gomaa, H.G., "Using in-line static mixers to intensify gas-liquid mass transfer processes", Chem. Eng. Sci., **60**, 6378-6390 (2005).

Al Taweel, A.M.; Rafi, M.S.; Luo, J.J.; Keast, B.; Yuet, P.; Odedra, D.; Boucher, H., "Dynamic surface characteristics of selected industrial streams and their impact on gas liquid contacting" paper to be presented at the 8th World Conference of Chemical Engineering, Montreal, Canada (2009).

Al-Masry, "Effects of Antifoam and Scaleup on Operations of Bioreactors", Chem. Eng. Process., **38**, 197-201 (1999).

Alves S.S., C.I. Maia and J.M.T. Vasconcelos, "Gas-liquid mass transfer coefficient in stirred tanks interpreted through bubble contamination kinetics", Chem. Engin. and Proc., **43**, 823–830 (2004)

Alves, S. S.; Vasconcelos, J. M. T.; Orvalho, S. P, "Mass transfer to clean bubbles at low turbulent energy dissipation", Chem. Eng. Sci., **61**, 1334-1337 (2006).

Alves, S.S., Orvalho, S.P., Vasconcelos, J.M.T., "Effect of bubble contamination on rise velocity and mass transfer", Chem. Eng. Sci., **60**, 1-9 (2005).

Amromin, E.; Kovinskaya, S., "Selection of gas-based drag reduction technology", Proceedings of ASME Fluids Engineering Division Summer Meeting 2006, 133-138, (2006).

Andersson, R., Andersson, B., Chopard, F., Noren, T., "Development of a multi-scale simulation method for design of novel multiphase reactors", Chem. Eng. Sci., **59**, 4911-4917 (2004).

Azizi, F., Al Taweel A.M., "Hydrodynamics of liquid flow through screens and screen-type static mixers", submitted for publication in Chem. Eng. Comm (2008).

Azizi, F., Al Taweel, A.M., "Population balance simulation of intensified gas-liquid contacting", Chem. Eng. Sci., **62**, 7436-7445 (2007).

Botes, F.G., Lorenzen, L., Van Deventer, J.S.J., "The development of high intensity gas-liquid jet reactors", Chem. Eng. Comm., **170**, 217-244 (1998).

Cancino, B., Roth, P., Reuß, M., "Design of high efficiency surface aerators. Part 1: Development of new rotors for surface aerators", Aquacult. Eng., **31**, 83–98 (2004).

Camarasda E., C. Vial, S. Poncin, G. Wild, N. Midouxd and J. Bouillard, "Influence of coalescence behaviour of the liquid and of the gas sparging hydrodynamics on bubble characteristics in a bubble column", Chem. Eng. Process., **38**, 329-344 (1999).

Chen C., "Dispersion and coalescence in static mixers", Ph.D. Thesis, Technical

University of Nova Scotia (1996)

Davies, J.T., "Turbulence phenomena at free surfaces" AIChE J, **18**, 169-73 (1972).

Ehrhardt, G., "Flow measurements for wire gauzes", Int. Chem. Eng., **23**, 455-465 (1983).

Hébrard, G., Zeng, J., Loubiere, K., "Effect of surfactants on liquid side mass transfer coefficients: a new insight", Chem. Eng. Sci., article in press (2008).

Hewgill, M. R.; Mackley, M. R.; Pandit, A. B.; Pannu, S. S., "Enhancement of Gas-Liquid Mass-Transfer Using Oscillatory Flow in a Baffled Tube", Chem. Eng. Sci., **48**, 799–809 (1993).

Heyouni, A., Roustan, M., Do-Quang, Z., "Hydrodynamics and mass transfer in gas-liquid flow through static mixers", Chem. Eng. Sci., **57**, 3325-3333 (2002).

Jackson, M.L., "Aeration in bernoulli types of devices", AIChE J, **10**, 836–842 (1964).

Kastánek,F, J. Zahradnik, J. Kratochvil, and J. Cermak, "Chemical reactors for gas-liquid systems", 279-285, 300-308, 340-389 (1993).

Koglin, B, J. Pawlowski and H. Schnoring, "Kontinuierliches emulgieren mit rotor/stator maschinen", Chem.-Ing.-Tech., **53**, 641-647 (1981).

Koide, K., S. Yamazoe, and S. Harada, "Effect of surface-active substances on gas holdup and gas-liquid mass transfer in bubble column", J. Chem. Eng. of Japan **18**, 287-292 (1985).

Kumar A., P.R. Gogate, A.B. Pandit, H. Delmas and A.M. Wilhelm," Gas-liquid mass transfer studies in sonochemical reactors", Ind. Eng. Chem. Res., **43**, 1812-1819 (2004)

Kuzmin, A.O.; Pravdina, M.K.; Yavorsky, A.I.; Yavorsky, N.I.; Parmon, V.N, "Vortex centrifugal bubbling reactor", Chem. Eng. J., **107**, 55-62 (2005).

Lezhnin, S., Eskin, D., Leonenko, Y., Vinogradov, O., "Dissolution of air bubbles in a turbulent water pipeline flow", Heat Mass Trans., **39**, 483-487 (2003).

Linek, V., Kordac, M., Fujasova, M., Moucha, T., "Gas-liquid mass transfer coefficient in stirred tanks interpreted through models of idealized eddy structure of turbulent in the bubble vicinity", Chem. Eng. Process., **43**, 1511-1517 (2004).

Linek, V., Kordac, M., Moucha, T., "Mechanism of mass transfer from bubbles in dispersions, Part II: mass transfer coefficients in stirred gas-liquid reactor and bubble column", Chem. Eng. Process., **44**, 121-130 (2005).

Luo J.J. "Bubble dispersion and coalescence in turbulent pipe flow", Ph.D. Thesis, Dalhousie University (2002)

Majirova, H.; Pinelli, D.; Machon, V.; Magelli, F., "Gas flow behavior in a two-phase reactor stirred with triple turbines", Chem. Eng. Tech., **27**, 304-309 (2004).

Middleton, J. C., "Motionless mixers as gas–liquid contacting devices", AIChE 71st annual meeting, Miami Beach, USA (1978).

Middleton, J.C.; Smith, J.M., "Gas-liquid mixing in turbulent systems", in "Handbook of industrial mixing : science and practice ", Paul, E. L.; Atiemo-Obeng, V. A.; Kresta, S. M., Eds., Wiley-Interscience: Hoboken, N.J., 585–638. (2004).

Painmanakul, P., Loubiere, K., Hebrard, G., Mietton-Peuchot, M., Roustan, M., "Effect of surfactants on liquid-side mass transfer coefficients", Chem. Eng. Sci., **60**, 6480-6491 (2005).

Reis, N., Pereira, R.N., Vicente, A.A., Teixeira, J.A., "Enhanced gas-liquid mass transfer of an oscillatory constricted-tubular reactor", Ind. Eng. Chem. Res., **47**, 7190-7201 (2008).

Roes, A. W. M., Zeerman, A. T., & Bukkems, F. H. J., "High-intensity gas–liquid mass transfer in the bubbly flow region during co-current up flow through static mixer", Int. Chem. Eng. Symposium Series, **38**, 231–238 (1984).

Rosso, D., Huo, D.L., Stenstrom, M.K., "Effects of interfacial surfactant contamination on bubble gas transfer", Chem. Eng. Sci., **61**, 5500-5514 (2006).

Sardeing, R., Painmanakul, P., Hébrard, G., "Effect of surfactants on liquid-side mass transfer coefficients in gas-liquid systems: a first step to modeling", Chem. Eng. Sci., **61**, 6249-6260 (2006).

Schubert, H.; Engel, R., "Product formulation engineering of emulsions", Chem. Eng. Res. Des., **82**, 1137-1143 (2004).

Sotiriadis A.A.; Thorpe, R.B.; Smith, J.M., "Bubble size and mass transfer characteristics of sparged downwards two-phase flow", Chem. Eng. Sci., **60**, 5917 – 5929 (2005).

Staudinger, J.; Roberts, P.V. "A critical compilation of Henry's law constant temperature dependence relations for organic compounds in dilute aqueous solutions", Chemosphere, **44**, 561–576, (2001).

Stenstrom, M.K., and Gilbert, R.G., "Effects of alpha, beta and theta factor upon the design, specification and operation of aeration systems", Water Research **15**, 643-654 (1981).

Takemura, F., Yabe, A., "Rising speed and dissolution rate of a carbon dioxide bubble in slightly contaminated water", J. Fluid Mech. **378**, 319–334 (1999).

Tamir, A.; Herskowits, D.; Herskowits, V., "Impinging jet absorbers", Chem. Eng. Proc., **28**, 165-172, (1990).

Thakur, R.K., C. Vial, K.D.P. Nigam, E.B. Nauman and G. Djelveh, "Static mixers in the process industries - a review", Chem. Eng. Res. Des., **81**, 787-826 (2003).

Vasconcelos J.M.T., J.M.L. Rodrigues, S.C.P. Orvalho,. S.S. Alves, R.L. Mendes and A. Reis, "Effect of contaminants on mass transfer coefficients in bubble column and airlift contactors", Chem. Eng. Sci., 58, 1431-1440 (2003)

Vasconcelos J.M.T., Orvalho, Sandra P.; Alves, Sebastiao S. "Gas-liquid mass transfer to single bubbles: Effect of surface contamination" AIChE Journal, 48, 1145-1154 2002

Vazquez G., G. Antorrena and J.M. Navaza, "Influence of surfactant concentration and chain length on the absorption of CO_2 by aqueous surfactant solutions in the presence and absence of induced marangoni effect", Ind. Eng. Chem. Res., **39**, 1088-1094 (2000)

Vazquez, G., M.A. Cancela, R. Varela, E. Alvarez and J.M. Navaza, "Influence of surfactants on absorption of CO_2 in a stirred tank with and without bubbling", Chem. Eng. J. **67**, 131-137 (1997).

Wagner M. and J. Popel, "Surface active agents and their influence on oxygen transfer", Water Sci. Technol., **34**, 249-256 (1996).

Walter, J. F. and H. W. Blanch, "Bubble breakup: gas-liquid bioreactors: breakup in turbulent flows", Chem. Eng. J., **32**, 7-17 (1986).

Wilde, F.D., "National field manual for the collection of water quality data", Handbook for water resources investigations, **9**, 28-32 (2005).

Zahradnik J., G. Kuncova and M. Fialova, "The effect of surface active additives on bubble coalescence and gas holdup in viscous aerated batches", Chem. Eng. Sci., **54**, 2401-2408 (1999).

Zhu, Z.M., Hannon, J., Green, A., "Use of high intensity gas-liquid mixers as reactors", Chem. Eng. Sci., **47**, 2847-2852 (1992).

Ziolkawski, D., and Morawski, J., "Flow characteristics of the liquid streams inside a tubular apparatus equipped with static mixing elements of a new type", Chemical Engineering and Processing, **21**, 131-139 (1987)

Zlokarnik, M., "Tower-shaped reactors for aerobic biological waste water treatment", In: Zlokarnik, M., Brauer, H., (Eds.), Biotechnology.VCH, Weiheim, Germany, 537–569 (1985).

Chapter 8.
Conclusion

This thesis is a compilation of various published and/or submitted manuscripts, and detailed conclusions regarding each section were given in the corresponding individual chapters. However, the most important conclusions can be highlighted in the following:

I. Hydrodynamics of flow through screens:

While no previous methods for modeling the local energy dissipation rate behind wire gauze are available in the literature, an approach based on extending the use of the homogeneous and isotropic turbulence decay equation to the anisotropic region of the flow was proposed. By fixing the values of the turbulence decay exponent and origin, it would become possible to determine the turbulence decay constant value by balancing the volume average energy dissipation rate, obtained from pressure drop measurements or estimations, with the estimated spatial average energy dissipation rate.

The proposed turbulence decay profile behind a grid was thus divided into two distinct regions. A region of constant high energy dissipation rate prevailing over a certain distance downstream of the grid, followed by a region of fast decay where the homogenous isotropic turbulence decay equation applies. Experimentally determined volume average energy dissipation rate data were then used to validate the proposed approach, and the calculated values were found to match the experimental data quite well.

II. PBE solution under high shear conditions:

While the previously developed algorithm for the numerical solution of the PBE (Al Taweel t al., 2002) rendered accurate and stable solutions at low and intermediate energy dissipation conditions, it was found unstable under high shear rate conditions. Therefore a new method for solving the discretized PBE was proposed and is similarly based on the use of the size distribution sampling approach proposed by Sovova and Prochazka (1981)

combined with a moving grid technique. In addition, an enhanced solution stability algorithm was proposed, which relies on monitoring the onset of errors in the various birth and death terms encountered in PBE. It consequently provides a much more sensitive indication of the numerical errors that can be introduced and allows for corrective action to be undertaken before the errors propagate in an uncontrollable fashion.

Using this approach for solving the PBE, the finite domain errors resulting from discretization were reduced if not eliminated while maintaining optimum drop size integration ranges to describe the population. This method was then tested under breakage and coalescence dominated conditions and was found to render a highly stable solution under low, moderate and high shear rate conditions.

III. Liquid-liquid and gas-liquid PBE:

Turbulently flowing gas-liquid and liquid-liquid dispersions were accurately simulated using the phenomenological model developed by Coulaloglou and Tavlarides (1977) for liquid-liquid dispersions. Experimental data obtained for gas-liquid and liquid-liquid mixtures flowing through a multi-stage screen-type static mixer contactor were used for validating this model. A major characteristic of the flow through such mixers is that nearly isotropic turbulent plug flow conditions would prevail, and the successive exposure of the flow to regions of high and low shear rates would provide very stringent conditions for testing and validating the model and for the development of accurate model parameters that may be used for simulating other more complex multiphase contactors such as MATs.

In the case of liquid-liquid dispersions, the predicted drop size distribution as well as the Sauter mean diameter (when quasi-steady state conditions were assumed to be reached) was compared with experimental results measured by photographic techniques and good agreement was obtained at different flow velocities and diverse screen geometries.

However, an accurate simulation of gas-liquid flows was only possible after incorporating the effect of virtual mass into the model of Coulaloglou and Tavlarides (1977). The predicted spatial variation of the interfacial area of contact and Sauter mean

diameter as well as the average Sauter mean diameter (when quasi-steady state conditions were assumed to be reached) were compared with experimental results and good agreement was obtained at different superficial velocities, dispersed phase volume fractions and interfacial characteristics of the system.

In addition to generating very uniform hydrodynamic conditions, another advantage of using this type of reactor is that it allows an easy optical access to each mixing element. This would be of great importance in experimentally determining breakage and coalescence processes under well controlled and well characterized turbulent conditions.

IV. Liquid-liquid mass transfer:

A new model capable of calculating the dispersed phase mass transfer coefficient in turbulently flowing dispersions was developed. It is based on Higbie's penetration theory combined with Kawase's surface renewal approach for the turbulent exposure time and can therefore account for the effect of turbulence in the continuous phase on the rate of surface renewal within the drop. The effect of surface contamination on the predicted turbulent mass transfer coefficient was also taken into account using a contamination factor the value of which reflects the degree of surface mobility of the drop.

This model was then incorporated in the previously developed population balance based simulation program and used to estimate the local dispersed phase mass transfer coefficients under the well known and controlled hydrodynamic conditions present in tubular contactors/reactors equipped with screen-type static mixers, and the average overall volumetric mass transfer coefficient obtained in such units. The value of the contamination factor, f_c, was determined by matching the predicted overall volumetric mass transfer coefficient with the experimental results.

Good correspondence between experimental and predicted values was obtained for the system water/ acetic acid / diesel over a wide range of dispersed phase holdup and local energy dissipation rates. This is a reflection of the ability of the hydrodynamic model to accurately predict the drop size distribution, and the ability of the newly developed mass transfer model to predict the effect of turbulence on the drop side mass transfer coefficient.

In addition, the proposed model provided a better fit of the entire experimental results than the commonly used eddy diffusivity model. Moreover, it provided a hydrodynamic explanation of the empirically determined effective diffusivity correction factor which is reported to vary between 1 and 50.

V. Gas-liquid mass transfer:

The ability of screen-type static mixers to focus the turbulent energy dissipation rate in a short distance downstream in addition to their ability to provide uniform hydrodynamic conditions throughout the reactor volume was taken advantage of to intensify gas-liquid inter-phase mass transfer. Values of the volumetric mass transfer coefficient, $k_L a$, as high as 4.08 s^{-1} were achieved, thus allowing substantial enhancements of the conversion, selectivity and inherent safety of fast multiphase reactions.

While the volumetric mass transfer coefficient was found to increase with an increase in the energy input to the system, the value of $k_L a$ was also found to increase with increasing gas holdups for slow and rapidly coalescent systems. Although the presence of SAA is known to decrease the value of the mass transfer coefficient, the increase in the interfacial area of contact between the phases due to coalescence retardation, outweighed the decrease in the value of k_L.

This contactor also showed a superior performance when compared to other commercially available units used for contacting gas-liquid systems. The screen-type static mixers not only achieved volumetric mass transfer coefficients that are orders of magnitude higher than most contactors, but also a higher mass transfer coefficient per unit volume of the bubbles.

Recommendations:

The following overall recommendations can be deduced from the findings of this work:

- A comparative evaluation between the various techniques used to solve PBE is needed where results should be quantitatively analyzed.

- Additional coalescence and breakage kernels should be incorporated in the PBE solution program, in order to give it a higher credibility and ability to simulate the wide range of multi-phase dispersions.
- Higher accuracy DSD measurement techniques are recommended to be used in order to match the model predictions especially under conditions where very small drop/bubble sizes are dominant.
- Utilizing plug flow reactors using screen-type static mixers is recommended over the use of the conventional mechanically agitated tanks especially when evaluating bubble/drop breakage and coalescence models because they allow a successive exposure of the flowing dispersion to breakage-dominated and coalescence dominated regions.
- In addition, micro-mixing and inter-phase mass transfer can be significantly enhanced at low total energy consumption rates.
- Such configuration would also allow an easy optical access to each mixing element thus facilitating the experimental determination of breakage and coalescence processes under well controlled and well characterized turbulent conditions.
- The use of the proposed turbulent mass transfer model to estimate the dispersed phase mass transfer coefficient is recommended.
- Furthermore, it can also be used to calculate the overall volumetric mass transfer coefficient in combination with PBE simulations; however, under more complex hydrodynamic conditions (*e.g.* those encountered in MAT and impinging jet reactors) accurate representation of the bulk flow is required.
- The use of screen type static mixers with short inter-screen spacing to promote gas-liquid inter-phase mass transfer is recommended over the use of conventional mixers even for the case of slowly coalescent dispersions.
- The effect of changing inter-screen spacing and screen geometry needs to be investigated in order to determine the optimum conditions for intensifying gas-liquid mass transfer operations.

REFERENCES

Al Taweel A. M. and Walker, L. D., "Liquid dispersion in-line mixers", Can. J. Chem. Eng., **61**, 527-533 (1983).

Al Taweel A.M., F. Azizi, K. Podila and A. Speers, "In-Line Processing for the Production of Large Compact Flocs", Technical report submitted to the Energy Technology Centre, CANMET, Devon Alberta (2008a).

Al Taweel, A. M.; Chen, C., "Novel static mixer for the effective dispersion of immiscible liquids", Chem. Eng. Res. Des., **74**, 445-450 (1996).

Al Taweel, A. M.; Li, C.; Gomaa, H. G.; Yuet, P, "Intensifying mass transfer between immiscible liquids: Using screen-type static mixers". Chem. Eng. Res. Des., **85**, 760-765 (2007).

Al Taweel, A.M., Azizi, F., Uppal, A., "Using static mixers to intensify diesel desulphurization reaction/operation", Paper presented at the International Symposium on Mixing in Industrial Processes VI, Niagara-on-the-Lake, Ontario, Canada (2008b).

Al Taweel, A.M., Landau, J., Picot, J.J.C., "Oxygen transfer in reciprocating plate columns", AIChE Symposium Series, **75**, 217-224 (1979).

Al Taweel, A.M., M. El-Ali, F. Azizi, B. Liekens, D. Odedra, A. Uppal and H.G. Gomaa, "In-Line Processing for Intensifying Multi-Phase Contacting Operations", Proceedings of the 5th Inter. Conf. Proc. Int. **5**, 59-73 (2003).

Al Taweel, A.M., Madhavan, S., Podila, K., Koksal, M., Troshko, A., and Gupta, Y.P., "CFD simulation of multiphase flow: closure recommendations for fluid-fluid systems", Proc. of 12th European Conference on Mixing, Bologna, Italy, 495-502 (2006).

Al Taweel, A.M., Webber, J.R., Devavarapu, R.C., Gupta, Y.P., Elsayed, A.S.I., "An algorithm for accurately solving population balance problems", Alexandria Eng. J., **41**, 1069-1075 (2002).

Al Taweel, A.M., Yan, J., Azizi, F., Odedra, D., Gomaa, H.G., "Using in-line static mixers to intensify gas-liquid mass transfer processes", Chem. Eng. Sci., **60**, 6378-6390 (2005).

Al Taweel, A.M.; Rafi, M.S.; Luo, J.J.; Keast, B.; Yuet, P.; Odedra, D.; Boucher, H., "Dynamic surface characteristics of selected industrial streams and their impact on gas liquid contacting" paper to be presented at the 8th World Conference of Chemical Engineering, Montreal, Canada (2009).

Alexopoulos, A.H. , Roussos, A.I., Kiparissides, C., « Part I: Dynamic evolution of the particle size distribution in particulate processes undergoing combined particle growth and aggregation", Chem. Eng. Sci., **59**, 5751–5769 (2004).

Alexopoulos, A.H., Maggioris, D., Kiparissides, C., "CFD analysis of turbulence non-homogeneity in mixing vessels a two-compartment model", Chem. Eng. Sci., **57**, 1735-1752 (2002).

Al-Masry, "Effects of Antifoam and Scaleup on Operations of Bioreactors", Chem. Eng. Process., **38**, 197-201 (1999).

Alopaeus, V., J. Koskinen and K.I. Keskinen, "Utilization of Population Balances in Simulation of Liquid-Liquid Systems in Mixed Tanks", Chem. Eng. Comm. **190**, 1468-1484 (2003).

Alopaeus, V., Koskinen, J., Keskinen, K.I., "Simulation of the population balances for liquid-liquid systems in a nonideal stirred tank. Part 1. Description and qualitative validation of the model", Chem. Eng. Sci., **54**, 5887-5899 (1999).

Alopaeus, V., Laakkonen, M., Aittamaa, J., "Solution of population balances with growth and nucleation by high order moment-conserving method of classes", Chem. Eng. Sci., **62**, 2277-2289 (2007).

Alopaeus, V., Laakkonen, M., Aittamaa, J., "Solution of population balances by high order moment-conserving method of classes: reconstruction of a non-negative density distribution", Chem. Eng. Sci., **63**, 2741-2751 (2008).

Alopaeus, V., Laakkonen, M., Aittamaa, J., « Solution of population balances with breakage and agglomeration by high-order moment-conserving method of classes", Chem. Eng. Sci., **61**, 6732-6752 (2006).

Alves, S. S.; Maia, C. I.; Vasconcelos, J. M. T. Gas-liquid mass transfer coefficient in stirred tanks interpreted through bubble contamination kinetics. Chem. Eng. Proc. **43**, 823-830 (2004).

Alves, S. S.; Vasconcelos, J. M. T.; Orvalho, S. P, "Mass transfer to clean bubbles at low turbulent energy dissipation", Chem. Eng. Sci., **61**, 1334-1337 (2006).

Alves, S.S., Orvalho, S.P., Vasconcelos, J.M.T., "Effect of bubble contamination on rise velocity and mass transfer", Chem. Eng. Sci., **60**, 1-9 (2005).

Amromin, E.; Kovinskaya, S., "Selection of gas-based drag reduction technology", Proceedings of ASME Fluids Engineering Division Summer Meeting 2006, 133-138, (2006).

Andersson, R., Andersson, B., Chopard, F., Noren, T., "Development of a multi-scale simulation method for design of novel multiphase reactors", Chem. Eng. Sci., **59**, 4911-4917 (2004).

Andersson, R.., Andersson, B., "On the breakup of fluid particles in turbulent flows", AIChE J., **52**, 2020-2030 (2006).

Attarakih, M., Fara, D.A., Sayed, S., "Dynamic modeling of a packed-bed glycerol - Water distillation column", Ind. Eng. Chem. Res., **40**, 4857-4865 (2001).

Attarakih, M.M., Bart, H., Faqir, N.M., "Numerical solution of the spatially distributed population balance equation describing the hydrodynamics of interacting liquid-liquid dispersions", Chem. Eng. Sci., **59**, 2567-2592 (2004).

Attarakih, M.M., Bart, H.-., Faqir, N.M., "Optimal moving and fixed grids for the solution of discretized population balances in batch and continuous systems: Droplet breakage". Chem. Eng. Sci., **58**, 1251-1269 (2003).

Attarakih, M.M., H. Bart and N.M. Faqir, "Solution of the Droplet Breakage Equation for Interacting Liquid-Liquid Dispersions: A Conservative Discretization Approach", Chem. Eng. Sci. **59**, 2547-2565 (2004).

Azizi, F., "Intensification of the fuels desulfurization processes", Dalhousie University, Halifax, N.S. (2004).

Azizi, F., Al Taweel A.M., "Hydrodynamics of liquid flow through screens and screen-type static mixers" Submitted for publication in Chem. Eng. Comm. (2008a).

Azizi, F.; Al Taweel, A. M., "Algorithm for the accurate numerical solution of PBE for drop breakup and coalescence under high shear rates", Chem. Eng. Sci., submitted for publication (2008b).

Azizi, F., Al Taweel A.M., "Turbulently flowing liquid-liquid dispersions. Part I: drop breakage and coalescence", submitted for publication in Chem. Eng. Sci. (2009a).

Azizi, F., Al Taweel A.M., "Turbulently flowing liquid-liquid dispersions. Part II: interphase mass transfer", submitted for publication in Ind. Eng. Chem. Res. (2009b).

Azizi, F., Al Taweel, A.M., "Population balance simulation of intensified gas-liquid contacting", Chem. Eng. Sci., **62**, 7436-7445 (2007).

Azizi, F., Al Taweel, A.M., "Reliable Design of Industrial Multiphase Contactors/Reactors", Paper presented at the North American Mixing Forum, Mixing XX; Parksville, BC, Canada, (2005).

Baines, W.D., Peterson, E.G., "Investigation of flow through screens", Am. Soc. Mech. Engrs – Trans., **73**, 467-477 (1951).

Bajpai, R.K., Ramkrishna, D., Prokop, A., "A coalescence redispersion model for drop-size distributions in an agitated vessel", Chem. Eng. Sci., **31**, 913-920 (1976).

Bakker, A., A.H. Haidari and L.M. Oshinowo, "Realize Greater Benefits from CFD", Chem. Eng. Prog. **97**, 45-53 (2001).

Bakker, A.; Van den Akker, H. E. A., "Computational model for the gas-liquid flow in stirred reactors", Chem. Eng. Res. Des., Trans. IChemE, **72**, 594-606 (1994).

Balliu, N.E., Cameron, I.T., Newell, R., "A comparative study of numerical methods for solving continuous population balance models for aggregation processes", Dev. Chem. Eng. Min. Proc., **12**, 277-291 (2004).

Bapat, P.M. and L.L. Tavlarides, "Mass Transfer in Liquid-Liquid CFSTR", AICHE J. **31**, 659-666 (1985).

Bart, H.J., "Reactive extraction in stirred columns - A review". Chem. Eng. Tech., **26**, 723-731 (2003).

Batterham, R.J., Hall, J.S., Barton, G., "Pelletizing kinetics and simulation of full-scale balling circuits". Proceedings of the 3rd Int ernational Symposium on Agglomeration, Nurnberg, Germany, A136 (1981).

Bennani, A., Gence, J.N., Mathieu, J., "Influence of a grid-generated turbulence on the development of chemical reactions", AIChE J., **31**, 1157-1166 (1985).

Bischof, F., M. Sommerfeld and F. Durst, "Mass transfer from bubbles under the influence of surface active agents", Chem. Ing. Tech **65**, 1365-1367 (1993).

Botello-Alvarez, E. J.; Navarrete-Bolanos, L. J.; Jimenez-Islas, H.; Estrada-Baltazar, A.; Rico-Martinez, R., "Improving mass transfer coefficient prediction in bubbling columns via sphericity measurements", Ind Eng Chem Res, **43**, 6527-6533 (2004).

Botes, F.G., Lorenzen, L., Van Deventer, J.S.J., "The development of high intensity gas-liquid jet reactors", Chem. Eng. Comm., **170**, 217-244 (1998).

Bouaifi, M.; Hebrard, G.; Bastoul, D.; Roustan, M., "Comparative study of gas hold-up, bubble size, interfacial area and mass transfer coefficients in stirred gas-liquid reactors and bubble columns", Chem. Eng. Proc., **40**, 97-111 (2001).

Bourne, J. R.; Lips, M., "Micromixing in grid-generated turbulence. Theoretical analysis and experimental study", Chem. Eng. J. Biochem. Eng. J., **47**, 155-162 (1991).

Briassulis, G., Agui, J.H., Andreopoulos, Y., "The structure of weakly compressible grid-generated turbulence", J. Fluid Mech., **432**, 219-283 (2001).

Brucato, A., M. Ciofalo, F. Grisafi and R. Tocco, "On the Simulation of Stirred Tank Reactors Via Computational Fluid Dynam", Chem. Eng. Sci., **55**, 291-302 (2000).

Calabrese, R.V.; Cheng, S.-H.; Lin, J.-C.; Gentry, J.W., "Effect of kernel on aggregation of coalescence of large clusters", Part. Sci. Tech., 13, (1995).

Cancino, B., Roth, P., Reuß, M., "Design of high efficiency surface aerators. Part 1: Development of new rotors for surface aerators", Aquacult. Eng., **31**, 83–98 (2004).

Camarasda E., C. Vial, S. Poncin, G. Wild, N. Midouxd and J. Bouillard, "Influence of coalescence behaviour of the liquid and of the gas sparging hydrodynamics on bubble characteristics in a bubble column", Chem. Eng. Process., **38**, 329-344 (1999).

Campos, F.B., Lage, P.L.C., "A numerical method for solving the transient multidimensional population balance equation using an Euler-Lagrange formulation", Chem. Eng. Sci, **58**, 2725-2744 (2003).

Camurdan, M. C.; Baird, I. M. H.; Taylor, P A., "Steady state hydrodynamics and mass transfer characteristics of a Karr extraction column", Can. J. Chem. Eng., **67**, 554-559 (1989).

Chaudhari, R.V., Hofmann, H., "Coalescence of gas bubbles in liquids", Rev. Chem. Eng., **10**, 131–190 (1994).

Chen C., "Dispersion and coalescence in static mixers", Ph.D. Thesis, Technical University of Nova Scotia (1996)

Chen, C., Al Taweel, A.M., (2007). An experimental investigation of gas-liquid contacting in screen-type static mixers, in preparation.

Chen, P., Sanyal, J., Dudukovic, M.P., "Numerical simulation of bubble columns flows: Effect of different breakup and coalescence closures", Chem. Eng. Sci., **60**, 1085-1101 (2005).

Chhabra, R.P., Richardson, J.F., "Flow of liquids through screens: relationship between pressure drop and flow rate", Chem. Eng. Sci., **40**, 313-316 (1985).

Comte-Bellot, G., Corrsin, S., "Use of contraction to improve isotropy of grid-generated turbulence", J. Fluid Mech., **25**, 657-682 (1966).

Coulaloglou, C.A., "Dispersed Phase Interactions in an Agitated Flow Vessel", PhD Thesis, Illinois Institute of Technology, Chicago, IL (1975).

Coulaloglou, C.A., Tavlarides, L.L., "Description of interaction processes in agitated liquid-liquid dispersions", Chem. Eng. Sci., **32**, 1289-1297 (1977).

Davies, J.T., "Turbulence Phenomena", Academic Press, New York (1972).

Davies, J.T., "Turbulence phenomena at free surfaces" AIChE J, **18**, 169-73 (1972).

Dehkordi, A., "Liquid-liquid extraction with chemical reaction in a novel impinging-jets reactor", AICHE J., 48, 2230-2239 (2002).

Diemer, R.B., Olson, J.H., "A moment methodology for coagulation and breakage problems: Part 2-Moment models and distribution reconstruction", Chem. Eng. Sci., **57**, 2211-2228 (2002).

Dorao, C.A., Jakobsen, H.A., "A least squares method for the solution of population balance problems", Comp. Chem. Eng., **30**, 535-547 (2006).

Ehrhardt, G., "Flow measurements for wire gauzes", Int. Chem. Eng., **23**, 455-465 (1983).

El-Ali, M., "Performance characteristics of a novel liquid-liquid contactor", Ph.D thesis, Dalhousie University, Canada (2001).

Farrauto, R.J., Lee, H.C., "Ammonia oxidation catalysts with enhanced activity", Ind. Eng. Chem. Res., **29**, 1125-1129 (1990).

Gad-el-hak, M., Corrsin, S., "Measurements of the nearly isotropic turbulence behind a uniform jet grid", J. Fluid Mech., **62**, 115-143 (1974).

Gelbard, F., Seinfeld, J.H., "Numerical solution of the dynamical equation for particulate systems", J. Comp. Phy., **28**, 357–375 (1978).

Groth, J., Johansson, A.V, "Turbulence reduction by screens", J. Fluid Mech., **197**, 139-155 (1988).

Handlos, A. E.; Baron, T., "Mass and heat transfer from drops in liquid-liquid extraction", AICHE J., **3**, 127-136, (1957).

Harris, C.K., D. Roekaerts, F.J.J. Rosendal, F.G.J. Buitendijk, P. Daskopoulos, A.J.N. Vreenegoor and H. Wang, "Computational Fluid Dynamics for Chemical Reactor Engineering", Chem. Eng. Sci., **51**, 1569-1594 (1996).

Hébrard, G., Zeng, J., Loubiere, K., "Effect of surfactants on liquid side mass transfer coefficients: a new insight", Chem. Eng. Sci., article in press (2008).

Henschke, M.; Pfennig, A., "Mass-transfer enhancement in single-drop extraction experiments", AICHE J., **45**, 2079-2086 (1999).

Hesketh, R.P., Etchells, A.W., Russell, T.W.F., "Experimental observations of bubble breakage in turbulent flows". Ind. Eng. Chem. Res., **30**, 831–845 (1991).

Hewgill, M. R.; Mackley, M. R.; Pandit, A. B.; Pannu, S. S., "Enhancement of Gas-Liquid Mass-Transfer Using Oscillatory Flow in a Baffled Tube", Chem. Eng. Sci., **48**, 799–809 (1993).

Heyouni, A., Roustan, M., Do-Quang, Z., "Hydrodynamics and mass transfer in gas-liquid flow through static mixers", Chem. Eng. Sci., **57**, 3325-3333 (2002).

Higbie, R., "The rate of absorption of a pure gas into a still liquid during a short time of exposure", Trans Amer Inst Chem Eng, **31**, 365 (1935).

Hounslow, M.J., "Discretized population balance for continuous systems at steady state", AICHE J., **36**, 106-116 (1990).

Hsia, M. A.; Tavlarides, L. L., "Simulation Model for Homogeneous Dispersions in Stirred Tanks", Chem. Eng. J. Biochem. Eng. J., **20**, 225-236 (1980).

Hsia, M.A., "The Modeling of Liquid-Liquid Extraction in Stirred Tanks by a Simulation Approach", Ph.D. Thesis, Illinois Institue of Technology, Chicago, IL (1981).

Jackson, M.L., "Aeration in bernoulli types of devices", AIChE J, **10**, 836–842 (1964).

Jairazbhoy, V., Tavlarides, L.L., "Numerical technique for the solution of integrodifferential equations arising from balances over populations of drops in turbulent flows", Comp. Chem. Eng., **23**, 1725-1735 (2000).

Jajuee, B.; Margaritis, A.; Karamanev, D.; Bergougnou, M. A., "Application of surface-renewal-stretch model for interface mass transfer", Chem. Eng. Sci., **61**, 3917-3929 (2006).

Jakobsen, H.A., Lindborg, H., Dorao, C.A., "Modeling of bubble column reactors: progress and limitations", Ind. Eng. Chem. Res., **44**, 5107-5151 (2005).

Johnson, A. I.; Hamielec, A. E., "Mass transfer inside drops", A.I.Ch.E. J., **6**, 145-149 (1960).

Joshi, J.B., "Computational flow modelling and design of bubble column reactors", Chem. Eng. Sci., **56**, 5893-5933 (2001).

Kamp, A.M., Chesters, A.K., Colin, C., Fabre, J., "Bubble coalescence in turbulent flows: A mechanistic model for turbulence-induced coalescene applied to microgravity bubbly pipe flow", Int. J. Multiphas. Flow, **27**, 1363-1396 (2001).

Kang, H. S.; Chester, S.; Meneveau, C., "Decaying turbulence in an active-grid-generated flow and comparisons with large-eddy simulation", J. Fluid Mech., 129-160 (2003).

Kasireddy, V.K., Al Taweel, A.M., "An improved light attenuation technique for measuring large interfacial areas", Can. J. Chem. Eng., **68**, 690-693 (1990).

Kastánek,F, J. Zahradnik, J. Kratochvil, and J. Cermak, "Chemical reactors for gas-liquid systems", 279-285, 300-308, 340-389 (1993).

Kawase, Y.; Halard, B.; Moo-Young, M., "Theoretical Prediction of Volumetric Mass Transfer Coefficients in Bubble Columns for Newtonian and Non-Newtonian Fluids", Chem. Eng. Sci., **42**, 1609-1617 (1987).

Koglin, B, J. Pawlowski and H. Schnoring, "Kontinuierliches emulgieren mit rotor/stator maschinen", Chem.-Ing.-Tech., **53**, 641-647 (1981).

Koide, K., S. Yamazoe, and S. Harada, "Effect of surface-active substances on gas holdup and gas-liquid mass transfer in bubble column", J. Chem. Eng. of Japan **18**, 287-292 (1985).

Konno, M., Matsunaga, Y., Arai, K., Saito, S., "Simulation model for breakup process in an agitated tank", J. Chem. Eng. Japan, **13**, 67-73 (1980).

Kostoglou, M. and A.J. Karabelas, "On the Attainment of Steady State in Turbulent Pipe Flow of Dilute Dispersions", Chem. Eng. Sci., **53**, 505-513 (1998).

Kostoglou, M., Karabelas, A.J., "Toward a unified framework for the derivation of breakage functions based on the statistical theory of turbulence", Chem. Eng. Sci., **60**, 6584-6595 (2005).

Kronig, R.; Brink, J. C., "On theory of extraction from falling droplets". App. Sci. Res., **A2**, 142-154 (1950).

Kumar A., P.R. Gogate, A.B. Pandit, H. Delmas and A.M. Wilhelm," Gas-liquid mass transfer studies in sonochemical reactors", Ind. Eng. Chem. Res., **43**, 1812-1819 (2004)

Kumar, A.; Hartland, S. Correlations for prediction of mass transfer coefficients in single drop systems and liquid-liquid extraction columns. Trans. IChemE, **77**, 372-384 (1999).

Kumar, S., Ramkrishna, D., "On the solution of population balance equations by discretization - I. A fixed pivot technique", Chem. Eng. Sci., **51**, 1311-1332 (1996a).

Kumar, S., Ramkrishna, D., "On the solution of population balance equations by discretization - discretization - II. A moving pivot technique", Chem. Eng. Sci., 51, 1333-1342 (1996b).

Kuzmin, A.O.; Pravdina, M.K.; Yavorsky, A.I.; Yavorsky, N.I.; Parmon, V.N, "Vortex centrifugal bubbling reactor", Chem. Eng. J., **107**, 55-62 (2005).

Laakkonen, M., Alopaeus, V., Aittamaa, J., "Validation of bubble breakage, coalescence and mass transfer models for gas-liquid dispersion in agitated vessel", Chem. Eng. Sci., **61**, 218-228 (2006).

Laakkonen, M., Moilanen, P., Alopaeus, V., Aittamaa, J., "Modelling local bubble size distributions in agitated vessels", Chem. Eng. Sci., **62**, 721-740 (2007).

Lance, M., Bataille, J., "Turbulence in the liquid phase of a uniform bubbly air-water flow", J. Fluid Mech., **222**, 95-118 (1991).

Lasheras, J.C., Eastwood, C., Martinez-Bazan, C., Montanes, J.L., "A review of statistical models for the break-up an immiscible fluid immersed into a fully developed turbulent flow", Int. J. Multiphas Flow, **28**, 247-278 (2002).

Laws, E.M., Livesey, J.L., "Flow through screens", Ann. Rev. Fluid Mech., **10**, 247-266 (1978).

Lee, C.K., Erickson, L.E., Glasgow, L.A., "Bubble breakup and coalescence in turbulent gas-liquid dispersions", Chem. Eng. Comm., **59**, 65-84 (1987).

Lehr, F., Mewes, D., "A transport equation for the interfacial area density applied to bubble columns", Chem. Eng. Sci., **56**, 1159-1166 (2001).

Lezhnin, S., Eskin, D., Leonenko, Y., Vinogradov, O., "Dissolution of air bubbles in a turbulent water pipeline flow", Heat Mass Trans., **39**, 483-487 (2003).

Linek, V., Kordac, M., Fujasova, M., Moucha, T., "Gas-liquid mass transfer coefficient in stirred tanks interpreted through models of idealized eddy structure of turbulent in the bubble vicinity", Chem. Eng. Process., **43**, 1511-1517 (2004).

Linek, V., Kordac, M., Moucha, T., "Mechanism of mass transfer from bubbles in dispersions, Part II: mass transfer coefficients in stirred gas-liquid reactor and bubble column", Chem. Eng. Process., **44**, 121-130 (2005).

Litster, J.D., Smit, D.J., Hounslow, M.J., "Adjustable discretized population balance for growth and aggregation", AICHE J., **41**, 591-603 (1995).

Luo J.J. "Bubble dispersion and coalescence in turbulent pipe flow", Ph.D. Thesis, Dalhousie University (2002)

Luo, H., Svendsen, H.F., "Theoretical model for drop and bubble breakup in turbulent dispersions", AICHE J., **42**, 1225-1233 (1996).

Maaß, S., Gäbler, A., Zaccone, A., Paschedag, A.R., Kraume, M., "Experimental investigations and modeling of breakage phenomena in stirred liquid/liquid systems", Chem. Eng. Res. Des., **85**, 703-709 (2007).

Mahoney, A.W. and D. Ramkrishna, "Efficient Solution of Population Balance Equations with Discontinuities by Finite Elements", Chem. Eng. Sci., **57**, 1107-1119 (2002).

Majirova, H.; Pinelli, D.; Machon, V.; Magelli, F., "Gas flow behavior in a two-phase reactor stirred with triple turbines", Chem. Eng. Tech., **27**, 304-309 (2004).

Marchisio, D.L., Fox, R.O., "Solution of population balance equations using the direct quadrature method of moments". J. Aerosol Sci., **36**, 43-73 (2005).

Marchisio, D.L., Pikturna, J.T., Fox, R.O., Vigil, R.D., Barresi, A.A., "Quadrature method of moments for population-balance equations", AICHE J., **49**, 1266-1276 (2003).

Martinez-Bazan, C.; Montanes, J.L.; Lasheras, J.C., "On the breakup of an air bubble injected into a fully developed turbulent flow. Part 2. Size PDF of the resulting daughter bubbles", J. Fluid Mech., **401**, 183 (1999).

Middleton, J. C., "Motionless mixers as gas–liquid contacting devices", AIChE 71st annual meeting, Miami Beach, USA (1978).

Middleton, J.C.; Smith, J.M., "Gas-liquid mixing in turbulent systems", in "Handbook of industrial mixing : science and practice ", Paul, E. L.; Atiemo-Obeng, V. A.; Kresta, S. M., Eds., Wiley-Interscience: Hoboken, N.J., 585–638. (2004).

Mohamed, M.S., LaRue, J.C., "Decay power law in grid-generated turbulence", J. Fluid Mech., **219**, 195-214 (1990).

Motz, S., Mannal, S., Gilles, E., "Integral approximation - an approach to reduced models for particulate processes", Chem. Eng. Sci., **59**, 987-1000 (2004).

Motz, S., Mitrovic, A., Gilles, E., "Comparison of numerical methods for the simulation of dispersed phase systems". Chem. Eng. Sci., **57**, 4329-4344 (2002).

Mudde, R.F., Simonin, O., "Two- and three-dimensional simulations of a bubble plume using a two-fluid model", Chem. Eng. Sci., **54**, 5061-5069 (1999).

Newman, A. B., "The Drying of Porous Solids - Diffusion Calculations", Trans Amer Inst Chem Eng, **27**, 310, (1931).

Ni, X., Mignard, D., Saye, B., Johnstone, J.C., Pereira, N., "On the evaluation of droplet breakage and coalescence rates in an oscillatory baffled reactor", Chem. Eng. Sci., **57**, 2101-2114, (2002).

Nicmanis, M., Hounslow, M.J., "A finite element method for the steady state population balance equation", AIChE J., **44**, 2258–2272 (1998).

Noh, H. S.; Baird, I. M. H., "Mass Transfer and Pressure Drop in a Cocurrent Reciprocating Plate Extraction Column", AICHE J., **30**, 120-127 (1984).

Nopens, I., Beheydt, D., Vanrolleghem, P.A., "Comparison and pitfalls of different discretised solution methods for population balance models: A simulation study", Comp. Chem. Eng., **29**, 367-377 (2005).

Oshinowo, L., Kuhn, D.C.S., "Turbulence decay behind expanded metal screens", Can. J. Chem. Eng., **78**, 1032-1039 (2000).

Painmanakul, P., Loubiere, K., Hebrard, G., Mietton-Peuchot, M., Roustan, M., "Effect of surfactants on liquid-side mass transfer coefficients", Chem. Eng. Sci., **60**, 6480-6491 (2005).

Patil, D.P., Andrews, J.R.G., "An analytical solution to continuous population balance model describing floc coalescence and breakage — A special case", Chem. Eng. Sci., **53**, 599-601 (1998).

Paul, E. L.; Atiemo-Obeng, V. A.; Kresta, S. M., "Handbook of industrial mixing : science and practice", Wiley-Interscience: Hoboken, N.J., (2004).

Pinker, R.A., Herbert, M.V., "Pressure loss associated with compressible flow through square-mesh wire gauzes", J. Mech. Eng. Sci., **9**, 11-23 (1967).

Podgorska, W., "Modelling of high viscosity oil drop breakage process in intermittent turbulence", Chem. Eng. Sci., **61**, 2986-2993 (2006).

Podila, K., Al Taweel, A.M., Koksal, M., Troshko, A., Gupta, Y.P., "CFD simulation of gas-liquid contacting in tubular reactors", Chem. Eng. Sci., 62, 7151-7162 (2007).

Polprasert, G., Al Taweel, A.M.,Webber, J., Gupta, P., Elsayed, A.S.I., "Improving the stability and accuracy of population balance numerical solutions: I- methods of describing drop size distribution", Alexandria Eng. J., **41**, 1059-1067 (2002).

Press, W.H., Teukolsky, S.A., Vetterling, W.T., Flannery, B.P., "Numerical recipes in C: the art of scientific computing, Cambridge University Press, Cambridge (2002).

Prince, M.J., Blanch, H.W., "Bubble coalescence and break-up in air-sparged bubble columns", AICHE J., **36**, 1485-1499 (1990).

Qamar, S., Ashfaq, A., Angelov, I., Elsner, M.P., Warnecke, G., Seidel-Morgenstern, A., "Numerical solutions of population balance models in preferential crystallization", Chem. Eng. Sci., **63**, 1342-1352 (2008).

Ramkrishna, D., "Population Balances: Theory and Applications to Particulate Processes in Engineering", Academic Press, New York, NY (2000).

Ramkrishna, D., "Status of population balances", Rev. Chem. Eng., **3**, 49-95 (1985).

Reis, N., Pereira, R.N., Vicente, A.A., Teixeira, J.A., "Enhanced gas-liquid mass transfer of an oscillatory constricted-tubular reactor", Ind. Eng. Chem. Res., **47**, 7190-7201 (2008).

Ribeiro, L.M.; Regueiras, P.F.R; Guimaraes, M.M.L.; Madureira, C.M.N.; Cruz-Pinto, J.J.C., "Dynamic behaviour of liquid-liquid agitated dispersions - I. The hydrodynamics", Comp.. Chem. Eng., **19**, 333-343 (1995).

Rigopoulos, S. and A.G. Jones, "Finite-Element Scheme for Solution of the Dynamic Population Balance Equation", AICHE J. **49**, 1127-1139 (2003).

Risso, F., Fabre, J., "Oscillations and breakup of a bubble immersed in a turbulent field", J. Fluid Mech., **372**, 323 (1998).

Rod, V., Misek, T., 'Stochastic modelling of dispersion formation in agitated liquid-liquid systems", Trans. IChemE, **60**, 48-53 (1982).

Roes, A. W. M.; Zeerman, A. T.; Bukkems, F. H. J., "High-intensity gas–liquid mass transfer in the bubbly flow region during co-current up flow through static mixer", Int. Chem. Eng. Symposium Series, **38**, 231–238 (1984).

Ross, S.L., F.H. Verhoff and R.L. Curl, "Droplet Breakage and Coalescence Processes in an Agitated Dispersion – 2. Measurement and Interpretation of Mixing Experiments", Ind. Eng. Chem. Fund., **17**, pp. 101-108 (1978).

Rosso, D., Huo, D.L., Stenstrom, M.K., "Effects of interfacial surfactant contamination on bubble gas transfer", Chem. Eng. Sci., **61**, 5500-5514 (2006).

Sahu, A.K., P. Kumar, A.W. Patwardhan and J.B. Joshi, "CFD Modelling and Mixing in Stirred Tanks", Chem. Eng. Sci., **54**, 2285-2293 (1999).

Saien, J.; Barani, M., "A combined mass transfer coefficient model for liquid-liquid systems under simultaneous effect of contamination and agitation", Can. J. Chem. Eng. **83**, 224-231 (2005).

Sardeing, R., Painmanakul, P., Hébrard, G., "Effect of surfactants on liquid-side mass transfer coefficients in gas-liquid systems: a first step to modeling", Chem. Eng. Sci., **61**, 6249-6260 (2006).

Schmidt, S. A.; Simon, M.; Attarakih, M. M.; Lagar G., L.; Bart, H., "Droplet population balance modelling - Hydrodynamics and mass transfer", Chem. Eng. Sci., **61**, 246-256 (2006).

Schubert, H.; Engel, R., "Product formulation engineering of emulsions", Chem. Eng. Res. Des., **82**, 1137-1143 (2004).

Scott, W.T., "Analytic studies of cloud droplet coalescence", J. Atm. Sci., **25**, 54-65 (1968).

Sherwood, T. K.; Evans, J. E.; Longcor, J. V. A., "Extraction in spray and packed columns", Ind. Eng. Chem., **31**, 1144-1150 (1939).

Skelland, P. A. H.; Lee, J. M., "Drop Size and Continuous-Phase Mass Transfer in Agitated Vessels", AICHE J., **27**, 99-111 (1981).

Slater, M. J., "Combined model of mass transfer coefficients for contaminated drop liquid-liquid systems". Can. J. Chem. Eng., **73**, 462-469 (1995).

Sommerfeld, M. and S. Decker, "State of the Art and Future Trends in CFD Simulation of Stirred Vessel Hydrodynamics", Chem. Eng. Tech., **27**, 215-224 (2004).

Sotiriadis A.A.; Thorpe, R.B.; Smith, J.M., "Bubble size and mass transfer characteristics of sparged downwards two-phase flow", Chem. Eng. Sci., **60**, 5917 – 5929 (2005).

Sovova, H., Prochazka, J., "Breakage and coalescence of drops in a batch stirred vessel - 1. comparison of continuous and discrete models", **36**, 163-171 (1981).

Staudinger, J.; Roberts, P.V. "A critical compilation of Henry's law constant temperature dependence relations for organic compounds in dilute aqueous solutions", Chemosphere, **44**, 561–576, (2001).

Steiner, L., "Mass Transfer Rates from Single Drops and Drop Swarms", Chem. Eng. Sci., **41**, 1979-1986 (1986).

Stenstrom, M.K., and Gilbert, R.G., "Effects of alpha, beta and theta factor upon the design, specification and operation of aeration systems", Water Research **15**, 643-654 (1981).

Stewart, E.J., Huq, P., "Dissipation rate correction methods", Exp. Fluids, **40**, 405-421 (2006).

Takemura, F., Yabe, A., "Rising speed and dissolution rate of a carbon dioxide bubble in slightly contaminated water", J. Fluid Mech. **378**, 319–334 (1999).

Tamir, A.; Herskowits, D.; Herskowits, V., "Impinging jet absorbers", Chem. Eng. Proc., **28**, 165-172, (1990).

Tcholakova, S., Vankova, N., Denkov, N., Danner, T., "Emulsification in turbulent flow : 3. Daughter drop-size distribution", J. Col. Int. Sci., 310, 570-589 (2007).

Thakur, R.K., C. Vial, K.D.P. Nigam, E.B. Nauman and G. D., "Static mixers in the process industries - a review", Chem. Eng. Res. Des., **81**, 787-826 (2003).

Turunen, I. and H. Haario, "Mass Transfer in Tubular Reactors Equipped with Static Mixers", Chem. Eng. Sci., **49**, 5257-5269 (1994).

Valentas, K.J., Amundson, N.R., "Breakage and coalescence in dispersed phase systems", Ind. Eng. Chem. Fund., **5**, 533-542 (1966).

Vanni, M., "Approximate Population Balance Equations for Aggregation–Breakage Processes", J. Col. Int. Sci., **221**, 143-160 (2000).

Vasconcelos J.M.T., J.M.L. Rodrigues, S.C.P. Orvalho,. S.S. Alves, R.L. Mendes and A. Reis, "Effect of contaminants on mass transfer coefficients in bubble column and airlift contactors", Chem. Eng. Sci., 58, 1431-1440 (2003)

Vasconcelos, J.M.T., S.P. Orvalho and S.S. Alves, "Gas-Liquid Mass Transfer to Single Bubbles: Effect of Surface Contamination", AICHE J. **48**, pp. 1145-1154 (2002).

Vasquez, V.; Bautista, R. G., "Mass transfer correlation coefficients for two-phase systems: A general review for liquid-liquid", Miner Process Extr Metal Rev, **17**, 239-255, 1997.

Vazquez G., G. Antorrena and J.M. Navaza, "Influence of surfactant concentration and chain length on the absorption of CO_2 by aqueous surfactant solutions in the presence and absence of induced marangoni effect", Ind. Eng. Chem. Res., **39**, 1088-1094 (2000)

Vazquez, G., M.A. Cancela, R. Varela, E. Alvarez and J.M. Navaza, "Influence of surfactants on absorption of CO_2 in a stirred tank with and without bubbling", Chem. Eng. J. **67**, 131-137 (1997).

Venneker, B. C. H.; Derksen, J. J.; Van den Akker,Harrie E.A., "Population balance modeling of aerated stirred vessels based on CFD", AICHE J., **48**, 673-685 (2002).

Wagner M. and J. Popel, "Surface active agents and their influence on oxygen transfer", Water Sci. Technol., **34**, 249-256 (1996).

Walter, J. F. and H. W. Blanch, "Bubble breakup: gas-liquid bioreactors: breakup in turbulent flows", Chem. Eng. J., **32**, 7-17 (1986).

Warhaft, Z., Lumley, J.L., "Experimental study of the decay of temperature fluctuations in grid-generated turbulence", J. Fluid Mech., **88**, 659-684 (1978).

West, F. B.; Robinson, P. A.; Morgenthaler, A. C.; Beck, T. R.; McGregor, D. K., "Liquid-Liquid Extraction from Single Drops", Ind. Eng. Chem., **43**, 234-238 (1951).

Wilde, F.D., "National field manual for the collection of water quality data", Handbook for water resources investigations, **9**, 28-32 (2005).

Zahradnik J., G. Kuncova and M. Fialova, "The effect of surface active additives on bubble coalescence and gas holdup in viscous aerated batches", Chem. Eng. Sci., **54**, 2401-2408 (1999).

Zhu, Z.M., Hannon, J., Green, A., "Use of high intensity gas-liquid mixers as reactors", Chem. Eng. Sci., **47**, 2847-2852 (1992).

Ziff, R.M., McGrady, E.D., "The kinetics of cluster fragmentation and depolymerisation", J. Phys. A: Mathematical and General, **18**, 3027-3037 (1985).

Ziolkowski, D., Morawski, J., "Flow characteristics of the liquid streams inside a tubular apparatus equipped with static mixing elements of a new type", Chem. Eng. Proc., **21**, 131-139 (1987).

Zlokarnik, M., "Tower-shaped reactors for aerobic biological waste water treatment", In: Zlokarnik, M., Brauer, H., (Eds.), Biotechnology.VCH, Weiheim, Germany, 537–569 (1985).

APPENDIX A: Complementary Information Regarding PBE Simulations of Gas-Liquid Systems

The following complementary information is incorporated in order to present a complete and comprehensive representation of the research undertaken.

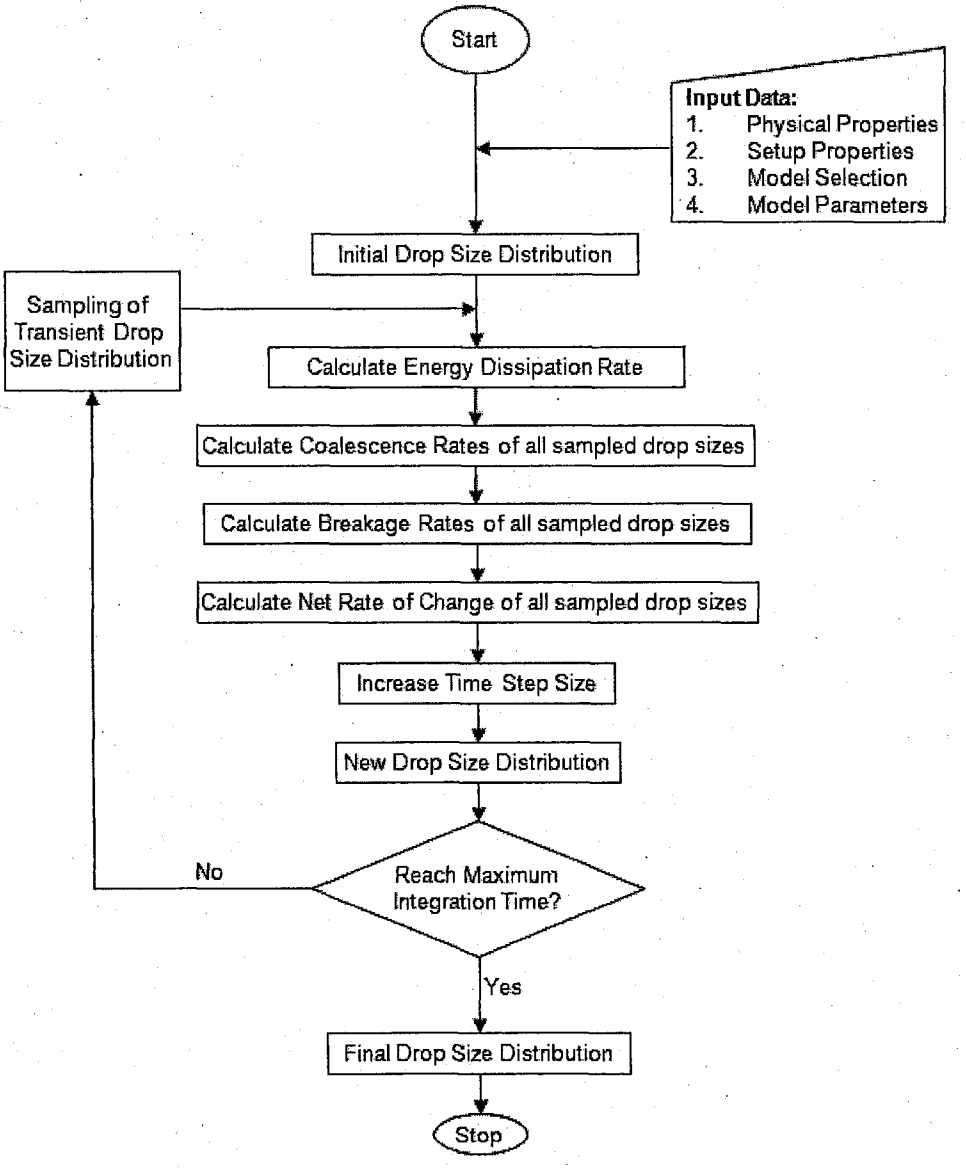

Figure A.1: Algorithm used for the numerical solution of the PBE in Chapter 2.

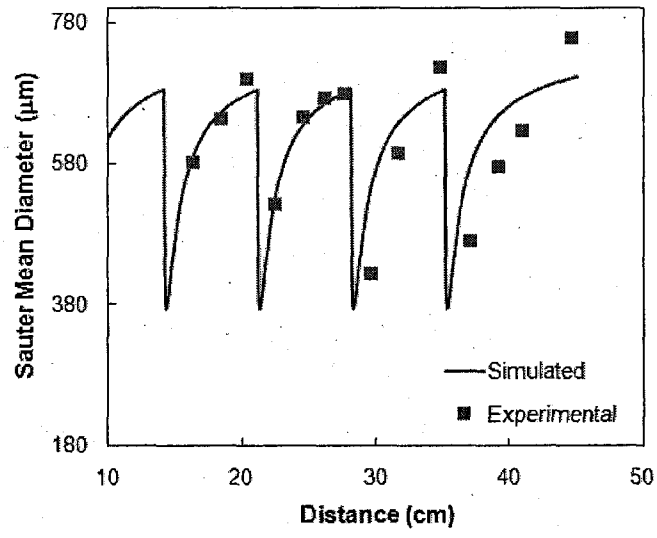

Figure A.2: Spatial variation of the Sauter mean diameter along the reactor/contactor length (U = 1.3 m/s; ϕ = 7%; C_{SDS} = 0 ppm)

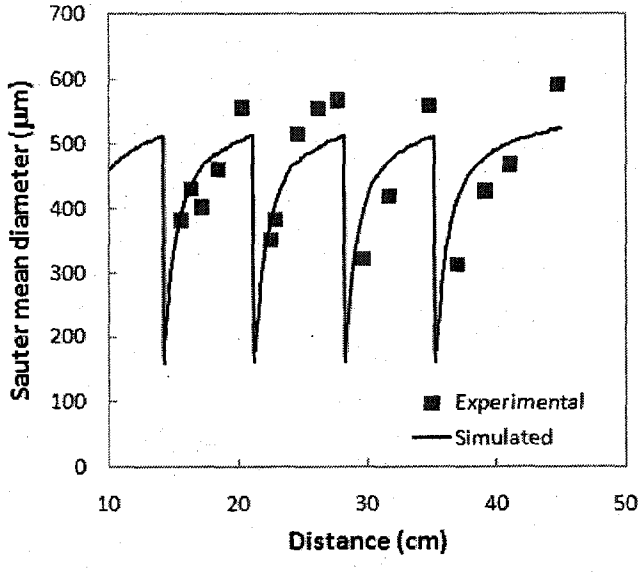

Figure A.3: Spatial variation of the Sauter mean diameter along the reactor/contactor length (U = 2.0 m/s; ϕ = 7%; C_{SDS} = 0 ppm)

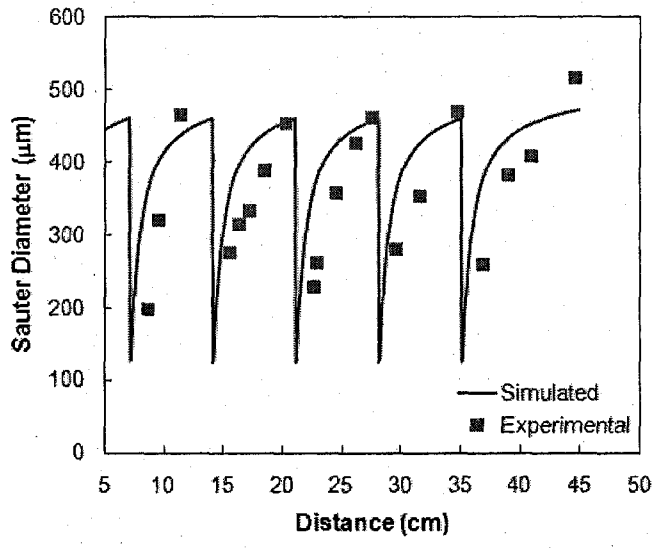

Figure A.4: Spatial variation of the Sauter mean diameter along the reactor/contactor length (U = 2.3 m/s; ϕ = 7%; C_{SDS} = 0 ppm)

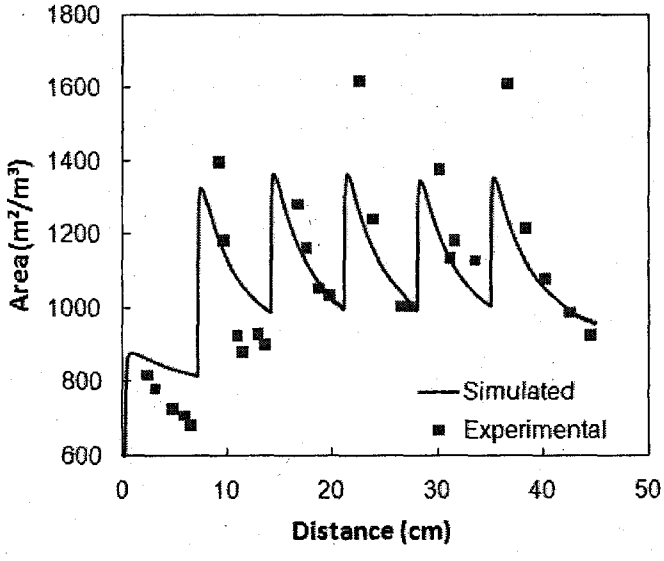

Figure A.5: Spatial variation of the Sauter mean diameter along the reactor/contactor length (U = 2.0 m/s; ϕ = 7%; C_{SDS} = 2 ppm)

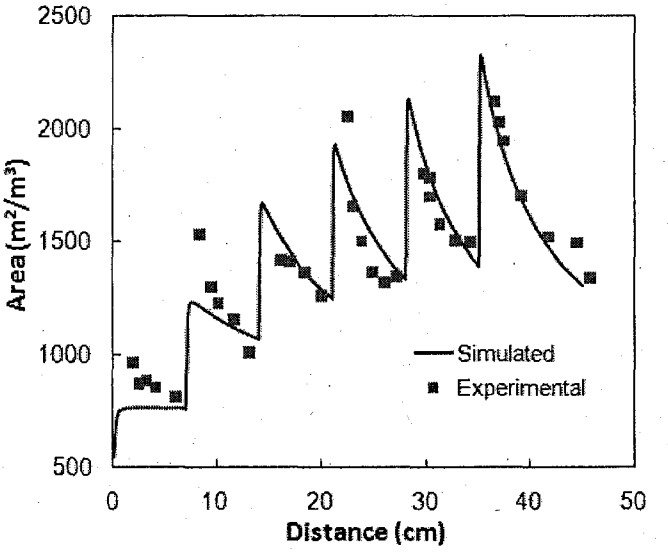

Figure A.6: Spatial variation of the Sauter mean diameter along the reactor/contactor length (U = 2.0 m/s; ϕ = 7%; C_{SDS} = 5 ppm)

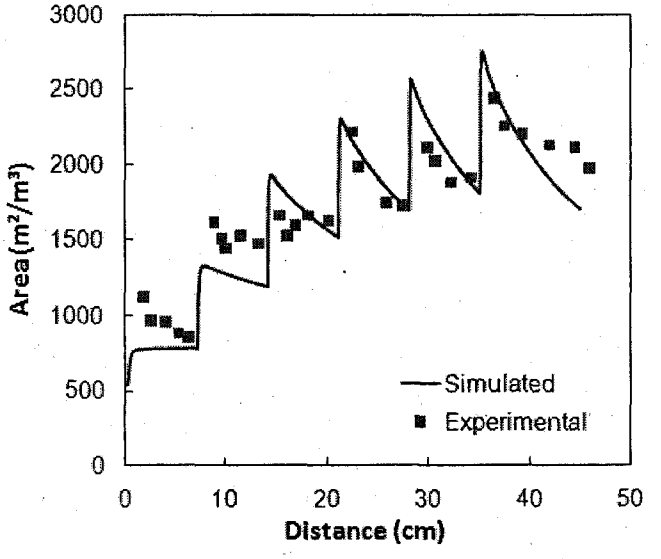

Figure A.7: Spatial variation of the Sauter mean diameter along the reactor/contactor length (U = 2.0 m/s; ϕ = 7%; C_{SDS} = 10 ppm)

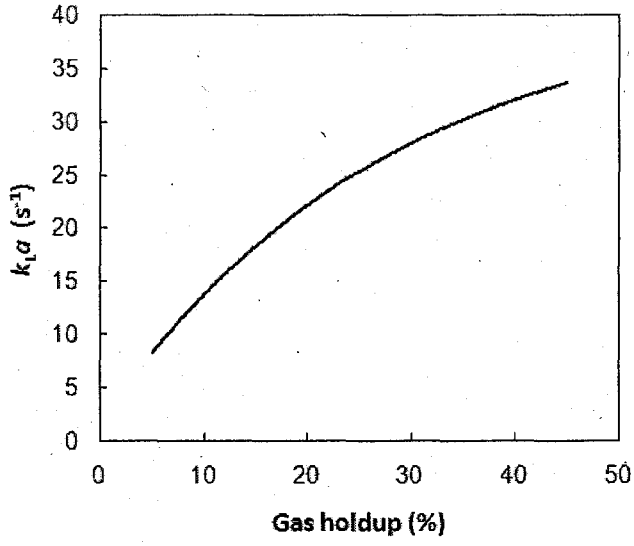

Figure A.8: Predicted mass transfer performance of the contactor/reactor (U = 2.3 m/s; L = 1 cm; C_{SDS} = 10 ppm)

APPENDIX B: Complementary Information Regarding the Pressure Drop and Energy Dissipation in Screens

The following complementary information is incorporated in order to present a complete and comprehensive representation of the research undertaken.

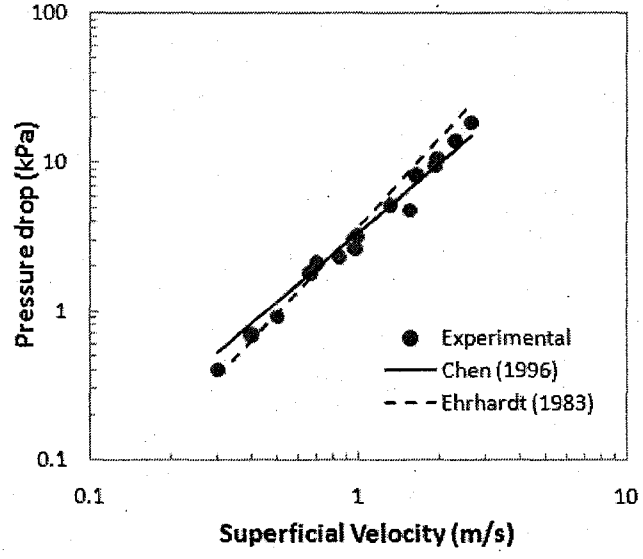

Figure B.1: Effect of superficial velocity on the pressure drop using Chen (1996) and Ehrhardt (1983) drag correlations (α = 27 %)

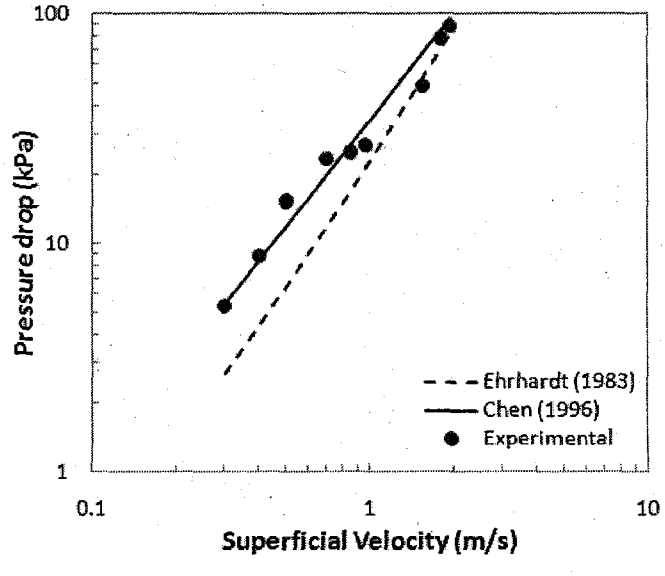

Figure B.2: Effect of superficial velocity on the pressure drop using Chen (1996) and Ehrhardt (1983) drag correlations (α = 33 %)

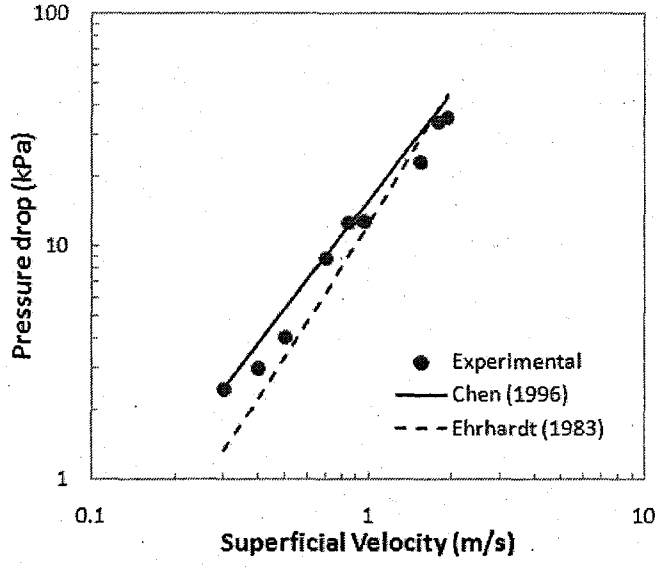

Figure B.3: Effect of superficial velocity on the pressure drop using Chen (1996) and Ehrhardt (1983) drag correlations ($\alpha = 41$ %)

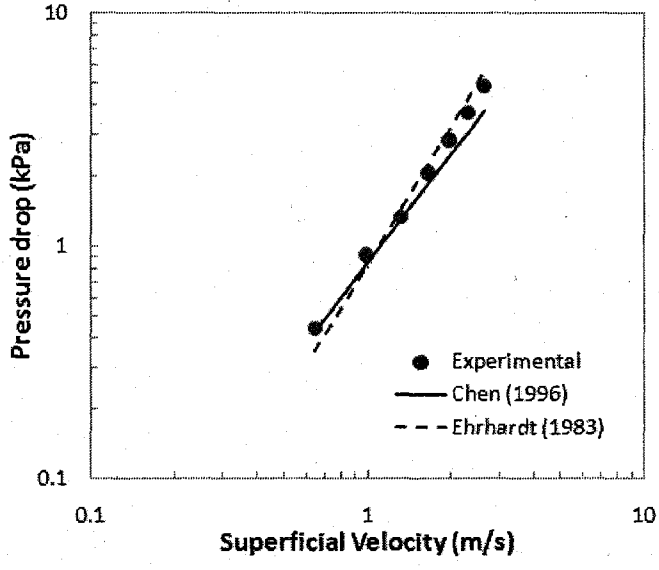

Figure B.4: Effect of superficial velocity on the pressure drop using Chen (1996) and Ehrhardt (1983) drag correlations ($\alpha = 48.4$ %)

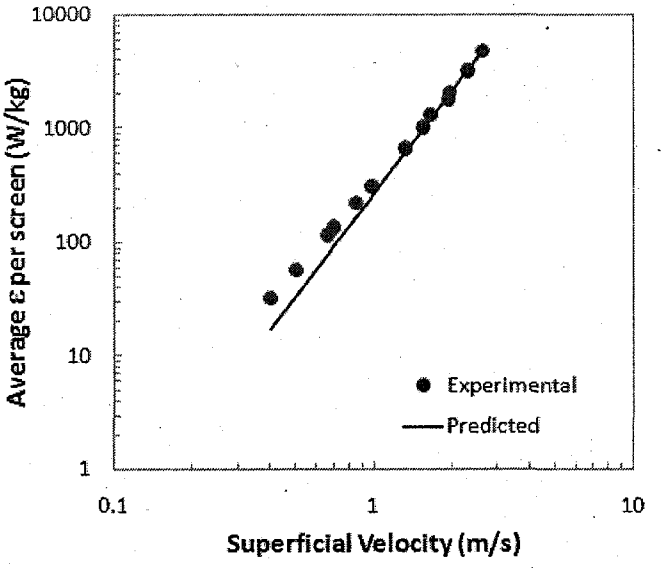

Figure B.5: Effect of superficial velocity on the average ε per screen ($C = 1.72$; $\alpha = 27$ %)

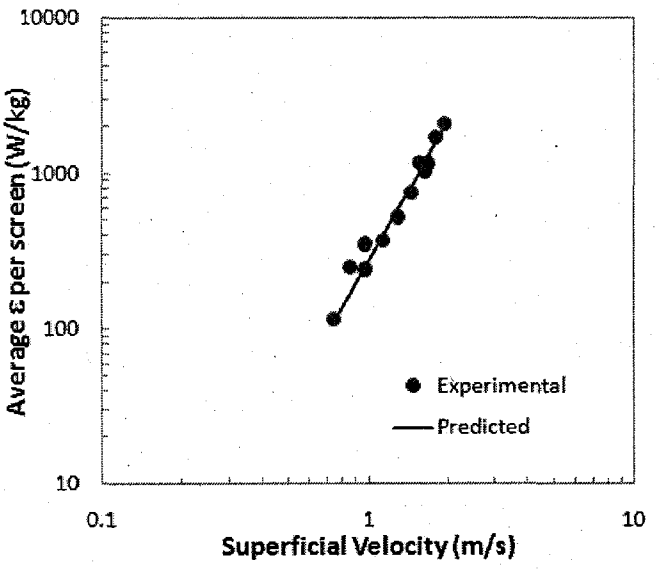

Figure B.6: Effect of superficial velocity on the average ε per screen ($C = 1.82$; $\alpha = 33$ %)

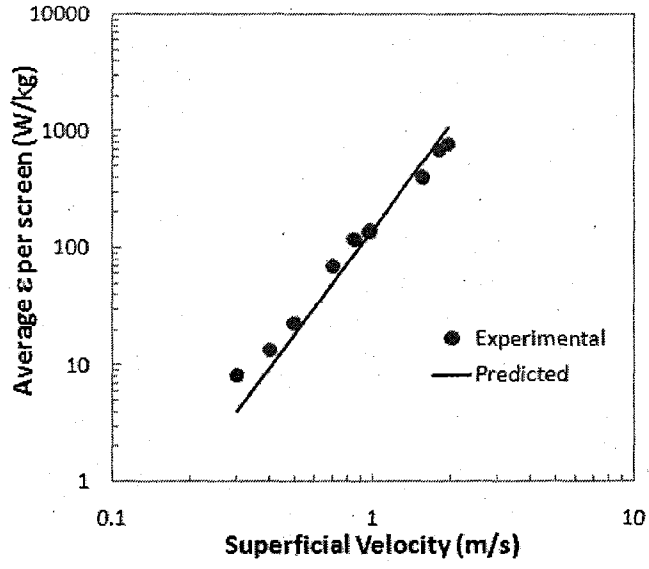

Figure B.7: Effect of superficial velocity on the average ε per screen ($C = 3.15$; $\alpha = 41$ %)

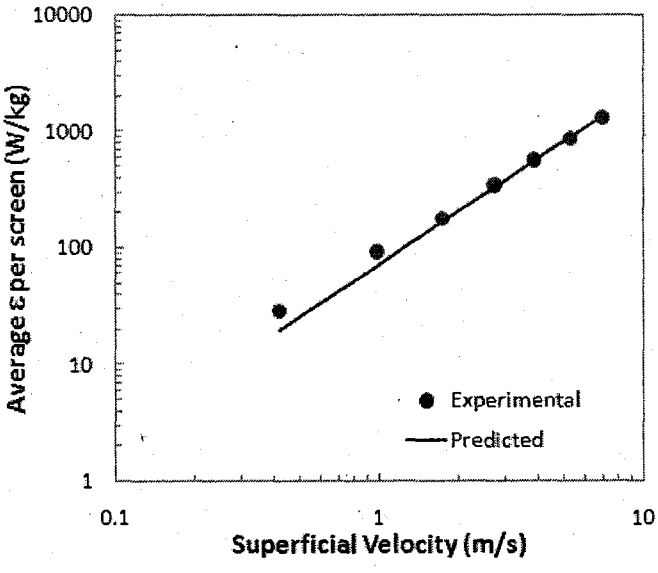

Figure B.8: Effect of superficial velocity on the average ε per screen ($C = 6.22$; $\alpha = 48.4$ %)

APPENDIX C: Complementary Information Regarding the Instabilities Encountered while Numerically Solving the PBE at High Shear Rates

The following complementary information is incorporated in order to present a complete and comprehensive representation of the research undertaken.

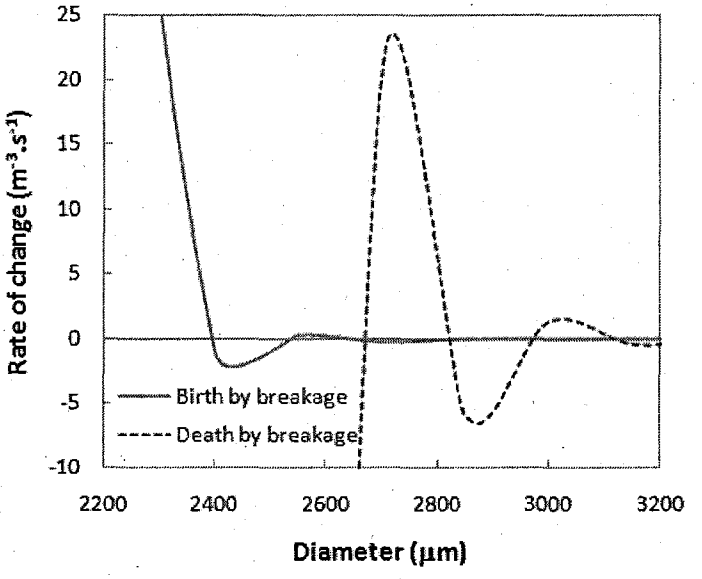

Figure C.1: Development of oscillatory numerical instabilities in the individual breakage rates.

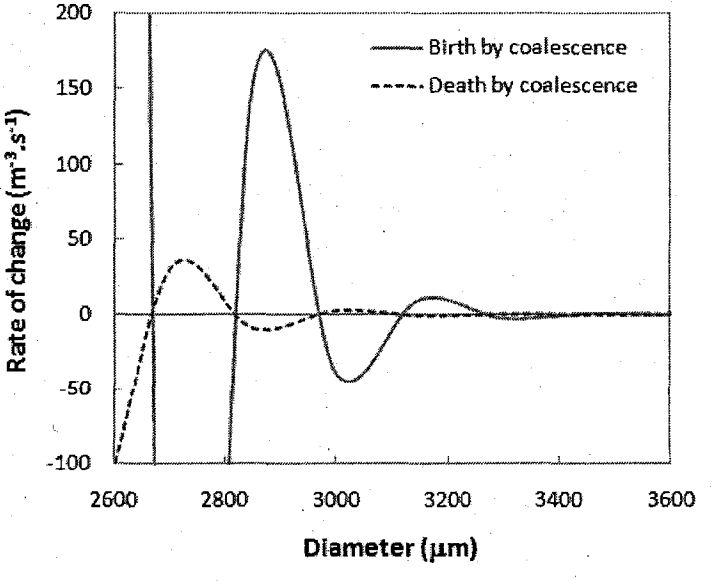

Figure C.2: Development of oscillatory numerical instabilities in the individual coalescence rates.

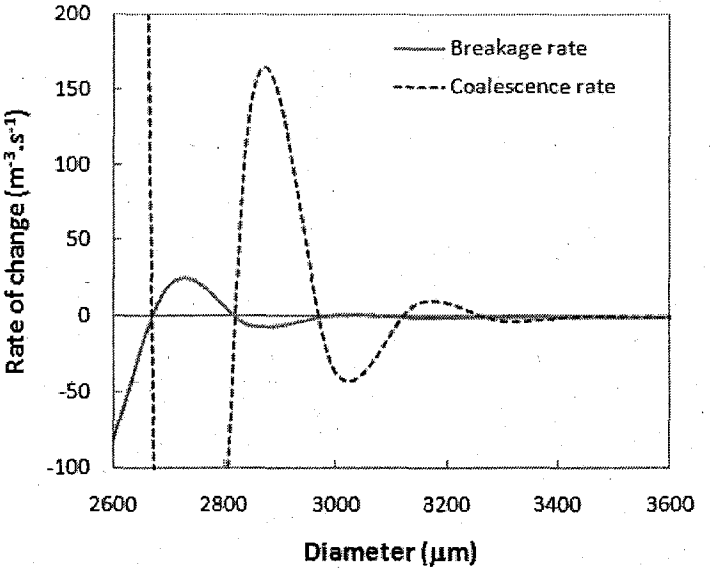

Figure C.3: Development of oscillatory numerical instabilities in the overall breakage and coalescence rates.

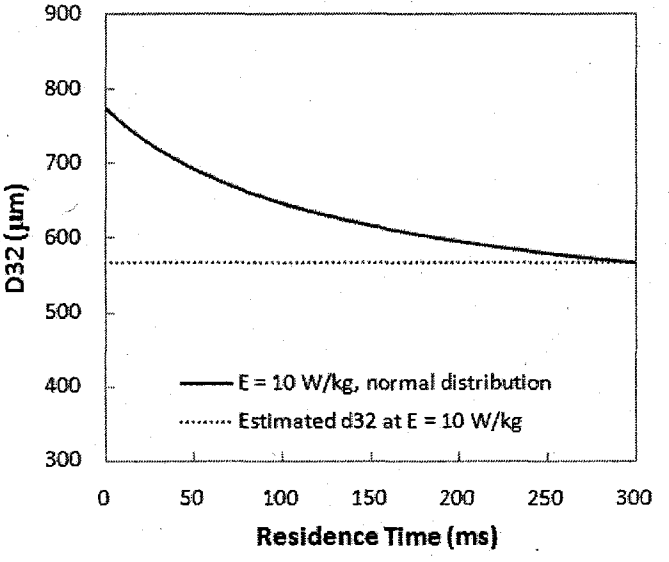

Figure C.4: Temporal variation of the Sauter mean diameter under breakage dominated conditions (obtained using the algorithm of Al Taweel et al. (2002), $\phi = 0.5$ %)

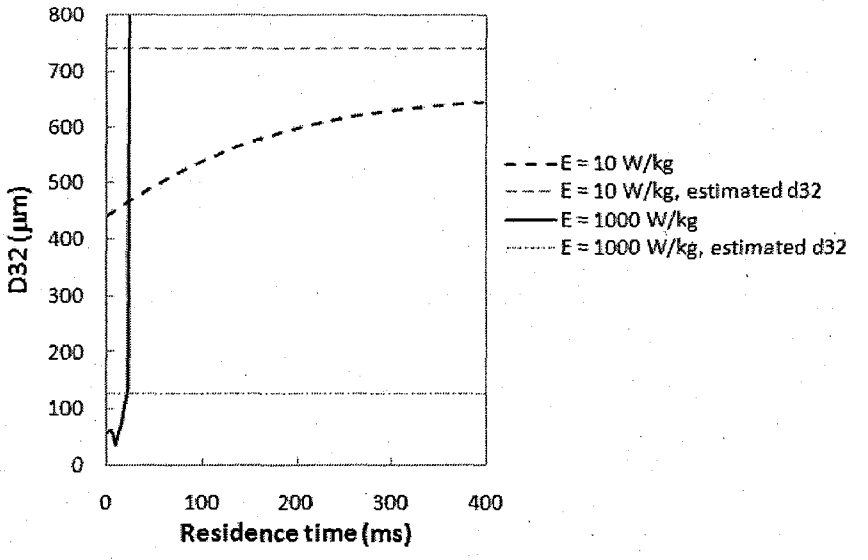

Figure C.5: Temporal variation of d_{32} under coalescence dominated conditions (obtained using only the relative drop number density approach for determining the upper limit, $\phi = 0.5\%$, coalescence frequency increased by 10-fold, $C_3 = 1$)

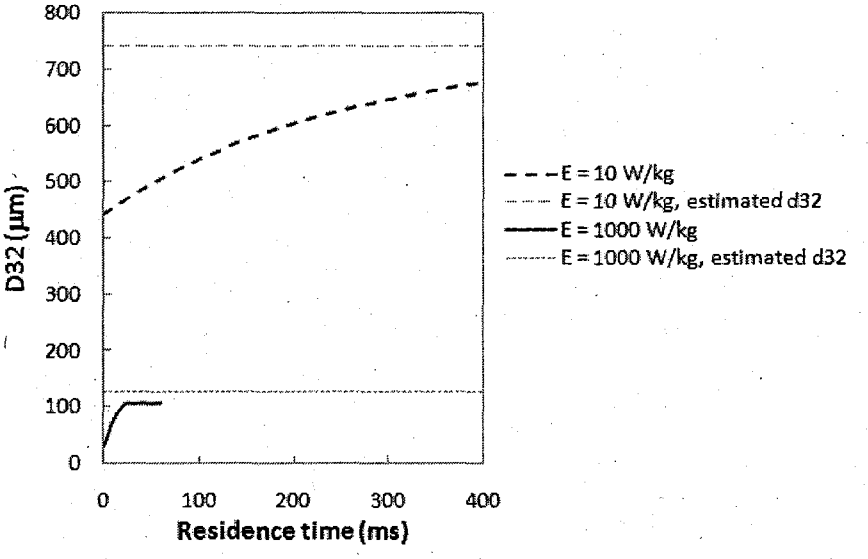

Figure C.6: Temporal variation of d_{32} under coalescence-dominated conditions (obtained using only the enhanced solution stability algorithm, $\phi = 0.5\%$, coalescence frequency increased by 10-fold, $C_3 = 1$)

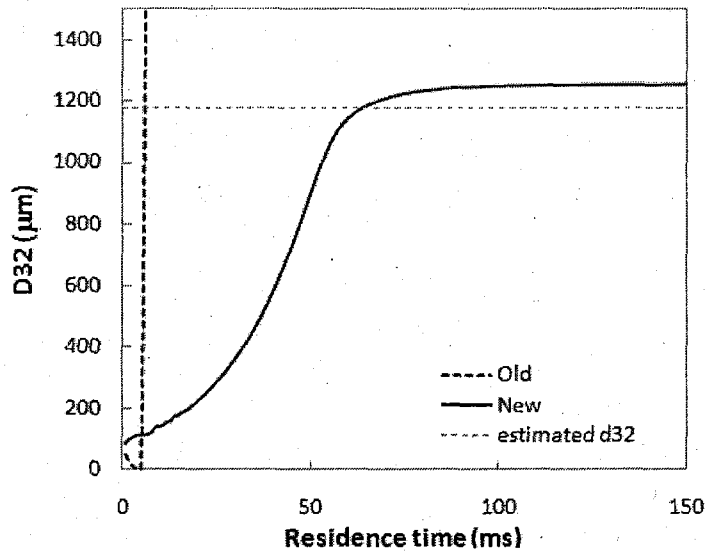

Figure C.7: Comparison between the temporal variations of the Sauter mean diameter under coalescence dominated conditions using the different solution methods ($\varepsilon = 10$ W/kg, $\phi = 0.5$ %, coalescence frequency increased by 1000-fold, $C_3 = 100$).

APPENDIX D: Complementary Information Regarding the PBE Simulations of Liquid-Liquid Systems

The following complementary information is incorporated in order to present a complete and comprehensive representation of the research undertaken.

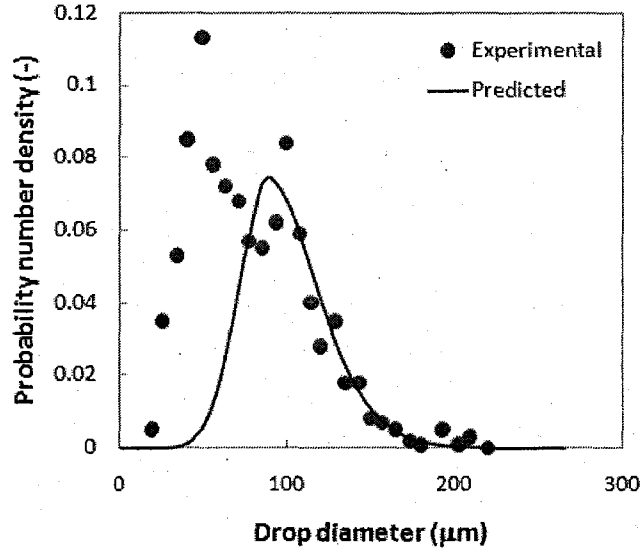

Figure D.1: Drop number density distribution ($\phi = 0.5$ %; $U = 0.9$ m/s; $\alpha = 27$ %)

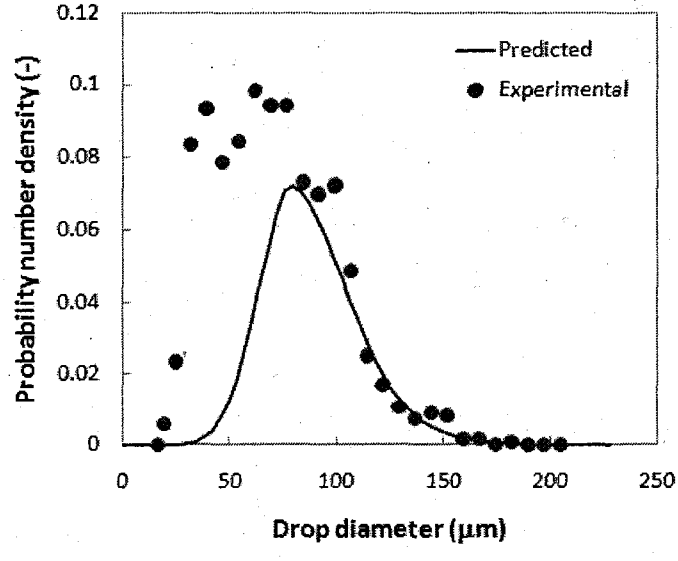

Figure D.2: Drop number density distribution ($\phi = 0.5$ %; $U = 0.97$ m/s; $\alpha = 27$ %)

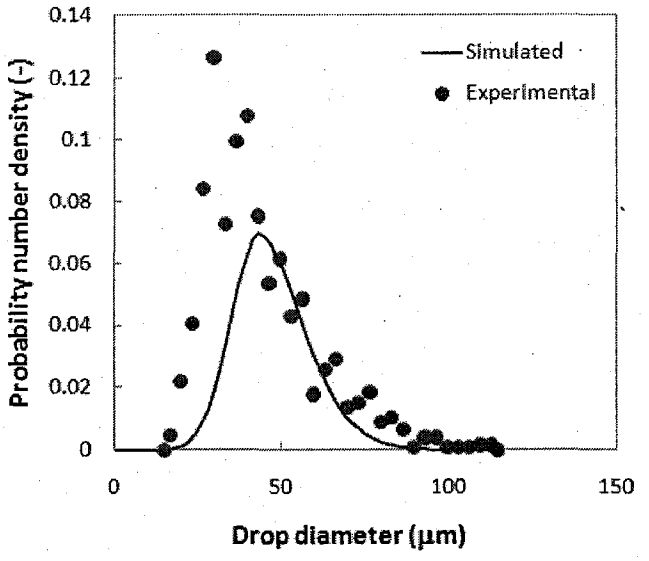

Figure D.3: Drop number density distribution ($\phi = 0.5$ %; $U = 1.55$ m/s; $\alpha = 27$ %)

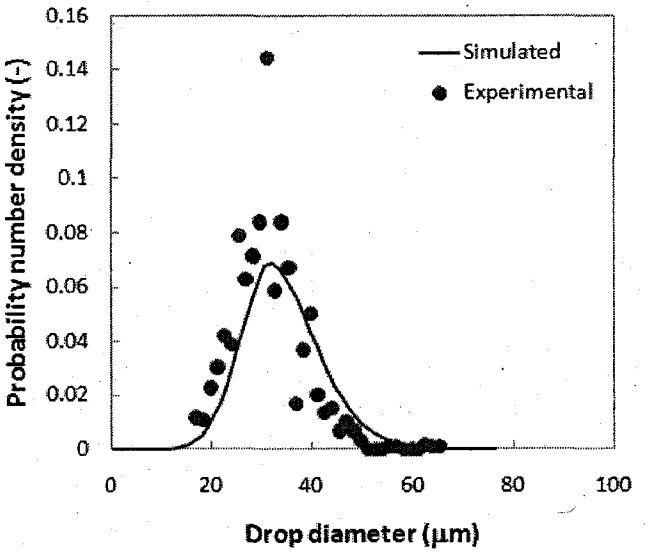

Figure D.4: Drop number density distribution ($\phi = 0.5$ %; $U = 1.94$ m/s; $\alpha = 27$ %)

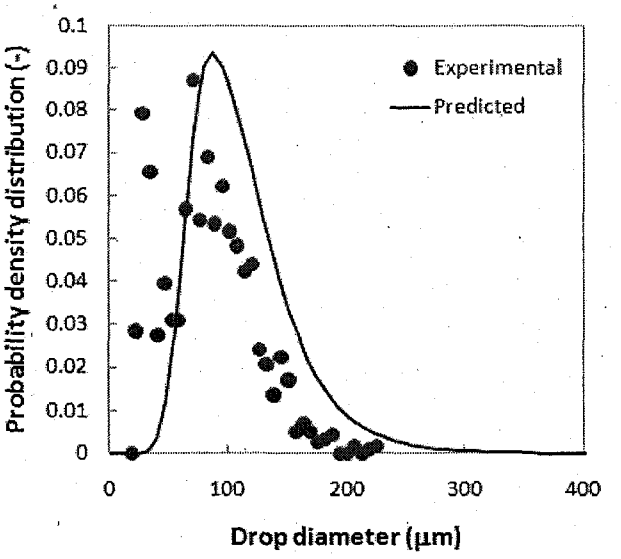

Figure D.5: Drop number density distribution ($\phi = 0.5$ %; $U = 0.85$ m/s; $\alpha = 33$ %)

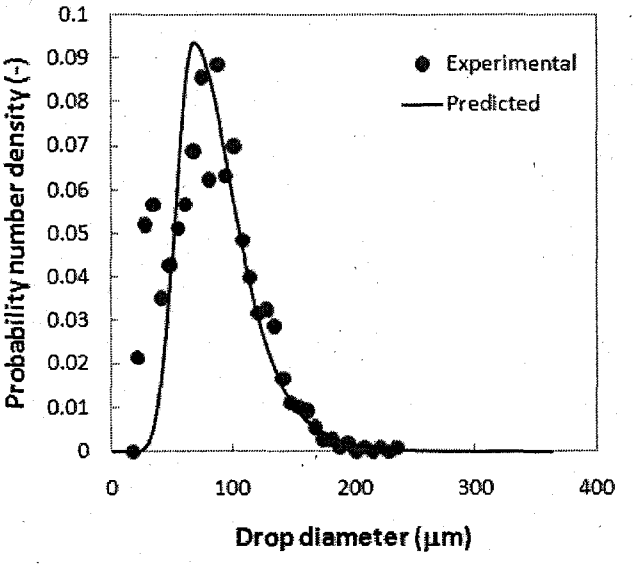

Figure D.6: Drop number density distribution ($\phi = 0.5$ %; $U = 0.97$ m/s; $\alpha = 33$ %)

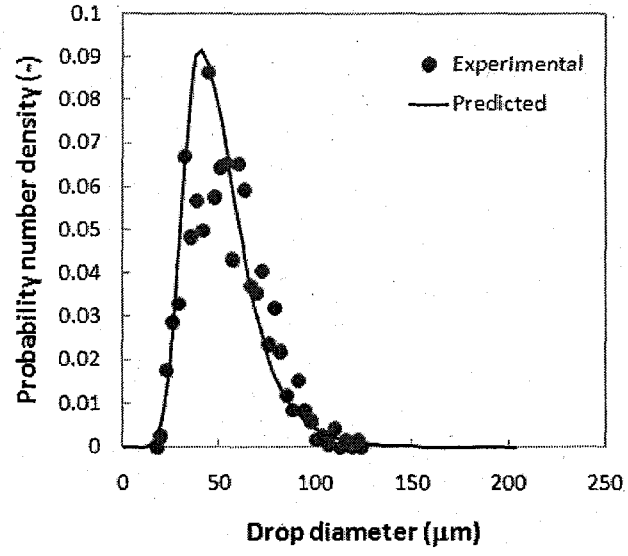

Figure D.7: Drop number density distribution ($\phi = 0.5$ %; $U = 1.55$ m/s; $\alpha = 33$ %)

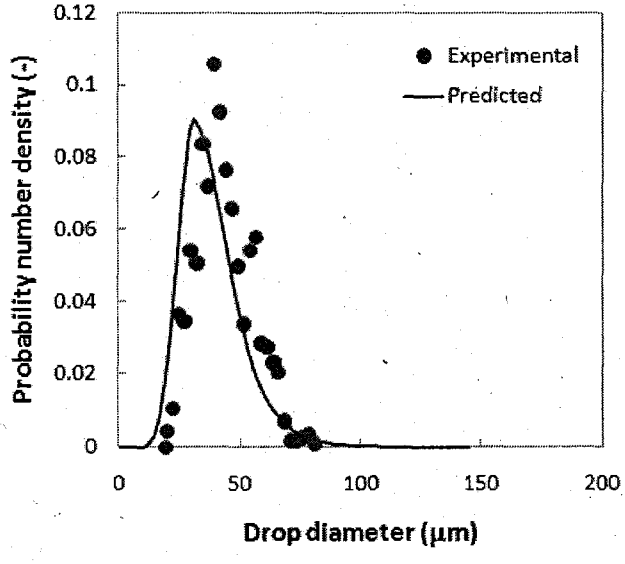

Figure D.8: Drop number density distribution ($\phi = 0.5$ %; $U = 1.8$ m/s; $\alpha = 33$ %)

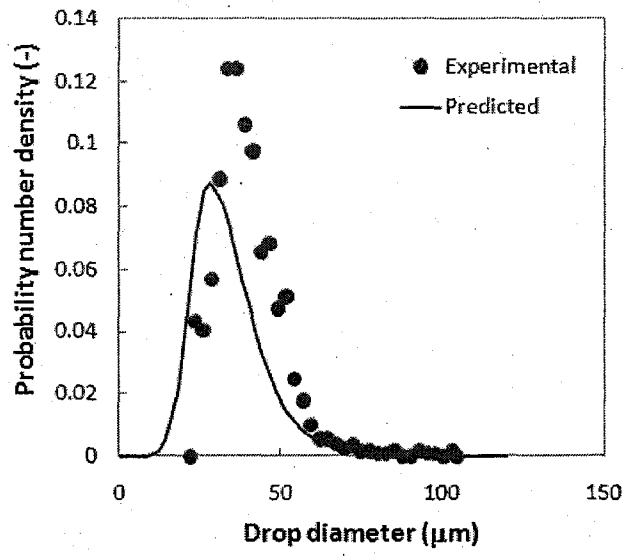

Figure D.9: Drop number density distribution (ϕ = 0.5 %; U = 1.94 m/s; α = 33 %)

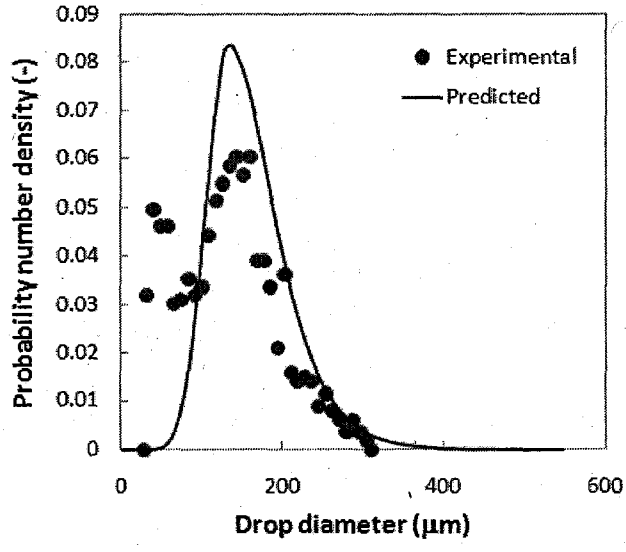

Figure D.10: Drop number density distribution (ϕ = 0.5 %; U = 0.85 m/s; α = 41 %)

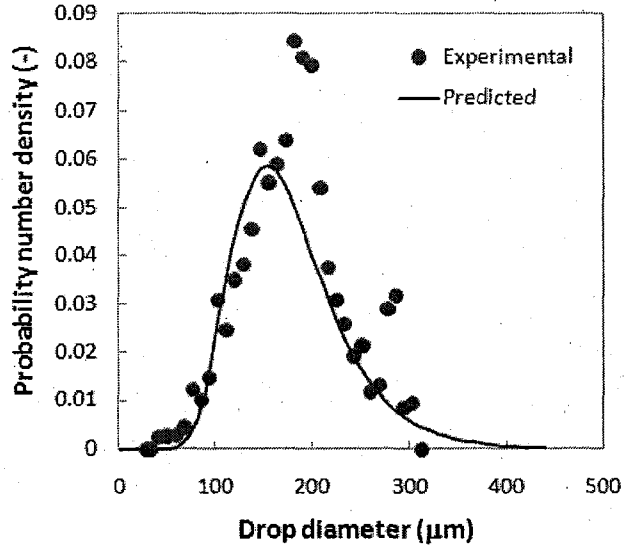

Figure D.11: Drop number density distribution ($\phi = 0.5$ %; $U = 0.97$ m/s; $\alpha = 41$ %)

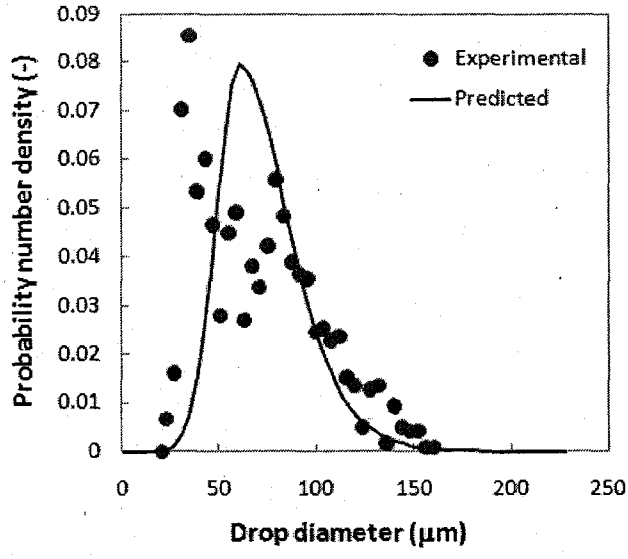

Figure D.12: Drop number density distribution ($\phi = 0.5$ %; $U = 1.55$ m/s; $\alpha = 41$ %)

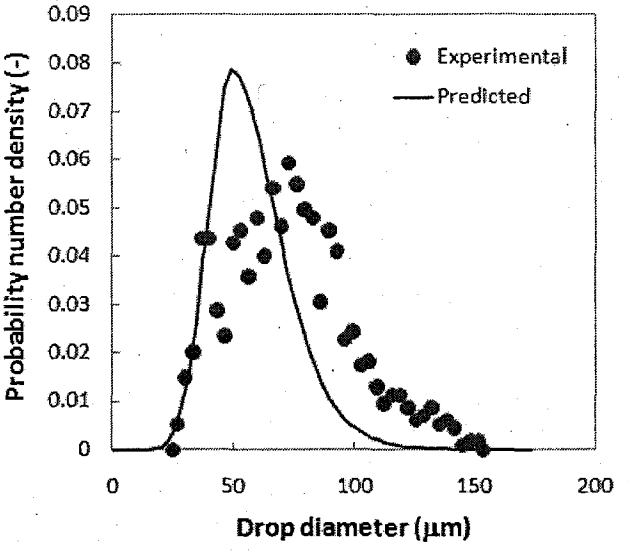

Figure D.13: Drop number density distribution ($\phi = 0.5$ %; $U = 1.8$ m/s; $\alpha = 41$ %)

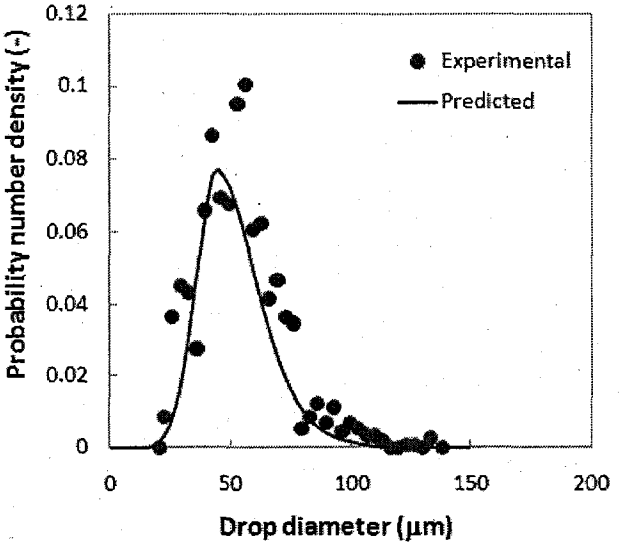

Figure D.14: Drop number density distribution ($\phi = 0.5$ %; $U = 1.94$ m/s; $\alpha = 41$ %)

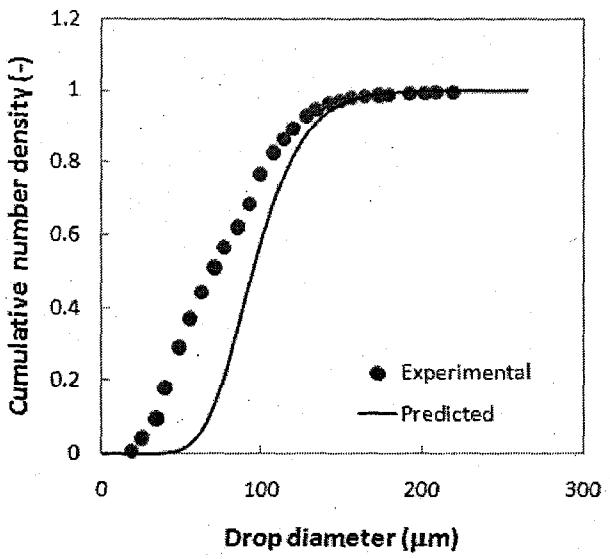

Figure D.15: Cumulative drop number density distribution
($\phi = 0.5$ %; $U = 0.9$ m/s; $\alpha = 27$ %)

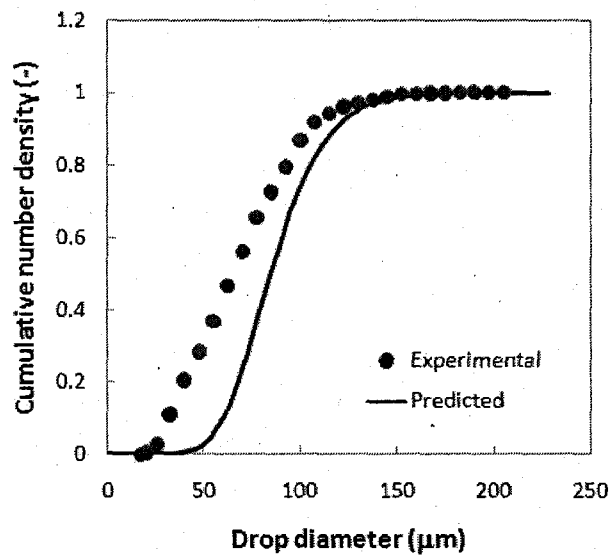

Figure D.16: Cumulative drop number density distribution
($\phi = 0.5$ %; $U = 0.97$ m/s; $\alpha = 27$ %)

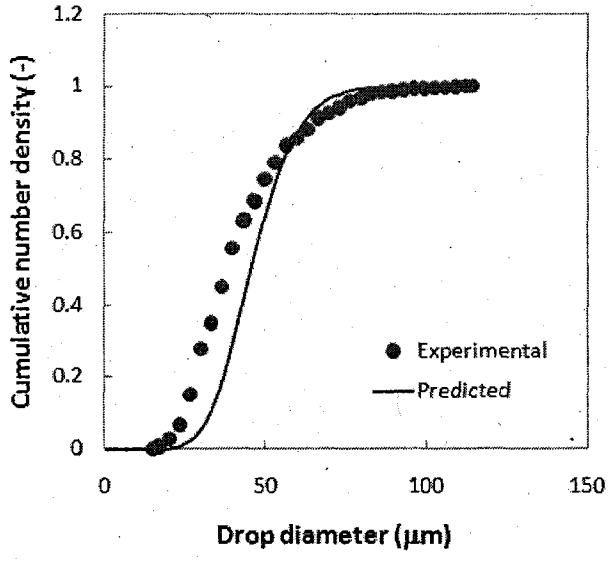

Figure D.17: Cumulative drop number density distribution
(ϕ = 0.5 %; U = 1.55 m/s; α = 27 %)

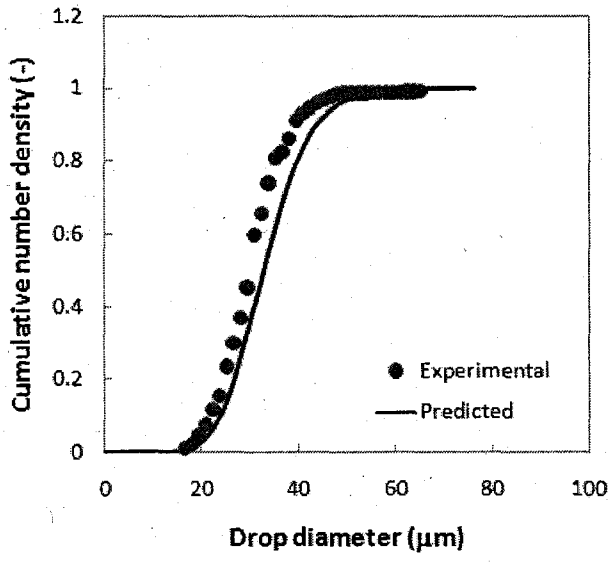

Figure D.18: Cumulative drop number density distribution
(ϕ = 0.5 %; U = 1.94 m/s; α = 27 %)

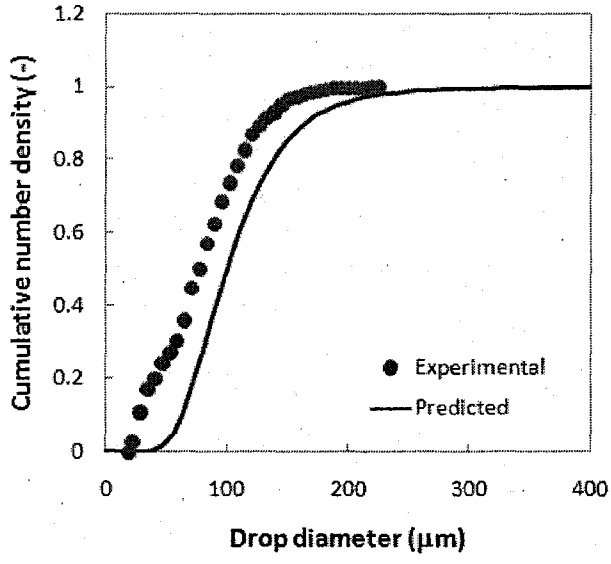

Figure D.19: Cumulative drop number density distribution
($\phi = 0.5$ %; $U = 0.85$ m/s; $\alpha = 33$ %)

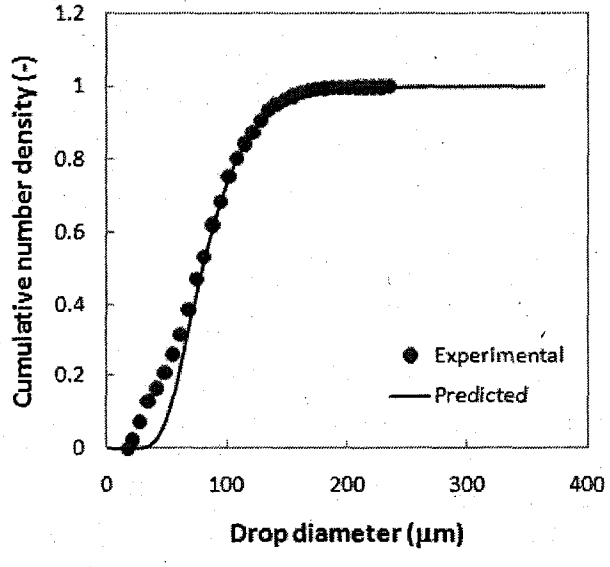

Figure D.20: Cumulative drop number density distribution
($\phi = 0.5$ %; $U = 0.97$ m/s; $\alpha = 33$ %)

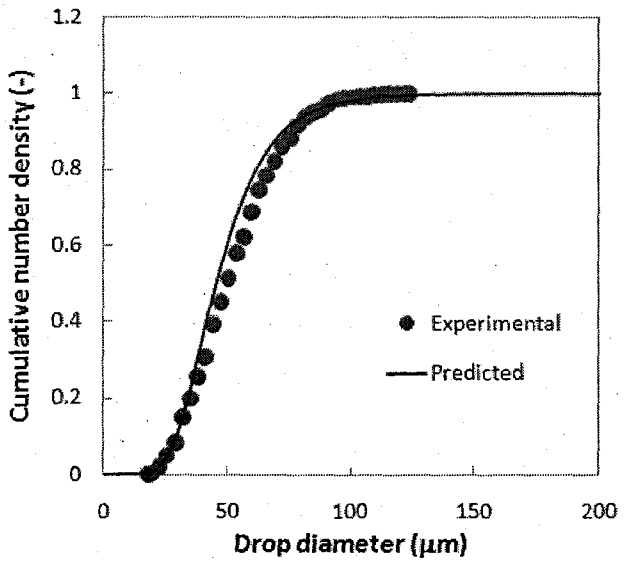

Figure D.21: Cumulative drop number density distribution
(ϕ = 0.5 %; U = 1.55 m/s; α = 33 %)

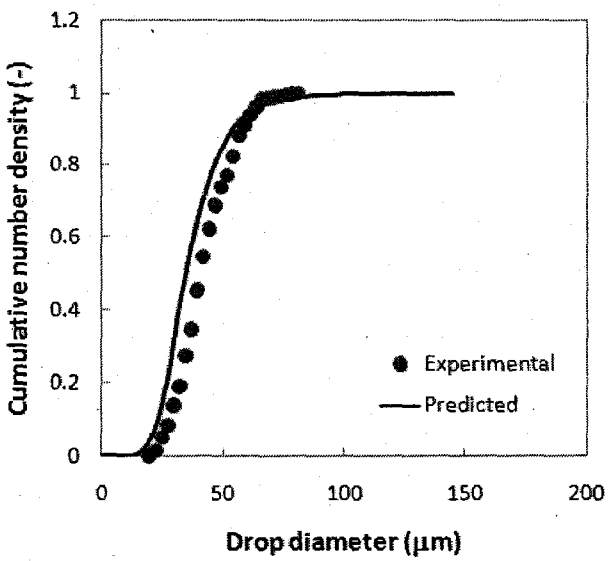

Figure D.22: Cumulative drop number density distribution
(ϕ = 0.5 %; U = 1.8 m/s; α = 33 %)

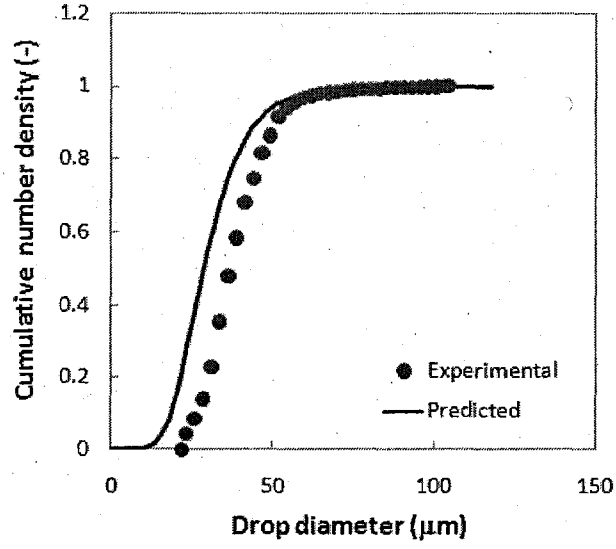

Figure D.23: Cumulative drop number density distribution
($\phi = 0.5$ %; $U = 1.94$ m/s; $\alpha = 33$ %)

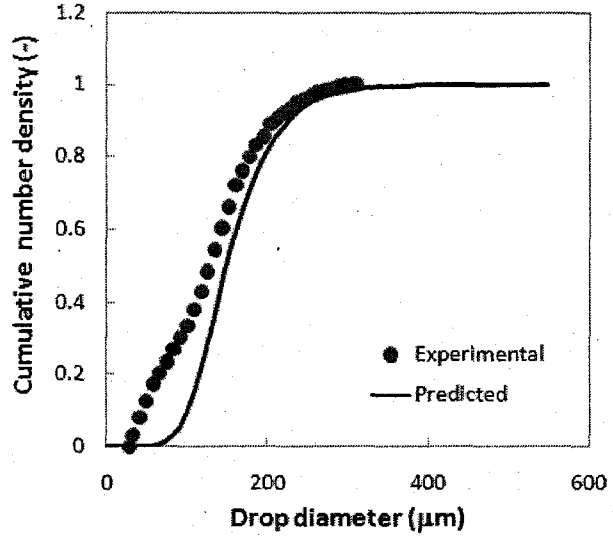

Figure D.24: Cumulative drop number density distribution
($\phi = 0.5$ %; $U = 0.85$ m/s; $\alpha = 41$ %)

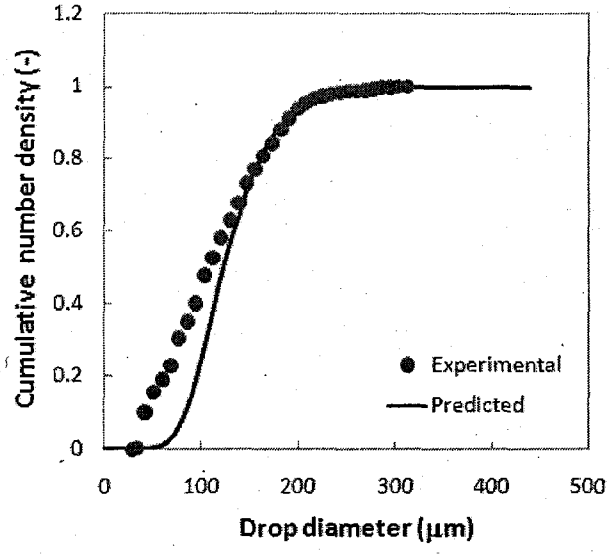

Figure D.25: Cumulative drop number density distribution
($\phi = 0.5$ %; $U = 0.97$ m/s; $\alpha = 41$ %)

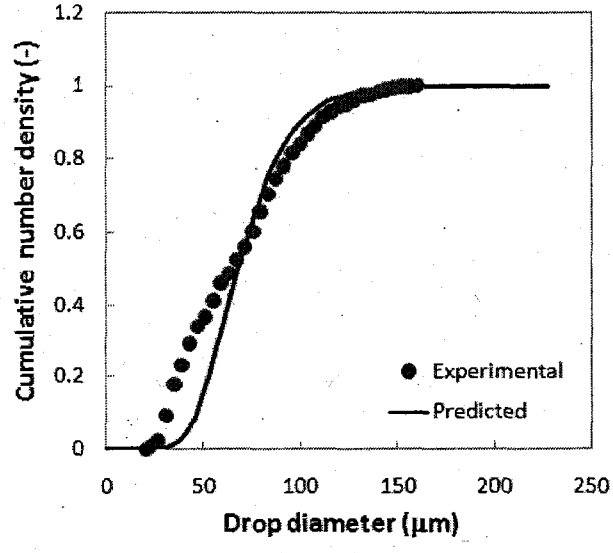

Figure D.26: Cumulative drop number density distribution
($\phi = 0.5$ %; $U = 1.55$ m/s; $\alpha = 41$ %)

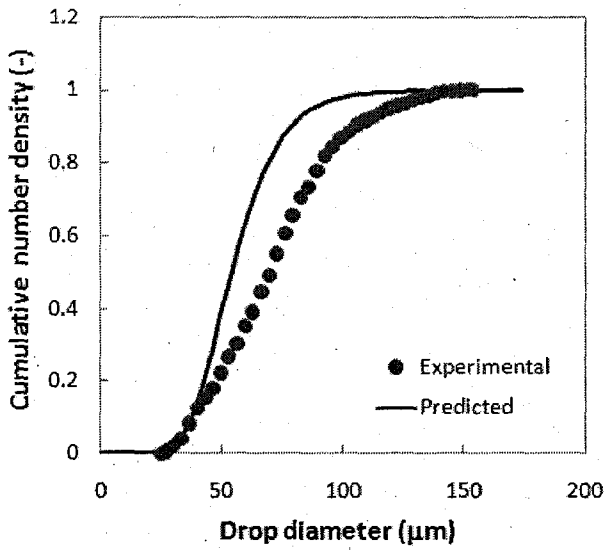

Figure D.27: Cumulative drop number density distribution
($\phi = 0.5$ %; $U = 1.8$ m/s; $\alpha = 41$ %)

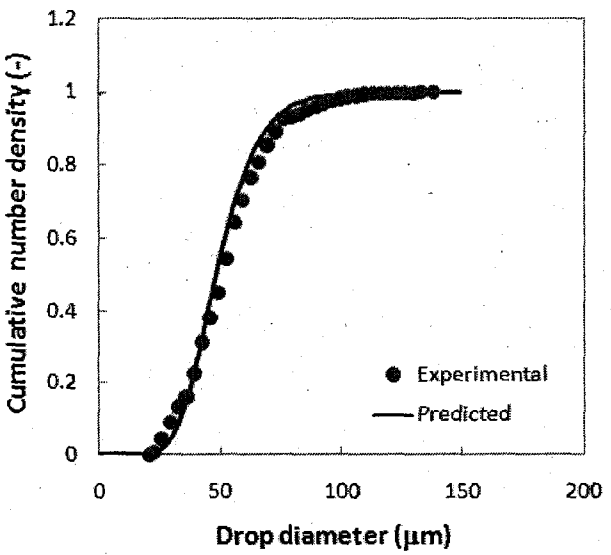

Figure D.28: Cumulative drop number density distribution
($\phi = 0.5$ %; $U = 1.94$ m/s; $\alpha = 41$ %)

APPENDIX E: Complementary Information Regarding Inter-Phase Mass Transfer in Liquid-Liquid Systems

The following complementary information is incorporated in order to present a complete and comprehensive representation of the research undertaken.

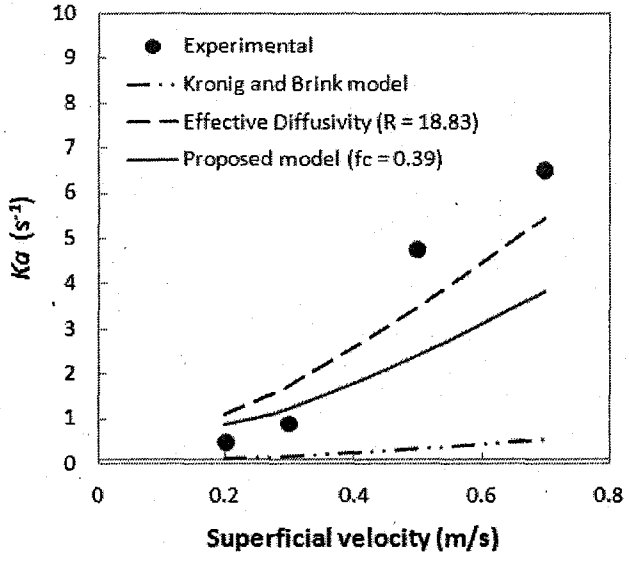

Figure E.1: Effect of the superficial velocity on Ka
($\alpha = 33$ %; $\phi = 47$ %; $L = 12.7$ mm)

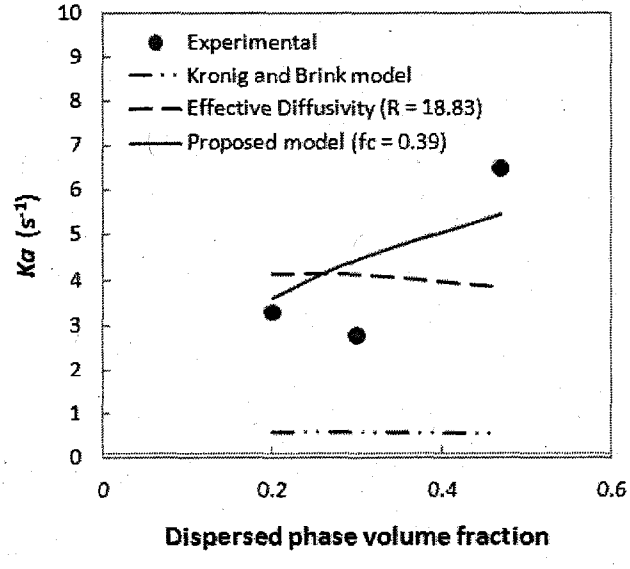

Figure E.2: Effect of the superficial velocity on Ka
($\alpha = 33$ %; $U = 0.7$ m/s; $L = 12.7$ mm)

APPENDIX F: Complementary Information Regarding Inter-Phase Mass Transfer in Gas-Liquid Systems

The following complementary information is incorporated in order to present a complete and comprehensive representation of the research undertaken.

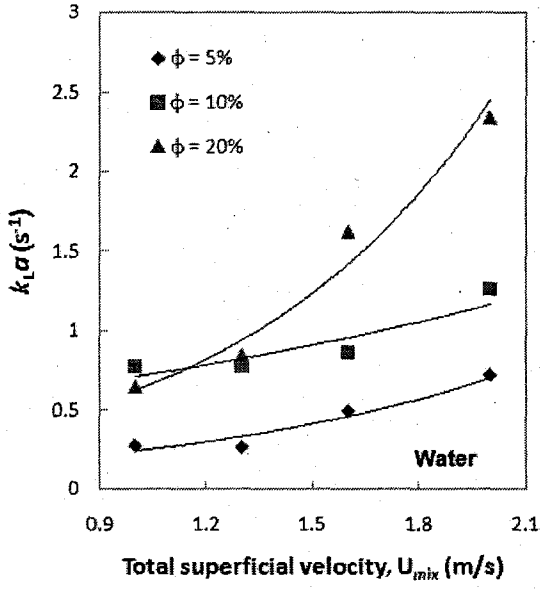

Figure F.1: Effect of gas-to-liquid flow ratio on k_La (C_{SDS} = 0 ppm)

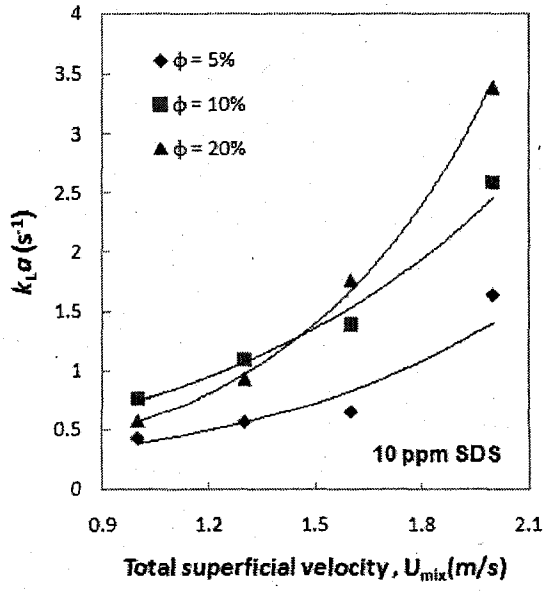

Figure F.2: Effect of gas-to-liquid flow ratio on k_La (C_{SDS} = 10 ppm)

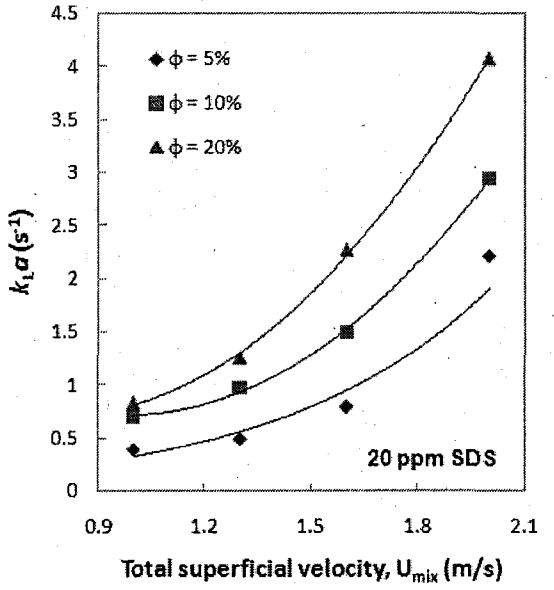

Figure F.3: Effect of gas-to-liquid flow ratio on $k_L a$ (C_{SDS} = 20 ppm)

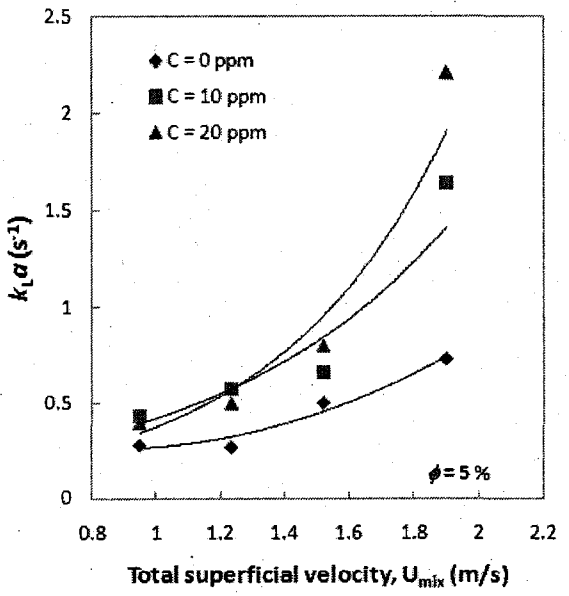

Figure F.4: Effect of SDS concentration on $k_L a$ (ϕ = 5 %)

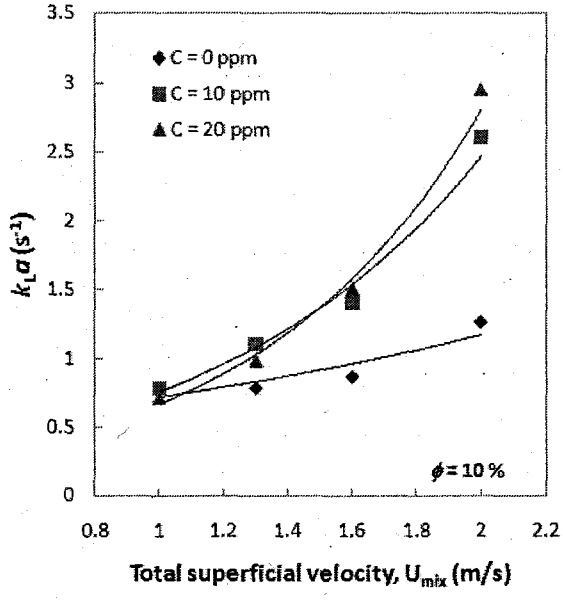

Figure F.5: Effect of SDS concentration on $k_L a$ (ϕ = 10 %)

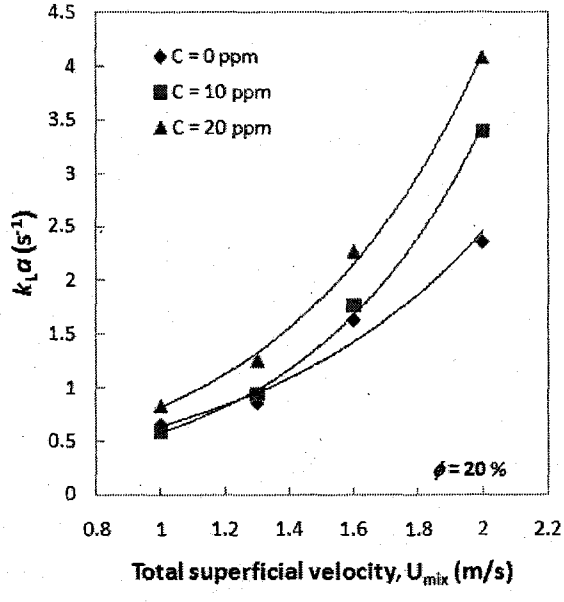

Figure F.6: Effect of SDS concentration on $k_L a$ (ϕ = 20 %)

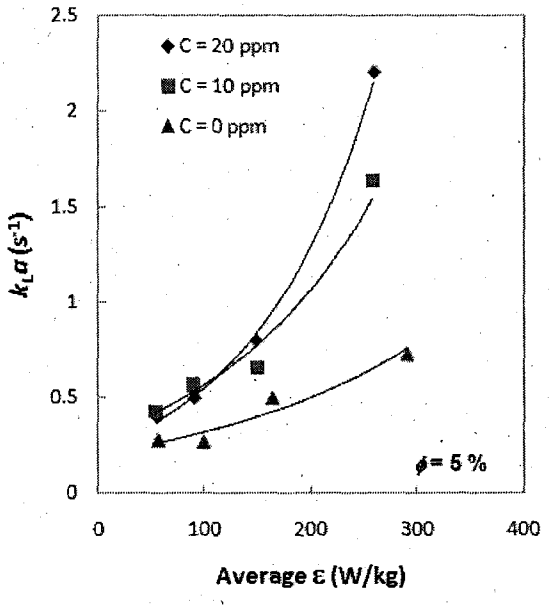

Figure F.7: Effect of average ε on k_La (ϕ = 5 %)

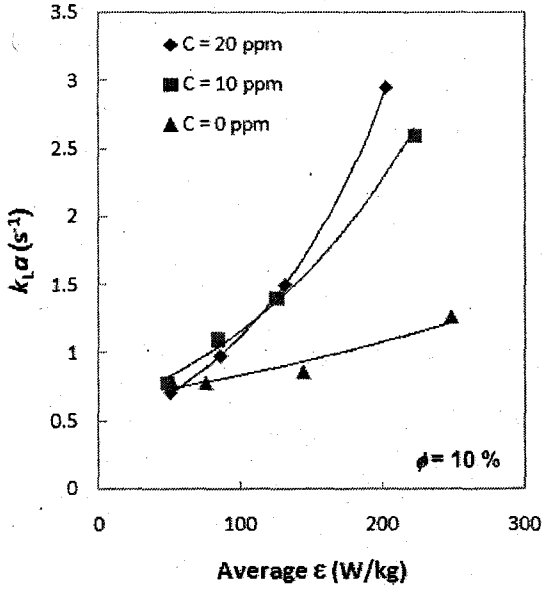

Figure F.8: Effect of average ε on k_La (ϕ = 10 %)

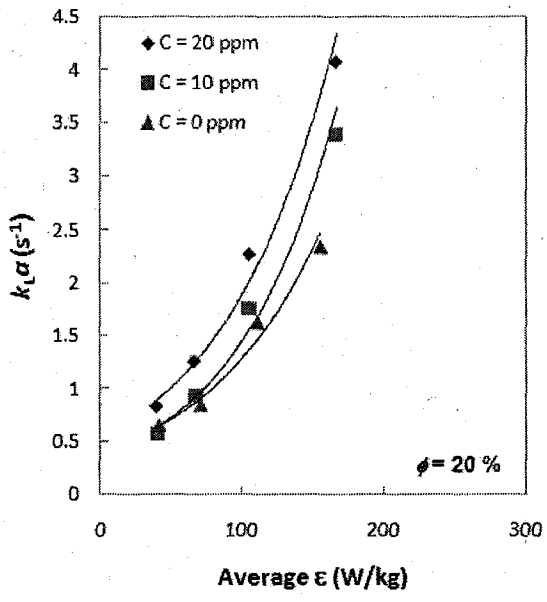

Figure F.9: Effect of average ε on $k_L a$ (ϕ = 20 %)

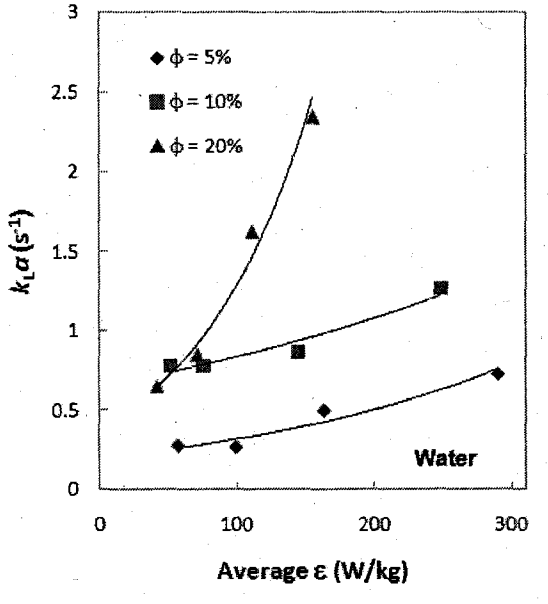

Figure F.10: Effect of average ε on $k_L a$ (C_{SDS} = 0 ppm)

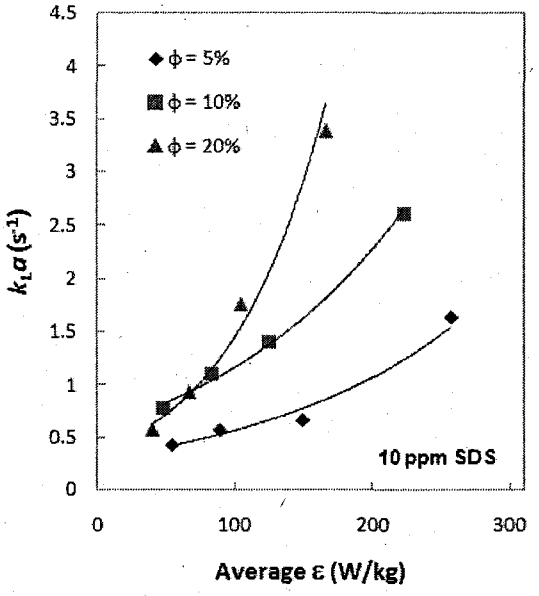

Figure F.11: Effect of average ε on k_La (C_{SDS} = 10 ppm)

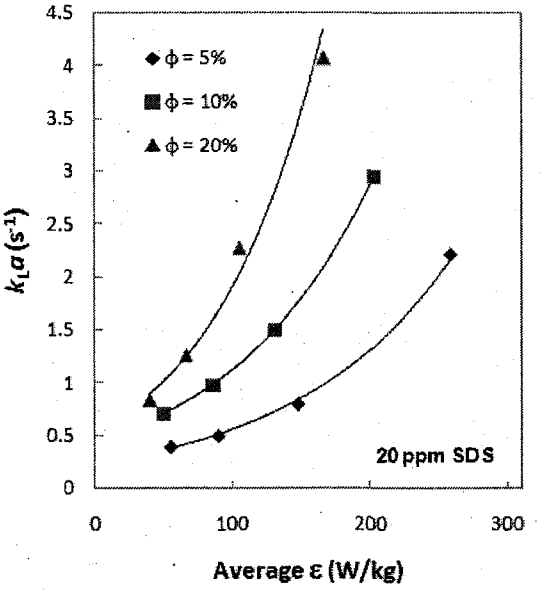

Figure F.12: Effect of average ε on k_La (C_{SDS} = 20 ppm)

APPENDIX G: Copyright Agreements

Chemical Engineering Science Copyright Permission

What follows are the rights retained by an author of the Chemical Engineering Science journal (an Elsevier publication). A complete list of rights and further copyright details can be found on the journal's website at:

(http://www.elsevier.com/wps/find/authorsview.authors/copyright#whatrights)

"As a journal author, you retain rights for large number of author uses, including use by your employing institute or company. These rights are retained and permitted without the need to obtain specific permission from Elsevier. These include:

- the right to make copies (print or electric) of the journal article for their own personal use, including for their own classroom teaching use;
- the right to make copies and distribute copies (including via e-mail) of the journal article to research colleagues, for personal use by such colleagues (but not for Commercial Purposes[1], as listed below);
- the right to present the journal article at a meeting or conference and to distribute copies of such paper or article to the delegates attending the meeting;
- **the right to include the journal article, in full or in part, in a thesis or dissertation;**
- the right to use the journal article or any part thereof in a printed compilation of works of the author, such as collected writings or lecture notes (subsequent to publication of the article in the journal); and
- the right to prepare other derivative works, to extend the journal article into book-length form, or to otherwise re-use portions or excerpts in other works, with full acknowledgement of its original publication in the journal."

---

[1] *Commercial Purposes includes the use or posting of articles for commercial gain including the posting by companies or their employee-authored works for use by customers of such companies (e.g. pharmaceutical companies and physician-prescribers); commercial exploitation such as directly associating advertising with such postings; the charging of fees for document delivery or access; or the systematic distribution to others via e-mail lists or list servers (to parties other than known colleagues), whether for a fee or for free.*

Chemical Engineering Communications Copyright Permission

What follows are the rights retained by an author of the Chemical Engineering Communications journal (a Taylor & Francis publication). A complete list of rights and further copyright details can be found on the publisher's website at:

(http://www.tandf.co.uk/journals/authorrights.pdf)

"What are my other retained rights as an author?

- patent rights, trademark rights, or rights to any process, product or procedure described in an article;
- the right to share with colleagues (but not on a commercial or systematic basis) copies of an article in its published form as supplied by Taylor & Francis as an electronic or printed offprint or reprint;
- **the right to include an article in a thesis or dissertation that is not to be published commercially, provided that acknowledgement to prior publication in the relevant Taylor & Francis journal is made explicit;**
- the right to present an article at a meeting or conference and to distribute printed copies of the Article to the delegates attending the meeting provided that this is not for commercial purposes, provided that acknowledgement to prior publication in the relevant Taylor & Francis journal is made explicit;
- the right to use the Article in its published form in whole or in part without revision or modification in personal compilations in print or electronic form or other publications of an Author's own articles, provided that acknowledgement to prior publication in the relevant Taylor & Francis journal is made explicit;
- the right to expand an article into book-length form for publication, provided that acknowledgement to prior publication in the relevant Taylor & Francis journal is made explicit."